Scuola di Dottorato in Ingegneria "Leonardo da Vinci"

UNIVERSITA' DEGLI STUDI DI PISA

Programma di Dottorato in Sicurezza Nucleare e Industriale

Experimental and computational analyses in support to the design of a SG mock-up prototype for LFR technology applications

Anno accademico 2013-2014

CANDIDATO

Davide ROZZIA

RELATORI

Dott. Ing. Mariano TARANTINO
Dott. Ing. Nicola FORGIONE
Dott. Alessandro ALEMBERTI
Prof. Francesco ORIOLO

(This page has been intentionally left blank)

Sommario

La configurazione di reattore veloce refrigerato a piombo messa a punto nel contesto dei più recenti progetti europei quali ELSY (European Lead cooled System) e LEADER (Lead-cooled European Advanced DEmonstration Reactor) prevede la realizzazione di un reattore molto compatto in cui l'intero sistema primario e i generatori di vapore sono locati all'interno di una piscina. In tale scenario, la progettazione dei generatori di vapore gioca un ruolo fondamentale nello sviluppo della filiera stessa in quanto detto componente rappresenta l'interfaccia tra l'isola nucleare e il circuito secondario. In particolare, la rottura di uno dei suoi tubi (che ammontano qualche migliaio), potrebbe propagarsi nei tubi ad esso adiacenti e generare una potenziale immissione di vuoti all'interno del core nonché una sovrappressione all'interno della piscina dovuta all'interazione tra piombo fuso e vapore ad alta pressione.

Una configurazione innovativa di generatore di vapore è stata proposta nel contesto del progetto LEADER: il generatore di vapore surriscaldato a perdite monitorabili grazie ad un fascio tubiero a baionetta con doppia parete. Questo tipo di design concettuale è stato studiato negli USA negli anni 60 per l'applicazione a reattori veloci a sodio. Un esempio di facility che opera con un componente di questo tipo è CIRCE (ENEA Brasimone) seppur con lo scopo di scambiatore di calore (non destinato alla produzione di vapore surriscaldato).

La singola unità verticale consiste di tre tubi concentrici. Partendo dal più piccolo, (feed-water tube), l'acqua di alimento entra dall'alto e lo percorre in flusso discendente. Al termine di questo tubo, il fluido entra nel meato anulare (annular-riser) realizzato tra il primo ed il secondo tubo ad esso concentrico risalendolo e cambiando di fase sino allo stato di vapore surriscaldato grazie allo scambio termico in controcorrente con il piombo fuso locato nello shell del generatore. Il piombo non è in contatto diretto con il secondo tubo: un terzo tubo concentrico provvede una doppia separazione tra la miscela acqua vapore ed il piombo realizzando la cosiddetta doppia parete.

Lo studio di questa particolare configurazione è motivato dal sostanziale aumento del margine di sicurezza apportato. Infatti, esso permette la doppia separazione fisica tra il lato fluido e il lato piombo riducendo pertanto la possibilità di interazione piombo acqua da rottura di tubi. Inoltre, pressurizzando il gap intermedio tra la doppia parete con gas elio, è possibile introdurre un sistema di rivelazione delle perdite (che ottempera tale funzione sia in caso di rottura lato piombo che in caso di rottura lato acqua), atto a prevenire scenari incidentali quali la rottura multipla di tubi dovuta all'interazione piombo acqua a seguito di rottura di un tubo.

Come rovescio della medaglia, occorre dimostrare l'efficace funzionamento di tale sistema e progettarlo cercando di mantenere il più possibile elevata l'efficienza termica del componente. In particolare, due aspetti del design sono di grande rilievo dal punto di vista economico per la realizzazione del tubo a baionetta a doppia parete monitorabile. Il primo concerne appunto il sistema di monitoraggio: l'introduzione di un gas a bassa conducibilità termica rende necessaria l'adozione di un mezzo poroso che lo possa contenere garantendo una più elevata conducibilità termica in modo da poter ridurre il più possibile lunghezza e/o numero dei tubi necessari ad asportare la potenza richiesta alla temperatura richiesta. Il secondo concerne l'isolamento termico tra acqua sottoraffreddata di alimento in discesa nel feed-water tube e vapore surriscaldato in risalita nell'annular-riser specialmente nella zona al di sopra del piombo al fine di evitare caduta

di temperatura del vapore e/o condensazione dello stesso nella superficie esterna del tubo di feed-water.

Il presente dottorato è co-finanziato da Ansaldo ed ENEA ed è direttamente connesso al progetto LEADER e al piano nazionale contenuto nell'Accordo Di Programma (ADP). L'attività ha come scopo di sostenere lo sviluppo del tubo a baionetta con doppia parete dotato di sistema di monitoraggio delle perdite e di investigare le sue performances termoidrauliche sia in via analitica che sperimentale. Al momento i seguenti obiettivi sono stati raggiunti e verranno presentati in questa tesi:

- *Analisi delle performances termoidrauliche del tubo a baionetta mediante codice RELAP-5.*
- *Design, costruzione ed esercizio della facility TxP (Tubes for Powders) avente come obiettivo la misura della conducibilità termica di polveri in geometria anulare. Il suo impiego è stato volto alla qualifica della conducibilità di polveri per la loro applicazione sia al tubo a baionetta per steam generator (prevedendo la possibilità di introduzione di elio in pressione) sia agli scambiatori di calore in uso presso il centro del Brasimone che utilizzano tale tecnologia per accomodare un gradiente termico tra due fluidi (generalmente acqua allo stato liquido monofase e piombo).*
- *Design e commissioning della test section HERO (Heavy liquid mEtal pRessurized water cOoled tubes) sulla base dei risultati ottenuti nelle campagne sperimentali condotte su TxP. La test section HERO è attualmente strumentata e collocate all'interno della facility CIRCE e consta di un bundle di 7 tubi a doppia parete a baionetta (monitorabili) che rappresentano il più possibile il generatore di vapore proposto in LEADER per il reattore ALFRED (1:1 in lunghezza, 1:1 in portata del singolo tubo).*

Abstract

The configuration of the Lead cooled Fast Reactor (LFR) pointed out in the framework of the European Lead cooled SYstem (ELSY) and Lead-cooled European Advanced DEmonstration Reactor (LEADER) EC founded projects deals with the compact pool type reactor in which the steam generators (SG) are located inside the reactor tank. In this scenario, the steam generator design plays an important role since it represents the interface between the nuclear island and the secondary system and one of the most impacting incidents connected to this is the Steam Generator Tube Rupture (SGTR) that may propagate to the near-bough tubes (which are located in the same vessel of the reactor core). In the framework of the LEADER project, an innovative configuration of SG has been proposed: the super-heated steam double wall once through bayonet type with leakage monitoring. This conceptual design was studied since 60' for Sodium Reactor application. An example of facility that operates with this concept is CIRCE (ENEA Brasimone), nevertheless the application is limited to the heat exchange function.

The single tube vertical unit consists of three concentric tubes. Starting from the smallest one (feed-water tube), the water crosses it in down-flow. At the end of this tube, it enters the second concentric tube (annular riser) in up-flow where it starts to boil due to the heat exchange with the liquid lead that flows in counter-current at the tube outer surface. The tube design allows the achievement of super-heated steam. The liquid lead is not in direct contact with the second tube. A third concentric tube, that creates an annulus, separates it from the steam-water sides realizing the so called double wall.

The study of this configuration is motivated by safety improvement. In fact, it allows the double physical separation between lead and water sides. Furthermore, by means of gap pressurization (with Helium), a leakage check system should be introduced between the double wall in order to prevent incident scenarios. On the other hands, the monitor-ability of the pressurized gap has to be demonstrated and the thermal efficiency of the unit has to be improved. In particular two main design issues are of great importance from the economic point of view. The first deals with monitor-ability of leakages: since a gas as helium is required and it has low conductivity, the gap between the tube should be minimized and a porous heat transfer enhancer should be introduced to reduce, as much as possible, the SG volume (tube length or tube number). The second deals with the thermal insulation of the feed-water descending tube. In fact, the water enters at its minimum temperature at the top of the SG, it is above the active length and it exchanges heat with the superheated stem that is leaving the SG unit. Therefore, in order to avoid steam condensation at the feed-water tube outer surface this tube should be designed with sandwich wall: steel - thermal insulator – steel.

This doctorate is co-financed by ANSALDO and ENEA and is directly connected to LEADER and Accordo Di Programma (ADP) national project. The activity aims to support the design of the double wall bayonet tube bundle SG with leakage monitoring and to investigate its TH performance both analytically and experimentally (into a representative prototype scaled down in power). The activity started in 2011 and is still ongoing. At present time the following objectives are reached and are presented in this thesis:

- *Assessment of the TH performance of the bayonet tube by means of RELAP-5.*

- *Design, construction, operation and disposal of the TxP (Tubes for Powders) facility devoted to powders conductivity measurement into an annular geometry. Its aim was to qualify the conductivity of powders for their application in the annular gap between the tubes that separate the fluids both for application as heat transfer enhancer (as for the ALFRED SG) and to both to accommodate a give temperature drop (as for the HX of facilities under operation at Brasimone).*
- *Design and commissioning of the HERO (Heavy liquid mEtal pRessurized water cOoled tubes) test section based on the results achieved during the experimental campaigns in TxP. This test section is actually located in CIRCE and aims to investigate the TH behavior of a bundle of seven tubes that represent, as much as possible, the ALFRED SG tubes (1:1 in length).*

Eight main sections and four attached appendixes constitute the structure of this work.

The first three sections have to be intended as introduction to the activity. Justification of the activity, framework and objective are given in section one. GEN-IV systems and LEADER project are briefly described in section 2. The third section presents the ALFRED SG. It includes also the historical development of double wall SG in the nuclear technology and a brief description of the HXs that have been operated or are under construction at ENEA CR Brasimone that make use of double wall concept.

The fourth and fifth sections are theoretical activities conducted in support to the R&D of the steam generator bayonet tube. In particular, section four is aimed to assess the TH performance of a single tube of the ALFRED SG by fixing, in a theoretical way (which is described in section five), some modeling issues still not defined in the ALFRED design (i.e. the powder material to be introduced between the double wall and its modeling). Section five aims to point out empirical models to treat the conductivity of powder media and to individuate candidate materials to be acquired and tested with the intent to design a double wall bayonet tube bundle test section. This last section includes an investigation on insulating materials for their application to the the feed-water tube.

Section six constitutes the core of this activity and has to be intended as a first step on R&D in support to the design of the bayonet tube steam generator with particular reference to the heat transfer enhancer porous medium placed between the double wall. The Tubes for Powders (TxP) facility has been designed (by ENEA), constructed (by LIMAINOX), instrumented (by ENEA) and operated to test the conductivity of powders both under un-pressurized air environment and under pressurized helium atmosphere. This process takes more than two years and gives rise to two main experimental campaigns. The first set of tests have been conducted to qualify the HXs of the facilities under operation at the Brasimone Research center while the second campaign aimed to support the design of the HERO (Heavy liquid mEtal pRessurized water cOoled tubes) test section.

The design of the HERO test section is still on-going. At present time the SG bayonet tube unit has been designed, constructed (by CRIOTEC), instrumented and connected to CIRCE (section seven). The secondary loop is under design phase.

Conclusions are finally given in section eight.

.

Ringraziamenti (acknowledgements)

Al termine di questo lungo percorso non privo di ostacoli ma anche portatore di soddisfazioni molte sono le persone che mi hanno di volta in volta sostenuto e che desidero ringraziare.

Partendo dai relatori, il primo ringraziamento va Mariano Tarantino per il sostegno datomi sotto il profilo scientifico, gestionale e umano specie nei momenti più critici di questo percorso.

Ringrazio i miei relatori presso UNIPI Nicola Forgione e Francesco Oriolo per avermi dato l’opportunità di trascorrere oltre tre anni all’interno di un centro sperimentale come il Brasimone. In particolare, ringrazio Nicola per essersi fatto carico di tutte le azioni volte a migliorare il mio status durante la permanenza al Brasimone e per quelle che hanno garantito la stessa anche oltre la durata effettiva della borsa di dottorato.

Ringrazio il mio relatore presso Ansaldo Nucleare Alessandro Alemberti per avermi sempre sostenuto durante tutti gli incontri avuti in questi anni.

Desidero ringraziare Gino Venturi per il lavoro svolto a supporto del design della facility TxP e Pierantonio Gaggini per il lavoro svolto a supporto del design della test section HERO.

Un ringraziamento particolare va ad Alessandro Del Nevo, mio tutor fin dalla tesi di laurea e compagno di lavoro fin da allora che ha attivamente contribuito a questo lavoro tramite gli insegnamenti dati nell’utilizzo del codice RELAP e il proprio sostegno morale.

Ringrazio sentitamente Giuseppe Fasano per l’enorme contributo datomi e senza il quale non sarebbe stato possibile il montaggio e l’esecuzione di tutta la campagna sperimentale su TxP.

Ringrazio tutto il personale dell’edificio PEC e dell’ente.

L’ultimo dei miei ringraziamenti va alla mia famiglia che mi sostiene da ormai oltre trent’anni.

CONTENTS

Abbreviations

ADP	Accordo Di Programma national project
ADS	Accelerator Driven System
ALFRED	Advanced Lead cooled Fast Reactor European Demonstrator
CIRCE	CIRColazione Eutettico facility
CIRTEN	Consorzio Interuniversitario per la Ricerca Tecnologica Nucleare
DHR	Decay Heat Removal system
DICI	Dipartimento di Ingegneria Civile e Industriale
EBR-I	Experimental fast Breeder Reactor – I
EBR-II	Experimental fast Breeder Reactor - II
EC	European Commission
ELFR	European Lead cooled Fast Reactor
ELSY	European Lead cooled SYstem
ENEA	Agenzia nazionale per le nuove tecnologie, l'energia e lo sviluppo economico sostenibile
ETDR	European LFR Technology Demonstrator Reactor
FA	Fuel Assembly
FBR	Fast Breeder Reactors
F/M	Ferritic/Martensitic steel
FR	Fast Reactor
FP	Fission Product
FP-7	7^{th} Framework Programme
GEN-IV	GENeration IV
GFR	Gas cooled Fast Reactor
GIF	Generation IV International Forum
HELENA	HEavy Liquid metal Experimental loop for advanced Nuclear Applications
HERO	Heavy liquid mEtal pRessurized water cOoled tubes
HLM	Heavy Liquid Metals
HNPF	Hallam Nuclear Power Facility
HX	Heat eXchanger
IAEA	International Atomic Energy Agency
ID	Inner Diameter
LBE	Lead Bismuth Eutectic
LEADER	European Advanced DEmonstration Reactor
LFR	Lead cooled Fast Reactor
LMC	Liquid Metal Coolants
LMFR	Liquid Metal cooled Fast Reactors
MHYRRA	Multi-purpose HYbrid Research Reactor
MOX	Mixed OXide (fuel)
MSR	Molten Salt Reactor
Na	Sodium
NACIE	NAtural CIrculation Experiment
NEA	Nuclear Energy Agency
NPP	Nuclear Power Plant
NRC	Nuclear Regulatory Commission
NSC	Nuclear Science Committee

OD	Outer Diameter
OECD	Organization for Economic Co-operation and Development
Pb	Lead
P/D	Pitch to Diameter
R&D	Research and Development
SFR	Sodium cooled Fast Reactor
SG	Steam Generator
SGBT	SG - Bayonet Tube
SGTR	SG – Tube Rupture
SCWR	Super-Critical Water-cooled Reactor
SS	Stainless Steel
TBC	Thermal Barrier Coatings
TH	Thermal Hydraulic
TxP	Tubes for Powder facility
UNIPI	Università di Pisa
VHTR	Very High Temperature Reactor
1-S	Single Step vibrated procedure
2-S	Double Step vibrated procedure

List of figures

List of tables

1 Foreword

1.1 Justification

The Generation IV International Forum (GIF), was chartered in July 2001 to promote the collaborative efforts of the world's leading nuclear technology nations to develop next generation nuclear technology. The main purpose of the initiative was and still remains to set-up innovative nuclear systems, candidate to reach technical and commercial maturity by 2040 [1][2].

Initially, a large number of innovative Generation IV systems was considered. Liquid Metal cooled Fast Reactors (LMFR) are the most promising conceptual solutions. Among the Liquid Metal Coolants (LMC), sodium (Na) has by far the most important cumulated experience both in experimental and industrial nuclear applications. Nevertheless, due to the advantages of these kind of coolants, lead (Pb) or Lead-Bismuth Eutectic (LBE) nuclear systems are proposed in the GIF together with sodium. Choosing LMCs for Fast Reactors (FR) is due to their high heat removal capabilities coupled with low interaction with neutrons.

The Lead cooled Fast Reactors (LFR) [3][4] operates in the fast-neutron spectrum and use a closed fuel cycle for an efficient conversion of fertile uranium. The use of lead as primary coolant is motivated by several advantages, which can be summarized as follow [5][6]:

- The promising nuclear properties, i.e. the low moderation rate.
- The non-existence of exothermic reactions between lead and water or air. This provides favorable conditions for the elimination of the intermediate circuit (typical of past Sodium cooled Fast Breeder Reactors, FBR).
- The high boiling point of lead (1749 °C at 1 bar). It allows to operate the reactor at low primary system pressure reducing the reactor vessel thickness. Furthermore, it eliminates the risk of core voiding due to coolant boiling.
- The high density of lead that favors fuel dispersion phenomena and prevents fuel compaction phenomena in case of core damage. This reduces the likelihood that fuel collects at the reactor vessel bottom in such a way that re-criticalities may occur.
- The high thermal capacity. It allows a significant grace time in case of loss-of-heat-sink accidents.
- The capability to retain FPs as iodine and cesium forming chemical compounds at temperatures up to 600 °C. This reduces the source term to the confinement/containment during accidents in which volatile fission products are released from the fuel matrix.
- The shielding capability against the γ-radiations.

Several Italian research institutions as ENEA, CIRTEN, UNIPI and industries as ANSALDO are involved in the development of LFR and GEN-IV nuclear systems. In particular, since the actual configuration of LFR (and in the general GEN-IV main concepts), deals with the compact pool type reactor in which the steam generators (SG) are located inside the reactor tank, the steam generator design is recognized to play an important role. The present activity aims to support the design of this last component.

1.2 Framework of the activity

The present activity has been conducted in the framework of the Lead-cooled European Advanced DEmonstration Reactor (LEADER) [7][8][9] project and Accordo Di Programma (ADP) national project. LEADER belongs to the 7th EC Framework Programme, FP-7 and started from the results achieved in the previous ELSY[10] (European Lead cooled SYstem) project with the intent to improve the reactor configuration pointed out at the end of ELSY – FP-6.

The main objective of LEADER deals with the conceptual design of a 300 MWth low cost and fully representative scaled down European LFR Technology Demonstrator Reactor (ETDR) named ALFRED (Advanced Lead Fast Reactor European Demonstrator). An additional objective of the project focuses on the development of a new industrial size consistent reactor conceptualization based on ELSY: the 600 MWe European Lead-cooled Fast Reactor (ELFR).

In this framework, a new configuration of Steam Generator (SG) has been proposed for the ETDR plant: the super-heated steam double wall once through bayonet tube type with leakage monitoring. This conceptual design was studied since 60' for Sodium Reactor application [12]. An example of facility that operates with this concept is CIRCE (at ENEA Brasimone) even if it is limited to the heat exchange function [13].

The double wall bayonet tube is constituted by three concentric tubes: in the smallest one, the coolant (i.e. water) enters in down flow and turns in the second concentric tube where it rises up removing the heat from a hot fluid (i.e lead) located into the SG shell side. The largest tube is placed between the second tube and the hot fluid to double separate the coolant from the hot fluid.

There are two primary reasons for this separation. The first is to increase the safety margin of the NPP by reducing the probability of interaction coolant-hot fluid. The second is that this configuration allows the possibility to monitor eventual leakages from the coolant or from the hot fluid by pressurizing the separation region (i.e by helium). On the other hand, since it is required to monitor the leakages (using a low conductivity material as a gas) and get high thermal performance of the unit, the annular space that separates the fluids should be filled with a porous heat transfer enhancer (i.e. powder). Therefore, R&D is mandatory to develop double wall bayonet tube bundle SGs. R&D on this concept has been constantly financed by ENEA as part of its main annual national programme: ADP.

1.3 Objective of the activity

This doctorate is co-financed by ANSALDO and ENEA and is directly connected to LEADER and ADP projects. The activity aims to support the design of the double wall bayonet tube bundle SG with leakage monitoring and to investigate its TH performance both experimentally and analytically.

In order to fulfill these objectives the Tubes for Powder facility has been designed and operated to cope one of the main R&D requirements of this configuration which is the selection of an appropriate porous material that allows leakage monitoring and acceptable TH performance. As sub-objective, TxP has also been operated to qualify three HXs under operation at the Brasimone Research center that adopt double wall tubes with intermediate powder as filler. The main results of these experimental campaigns lead to the design and the construction of a prototypic SG bayonet tube bundle of seven tubes which is retained a representative scaled down (in power) model of the

ALFRED SG. The activity started in 2011 [14] and is still ongoing. At present time the following objectives are reached:

- Assessment of the TH performance of the bayonet tube by means of RELAP-5.
- Design, construction, operation and disposal of the TxP (Tubes for Powders) facility devoted to powders conductivity measurement into an annular geometry. Its aim was to qualify the conductivity of powders for their application in the annular gap between the tubes that separate the fluids both for application as heat transfer enhancer (as for the ALFRED SG) and to accommodate a give temperature drop (as for the NACIE-UP HX).
- Design and commissioning of the HERO (Heavy liquid mEtal pRessurized water cOoled tubes) test section based on the results achieved during the experimental campaigns on TxP. This test section is actually located in CIRCE and aims to investigate the TH behavior of a bundle of 7 tubes that represent, as much as possible, the ALFRED SG tubes (1:1 in length).

1.4 Structure of the thesis

Eight main sections and four attached appendixes constitute the structure of the work.

The first three sections have to be intended as introduction to the activity. Justification of the activity, framework and objective are given in this section. GEN-IV systems and LEADER project are briefly described in section 2. The third section presents the ALFRED SG. It includes also the historical development of double wall SG in the nuclear technology and a brief description of the HXs that have been operated or are under construction at ENEA CR Brasimone that make use of double wall concept.

The fourth and fifth sections are theoretical activities conducted in support to the R&D of the steam generator bayonet tube. In particular, section four is aimed to assess the TH performance of a single tube of the ALFRED SG fixing, in a theoretical way (which is described in section five) some modeling issues still not defined in the ALFRED design (i.e. the powder material to be introduced between the double wall and its modeling). Section five aims to point out empirical models to treat the conductivity of powder media and to individuate candidate materials to be acquired and tested with the intent to design a double wall bayonet tube bundle test section. This last section includes an investigation of insulating materials for their application between the feed-water tube and the annular riser.

Section six constitutes the core of this activity and has to be intended as a first step on R&D in support to the design of the bayonet tube steam generator with particular reference to the heat transfer enhancer porous medium placed between the double wall. The Tubes for Powders (TxP) facility has been designed (by ENEA), constructed (by LIMAINOX), instrumented (by ENEA) and operated to test the conductivity of powders both under un-pressurized air environment and under pressurized helium atmosphere. This process takes more than two years and gives rise to two main experimental campaigns. The first set of tests have been conducted to qualify the HXs of the facilities under operation at the Brasimone Research center while the second campaign aimed to support the design of the HERO (Heavy liquid mEtal pRessurized water cOoled tubes) test section which is a 1:1 hexagonal wrapped tube bundle that represents the ALFRED SG.

The design of the HERO test section is still on-going. At present time the SG bayonet tube unit has been designed, constructed (by CRIOTEC), instrumented and connected to CIRCE (section seven). The secondary loop is under design phase.

Conclusions are finally given in section eight.

Appendix A reports the RELAP-5 input deck developed to assess the single bayonet tube as designed for the ALFRED-SG. Appendix B includes the constructive design of the TxP facility. Appendix C reports the granular-metric measurements performed by FN on AISI-316 powder. Appendix D contains the constructive design of the HERO-CIRCE SGBT test section.

2 Introduction

2.1 GEN-IV systems with focus on LMC

Nuclear power technology has evolved through three main generations of system designs.

- A first generation of prototypes implemented during the period 1950 to 1970.
- A second generation of industrial power plants built from 1970 to the turn of the century, most of which are still in operation today.
- A third generation, usually called Generation III/III+, of evolutionary advanced reactors which incorporate technical progress based on lessons learnt through more twelve thousand reactor-years of operation.

The Generation IV International Forum (GIF), was chartered in July 2001 to promote the collaborative efforts of the world's leading nuclear technology nations to develop next generation nuclear energy systems. The main purpose of the initiative is to set-up innovative nuclear systems, candidate to reach technical and commercial maturity by 2040 [1][2].

The Generation IV project is guided by a technology roadmap that identifies Research and Development (R&D) pathways for the most promising technologies [15]. The roadmap defines R&D objectives, activities, sequencing of tasks, cost estimates and opportunities for national and international cooperation for selected nuclear energy systems.

On the basis of specific GEN-IV requirements, the GIF identified six most promising reactor systems and fuel cycle concepts:

- VHTR: Very High Temperature Reactor.
- SFR: Sodium cooled Fast Reactor.
- SCWR: Super-Critical Water-cooled Reactor.
- GFR: Gas-cooled Fast Reactor.
- LFR: Lead cooled Fast Reactor.
- MSR: Molten Salt Reactor.

The appropriate choice of the primary coolant is of great significance for achieving high Fast Reactor (FR) performances. This determines also the main design approaches of FR and the technical and economical characteristics of the Nuclear Power Plant (NPP). Liquid Metal cooled Fast Reactors (LMFR) are the most promising conceptual solutions proposed in GEN-IV. Choosing Liquid Metal Coolants (LMC) for FR is due to their high heat removal capabilities coupled with low interaction with neutrons.

Among the liquid metal coolants, it is sodium that has gained the widest acceptance and is indicated as main GEN-IV concept in Europe, this is because it has the largest cumulated reactor experience. In fact, this coolant has been chosen for Fast Breeder Reactor (FBR) because of its good thermal and physical properties. Sodium offers the possibility to achieve high specific power densities in the core and thus the shortest doubling time. This was the world-wide strategic line of FBR development in the 1960s, and is still continuing in some countries at present. Industrial experience has been already gained with sodium cooled fast reactor operation. Sodium is practically non-

corrosive to stainless steel. Nevertheless, the use of sodium as a coolant poses fire danger in case of its leakage and interaction with air or water. Operating experience testifies the possibility of coping with the mentioned problem, but the quest for excellence calls for future improvement in LMFRs technology.

The changing of the strategic line (from breeding to non-proliferation resistance), the delaying of massive FRs commercial introduction and some drawbacks of sodium technology related in some demonstration LMFRs have given the rise to the question to reverse the trend of the last 20 years, which focused FR Research and Development (R&D) on SFR option. There is an opportunity to investigate alternative technical solutions. The objective is to obtain complete knowledge of their characteristics allowing to make, when the time has come, the best choice. Among these alternative solutions, Heavy Liquid Metals (HLM) were proposed and investigated as coolants for fast reactors, and mainly lead (Pb) and lead-bismuth eutectic (LBE) are considered at present as potential candidates for the new generation fast reactors and Accelerated Driven Systems (ADS) [6][15].

The lead content in the earth's crust is about 4 10^{-3} wt.%. Lead is a heavy, soft and ductile metal which falls into subgroup 4 of Period VI in the periodic system of elements. The atomic number of lead is 82, atomic mass is 207.19 and atomic volume 18.27 10^{-6} m^3/mole. Its atomic radius in the metallic form is 0.175 nm. Lead is found in more than 200 minerals: galenite PbS, anglesite $PbSO_4$ and cerussite $PbCO_3$ are of industrial importance. Lead has four stable isotopes, namely: 204, 206, 207 and 208. The last three are the products of U, Ac and Th decay.

The bismuth content in the earth's crust is about 2 10^{-5} wt.%. Bismuth deposits are few and far between, its recovering from the bismuth bearing ores is a very complicated multistage process.

The Lead cooled Fast Reactor (LFR) [4] operates in the fast-neutron spectrum and use a closed fuel cycle for an efficient conversion of fertile uranium. The use of lead as primary coolant is motivated by several advantages, which can be summarized as follow:

- The good nuclear properties, i.e. the low moderation rate.
- The non-existence of exothermic reactions between lead and water or air. This provides favorable conditions for the elimination of the intermediate circuit (typical of past Sodium cooled Fast Reactors), which reduces the overall footprint and the cost of the plant.
- The high boiling point of lead (1749 °C at 1 bar) makes it possible to operate the reactor at low primary system pressure, which allows reduced reactor vessel thickness. Furthermore, it eliminates the risk of core voiding due to coolant boiling.
- The high density of lead favors fuel dispersion phenomena and prevents fuel compaction phenomena in case of core damage. This reduces the likelihood that fuel collects within the primary system, especially at the reactor vessel bottom in such a way that re-criticalities may occur.
- The high thermal capacity allows a significant grace time in case of loss-of-heat-sink accidents.
- Lead appears to form compounds with iodine and cesium at temperatures up to 600 °C. This reduces the source term to the confinement/containment during accidents in which volatile fission products are released from the fuel matrix.
- Lead shields γ-rays effectively.

Nevertheless, the molten is not free from drawbacks. In fact, lead is a heavy metal and its chemical properties imply corrosion and erosion problems with the structural materials. To partially mitigate them it is mandatory to work at relatively low temperatures compared to the other GEN-IV reactors. Moreover, lead solidification may occur due to the high melting temperature (327 °C).

LBE was chosen in the past as the coolant for a number of alpha class submarine reactors in the former Soviet Union, which led to extensive R&D on the coolant technology and the materials. LBE has been considered as coolant for fast reactors, in particular it is expected to be used in most of ADS systems, mainly due to its low melting temperature of 124 °C (resulting in lower corrosion rates and in easier maintenance) and its low volume increase upon melting. However, several limitations are related to LBE. Upon neutron radiation, bismuth-209, forms the alpha emitter polonium-21 which poses potential radiological hazard.

The main thermo-physical properties of Sodium, Lead and LBE are summarized in *Tab. 1*, nuclear properties are also included. Detailed thermo-physical properties and TH recommended correlations applicable to molten lead and molten LBE are reported in *Tab. 2* and *Tab. 3* respectively. The tables report an indication of the accuracy of each correlation [5].

Properties (at 0.1 MPa)	Na	Pb	LBE (44.5% Pb; 55.5% Bi)
Atomic number	11	82	--
Atomic mass	22.99	207.2	--
Macroscopic capture cross-section relative to sodium (Calculated for spectrum specific to each reactor type)	1	6	
Moderating power	0.0078	0.0024	
Moderating Ratio	19	370	
Relative moderating power [/]	1.80	1	0.82
Neutron Absorption cross-section (1 MeV) [m-barn]	0.230	6.001	1.492
Neutron Scattering cross-section [barn]	3.2	6.4	6.9
Melting temperature [°C]	98	327.4	125
Boiling temperature [°C]	883	1745	1670
Heat of melting [kJ/kg]	114.8	24.7	38.8
Heat of vaporization [kJ/kg]	3871	856.8	852
Density [kg/m^3] at 20 °C (solid)	966	11340	10474
Density [kg/m^3] at 450 °C (liquid)	845	10520	10150
Heat capacity [kJ/kg K] at 20 °C (solid)	1.230	0.127	0.128
Heat capacity [kJ/kg K] at 450 °C (liquid)	1.269	147.3	146
Thermal conductivity [W/m K] at 20 °C (solid)	130	35	12.6
Thermal conductivity [W/m K]at 450 °C (liquid)	68.8	17.1	14.2
Kinematic viscosity [m^2/s] at 450 °C (liquid)	$3\ 10^{-7}$	$1.9\ 10^{-7}$	$1.4\ 10^{-7}$
Prandtl number at 450 °C (liquid)	0.0048	0.0174	0.0147
Thermal Expansion Coefficient (%V/K) at 450°C	0.029	0.011	
Surface tension [mN/m] at 450 °C (liquid)	163	480	392
Volume change with melting [%]	+2.65	+3.6	+0.5

Tab. 1 - Basic characteristics of LMFR coolants.

Properties [0.1 MPa]	SI unit	Correlation	Temp. range (K)	Estimated error
Melting temperature	K	$T_{melt} = 600.6$	--	0.1 K
Latent heat of melting	kJ kg^{-1}	$Q_{melt} = 23.8$	--	0.7 kJ kg^{-1}
Boiling temperature	K	$T_{boil} = 2016$	--	10 K
Latent heat of boiling	kJ kg^{-1}	$Q_{boil} = 858.2$	--	1.9 kJ kg^{-1}
Saturated vapor press.	Pa	$P_s = 6.5715\times10^{9}$ _exp$^{(-22247/T)}$	610-2016	15%
Surface tension	N m^{-1}	$\sigma = 0.519 - 1.13 \times 10^{-4} T$	601-1200	5%
Density	kg m^{-3}	$\rho = 11367 - 1.1944 T$	601-1900	0.7%
Sound velocity	m s^{-1}	$u_s = 1951.75 - 0.3423 T + 7.635 \times 10^{-5} T^2$	601-2000	0.05% ?
Bulk modulus	Pa	$Bs = (42.15 - 1.652 \times 10^{-2} T + 3.273 \times 10^{-6} T^2) \times 10^9$	601-2000	--
Isobaric specific heat	Jkg^{-1}K^{-1}	$cp = 175.1 - 4.961\times10^{-2} T + 1.985\times10^{-6} T^2 - 2.099 \times 10^{-9} T^3 - 1.524 \times 10^{6} T^{-2}$	601-1300	7% ?
Dynamic viscosity	Pa s	$\eta = 4.55 \times 10^{-4} \exp^{(1069/T)}$	601-1470	4%
Electric resistivity	Ω m	$r = (66.6 + 0.0479 T) \times 10^{-8}$	601-1300	1%
Thermal conductivity	Wm^{-1}K^{-1}	$\lambda = 9.2 + 0.011 T$	601-1300	10% ?

Tab. 2 - Basic properties of molten lead.

Properties [0.1 MPa]	SI unit	Correlation	Temp. range [K]	Estimated error
Melting temperature	K	$T_{melt} = 397.7$	--	0.6 K
Latent heat of melting	kJ kg^{-1}	$Q_{melt} = 38.6$	--	0.2 kJ kg^{-1}
Boiling temperature	K	$T_{boil} = 1943$	--	10 K
Latent heat of boiling	kJ kg^{-1}	$Q_{boil} = 854$	--	2 kJ kg^{-1}
Saturated vapor press.	Pa	$P_s = 11.1\times10^{9}$ _exp$^{(-22552/T)}$	508-1943	50%
Surface tension	N m^{-1}	$\sigma = (437.1 - 0.066 T) \times 10^{-3}$	423-1400	5%
Density	kg m^{-3}	$\rho = 11096 - 1.3236 T$	403-1300	0.8%
Sound velocity	m s^{-1}	$u_s = 1773 + 0.1049 T - 2.873 \times 10^{-4} T^2$	403-1300	--
Bulk modulus	Pa	$Bs = (35.18 - 1.541 \times 10^{-3} T - 9.191 \times 10^{-6} T^2) 10^9$	430-605	0.05%
Isobaric specific heat	Jkg^{-1}K^{-1}	$cp = 159 - 2.72 \times 10^{-2} T + 7.12 \times 10^{-6} T^2$	430-605	7% ?
Dynamic viscosity	Pa s	$\eta = 4.94 \times 10^{-4} \exp^{(754.1/T)}$	400-1100	5%
Electric resistivity	Ω m	$r = (86.334 + 0.0511 T) 10^{-8}$	403-1100	6%
Thermal conductivity	Wm^{-1}K^{-1}	$\lambda = 3.61 + 1.517 \times 10^{-2} T - 1.741 \times 10^{-6} T^2$	403-1100	5% ?

Tab. 3 - Basic properties of molten LBE.

2.2 The LEADER Project

The European project LEADER [7][8][9] (Lead-cooled European Advanced DEmonstration Reactor, 2010-2013) started from the results achieved in the ELSY Project [10][17] (2006 to 2010) with a deep analysis of the hard points of the reactor configuration. The objective of ELSY was to design a system that complies with all Generation IV goals and which gives assurance of investment protection. In particular, the main purposes of the project can be summarized as follows:

- Demonstration of the technical feasibility of the LFR concept (possibility to design an economically competitive and safe lead-cooled fast reactor adopting innovative and simple engineering features).
- Demonstration of the capability to fully comply with Generation IV goals.

The main goal of LEADER was to design a low cost and fully representative scaled down demonstrator of the LFR technology (European LFR Technology Demonstrator Reactor – ETDR) named ALFRED (Advanced Lead Fast Reactor European Demonstrator). The project aimed also to achieve a conceptual design of an industrial size LFR plant (the 600 MWe European Lead-cooled Fast Reactor – ELFR).

The configuration pointed out in the ELSY project has been investigated and modified to meet ETDR (ALFRED) and ELFR constrains and to reach a new consistent reactor configuration by improving plant safety and efficiency [3][18][19] the main features are listed in *Tab. 4*.

The overview of the ALFRED and ELFR primary pool configuration is reported in *Fig. 1* and *Fig. 2*. The indicated dimensions are considered preliminary.

The structural materials preliminary fixed are presented in *Tab. 5*. The main difference between the two concepts is represented by the cladding material. The 15-15 Ti is selected in the ALFRED design mainly because of nuclear qualification feasibility in the short term. At present time, T91 cannot be licensed because of several reasons: the most important is the lack in irradiation experience on T91 fueled rods. The wrapper material remains T91. Nevertheless, must be mentioned that data on T91 welded joint irradiation is still missing therefore, a possible alternative solution may be F/M steel named EM10.

Hexagonal, wrapped with spacer grid element has been selected in both the reactors. This allows to monitoring the outlet temperature and to reveal clad failure for each FA. The FA extends up to the cover gas space with an upper grid positioned in the cover gas. The upper grid coupled with a preloaded spring and a ballast acts against the lead buoyancy and maintain the FA in the correct position. The FA is not floating in lead, a lower grid had introduced to fix it. The control/shut down rod mechanisms are those of MHYRRA [20]. ALFRED core relies on proven MOX fuel. The maximum enrichment (30%), the active height (600 mm), and the rod geometry (rod OD 10.5mm, pellet OD 8 mm and gap width of 150 μm) have been definitively fixed. Preliminary calculations pointed out that two enriched core radial zones pursuit a good flux radial flattening [21],[22]. The core is composed of 171 FAs, 4 Control Rods, 12 Safety Rods and 108 Dummy Elements. Only the maximum enrichment (30%), the active height (600 mm), and the inner diameter of the annular pellets (2 mm) have been definitively fixed up to now. Preliminary calculations pointed out that two enriched radial zones pursuits a good flux radial flattering. It is composed of 171 FAs, 4 Control Rods 12 Safety Rods and 108 Dummy Elements. The ELFR core is presently the same analyzed in the ELSY project for the hexagonal FA solution. The cores are depicted in *Fig. 3* the FA preliminary design is shown in *Fig. 4* and *Fig. 5*.

The reactor vessel and the cylindrical inner vessel are given in *Fig. 6* and *Fig. 7*. The main innovations are represented by the two grids (*Fig. 7*). The dimensions are not reported.

Several systems for the Decay Heat Removal (DHR) function have been conceived and designed for ALFRED. One non safety-grade system, the secondary system, is used for the normal decay heat

removal following the reactor shutdown. Two independent, high reliable and redundant safety-related Decay Heat Removal systems (DHR N1 and DHR N2) are provided, *Fig. 8*. In case of unavailability of the secondary system, the DHR N1 system is called upon and in the unlike event of unavailability of the first two systems the DHR N2 starts to evacuate the decay heat. DHR N1 is an improvement of the ELSY DHR (the improvement consists in passive activation of the system) and it relies on the Isolation Condenser system connected to four out of eight SGs [3]. DHR N2 relies on an Isolation Condenser system connected to remaining four SGs. The final configuration of DHR-2 could be changed because system diversification cannot be demonstrated (both the systems are based on the same physical principle) [3].

A detailed description of the ALFRED steam generators system is included in section 3.2.

Item	ELSY	ELFR	ALFRED
Electrical Power	600 MWe	600 MWe	120 MWe
Primary Coolant	Pure Lead	Pure Lead	Pure Lead
Primary System	Pool type, Compact	Pool type, Compact	Pool type, Compact
Max. Lead velocity	2 m/s	2 m/s	2 m/s
Core Inlet T.	400 °C	400 °C	400 °C
SG Inlet T.	480 °C	480 °C	480 °C
Secondary Coolant	Water-S-Steam	Water-S-Steam	Water-S-Steam
Feed-water T.	335 °C	335 °C	335 °C
Steam Pressure	18 MPa	18 MPa	18 MPa
Plant efficiency	~ 43 %	~ 43 %	~ 40 %
Reactor vessel	Austenitic SS, Hung	Austenitic SS, Hung	Austenitic SS, Hung
Safety Vessel	Anchored to reactor pit	Anchored to reactor pit	Anchored to reactor pit
Inner Vessel (Core Barrel)	Cylindrical, Removable	Cylindrical, Integral with the core support grid, Removable	Cylindrical, Integral with the core support grid, Removable
Steam generators	Plane-Spiral type, Integrated in the reactor vessel, Removable	ELSY Spiral type or alternate solution (i.e. double walls bayonet type)	Bayonet type with double walls, Integrated in the reactor vessel, Removable
Primary pumps	Mechanical pumps in the hot collector, Removable	Mechanical pumps in the hot collector, Removable	Mechanical pumps in the hot collector, Removable
Max. Structural material dpa	2 dpa	2 dpa	2 dpa
Fuel Assembly	Open (wrapper-less), Square	Closed (with wrapper), Hexagonal, Weighed down when primary pumps are off, Forced in position by springs when primary pumps are on	Closed (with wrapper), Hexagonal, Weighed down when primary pumps are off, Forced in position by springs when primary pumps are on
Fuel type	MOX (max Pu en. 20%)	MOX	MOX (max Pu enrich. 30%)
Max. burn-up	100 MWd/kg-HM	100 MWd/kg-HM	between 90-100 MWd/kg-HM
Fuel resident time	5 y	5 y	5 y
Fuel Clad Material	T91 (coated)	T91 (coated)	15-15 Ti (possibility of coating)
Max. Clad Neutron Damage	100 dpa	100 dpa	100 dpa
Max. Clad T.	550 °C	550 °C	550 °C
Max. core Δp	0.1 MPa	0.1 MPa	0.1 MPa
Control/Shutdown System	3 Independent systems moving in empty (Argon) box beams of each FA	2 diverse and redundant systems of the same concept derived from CDT	2 diverse and redundant systems of the same concept derived from CDT
1st System for Shutdown	8 Massive Conventional Absorber Rods	Pneumatic Inserted Absorber Rods: passively inserted by (by depressurization) from the core top.	Pneumatic Inserted Absorber Rods: passively inserted by (by depressurization) from the core top.
2ndSystem Control/Shutdown	32 Finger Absorbers Rod passively inserted by gravity (only shut-down)	Buoyancy Absorbers Rods: passively inserted by buoyancy from the core bottom.	Buoyancy Absorbers Rods: passively inserted by buoyancy from the core bottom.
3rd System Control/Shutdown	38 FARs motorized	Not any	Not any
Refueling System	No refueling machine stored inside the RV	No refueling machine stored inside the Reactor Vessel	No refueling machine stored inside the Reactor Vessel
DHR	2 diverse and redundant systems (DHR1 & DHR2) + 1 complementary system (RVACS)	2 diverse and redundant systems (actively actuated, passively operated). No RVACS	2 diverse and redundant systems (actively actuated, passively operated). No RVACS
DHR1	4 independent loops, immersed in the lead pool. Passively operated	Alternate solution to ELSY W-DHR should be exploited	Under investigation (I.e. 4 IC connected to the 4 remaining SG: 1/4 redundancy
DHR2	Isolation Condenser connected to the SG: 4 units provided on 4/8 SGs	Isolation Condenser connected to the SG: 4 units provided on 4/8 SGs	Isolation Condenser connected to the SG: 4 units provided on 4/8 SGs
Seismic Dumping Devices	2D isolator below reactor building	2D isolator below reactor building	2D isolator below reactor building

Tab. 4 - LEADER Project, ALFRED and ELFR updated configurations (compared to ELSY).

Components	ALFRED	ELFR
Reactor Vessel, Cover and Support	AISI316L	AISI316L
Safety Vessel (Cavity Liner)	AISI316L	AISI316L
Inner Vessel	AISI316LN	AISI316LN
Core Lower and Upper Grids	AISI316LN	AISI316LN
SG	T91	T91
Primary Pump Duct and Shaft	AISI316LN	AISI316LN
Primary Pump Impeller	To Be Defined (MAXTAL)	To Be Defined (MAXTAL)
Deep Cooler	--	AISI316LN
Cladding	15-15 Ti (coated?)	T91 (coated)
FA grids	15-15 Ti	T91
Wrapper	T91 (?)	T91

Tab. 5 - LEADER Project, ALFRED and ELFR structural materials.

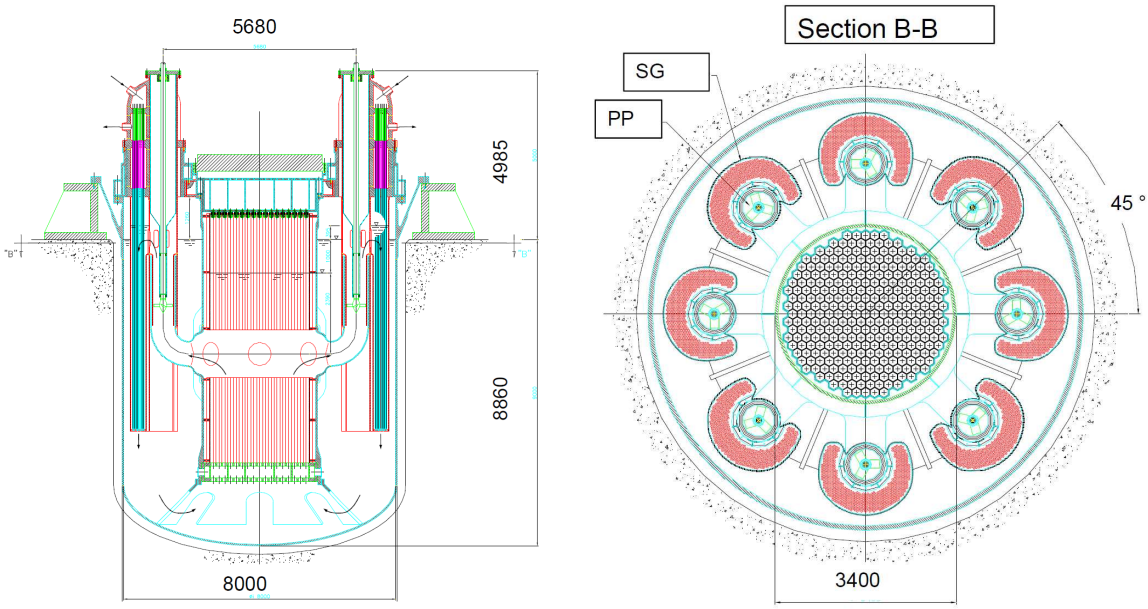

Fig. 1 – LEADER Project, ALFRED: preliminary lay-out of the primary pool.

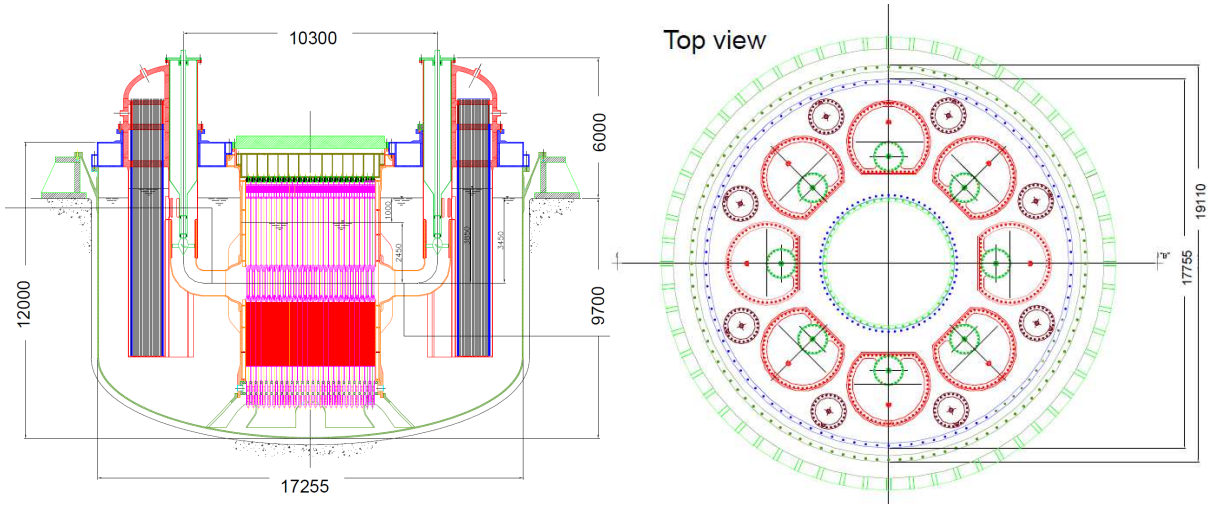

Fig. 2 – LEADER Project, ELFR: preliminary lay-out of the primary pool.

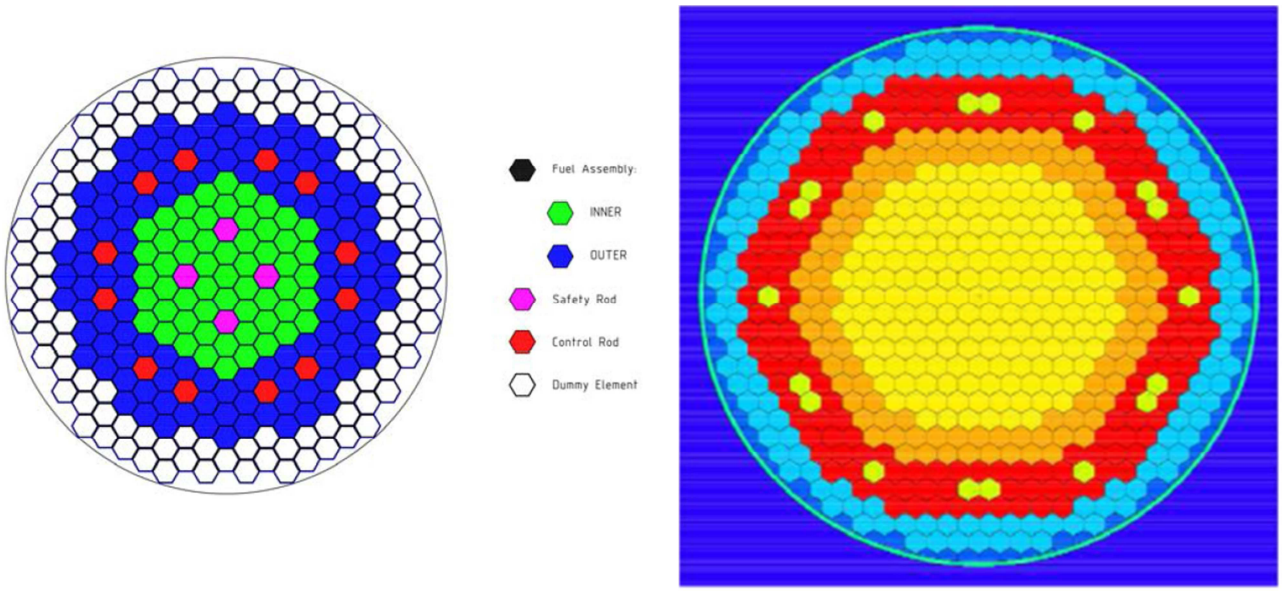

(a) ALFRED (b) ELFR

Fig. 3 – LEADER Project, ALFRED and ELFR core horizontal section.

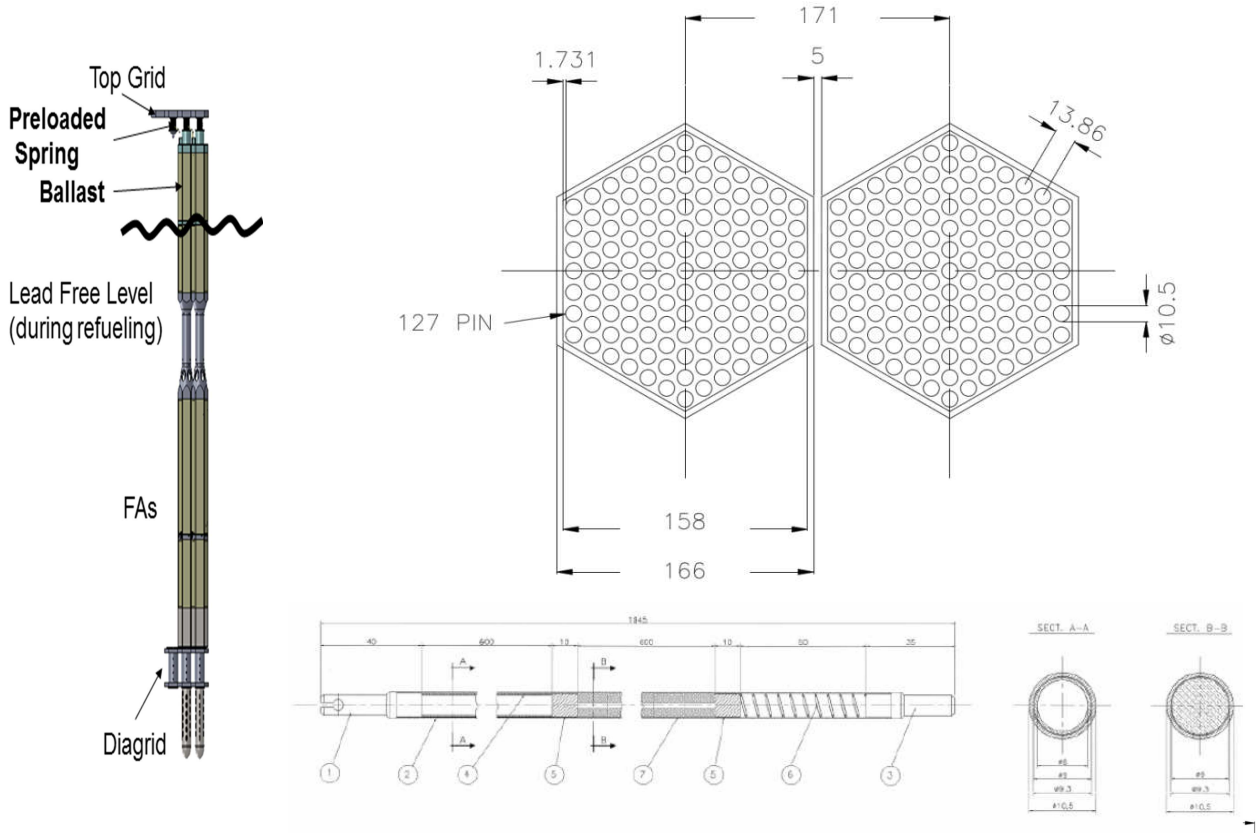

Fig. 4 – LEADER Project, ALFRED: preliminary lay-out of the FA.

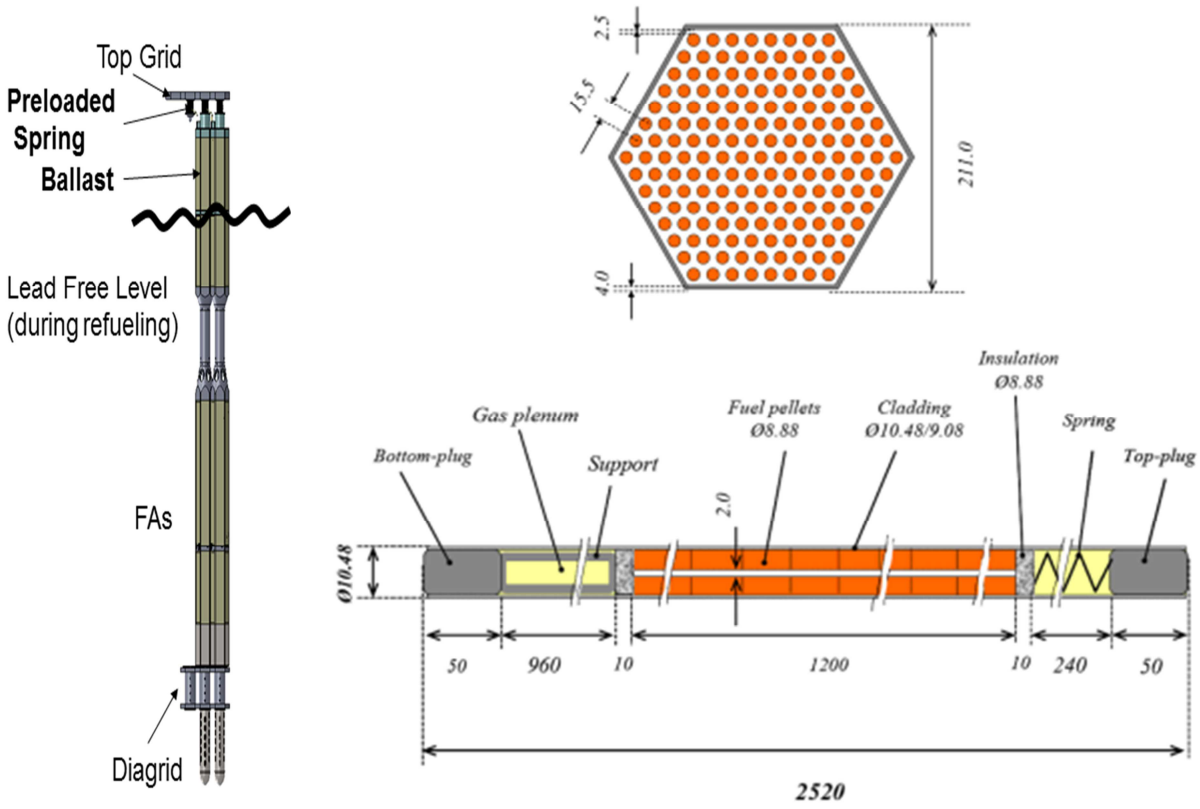

Fig. 5 – LEADER Project, ELFR: preliminary lay-out of the FA.

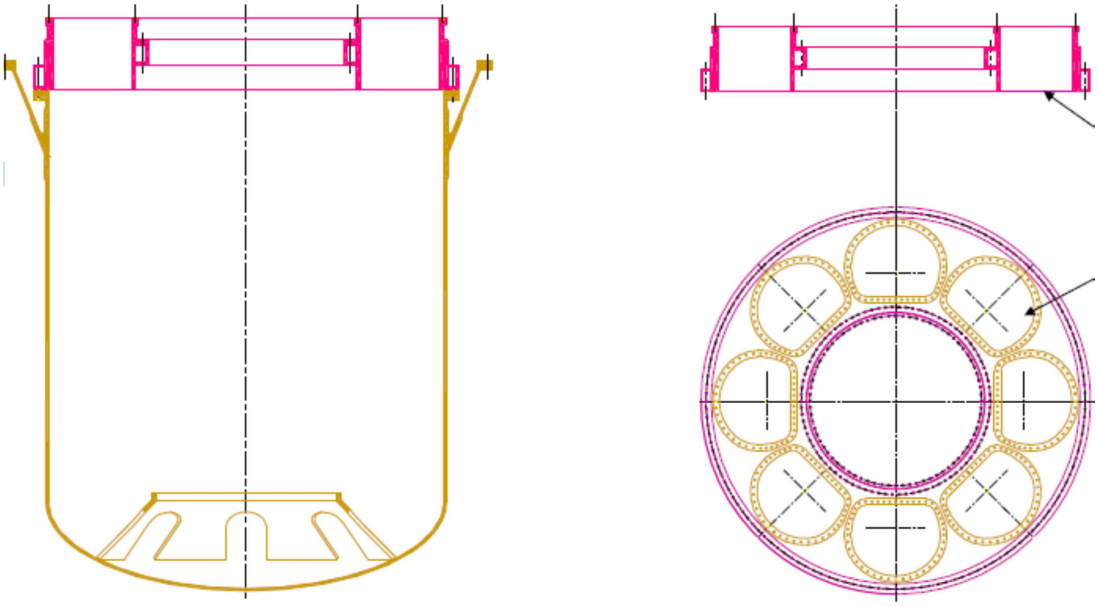

Fig. 6 – LEADER Project, ALFRED/ELFR: reactor vessel and cover.

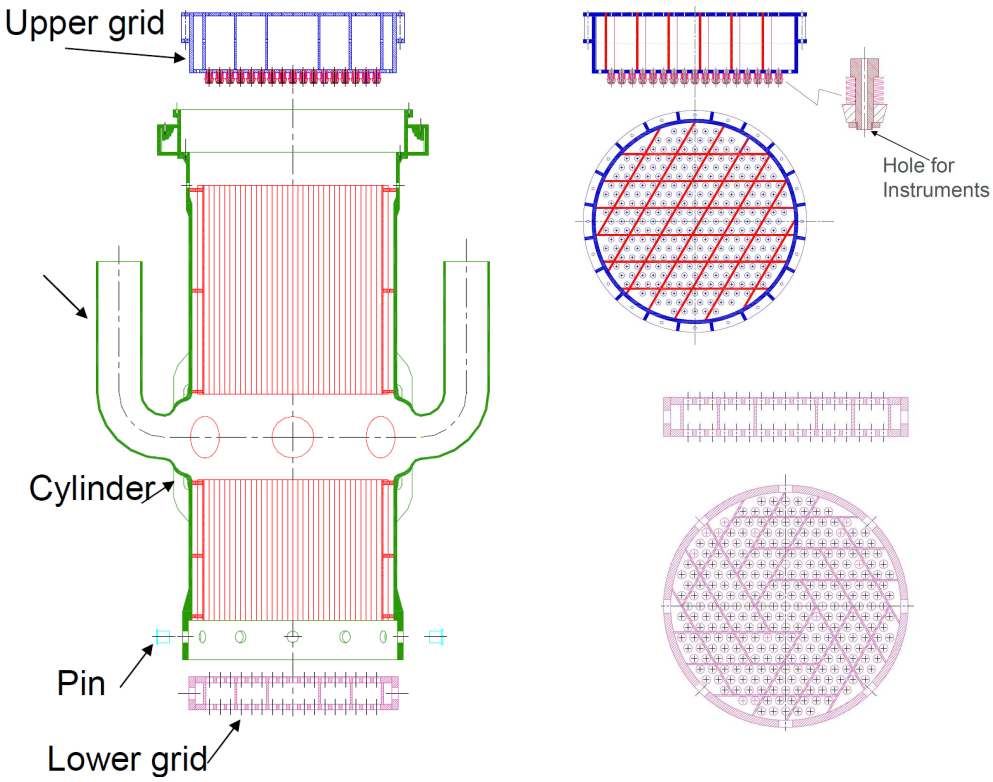

Fig. 7 – LEADER Project, ALFRED/ELFR: cylindrical inner vessel and grids.

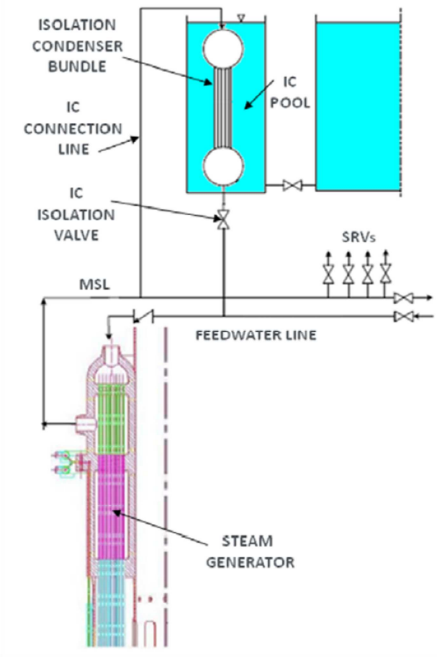

Fig. 8 – LEADER Project, ALFRED DHR schematic view.

3 DOUBLE WALL TUBE SG – HXs

The double wall tube bundle heat exchanger is usually constituted by two (in this case it is generally straight tube type) or three (called double wall bayonet) concentric tubes. It is based on the concept to provide a double physical separation between two fluids: the coolant (i.e. water) and the hot fluid (i.e. lead). There are two primary reasons for the separation of the fluids.

- The first is to maintain a given temperature drop between the hot fluid and the coolant. In this case one has to speak about HX since the main function of the unit is to accommodate an high temperature drop between the fluids avoiding stresses due to thermal shocks.
- The second is to increase the safety margin of the unit by reducing the probability of interaction between the coolant and the hot fluid. Furthermore, this configuration allows the possibility to monitor eventual leakages from the coolant or from the hot fluid by pressurizing the annular region between the double wall.

The main drawback of double wall tube bundle heat exchanger with leakage monitoring stays in its economic feasibility when it is necessary to achieve high TH performance of the unit, as in the case of a SG. In fact, the presence of a second tube and the presence of an annular space filled with a low conductivity material (as a gas), makes this unit more expensive and more bulky compared to the single wall tube. Therefore, the annular space that separates the fluids should be filled with a porous heat transfer enhancer (i.e. sintetic diamond powder, stainless steel-SS powder) in order to preserve both leakage monitor-ability and appropriate thermal performance into an economically acceptable geometry.

Several applications of double wall HXs have been experienced at ENEA CR Brasimone.

- NACIE and its updated version NACIE-UP [27], HELENA and CIRCE-HERO are facilities/test sections whose HX is based on double wall tubes and make use of SS powder (AISI-304 or AISI-316) located into the annular region that separates the fluids to provide a temperature drop or to accommodate leakage monitoring and heat transfer enhancement.
- CIRCE-ICE [13] test section has a double wall bayonet tube HX with annular region filled by helium (to accommodate a temperature drop).

Excepts CIRCE-HERO, these HXs are designed to remove the generated power without steam production, therefore the double wall concept is applied to accommodate a temperature drop. Their main features are given in *Tab. 6*.

In particular, NACIE and CIRCE-ICE have been extensively operated, NACIE-UP and HELENA are prone for the first start up and CIRCE-HERO is under construction, it is described in section 7.

Main features					
Description	**NACIE-HX**	**NACIE-UP-HX**	**HELENA-HX**	**CIRCE-HERO-HX**	**CIRCE-ICE-HX**
HX type/ Test section	Double wall straight	Double wall straight	Double wall straight	Double wall bayonet	Double wall bayonet
N° of tubes	1	7	7	7	91
Power	30 kW	250 kW	250 kW	500 kW	925 kW
Coolant	Water, HX shell	Water, HX shell	Water, HX shell	Water-steam, HX tubes	Water-steam, HX tubes
Max coolant T.	100	200°C	310	410°C	100°C
Coolant p	1 bar	16 bar	100 bar	172 bar	1 bar
Fluid	Pb / LBE HX tubes	Pb / LBE HX tubes	Pb HX tubes	LBE HX shell	LBE HX shell
Max fluid temp.	480°C	480°C	500°C	480°C	480°C
HLM p	Hydraulic head	Hydraulic head	Hydraulic head	Hydraulic head	Hydraulic head
Double wall tubes features					
Description	**NACIE-HX**	**NACIE-UP-HX**	**HELENA-HX**	**CIRCE-HERO-HX**	**CIRCE-ICE-HX**
Filling powder	AISI 304	AISI 316	AISI 316	AISI 316	None
Filling gas	Air	Air	Air	He 4bar	He 4 bar
Inner tube OD	73.03mm	73.03mm	73.03mm	25.40mm	19.05mm
Outer tube OD	88.90mm	88.90mm	88.90mm	33.40mm	25.40mm
Gap size	5.80mm	5.80mm	2.50mm	0.62mm	1.06mm

Tab. 6 - Main features of the double wall HXs located at ENEA Brasimone.

3.1 Historical development of SG with double wall tubes

Past FR experience was mainly concentrated on loop type (and few pool type) Sodium cooled FBR with Intermediate Heat eXchanger (IHX) to avoid direct interaction between water and primary coolant. In general, their SGs are once-through type with single wall, *Tab. 7*. Double wall straight tubes were adopted only in two reactors: EBR-I (4 MWth) and EBR-II (62.5MWth) [23]. The operation of FBRs indicated that a major cause of unreliability associated with such systems is the possibility of a sodium-water reaction being therefore the SG design a main issue that impacts the efficient operation of these type of NPPs. Should such reaction occur, as a result of leakage at the sodium/ water interface, the unit could be damaged significantly and lead to the plant being shut down for repairs.

It is clear that Steam Generator employing single walled heat transfer tubes represents the most economical capital cost design (and the main concept that has been experienced up to now). However, the use of double walled or so called "duplex" tubes proved to be more economical in terms of overall plant life cost since initial fabrication costs could be more than offset by less operational downtime due to leakage and removal of sodium/water reaction products and steam dump systems. These considerations had been strongly substantiated by the double walled Experimental Breeder Reactor-II (EBR-II) steam generators which have accumulated almost several years of operating experience unhampered by shutdowns due to tube leakage [12]. In addition, a double walled unit is inherently safer than a single walled unit. These reasons promoted the

investigation of duplex tube steam generators for SFR application during 60' and 70' in several research US centers.

Due to the presence of the IHX, double wall bayonet tube SG has never been used in experimental reactors. However, it is the logical development of a Duplex SG directly located inside the reactor pool without IHX as in the case of LFR. This innovative concept is further improved with the introduction of leakage monitor-ability.

Reactor	Classification	Thermal power	SG type	Operation
RAPSODIE (France)	Exp. reactor	40 MWth	No SG	1967 - 1983
KNK-II (Germany)	Exp. reactor	58 MWth	Once-through evaporator, twin tubes	1971 - 1991
FBTR (India)	Exp. reactor	40 MWth	Once through; triple S shaped tubes	1985 -
PEC (Italy)	Exp. reactor	120 MWth	No SG	Never operated
JOYO (Japan)	Exp. reactor	140 MWth	No SG	1977 -
DFR (UK)	Exp. reactor	60 MWth	Parallel tubes in copper heat transfer block	1959 - 1977
BOR-60 (Russia)	Exp. reactor	55 MWth	7 types of once through SGs	1968 -
EBR-I (USA)	Exp. reactor	4 MWth	**Once through; straight double wall tubes**	1951 - 1970
EBR-II (USA)	Exp. reactor	62.5 MWth	**Once through; straight double wall tubes**	1964 - 1994
FFTF (USA)	Exp. reactor	200 MWth	No SG	1980 - 1996
BR-10 (Russia)	Exp. reactor	8 MWth	No SG	1958 - 2003
CEFR (China)	Exp. reactor	65 MWth	Once through; straight tubes, evaporator and super-heater	2011 -
Phenix (France)	DEMO	350 MWth	Once-through, vertical bank of large S-shaped tubes, each containing small pipes for water	1973 - 2010
SNR-300 (Germany)	DEMO	762 MWth	Once-through evaporator and separate super-heater, tubes straight in 2 loops, helical in 3rd	Never operated
MONJU (Japan)	DEMO	714 MWth	Once-through evaporator and separate super-heater; helical coiled; intermediate coolant on shell side	1994 - ?
PFR (UK)	DEMO	650 MWth	Forced recirculation evaporator and drum separate super-heater; separate re-heater	1974 - 1994
BN-350 (Kazakhstan)	DEMO	750 MWth	Shell and tubes, Fild's tubes in evaporator, U-tubes in super-heater	1972 - 1999
BN-600 (Russia)	DEMO	1470 MWth	Shell and straight tubes, module type	1980 -
Super-Phenix	Commercial	2990 MWth	Once-through evaporator and super-heater with helical tubes	1985 - 1998
BN-800 (Russia)	Commercial	2100 MWth	Shell-and straight tubes, module type	2012 -

Tab. 7 - Experience on FBR SGs.

3.1.1 EBR-I SG

The EBR-I Steam Generator consisted of nine units of the design shown in *Fig. 9*, connected in series [23][24]. This arrangement provided the economizer, boiler, and super-heater for the small experimental plant (approximately 4 MW(th) total rating). The heat transfer tube assembly of each component consisted of an inner and outer nickel tube and an intermediate copper tube. The assemblies were fabricated by mechanically drawing the tubes together and subsequently bonding the interfaces by thermal diffusion to enhance the heat transfer characteristics. The heat transfer tube assembly had an outside diameter of 2. 625 inches and a total wall thickness of 0.313 inches. The individual tube wall thicknesses were 0.063, 0.125 and 0.0125 inches respectively for the outer, intermediate and inner tubes. Thus, the composite wall was 60% nickel and 40% copper.

The tubes were mechanically drawn together by passing them over a mandril to enlarge the inner tube and through a die to reduce the outer tube. The assemblies were then heated to form a copper-nickel alloy at the interfaces. This process yielded heat transfer coefficients of 204 BTU/hr-ft^2-°F and 508 BTU/hr-ft^2-°F for the film boiling and nucleate boiling sections respectively.

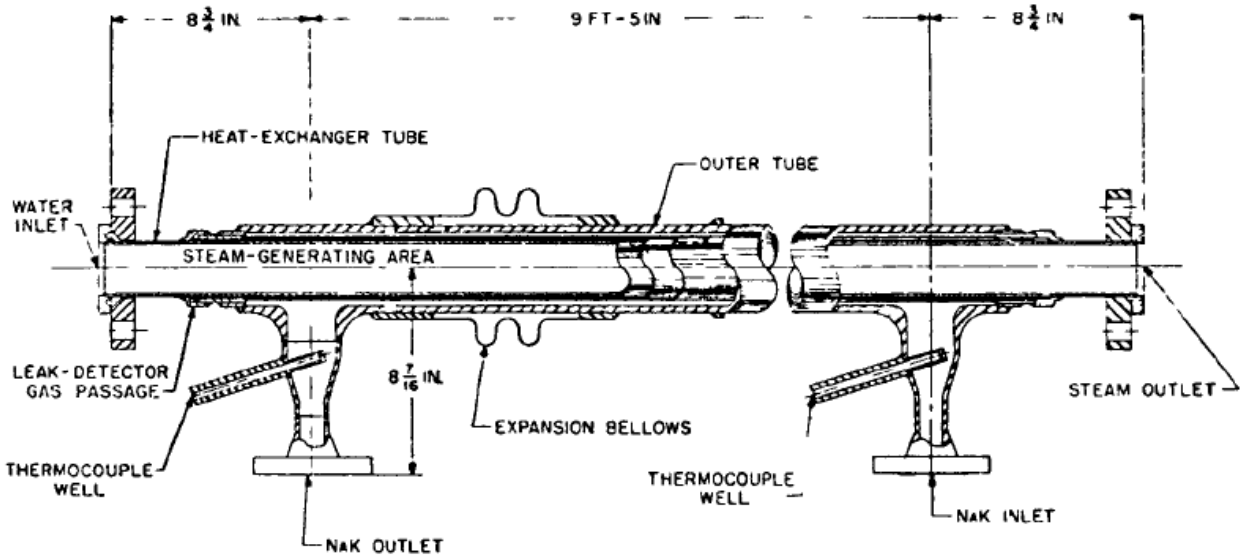

Fig. 9 – EBR-I SG.

3.1.2 EBR-II SG

The EBR-II Steam Generator consisted of evaporator and super-heater units, *Fig. 10, Fig. 11* and *Fig. 12*. The SG and distribution system uses the heat delivered by the primary cooling system to produce superheated steam at 438°C, 1250 psig, and delivers at a rate of 108862 kg/h when the reactor is operating at full power of 62.5 MW to a conventionally designed turbine generator to produce 20 MWe [23][24][25]. The basic steam generator components are: a steam drum with moisture-separating components, two shell-and-tube type once- through super-heaters, and seven shell-and-tube type recirculating evaporators. The feed-water flows out of the drum through the down-comer pipes to the bottom of seven parallel-connected evaporators. The feed-water rises through the duplex tubes, absorbing heat from the sodium flowing in the shell, and is returned to the steam drum through the riser nozzles. The saturated steam-water mixture [six parts water and one part steam at

303.8°C at full power] hits the moisture-separating components, the condensed water recirculates through the down-comer, and the dry steam flows into the super-heater section.

The evaporator assembly has an overall length of about 9 m and a maximum diameter of about 140 cm. It consists of a shell assembly through which the sodium flows and a duplex tube assembly through which the water flows (73 duplex tubes). The shell assembly consists of a pipe, two tee headers, a baffle nest assembly, and two sodium sheets with thermal plates. The super-heater assembly has exactly the same dimensions as the evaporators because it is an inverted and modified evaporator assembly. The modification is made by inserting core tubes in the duplex tubes. The core tubes decrease the cross-sectional area of the duplex tubes to cause the steam velocity to be increased.

The double walled heat transfer tubes were manufactured from 2-1/4 Ch. 1 Mo. The duplex tube outermost diameter was 36.53mm (2.39mm thickness) the inner tube outer diameter was 31.75mm (2.35 mm thickness). Two types of duplex tubing were used in the fabrication of the units. Four evaporators contain mechanically bonded duplex tubes, and four units contain metallurgically bonded tubes. Fabrication of both types of tubes consisted of placing the outer tube over the inner tube, drawing the two tubes together through a die and over a pin. This was followed by expanding the duplex tubes by drawing a pin through the I.D. without restraining the O.D. Metallurgical bonding required a final operation of heating to flow the nickel-nickel phosphorous alloy between the tubes to produce a brazed tube-to-tube-bond. The heating operation annealed out the pre-stress, which was introduced during the drawing operation, the mechanically bonded tubes were left in the stressed condition of outer tubes in tension and inner tubes in compression.

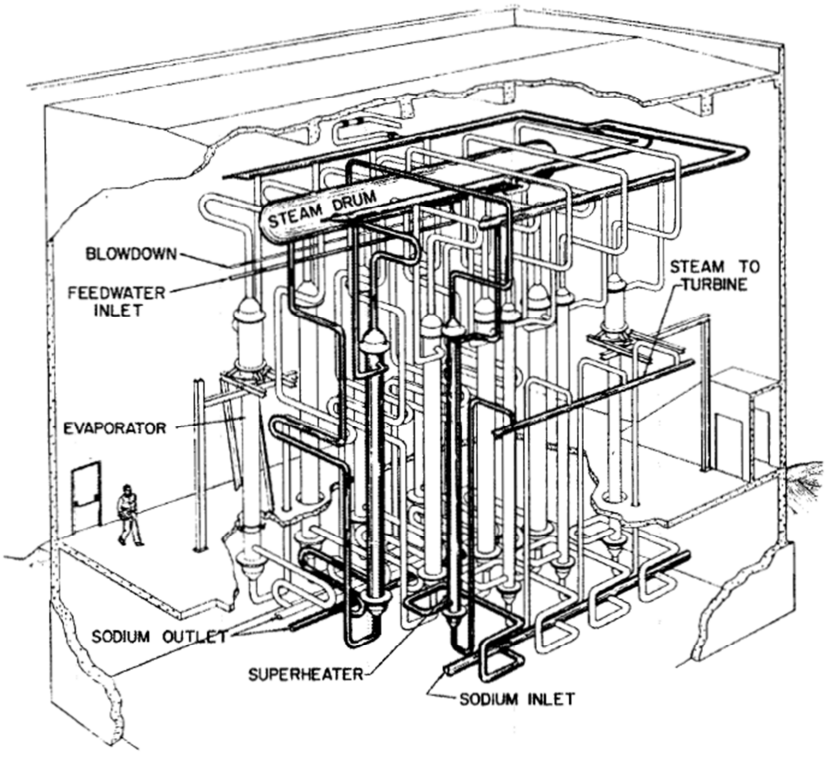

Fig. 10 – EBR-II Steam generating station.

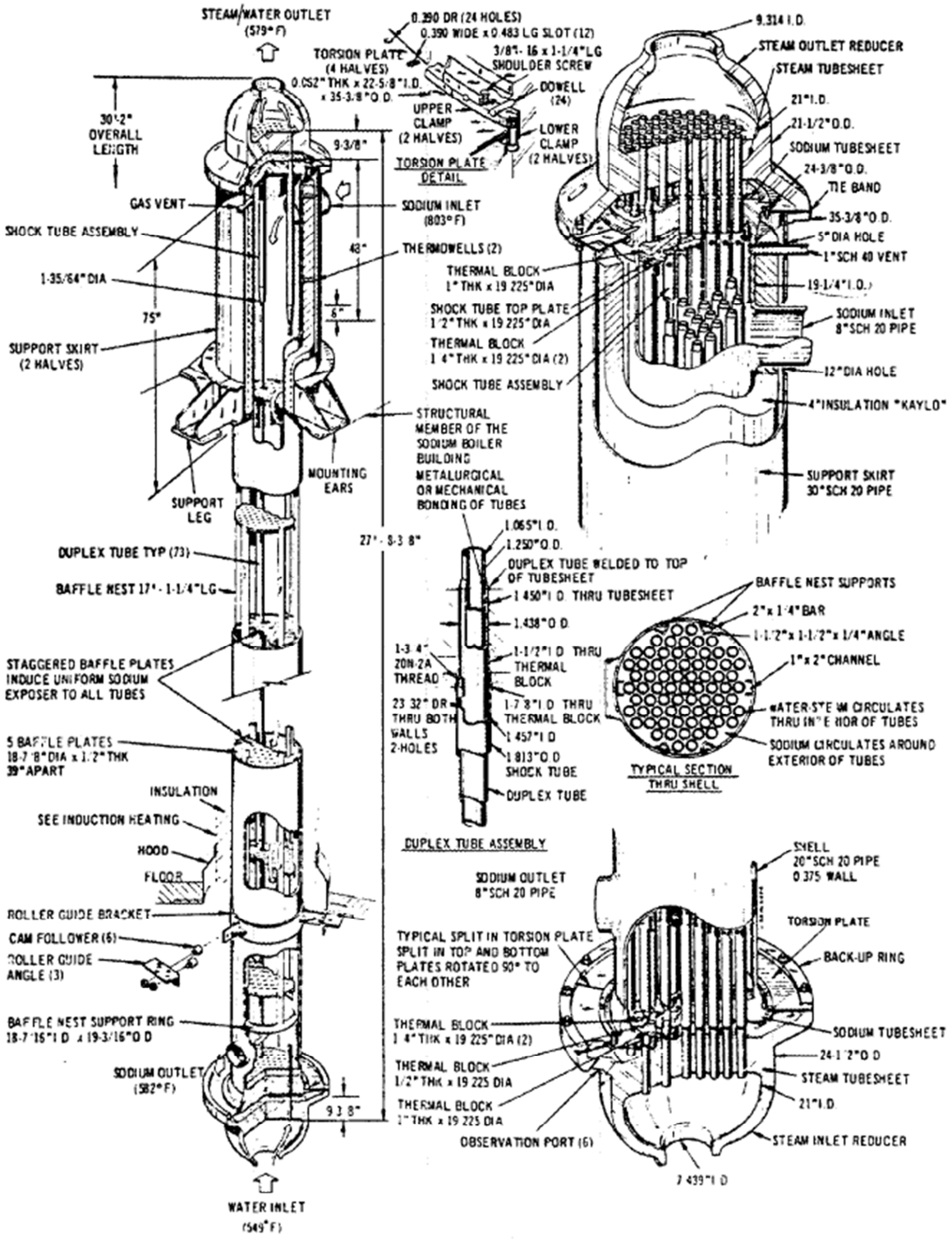

Fig. 11 – EBR-II SG, evaporator.

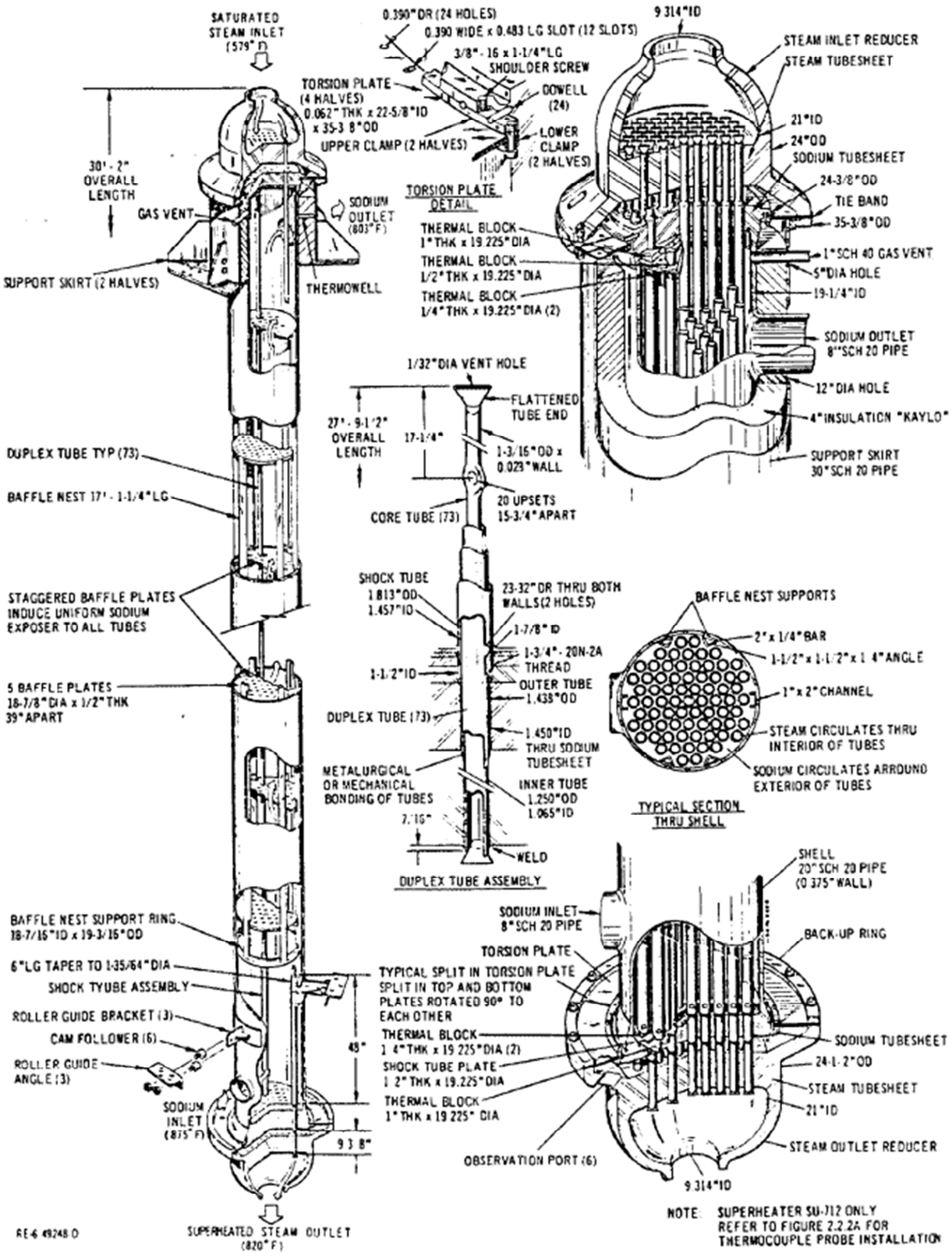

Fig. 12 – EBR-II SG, super-heater.

3.1.3 HNPF SG

(This facility has been mentioned even if there is few material available from literature since it is close to the concept of double wall bayonet tube with intermediate monitoring proposed for ALFRED). The Hallam Nuclear Power Facility (HNPF) successfully operated for several years with a steam generator in which sodium flowed into horizontal bayonet tubes as shown in *Fig. 13*. These units physically share many characteristics of C-E's Duplex Bayonet Tube SG and they provided an enclosed leakage monitoring gas system between the double tube walls and the dual tube-sheets [24]. The overall heat transfer coefficients noted during operation were high (800 BTU/hr-ft^2-°F initially for the evaporator) indicating a good interfacial conductance.

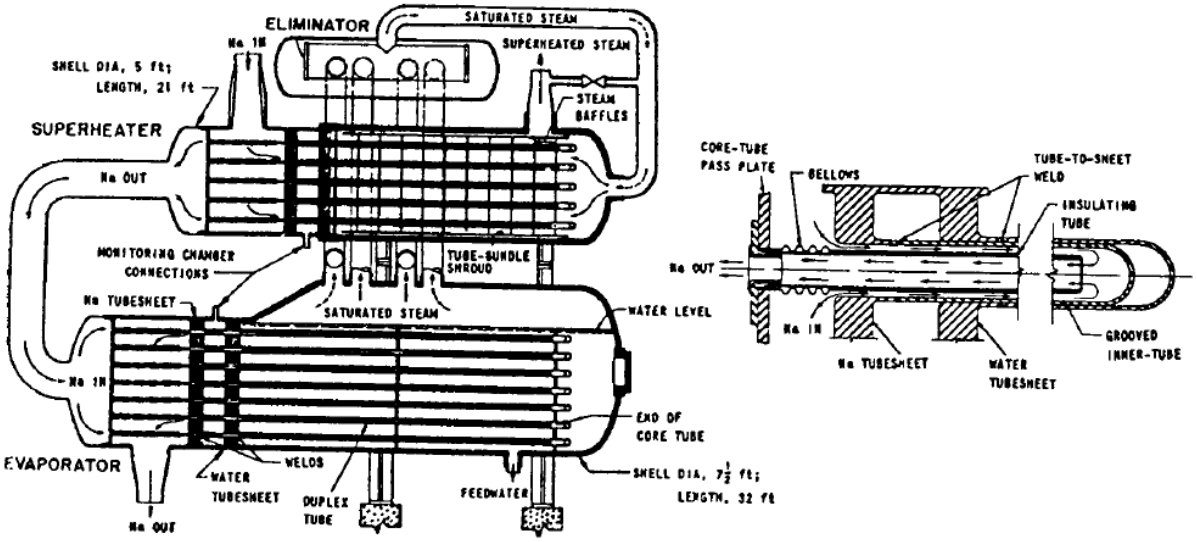

Fig. 13 – HNPF SG.

3.2 ALFRED SG

ALFRED conceptual design relies on innovative SG. Its tube bundle is the Double Wall once through Bayonet Tube type (SGBT) with leakage monitoring. It is capable to generate super-heated steam and has been conceptualized by ANSADO Nucleare in the framework of the LEADER Project.

ALFRED reactor includes eight SGs [8][19][26] whose transversal sections look like half of a moon. Preliminary calculations indicate that each SG has 510 tubes. The main data are given in *Tab. 8* and the scheme of ALFRED SG is shown in *Fig. 14* and *Fig. 15.* The single unit is capable to remove 37.5 MW, it consists of the SG coupled with its axial pump located in the hot side and integrated in the SGs (axial pump is the reference solution, jet pump is the alternative), *Fig. 16.*

The feed water enters each SG from its top head at 335°C, 180 bar and is distributed to the bayonet tubes anchored to the upper grid through eight collectors located in the top of the SG. It crosses each tube in down flow and then in up-flow. The rising annular zone is designed to remove the heat from the lead that flows in countercurrent and to generate superheated steam. The steam leaves the SG at its top nozzles (located below the bayonet tube top plate) at 450 °C and enters the steam plenum.

The lead is pumped from eight nozzles located into the cylindrical inner vessel (positioned above the reactor core). Each nozzle is connected to one suction line that consists of the structure that allows the lead to flow in the direction of the pump. The pump suction is directly located above the reactor core, the lead flows into the pump and leaves its casing through appropriate fissures (located above the tube bundle active height) that connect the pump to the SG tube bundle. The lead enters the bayonet tube bundle at 480 °C and crosses it in down flow. It leaves the SG at its bottom end at 400 °C and moves to the bottom part of the reactor core. The SG active length is 6 m, the top head of the reactor pool is filled by Ar (1 m in height).

Each bayonet tube removes 74 kW and consists of three concentric tubes, *Fig. 17*, *Fig. 18* and *Tab. 8*. The feed-water flows downward in the inner tube and enters the annular space between the first and the second tube in up-flow where it starts to boil because of the heat exchange with the liquid lead that flows in counter-current [11].

The design requires the achievement of high temperature super-heated steam (450 °C, 180 bar). The molten lead is not in contact with the second tube. The third concentric tube separates it from the water-steam side providing a double barrier and the capability to monitor leakages from the tubes. This last safety function is achieved by means of pressurization of the annular gap with helium.

The study of this configuration is motivated by safety improvement. In fact, it allows the double physical separation between lead and water sides. Furthermore, the leakage check system should prevent incident scenarios, as Steam Generator Tube Rupture (SGTR). On the other hands, the thermal efficiency of this configuration needs to be investigated and improved. In particular, two open points should be carefully investigated and constitute main R&D issues for economic feasibility of this unit:

- The first is the achievement of high temperature superheated steam that requires the selection of an appropriate material to be placed within the gap between the second and the third tube. This material should have a certain porosity to preserve leakage monitor-ability by helium pressurization.
- The heat exchange between the feed-water that crosses in down-flow the first tube and the superheated steam that rises up in the annular space should be minimized.

The candidate materials considered for the lead - annular riser gap are high conductivity materials (i.e. powders). The reference material was considered to have a conductivity 55 times that of He.

An insulator layer has been introduced between the super-heated steam riser and the descending feed water in order to prevent the loss of efficiency in the SG zone located above the active height, *Fig. 18*. The preliminary solution proposed by ANSALDO Nucleare consists of a paint with a thermal conductivity in the order of 0.05 W/mK: namely paint RHy12. The paint is located between the feed-water tube and the left boundaries of the annular cavity.

Steam Generator general properties			
Description	**Quantity**	**Description**	**Quantity**
Removed Power [MW]	37.5	Number of tubes	510
Feed-water flow rate [kg/s]	24.1	Water pressure [bar]	180
Bundle geometry	triangular	Pitch / tube diameter	1.42
Feed-water temperature [°C]	335	Steam outlet temperature [°C]	450
Lead inlet temperature [°C]	480	Lead outlet temperature [°C]	400
Bayonet tube geometry			
Description	**Quantity**	**Description**	**Quantity**
Slave tube outer diameter [mm]	9.52	Slave tube thickness [mm]	1.07
Inner tube outer diameter [mm]	19.05	Inner tube thickness [mm]	1.88
Second tube outer diameter [mm]	25.40	Second tube thickness[mm]	1.88
Third tube outer diameter [mm]	31.37	Third tube thickness [mm]	2.11
Powder annular gap width [mm]	1.07	Length of heat exchange [mm]	6000
Argon plenum height [mm]	1000	He plenum height [mm]	800
Steam plenum height [mm]	800	T91 plates thickness [mm]	250
Feed-water flow rate [g/s]	47.3		

Tab. 8 - ALFRED SG main data (from the conceptual design).

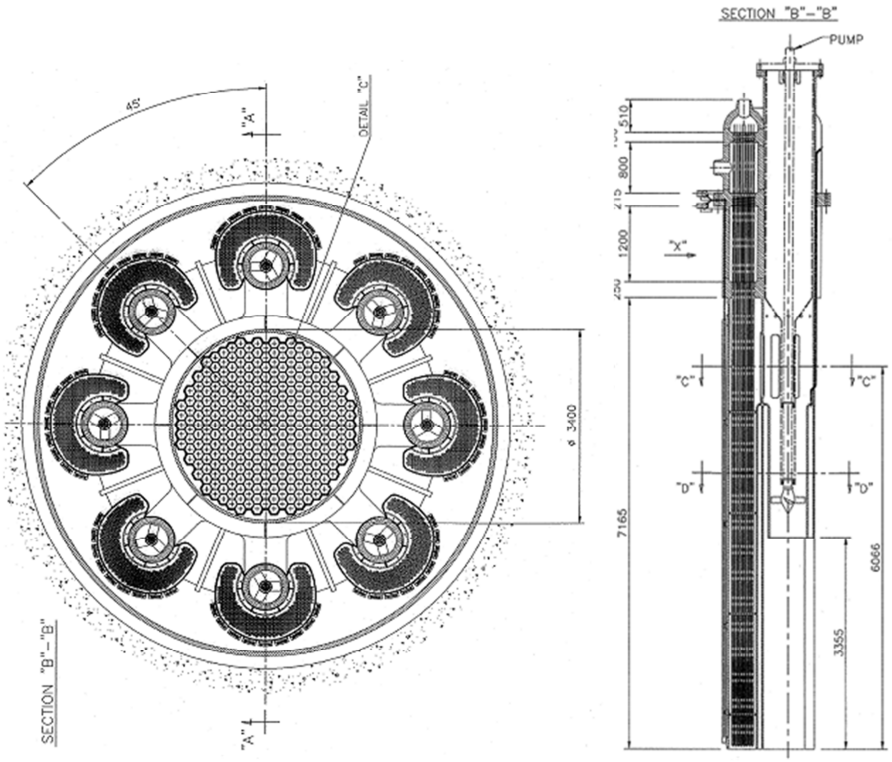

Fig. 14 – ALFRED SG view.

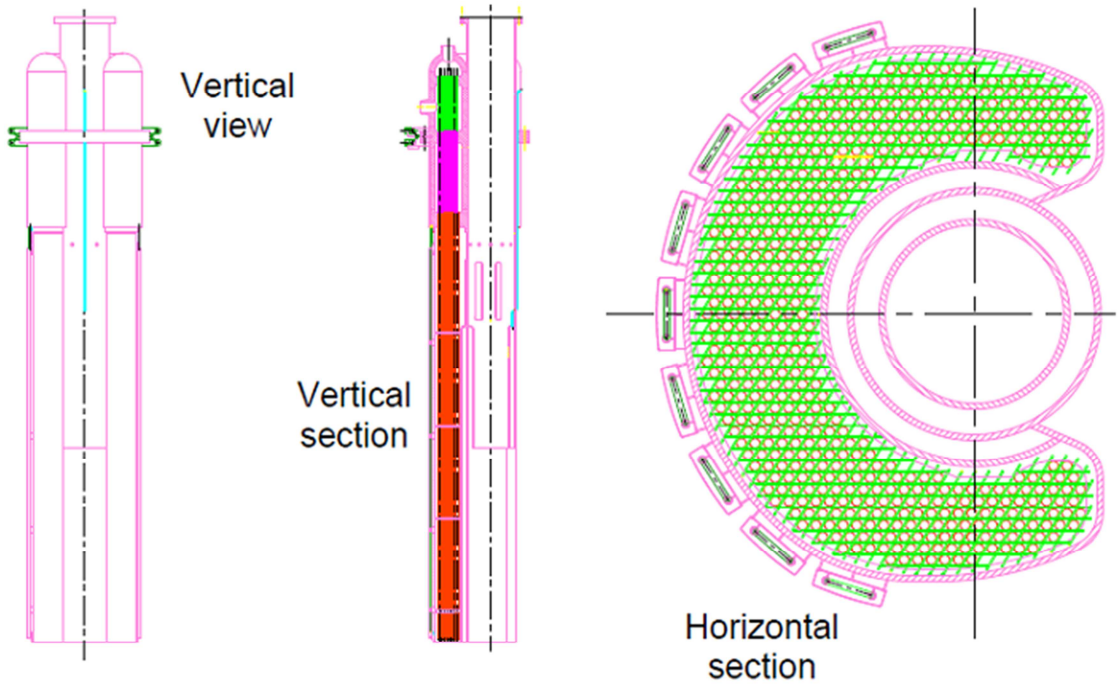

Fig. 15 – ALFRED SG scheme.

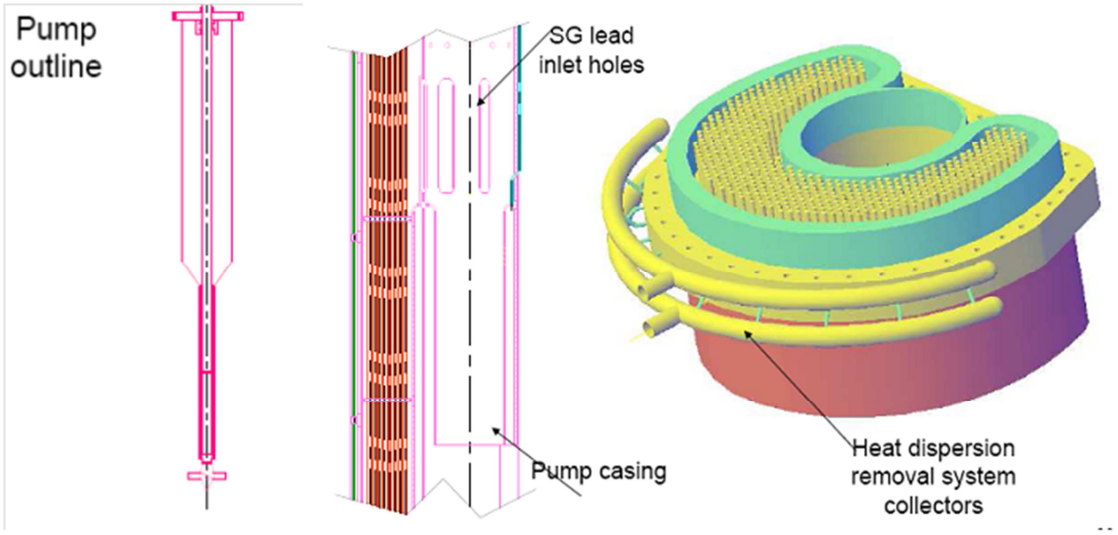

Fig. 16 – ALFRED pump, pump casing and Heat dispersion removal system.

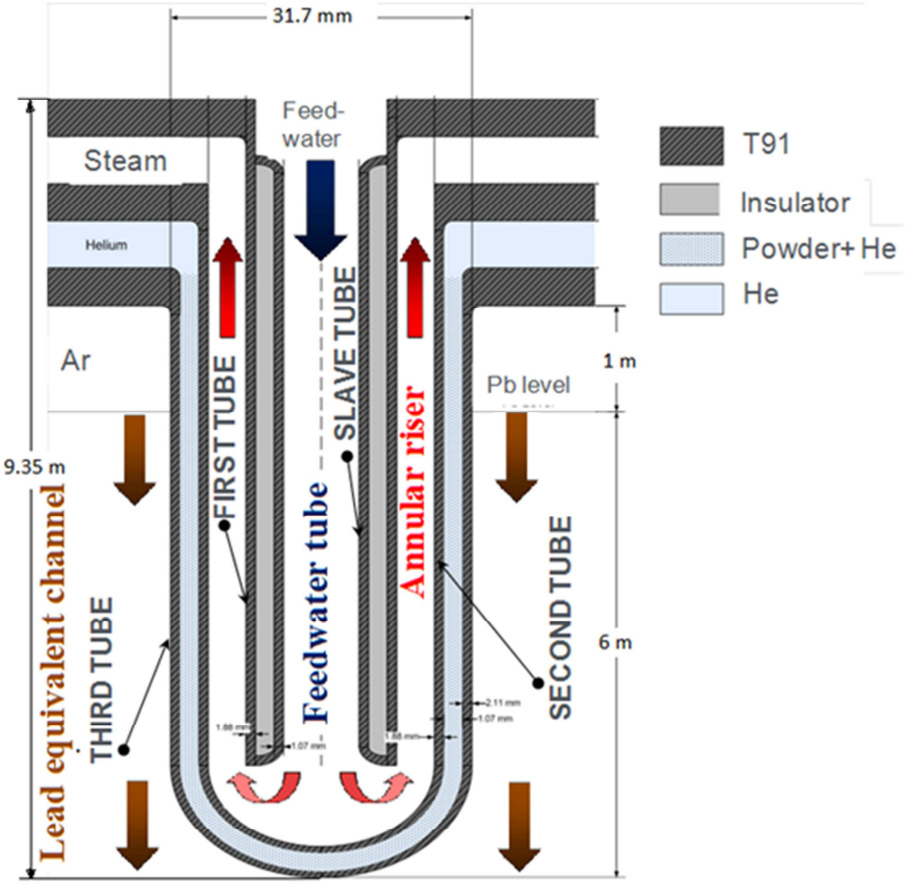

Fig. 17 – Scheme of the SG double wall bayonet tube of ALFRED, axial section.

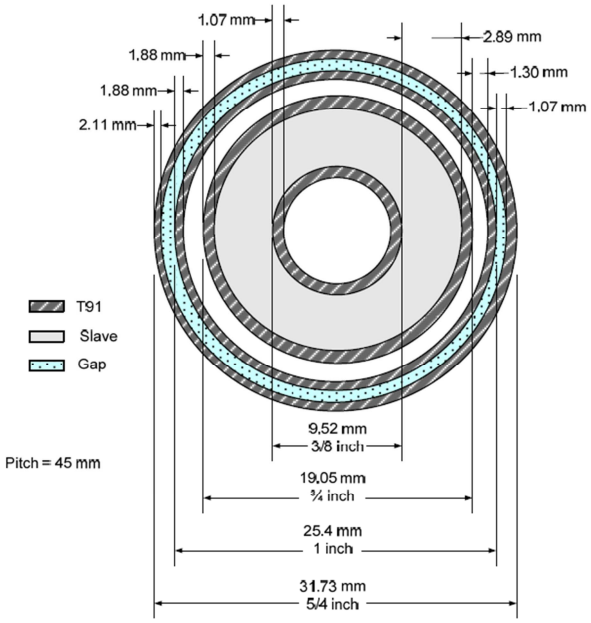

Fig. 18 – Scheme of the SG double wall bayonet tube of ALFRED: transversal section.

3.3 Conclusive remarks and connection to the present activity

The double wall bayonet tube with leakage monitoring SG proposed for ALFRED is a promising concept that allows to enhance the safety margin of a NPP in which the SG is directly located inside the reactor pool.

Since this is an innovative configuration that has never been experienced in the nuclear technology, there are still several open points that require R&D mainly related to economic feasibility. In particular:

- The achievement of high temperature superheated steam requires the selection of an appropriate material to be placed between the double wall. It should has a certain porosity to preserve leakage monitor-ability by helium pressurization.
- The heat exchange between the feed-water that crosses in down-flow the feed-water tube and the superheated steam that rises up in the annular riser should be minimized with an insulator to avoid loss of efficiency of the unit or condensation of steam at its outlet (which correspond to the feed-water inlet).

Considering that ENEA Brasimone has a certain experience with facilities that operate with HXs based on double wall straight and bayonet tubes (even if they have never been designed and operated to produce steam), it has been decided to concentrate R&D efforts on the experimental investigation of porous heat transfer enhancers since the thermal insulation between feed-water and steam is retained feasible.

The Tubes for Powder (TxP) facility has been designed and operated with this purpose and to qualify the existing HXs. The main results of these experimental campaigns lead to the design and the construction of a prototypic SG bayonet tube bundle of seven tubes which is retained a representative scaled down (in power) model of the ALFRED SG: the CIRCE-HERO (Heavy liquid mEtal pRessurized water cOoled tubes) test section.

4 Assessment of the ALFRED SG by means of RELAP-5

The present section focuses on the investigation of the thermal-hydraulic performance of the single double wall bayonet tube of ALFRED by means of RELAP-5. The main aim of this work is to check the conceptual design proposed by Ansaldo, to identify the main aspects that impact on the tube performance and to provide well understood boundary conditions in support to the design of the CIRCE-HERO test section on the basis of an in depth analysis by RELAP-5 modeling.

4.1 Development of the reference input deck

The single bayonet tube has been modeled by means of RELAP version 5.3.3. RELAP-5 is a light water reactor transient analysis code developed by the U.S. Nuclear Regulatory Commission (NRC) for use in rulemaking, licensing audit calculations, evaluation of operator guidelines and as a basis for a nuclear plant analyzer. It is a highly generic code that, in addition to calculating the behavior of a reactor coolant system during a transient, can be used for simulation of a wide variety of hydraulic and thermal transients in both nuclear and non-nuclear systems involving mixtures of steam, water, non-condensable and solute [28][29][30]. In particular the version 5.3.3 has the capability to include the lead and LBE as coolant material.

Due to the pitch to diameter ratio (P/D = 1.42) of this bundle, the model is considered representative of the SG. In fact, as reported in the literature [31], for P/D > 1.35 the single unit can be considered un-coupled with the boundary units. A schematic overview of the nodalization adopted is reported in *Fig. 19*. The model includes: the feed-water tube, the annular steam riser and the equivalent lead channel. The analysis has been developed on the basis of the following assumptions:

- The heat exchange between the annular steam riser and the Argon zone has been neglected, that means adiabatic behavior of the non-active outer-side tube surface region.
- The conductivity of the insulating paint has been fixed, in agreement with ANSALDO Nucleare recommendations, to 0.05 W/mK (RHY-12 insulating paint).
- The material adopted for the tubes is T91 (according to ANSALDO design).
- The filling powder is assumed as 0.3 porosity sintetic diamond. Its conductivity has been selected on the basis of section 5.1.1. Therefore, two different equations are adopted to calculate this quantity, it is assumed that they provide a boundary of the effective conductivity (see also section 4.2). They are labeled as Case 1 and Case 2.
- The heat transfer between the lead side and the annular riser is modeled according to the Mikityuk correlation that has been developed for fuel rod bundle [32][33].

The detailed description of the hydrodynamic components is given in section 4.1.1. Section 4.1.2 reports the characterization of the heat structures and the complete input deck is given in Appendix A and Refs [34], [35] and [36].

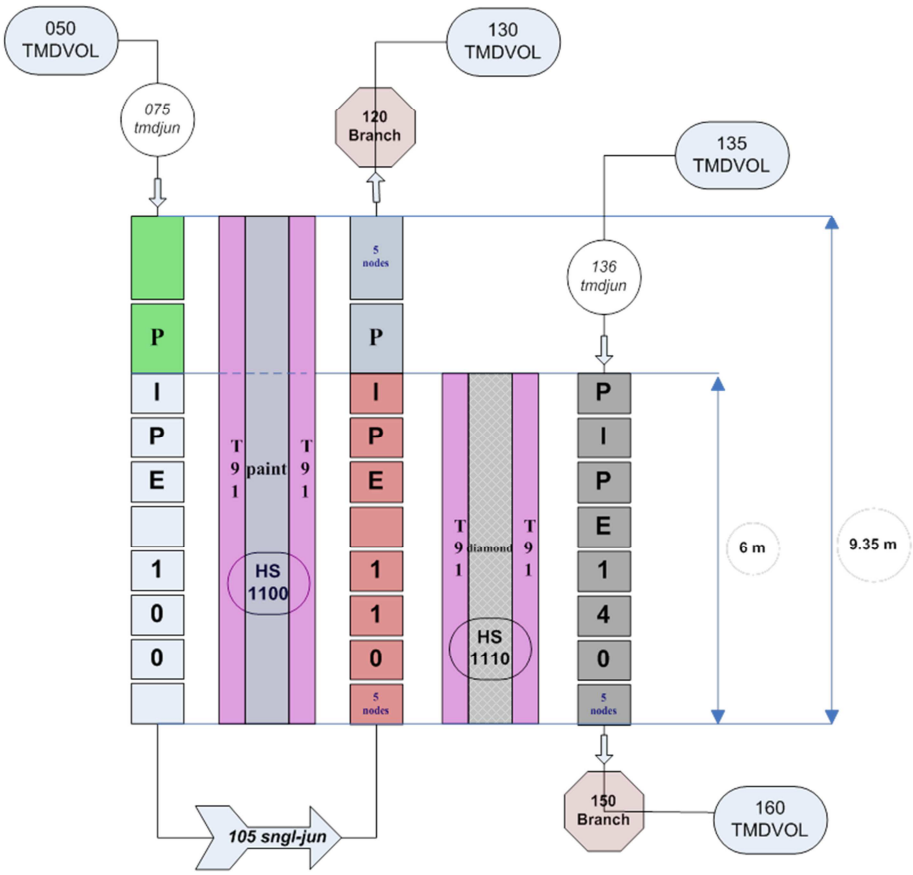

Fig. 19 – ALFRED SG double wall bayonet tube, RELAP-5.3.3 model.

4.1.1 Modeling of the hydrodynamic components

The description of the hydrodynamic components is reported from *Tab. 9* to *Tab. 11*. They are: the feed-water tube (pipe-100), the annular steam riser (pipe-110), and the equivalent lead channel (channel-140). The tables include the correlations adopted to calculate the quantities derived from the thermal-hydraulic and geometrical data attached in *Tab. 8* (section 3.2). The hydraulic diameter of the equivalent lead channel is calculated assuming triangular array infinite bundle (that means hydraulic diameter equal to heated diameter).

COMPONENT LABEL		**TYPE**	**DESCRIPTION**
Pipe 100		Hydrodynamic component	Feed-water tube
Id.	**Parameter**	**Quantity**	**Notes**
a	Axial node height	0.33500 m	--
b	N° axial nodes	10	--
c	Axial node height	0.15000	--
d	N° axial nodes	40	--
e	Inner radius	0.00369 m	--
f	Flow area	$4.27762*10^{-5}$ m^2	$f = \pi e^2$
g	Operating pressure	180 bar	--
h	Inlet temperature	335 °C	--
i	Mass flow	0.047255 kg/s	
j	Hydraulic diameter	0.00738 m	j = 2*e

Tab. 9 - ALFRED SG, hydrodynamic modeling of the feed-water tube.

COMPONENT LABEL		**TYPE**	**DESCRIPTION**
Pipe 110		Hydrodynamic component	Steam riser
Id.	**Parameter**	**Quantity**	**Notes**
a	Axial node height	0.15000 m	--
b	N° axial nodes	40	--
c	Axial node height	0.33500 m	--
d	N° axial nodes	10	--
e	*Annulus inner radius*	*0.00952 m*	--
f	*Annulus outer radius*	*0.01082 m*	--
g	Flow area	$8.27708*10^{-5}$ m^2	$g = (f^2 - e^2)*\pi$
h	Operating pressure	180 bar	--
i	Inlet temperature	335 °C	--
j	Mass flow	0.047255 kg/s	--
k	Hydraulic diameter	0.00259 m	$k = 4*g / [2 \pi*(f + e)]$

Tab. 10 - ALFRED SG hydrodynamic modeling of the annular steam riser.

COMPONENT LABEL		**TYPE**	**DESCRIPTION**
Pipe 140		Hydrodynamic component	Lead channel
Id.	Parameter	Quantity	Notes
a	Axial node height	0.15000 m	--
b	N° axial nodes	40	--
c	*Tube bundle pitch (triangular)*	*0.04500 m*	--
d	*Inner radius*	*0.01586 m*	--
e	Equivalent flow area	$9.629680*10^{-4}$ m^2	$e= \{[(c^2*2)*(\cos(\pi / 6))] - [(\pi/*d^2)/2]\}*2$
f	Operating pressure	1.6 bar	--
g	Inlet temperature	335 °C	--
h	Mass flow	6.367647 kg/s	--
i	Hydraulic diameter (heated)	0.03864 m	$i = 4*e / 2 \pi*d$

Tab. 11 - ALFRED SG, hydrodynamic modeling of the lead channel.

4.1.2 Modeling of the heat structures

The description of the heat structure between the feed-water tube and the annular riser is given in *Tab. 12*. The main features of the heat structure between the annular riser and the equivalent lead channel are summarized in *Tab. 13*. The first is constituted by a sandwich T91 – RHY12 – T91. The second is T91 – sintetic diamond – T91.

COMPONENT LABEL		**TYPE**	**DESCRIPTION**
1100		Heat structure	Heat transfer between 100-110
Id.	Parameter	Quantity	Notes
a	Axial node height	0.33500 m	--
b	N° axial nodes	10	--
c	Axial node height	0.15000 m	--
d	N° axial nodes	40	--
e	Inner radius	0.00369 m	--
f	Radial interval width	$2.14000*10^{-4}$ m	T91
g	N° radial intervals	5	T91
h	Radial interval width	$3.20556*10^{-4}$ m	Insulator
i	N° radial intervals	9	Insulator
j	Radial interval width	$3.76000*10^{-4}$ m	T91
k	N° radial intervals	5	T91
l	Initial temperature	335 °C	--
m	*Inner flow area*	$4.27762*10^{-5}$ m^2	$m= \pi c^2$
n	Left boundary heated diameter	0.00738 m	n = 4*m / 2 π*e
o	*Annulus inner radius*	*0.00952 m*	--
p	*Annulus outer radius*	*0.01082 m*	--
q	*Equivalent flow area*	$8.27708*10^{-5}$ m^2	$q = (p^2 - o^2)*\pi$
r	Right boundary heated diameter	0.00553 m	r = 4*q / 2 π*o

Tab. 12 - ALFRED SG, modeling of the heat structure between the feed-water tube and the annular riser.

COMPONENT LABEL		**TYPE**	**DESCRIPTION**
1110		Heat structure	Heat transfer between 110-140
Id.	Parameter	Quantity	Notes
a	Axial node height	0.15000 m	--
b	N° axial nodes	40	--
c	Inner radius	0.01082 m	--
d	Radial interval width	$1.88000*10^{-4}$ m	T91
e	N° radial intervals	10	T91
f	Radial interval width	$1.07000*10^{-4}$ m	Insulator
g	N° radial intervals	10	Insulator
h	Radial interval width	$2.09500*10^{-4}$ m	T91
i	N° radial intervals	10	T91
j	Initial temperature	335 °C	--
k	*Annulus inner radius*	*0.00952 m*	--
l	*Annulus outer radius*	*0.01082 m*	--
m	*Flow area*	$8.27708*10^{-5}$ m^2	$m = (l^2 - k^2)*\pi$
n	Left boundary heated diameter	0.00487 m	n = 4*m / 2 π*l
o	Riser natural circulation height	9.35000 m	--
p	Left boundary fouling factor	1.105	--
q	Tube bundle pitch (triangular)	0.04500 m	--
r	*Right boundary outer radius*	*0.01586 m*	--
s	*Equivalent flow area*	$96.29680*10^{-5}$ m^2	$s = \{[(q^2*2)*(\cos(\pi / 6))] - [(\pi*r^2)/2]\}*2$
t	Right boundary heated diameter	0.03864 m	t = 4*s / 2 π*r
u	Lead natural circulation height	6.00000 m	--
v	Pitch to diameter ratio	1.4182	v = q / 2*r
w	Right boundary fouling factor	1.105	--

Tab. 13 - ALFRED SG, modeling of the heat structure between the annular riser and the lead channel (active height only).

4.1.3 Development of the reference nodalization

The selection of the axial node length is a crucial issue. In fact, the heat transfer correlations selected by the code during the phase change depend on the flow regime. Since they are selected based on average parameters (i.e. void fraction, fluid velocity) within the volume of a node, the node length is an essential quantity. From one hand, the smaller is the node length, the higher is the accuracy of the prediction. From the other hand, the higher is the node number, the higher is computational time. A preliminary analysis is conducted with the aim to find a compromise between these last two issues. The steam temperature is selected as reference parameter to check the influence of the nodalization. The results are reported in *Fig. 20*: 40 nodes in the active length seem to be an appropriate choice.

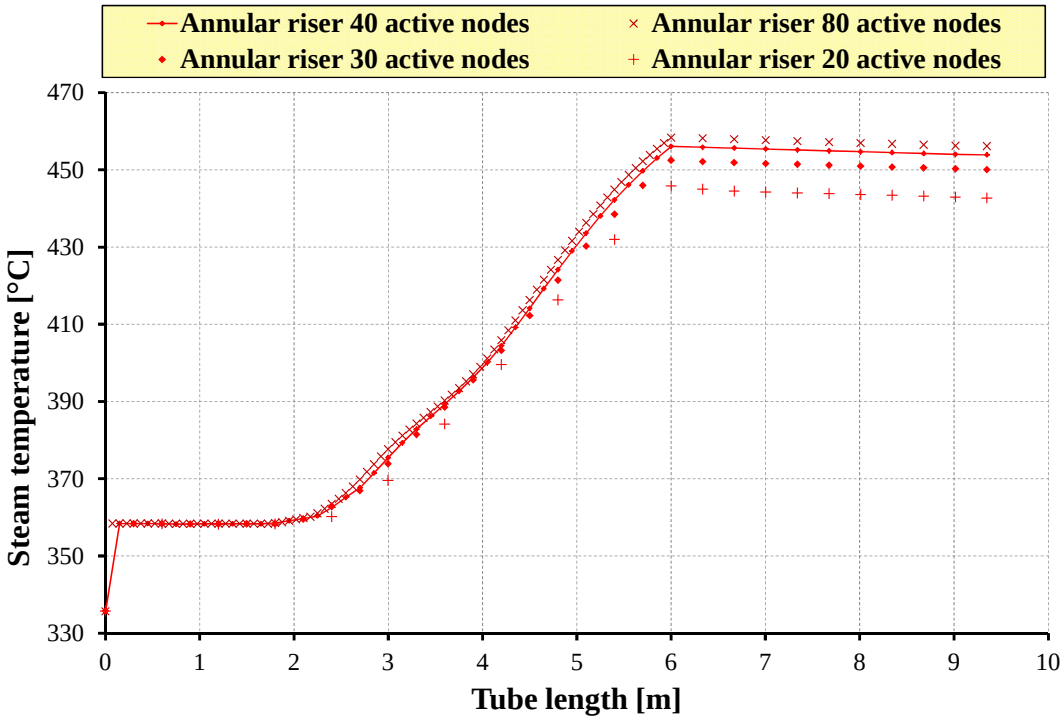

Fig. 20 – Preliminary analysis on node numbers, steam temperature along the tube.

4.2 Analysis of the reference configuration

Two distinct cases are analyzed in the reference simulations. They are labeled as case 1 and case 2. Both the calculations assume the annular gap filled by diamond powder at 0.3 porosity. The thermal conductivity of diamond is calculated based on *Eq. 5* (Case 1) and *Eq. 16* (Case 2).

The conductivity of diamond powder as function of porosity is depicted in *Fig. 21*. It should be pointed out that each correlation calculates the conductivity based on a simple function that depends upon three parameters:

- The conductivity of the solid material (99.5% dense);
- The conductivity of the fluid dispersed in the powder;
- The porosity.

The weakness points of the correlations can be summarized as follow:

- They are ideal correlations, and apply in specific range of porosity.
- Each correlation assumes spherical particles and does not account for the particle shape influence.
- The influence of the particles diameter is not considered.
- Open porosity is not accounted for.

However, they are considered to provide a lower band to the effective conductivity.

The analysis is subdivided in three main parts. The first one deals with the assessment of the hydrodynamic components. The second one focuses on the thermal structures, and the last one highlights the thermal-hydraulic behavior of the bayonet tube. Systematic comparison between the reference simulations and the results obtained by ANSALDO Nucleare is performed (when data are available).

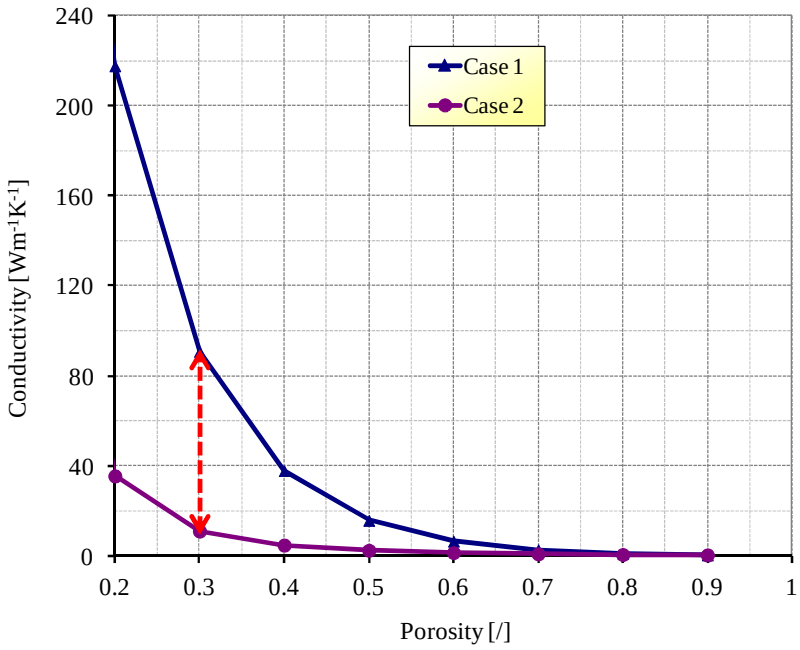

Fig. 21 – Thermal conductivity of diamond powder as function of porosity, calculated by Case 1 and Case 2 correlations.

4.2.1 Assessment of the hydrodynamic components

The results of the simulations are summarized in *Tab. 14*. The table contains the inlet and outlet temperatures, the void fraction at tube outlet, the pressure drop in the bayonet unit and the lead velocity in the equivalent channel. The quantities refer to Case 1, Case 2 and ANSALDO Nucleare calculations [37][38].

Fig. 22 a) and *b)* deal with Case 1 and Case 2 respectively. Each figure reports:

- The feed-water tube temperature as function of the tube length,
- The water-steam temperature in the annular riser as function of its length,
- The primary coolant temperature (only the lead submerged length) and
- The void fraction as function of annular riser axial elevation.

In agreement with ANSALDO, both the reference simulations predict a temperature increase in the feed-water tube in the range of 1.0 °C – 1.2 °C. The maximum steam temperature is in the range 438-456 °C depending on the conductivity correlation adopted to model the sintetic diamond powder (Case 2 and Case1 respectively). The ANSALDO simulation agrees with Case 1.

Each simulation confirms a lead temperature drop is in the order of 80 °C. Superheated steam is always predicted, being the void fraction close to 1 within the first 3 meters of the annular riser (Case 1, Case 2 and ANSALDO).

Pressure drops and velocities are represented in *Fig. 23* and *Fig. 24* (the indexes *a)* and *b)* refer to Case 1 and Case 2, respectively). The figures report:

- The feed-water pressure drop as function of the tube length.
- The water-steam pressure drop in the annular riser as function of its length.
- The lead velocity (only in the immersed tube length).
- The feed-water velocity as function of the tube length.
- The water phase velocity in the annular riser as function of axial elevation.
- The steam phase velocity in the annular riser as function of its length.

The total pressure drop in the bayonet tube is predicted in the range of 2.6 bar – 2.8 bar. These values are close to the ANSALDO results even if they are higher. This is connected with the choice of the tubes roughness. In the reference simulations, the lead and the feed-water velocities are characterized by approximately constant values along the tube length. The lead velocity is equal to about 0.65 m/s and is acceptable in terms of corrosion erosion phenomena. The water and steam phase velocities increase within the lead submerged height (first 6 meters) because of heat exchange between water-steam mixture and lead. At the end of the active length, the super-heated steam velocity is predicted to have a maximum value in the range of 8 m/s – 8.5 m/s which is retained again acceptable.

Parameter	Unit	Calc. Ref. CASE 1	Calc. Ref. CASE2	Calc. ANSALDO
Lead inlet temperature	°C	*479.3*	*479.0*	*480.0*
Lead outlet temperature	°C	*398.7*	*402.1*	*401.5*
Feed-water inlet temperature	°C	*334.4*	*334.4*	*335.0*
Feed-water tube temperature drop	°C	*1.2*	*1.0*	*<5.0*
Immersed tube steam temperature	°C	*456.1*	*438.3*	*451.5*
Superheated steam outlet temperature	°C	*453.9*	*436.1*	*450.1*
Void fraction	--	*1.0*	*1.0*	*1.0*
Pressure drop	bar	*2.8*	*2.6*	*3.3*
Lead velocity	m/s	*0.652*	*0.652*	--
Lead velocity peak factor	--	*1.004*	*1.004*	--

Tab. 14 - SGBT vs. RELAP5 v 3.3, reference simulations, assessment of hydrodynamic components.

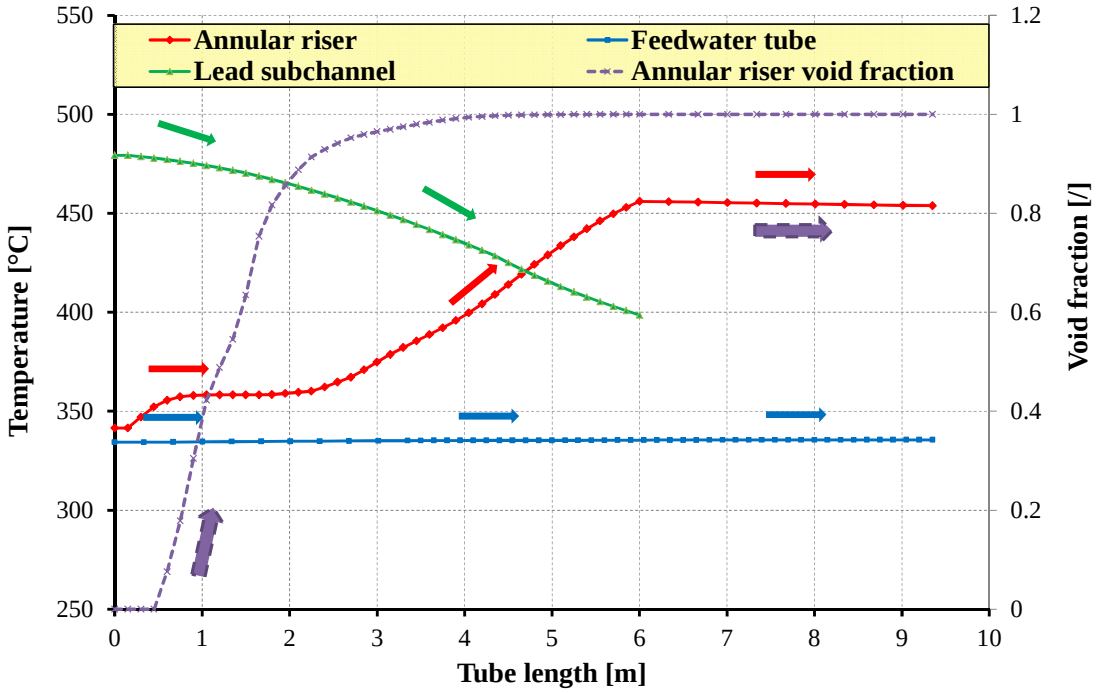

a) Case 1

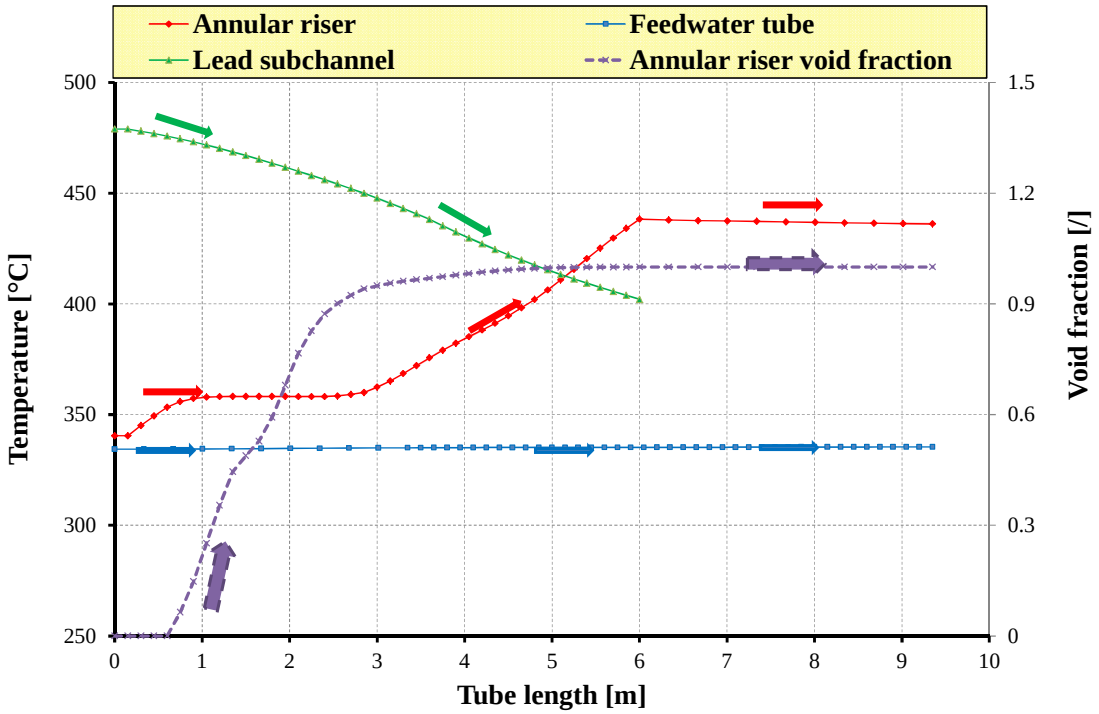

b) Case 2

Fig. 22 – SGBT vs. RELAP5 v 3.3, reference simulations, void fraction, water, steam and lead temperatures as function of tube length.

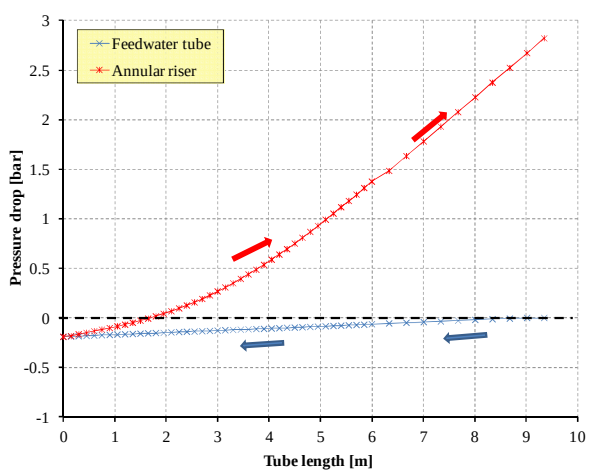

a) Case 1

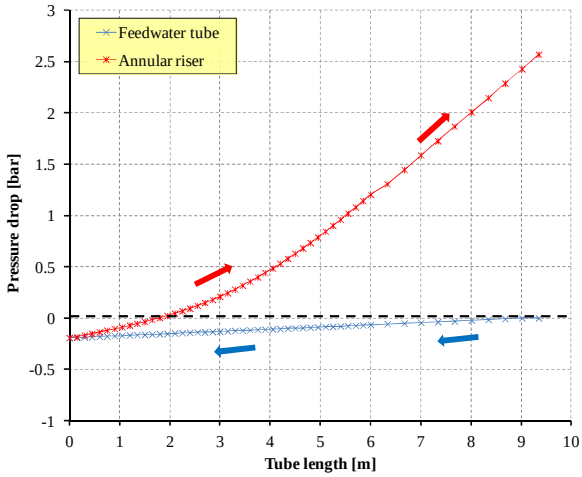

b) Case 2

Fig. 23 – SGBT vs. RELAP5 v 3.3, reference simulations, total pressure drops.

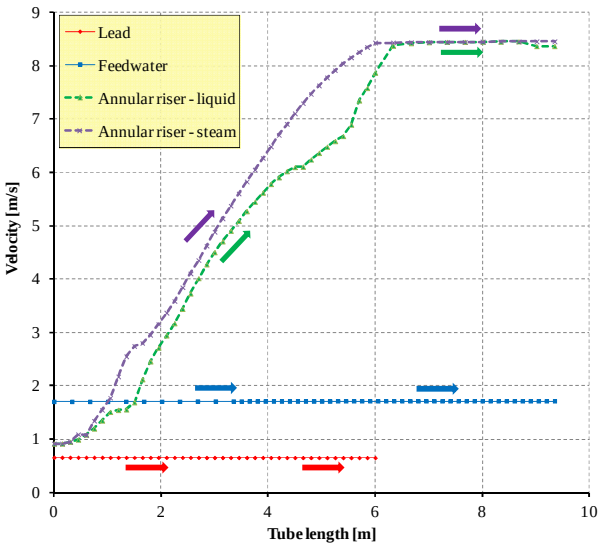

a) Case 1

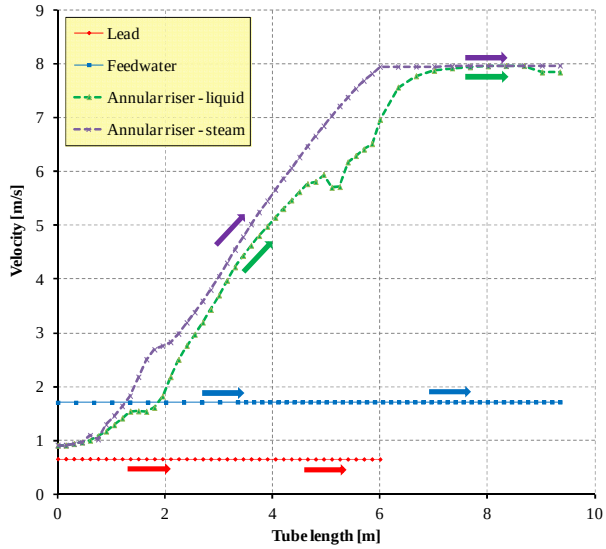

b) Case 2

Fig. 24 – SGBT vs. RELAP5 v 3.3, reference simulations, velocities.

4.2.2 Assessment of the heat structures

The assessment of the heat structures is summarized in *Tab. 15*. The table contains the average heat fluxes and surface temperatures at feed-water tube and annular riser surface boundaries. The axial peak factor is also reported. Moreover, it includes the total power exchanged by the annular riser outer surface with the lead side. The quantities refer to Case 1, Case 2 and ANSALDO Nucleare calculations (when available) [38].

The feed-water tube is analyzed from *Fig. 25* to *Fig. 27*. The annular riser is given from *Fig. 28* to *Fig. 30*. The indexes *a)* and *b)* refer to Case 1 and Case 2 respectively. The figures include the following quantities:

- The heat flux that crosses the inner surface as function of the tube length.
- The heat flux that crosses the outer surface as function of the length.

- The Heat Transfer Coefficient (HTC) at the inner surface as function of the tube length,
- The HTC at the outer surface as function of the length.
- The temperature at the inner surface as function of the tube length.
- The temperature at the outer surface as function of the length.

Feed-water tube: the heat flux at the inner side shows three discontinuities, *Fig. 25*. The first one is at the steam outlet, the second one is about 4 meters far from the outlet, close to the end of the active region and, the last one, is in the active region between 5-7 m. The outer side heat flux trend is similar to the inner side, it is scaled by the outer to inner surface ratio. The inner side HTC and surface temperature are approximately constant, this is due to the contact with sub-cooled water. The outer side HTC and surface temperature have a discontinuous behavior that reveals the occurrence of several heat transfer regimes, *Fig. 26* and *Fig. 27*. In order to explain these trends, further investigations are given in section 4.2.3.

Annular riser: both the simulations highlight a continuous increase of the heat flux at the outer and inner sides within the first 2.0 - 2.5 meters, *Fig. 28*. In fact, at the tube bottom, the water reaches saturation and begins to boil. This is reflected in the corresponding high HTC (*Fig. 29*). When superheated steam is reached both the HTC and the heat flux at the inner side tend to decrease. At the outer side, the HTC is approximately constant, according to the Mikityuk correlation. The maximum predicted temperature is close to 470 °C and it is reached at the end of the active length, *Fig. 30*. In agreement with ANSALDO calculations, the total power removed by the bayonet tube is in the range of 71.3 kW – 74.5 kW.

Parameter	Unit	Calc. Ref. CASE 1	Calc. Ref. CASE2	Calc. ANSALDO
Average heat flux feed-water tube ID	W/m^2	*1769*	*1470*	--
Heat flux peak factor feed-water tube ID	--	*1.940*	*1.997*	--
Average heat flux feed-water tube OD	W/m^2	*722*	*569*	--
Heat flux peak factor feed-water tube OD	--	*3.540*	*2.028*	--
Average heat flux annular riser ID	W/m^2	*182675*	*174951*	--
Axial heat flux peak factor annular riser ID	--	*1.700*	*1.512*	--
Average heat flux annular riser OD	W/m^2	*124585*	*119316*	--
Heat flux peak factor annular riser OD	--	*1.700*	*1.512*	--
Average temperature feed-water tube ID	°C	*335.3*	*335.2*	--
Axial temperature peak factor feed-water tube ID	--	*1.001*	*1.001*	--
Average temperature feed-water tube OD	°C	*397.3*	*386.8*	--
Axial temperature peak factor feed-water tube OD	--	*1.147*	*1.132*	--
Average temperature annular riser ID	°C	*408.8*	*395.0*	
Axial temperature peak factor annular riser ID	--	*1.146*	*1.155*	--
Average temperature annular riser OD	°C	*431.8*	*430.3*	--
Axial temperature peak factor annular riser OD	--	*1.101*	*1.099*	--
Total power removed annular riser OD	kW	*74.5137*	*71.3623*	*73.7640*

Tab. 15 - SGBT vs. RELAP5 v 3.3, reference simulations, assessment of heat structures.

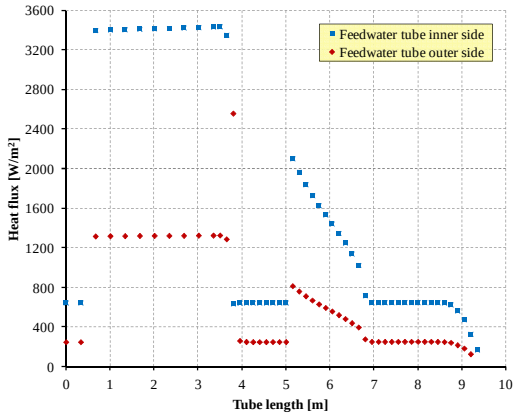

a) Case 1

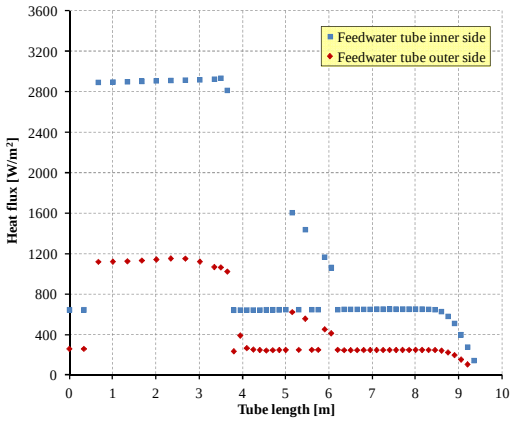

b) Case 2

Fig. 25 – SGBT vs. RELAP5 v 3.3, reference simulations, heat flux in the feed-water tube as function of tube length.

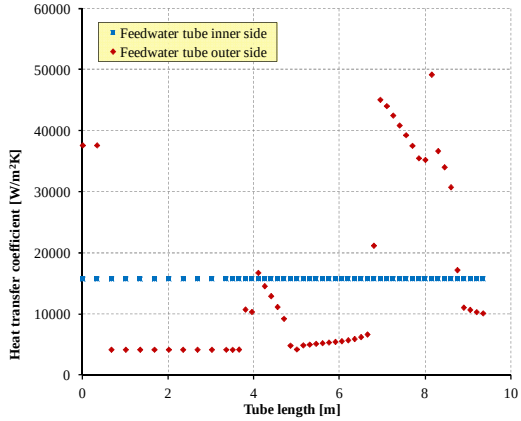

a) Case 1

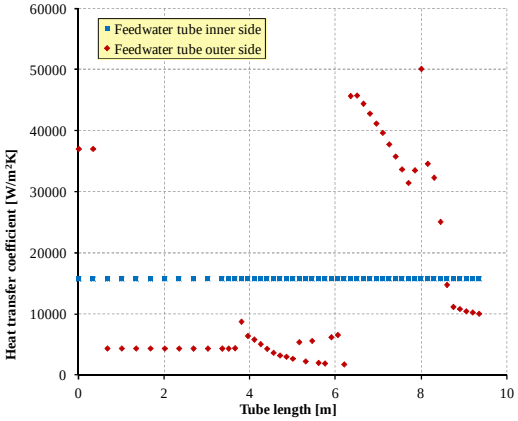

b) Case 2

Fig. 26 – SGBT vs. RELAP5 v 3.3, reference simulations, convection HTC at the feed-water tube surfaces as function of tube length.

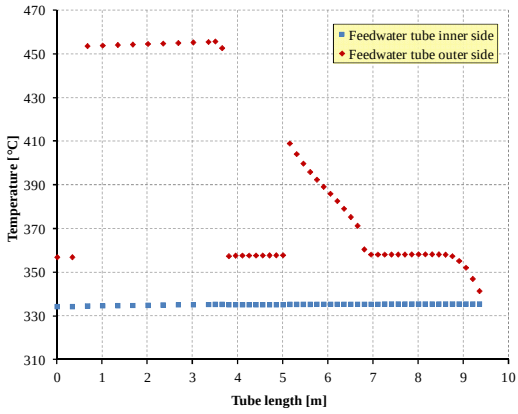

a) Case 1

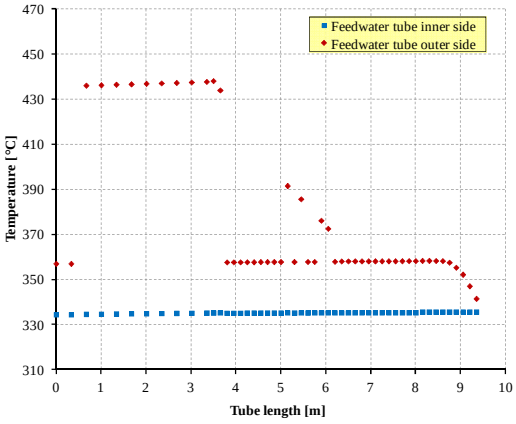

b) Case 2

Fig. 27 – SGBT vs. RELAP5 v 3.3, reference simulations, temperatures at the feed-water tube surfaces as function of tube length.

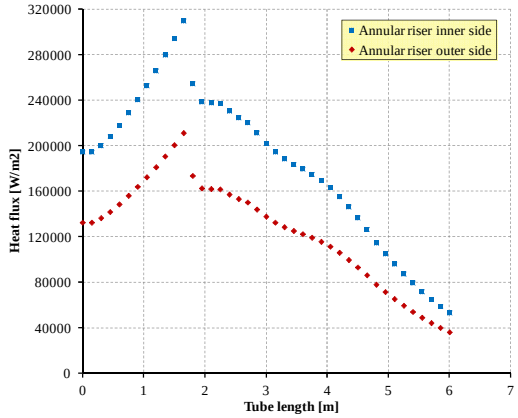

a) Case 1

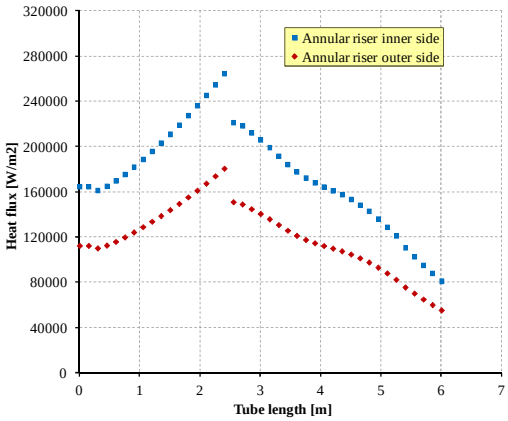

b) Case 2

Fig. 28 – SGBT vs. RELAP5 v 3.3, reference simulations, heat flux in the annular riser as function of tube length.

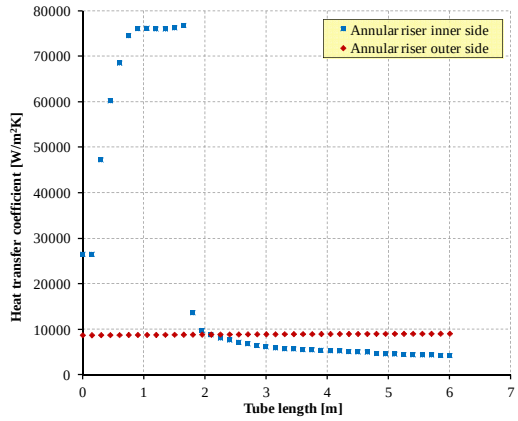

a) Case 1

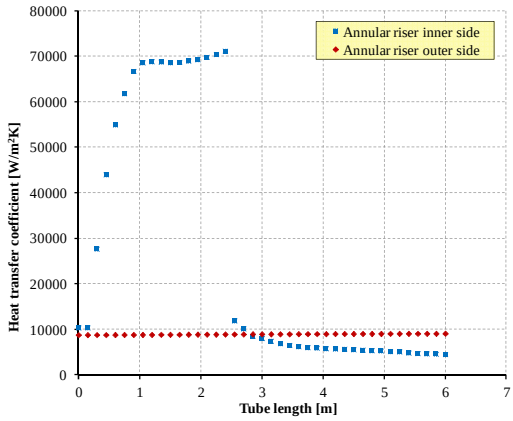

b) Case 2

Fig. 29 – SGBT vs. RELAP5 v 3.3, reference simulations, convection HTC in the annular riser as function of tube length.

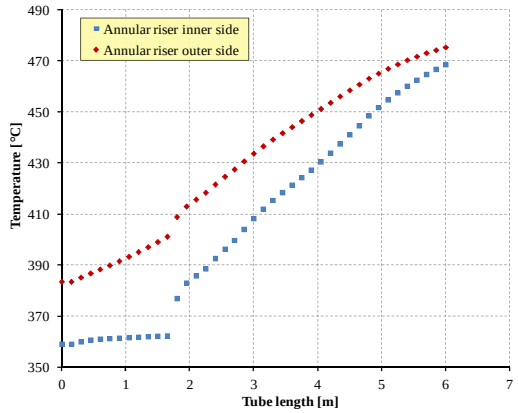

a) Case 1

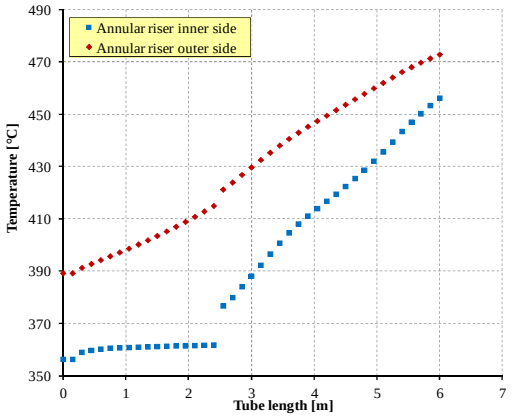

b) Case 2

Fig. 30 – SGBT vs. RELAP5 v 3.3, reference simulations, temperatures at annular riser surfaces as function of tube length.

4.2.3 Assessment of 2ϕ Dynamics in the Water Steam Side

The present section is aimed to point out the main thermal-hydraulic phenomena that occur in the water-steam side of the bayonet tube. RELAP5 code selects the flow regime in the two-phase bulk through a series of parameters, such as the void fraction (to switch the flow regime) and the ΔT_{gw} "wall surface temp. – steam temp difference" (to reach and overpass CHF conditions) [28], *Fig. 31*. In this way it is possible to predict the interfacial heat transfer mode inside each volume. The heat transfer mode between the tube surfaces and the steam-water mixture is selected according to the boiling curve used in RELAP5 to govern the selection of heat transfer correlations [28] (*Fig. 32*, in which T_{spp} is the saturation temperature based on the partial pressure of steam in the bulk, T_w is the wall surface temperature and T_{spt} is the saturation temperature based on the total pressure).

Three pictures are given in *Fig. 33*, they are representative of Case 1.

- The heat transfer modes at the feed-water tube outer wall are reported in the first picture. The figure includes the temperature difference ΔT_{gw} "steam - wall surface" and the HTC at the tube wall. The following modes are predicted:
  - Single-phase liquid convection at low void fractions.
  - Two large zones in which condensation takes place at low and high void fractions (>0.9). They are separated by a zone in which relatively high temperature liquid film is predicted at tube surface ($\Delta T_{gw} < 0$ in this zone) that induces the code to assume single-phase liquid convection at supercritical pressure mode.
  - Wall drying and single-phase vapor convection takes place in the higher part of the active length.
  - Condensation starts again at the tube outlet, 2.5m far from the active length. The liquid fraction is very low and the code predicts a liquid fraction of $1.15379*10^{-6}$.
  - This sequence of heat transfer modes (in particular the condensation) explains the discontinuities of the heat fluxes and surface temperatures in the feed-water tube.
- In the intermediate picture, the flow regimes and the corresponding void fraction in the annular riser are reported:
  - Bubbly flow, slug flow and annular mist flow are predicted to occur within 2 meters in the void fraction range 0.0-0.9.
  - Mist flow dominates the remaining part of the active length with the exception of the last nodes in which post CHF mist flow takes place (that corresponds to feed-water tube wall post dry-out).
  - Above the active length pre CHF mist flow is predicted, this could be connected with the condensation that occurs at tube outlet and with the adiabatic conditions at annular riser outer surface.
- In the third picture the heat transfer regimes at the annular riser inner wall are reported. The figure includes the temperature difference ΔT_{gw} "wall surface – steam" and the HTC at the tube wall. The following regimes are predicted:
  - Sub-cooled nucleate boiling at low void fractions.
  - Saturated nucleate boiling and saturated transition boiling up to void fraction of about 0.85.
  - When ΔT_{gw} becomes negative (-30°C) the wall temperature largely exceed the steam temperature, it is the film boiling mode.
  - Wall drying and single-phase vapor convection takes place in the higher part of the active length.

Case 2 is depicted in *Fig. 34*. The considerations reported above apply to this case too. Should be pointed out that RELAP5 code has been designed for Light Water Reactor (LWR) and it is suitable for their types of SG. Therefore, it is not completely accurate in simulating the bayonet tube configuration. Nevertheless, although the accuracy of the results should be verified, condensation phenomena occur and, in particular, those that appear at the feed-water tube surface ends seem to reflect a numerical noise due to input deck initialization. In fact, the initial conditions selected in the reference simulations are the following ("cold start-up"):

- Time 0 s: the temperature is equal to the feed-water temperature (335 °C) in the water and lead sides and in the heat structures. Water is flowing in the feed-water tube, lead is stagnant.
- Up to 500s: The lead side temperature gradually increases up the maximum value of 480 °C. The lead flow rate gradually increases up to the steady value of 6.3676 kg/s (at 500 s).
- After 1100s the system is found to be in equilibrium (based on simulations extended up to 6000 s).

If has been found as sensitivity analysis that there are no major difference compared to the reference results excepts the occurrence of condensation at feed-water –tube surface end (it disappears) if the following initial conditions are fixed ("hot start-up"):

- Time 0 s: the lead side is at 480 °C and the heat structures 1100 and 1110 are initialized at 450 °C. The mass flow rate of lead and water is null.
- Up to 50 s: The lead and water flow rate increases to their steady value: 0.0473 kg/s for water and 6.3676 kg/s for lead.
- The calculation has been extended to 6000 s in order to reach steady state conditions with high confidence.

The complete documentation of this sensitivity analysis is given in Ref. [36].

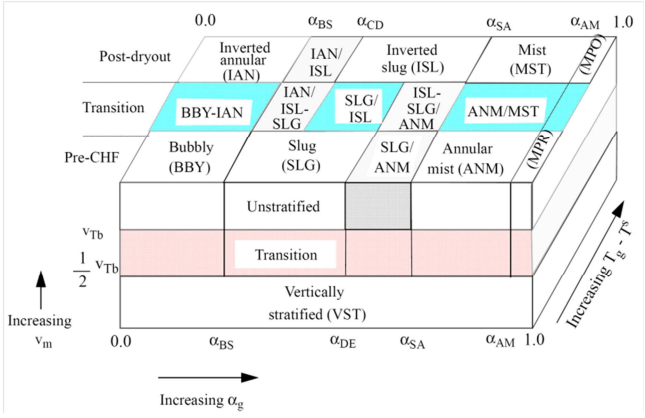

Fig. 31 – Flow regimes for vertical ducts for vertical ducts according to RELAP-5.

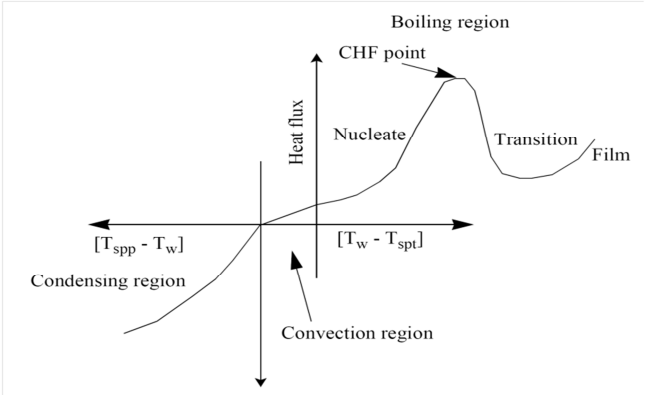

Fig. 32 – Heat transfer mode map at heat structures boundaries according to RELAP-5.

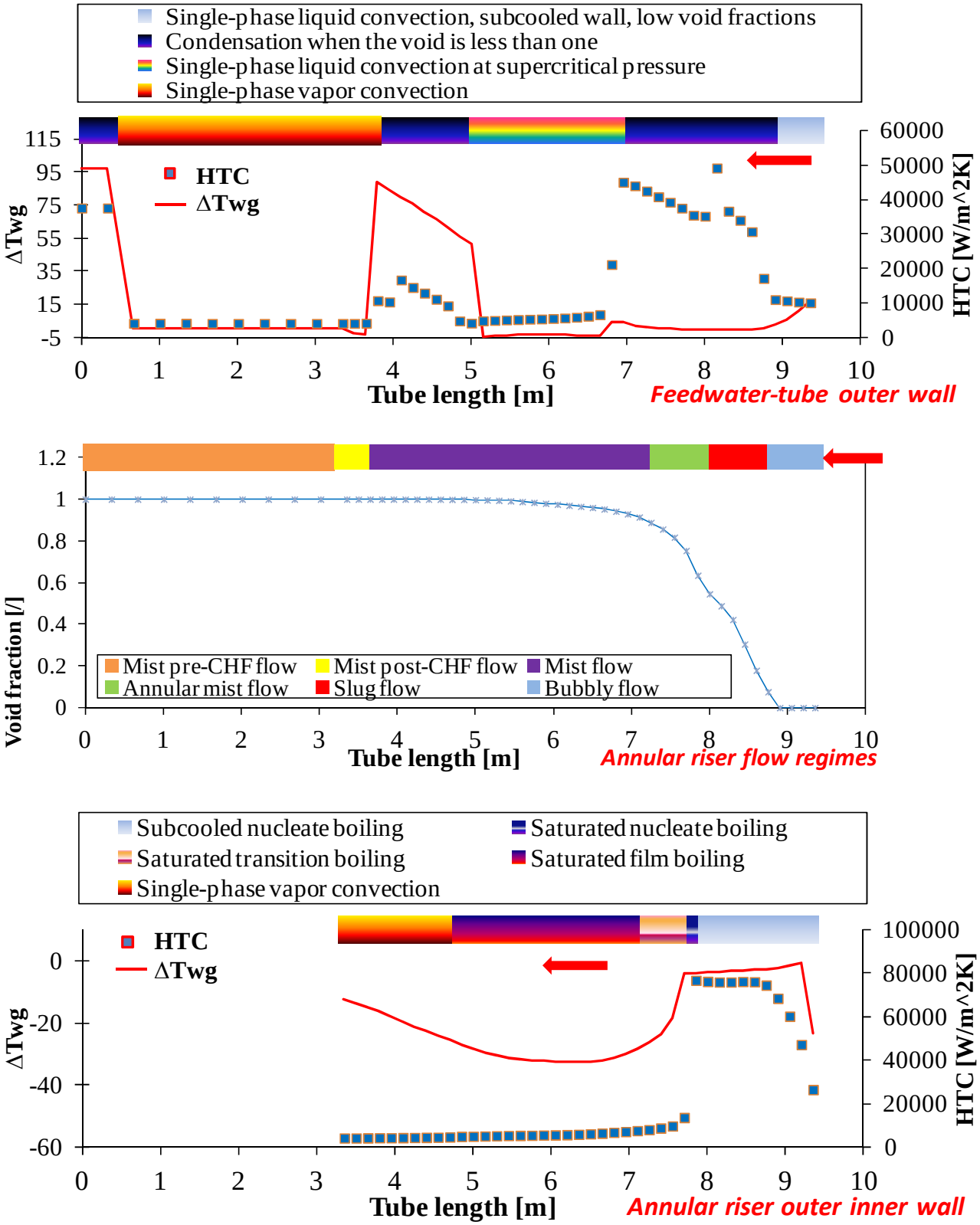

Fig. 33 – SGBT vs. RELAP5 v 3.3, reference simulation Case 1, flow regimes and heat transfer regimes at tube walls in the water-steam side.

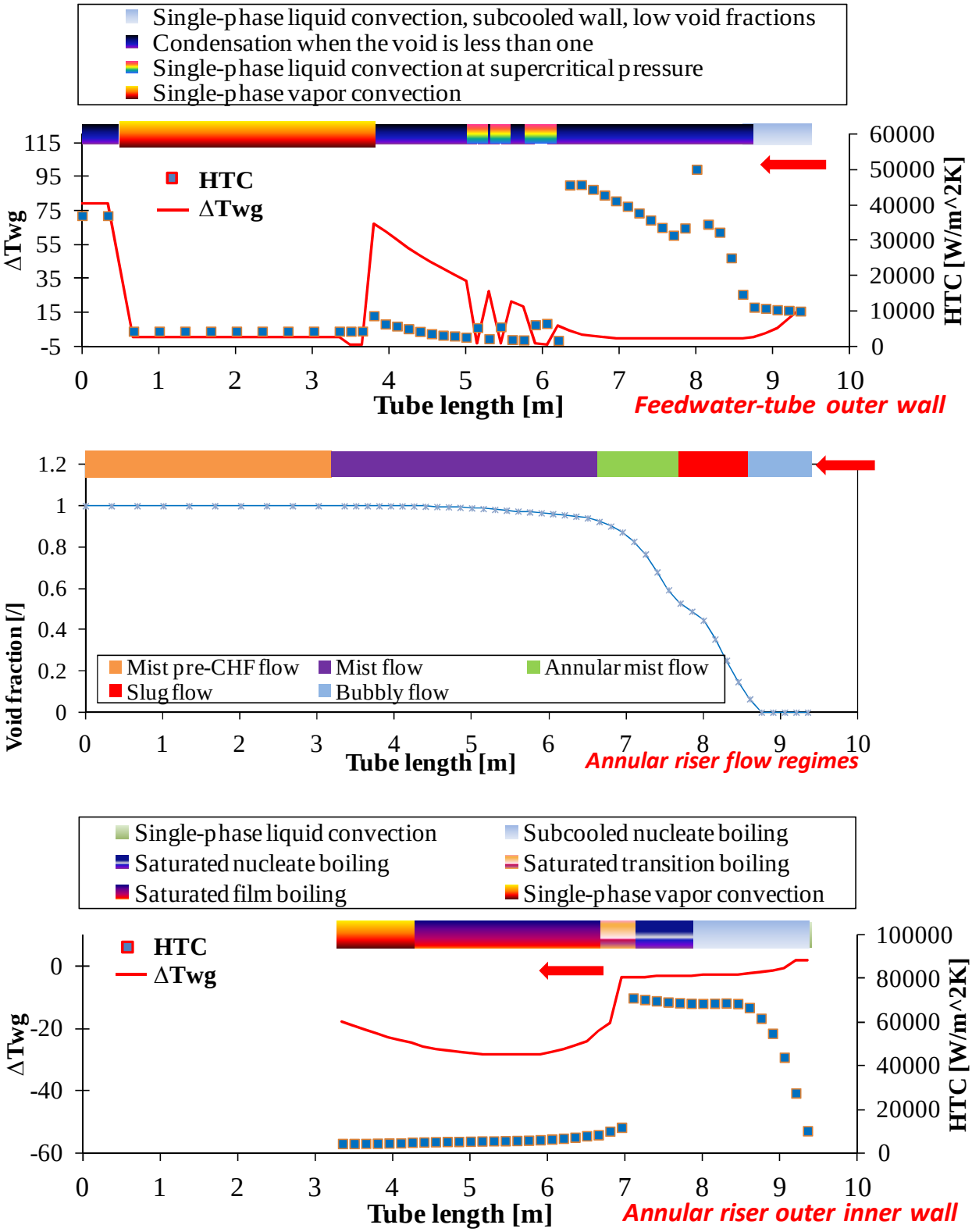

Fig. 34 – SGBT vs. RELAP5 v 3.3, reference simulation Case 2, flow regimes and heat transfer regimes at tube walls in the water-steam side.

4.3 Sensitivity analyses

The sensitivity analysis is a fundamental tool for the assessment of the code capabilities and the design options. Different objectives shall be fulfilled such as to demonstrate the robustness of the calculation, to characterize the reasons for possible discrepancies between calculated trends, to optimize code results and user option choices, to improve the knowledge of the code by the user and to optimize the detailed design. These simulations pursuit the following main objectives:

- To assess the nodalization effects
- To assess materials changes
- To assess alternative design solutions
- To assess the tube bundle geometry
- To assess the influence of different boundary and initial conditions

In the present section, the focus is limited to the steam outlet temperature as main figure of merit of the tube performance; however, they have been completely documented in Ref. [36] taking into account several TH parameters.

The sensitivity analyses are summarized in *Tab. 16* and *Tab. 17*, the following conclusions may be drawn:

- The number of axial nodes in the active length has minor influence above the reference choice (40 nodes).
- The porosity assumed to model the powder (0.3 in the reference calculations) impacts on the steam outlet temperature. If 0.55 porosity is assumed the temperature drop may range between 22°C (case1) and 95°C (case2) being the correlation adopted to model the powder conductivity largely affected by porosity, especially those of case 2.
- The annulus component has a minor influence on the steam outlet temperature if it is assumed to simulate the annular riser instead of the pipe component.
- Copper, Si-C, Al-N and brass powders are potential alternative to sintetic diamond since they allow to reach acceptable steam outlet temperatures. AISI-316 powder could be assumed only as back-up solution for scaled down experimental prototype of SG with double wall bayonet tube. Additional details are given in section 5.1.5.
- Insulating material such as Stone wool, Gemcowool®, Pyrogel®, Supertherm, Vacuum and air are potential alternative to RHY-12 paint. They are analyzed in section 5.2.2.
- Surface finned annular riser and a variation of tube length in the order of +/- 0.5m have minor influence on the steam outlet temperature.
- As discussed in 4.2.3, the hot initialization eliminates steam condensation on the outer surface of the feed-water tube at its inlet.

Id	Description	Sub RUN	Modification	Steam outlet temperature
RUN#0	**Powder conductivity according to Case1**	**RUN#0a**	**--**	**453.9°C**
RUN#1a	Number of axial nodes	RUN#1.1a	10 axial nodes in the active length instead of 40	442.7
		RUN#1.2a	20 axial nodes in the active length instead of 40	450.0
		RUN#1.1a	80 axial nodes in the active length instead of 40	456.1
RUN#2a	As reference different powder porosity	RUN#2.1a	Porosity equal to 0.35 instead of 0.30	452.5°C
		RUN#2.2a	Porosity equal to 0.40 instead of 0.30	449.5°C
		RUN#2.3a	Porosity equal to 0.45 instead of 0.30	445.1°C
		RUN#2.4a	Porosity equal to 0.50 instead of 0.30	440.8°C
		RUN#2.5a	Porosity equal to 0.55 instead of 0.30	431.5°C
RUN#3a	As reference ANNULUS component checked	RUN#3.1a	Annulus 110 instead of pipe-110	459.2
RUN#4a	As reference with different powder materials	RUN#4.1a	Si-C powder instead of sintetic diamond	446.6
		RUN#4.2a	Al-N powder instead of sintetic diamond	443.6
		RUN#4.3a	Cu powder instead of sintetic diamond	451.9
		RUN#4.4a	Brass powder instead of sintetic diamond	446.9
		RUN#4.5a	AISI-316 powder instead of sintetic diamond	408.2
RUN#5a	As reference with different insulating materials	RUN#5.1a	Stone wool instead of RHY-12	452.3
		RUN#5.2a	Gemcowool® instead of RHY-12	453.3
		RUN#5.3a	Pyrogel® instead of RHY-12	454.0
		RUN#5.4a	Supertherm instead of RHY-12	454.4
		RUN#5.5a	$BaLa_2Ti_3O_{10}$ outer coated (400μm) instead of RHY-12 sandwich	444.0
		RUN#5.6a	Vacuum	455.1
		RUN#5.7a	Air	452.8
RUN#6a	As reference with finned annular riser	RUN#6.1a	As reference 120% heated perimeter	455.1
RUN#7a	As reference with different tube active length	RUN#7.1a	Active length 5.5m instead of 6m	446.1
		RUN#7.2a	Active length 6.5m instead of 6m	459.9
RUN#8a	Initialization	RUN#8.1a	As reference "hot conditions at start up" (to avoid condensation at feed-water tube outer surface)	453.9°C

Tab. 16 - SGBT vs. RELAP5 v 3.3, sensitivity analyses: steam outlet temperatures case 1.

Id	Description	Sub RUN	Modification	Steam outlet temperature
RUN#0	**Powder conductivity according to Case2**	**RUN#0b**	**--**	**436.1°C**
RUN#1b	Number of axial nodes	RUN#1.1b	10 axial nodes in the active length instead of 40	424.9
		RUN#1.2b	20 axial nodes in the active length instead of 40	431.4
		RUN#1.1b	80 axial nodes in the active length instead of 40	438.1
RUN#2b	As reference different powder porosity	RUN#2.1b	Porosity equal to 0.35 instead of 0.30	424.6
		RUN#2.2b	Porosity equal to 0.40 instead of 0.30	410.5
		RUN#2.3b	Porosity equal to 0.45 instead of 0.30	394.1
		RUN#2.4b	Porosity equal to 0.50 instead of 0.30	380.0
		RUN#2.5b	Porosity equal to 0.55 instead of 0.30	368.0
RUN#3b	As reference ANNULUS component checked	RUN#3.1b	Annulus 110 instead of pipe-110	442.2
RUN#4b	As reference with different powder materials	RUN#4.1b	Si-C instead of sintetic diamond	420.9
		RUN#4.2b	Al-N powder instead of sintetic diamond	Not executed
		RUN#4.3b	Cu powder instead of sintetic diamond	Not executed
		RUN#4.4b	Brass powder instead of sintetic diamond	Not executed
		RUN#4.5b	AISI-316 powder instead of sintetic diamond	Not executed
RUN#5b	As reference with different insulating materials	RUN#5.1b	Stone wool instead of RHY-12	435.2
		RUN#5.2b	Gemcowool® instead of RHY-12	435.8
		RUN#5.3b	Pyrogel® instead of RHY-12	436.2
		RUN#5.4b	Supertherm instead of RHY-12	436.4
		RUN#5.5b	BaLa2Ti3O10 outer coated (400μm) instead of RHY-12 sandwich	430.3
		RUN#5.6b	Vacuum	436.8
		RUN#5.7b	Air	435.7
RUN#6b	As reference with finned annular riser	RUN#6.1b	As reference 120% heated perimeter	438.3
RUN#7b	As reference with different tube active length	RUN#7.1b	Active length 5.5m instead of 6m	425.8
		RUN#7.2b	Active length 6.5m instead of 6m	444.2
RUN#8b	Initialization	RUN#8.1b	As reference "hot conditions at start up" (to avoid condensation at feed-water tube outer surface)	436.1 °C

Tab. 17 - SGBT vs. RELAP5 v 3.3, sensitivity analyses: steam outlet temperatures case 2.

5 Theoretical activities in support to the development of SGBT

5.1 Porous materials

Porous material are here analysed with the aim to assess high thermal conductivity filling materials for the application to the SGBT, between the double wall. Porous medium deals with materials consisting of a solid matrix with an interconnected void. It is assumed that the solid matrix is either rigid (the usual situation) or it undergoes small deformation. The interconnectedness of the void (the pores) allows the flow of one or more fluids through the material. In the simplest situation ("single-phase flow"), a single fluid saturates the void [39]. The porosity φ of a porous medium is defined as the fraction of the total volume of the medium that is occupied by void space, *Eq. 1*. Thus, (1 - φ) is the fraction that is occupied by solid. Assuming the solid fraction Ψ = (1 - φ) their relations with densities are expressed by (*Eq. 2*):

$$\varphi = \frac{(\rho_s - \rho_m)}{(\rho_s - \rho_f)} \qquad \textit{Eq. 1}$$

$$1\text{-}\varphi = \Psi = \frac{(\rho_m - \rho_f)}{(\rho_s - \rho_f)} \qquad \textit{Eq. 2}$$

Where:

s, f, m refers to solid, fluid and overall volume respectively,
φ porosity [/],
ρ density [kg/m^3],
v average fluid velocity [m/s],
Ψ solid fraction [/],

For an isotropic medium the "surface porosity" (that is, the fraction of void area to total area of a typical cross section), will normally be equal to φ. If the medium is generic, the total porosity will depends on three main contributors:

- The void space between particles (which depends on particle shape and size and on the compaction grade of the mixture);
- The void space inside the particle which communicates with the void space between particles by means of its boundaries (named open porosity) and
- The void space inside the particles which does not communicate with the void space between particles (named closed porosity).

Heat transport through porous media is of great interest in chemical, mechanical, geological, environmental and petroleum applications [40]. Packed beds are widely used in various industrial equipment including heat exchangers, dryers, absorbers, distillation and extraction columns, chemical reactors, calcinators, and incinerators. Porous media applications arise also in the design of cryocoolers, heat pipes, enhanced oil recovery, and geothermal and petroleum applications (involving porous rocks and soil). Recent applications of porous media arise in microelectronics for electronic packaging (device encapsulation) as thermal interface materials (TIM) for efficient disposal of the generated heat.

5.1.1 Conductivity of porous media

In general, the structure of a porous medium is very complex, consisting of different grain (pore) sizes and geometries. A detailed prediction of the effective thermal conductivity of heterogeneous media requires knowledge of the shape, size, location (distribution) and conductivity of each particle in the system together with interaction between particles [39].

If the heat conduction in the solid and fluid phases occurs in parallel, *Eq. 3* gives the overall conductivity k_A. On the other hand, if the structure and orientation of the porous medium is such that the heat conduction takes place in series, with all of the heat flux passing through both solid and fluid, then the overall conductivity k_H is given by *Eq. 4*:

$$k_A = (1-\varphi)k_s + \varphi k_f \qquad \textit{Eq. 3}$$

$$\frac{1}{k_H} = \frac{(1-\varphi)}{k_s} + \frac{\varphi}{k_f} \qquad \textit{Eq. 4}$$

We always have $k_H \leq k_A$, with equality if and only if $ks = k f$. Therefore, k_A and k_H will provide upper and lower bounds, respectively, on the effective conductivity k_m.

For practical purposes, a rough and ready estimate for k_m is provided by k_G, the weighted geometric mean of k_s and k_f , defined by [39]:

$$k_G = k_s^{(1-\varphi)} \cdot k_f^{\varphi} \qquad \textit{Eq. 5}$$

For a sufficiently dilute dispersion (suspension) of spheres, Maxwell (1865) obtained the following expression for the stagnant thermal conductivity of a packed-sphere bed [40]:

$$\frac{k_m}{k_f} = \frac{[2\varphi + (k_s/k_f)(3-2\varphi)]}{[(3-\varphi) + (k_s/k_f)\varphi]} \qquad \textit{Eq. 6}$$

Assuming $\lambda = (k_s / k_f)$

$$\frac{k_m}{k_f} = \frac{[\lambda + 2 - 2\Psi(1-\lambda)]}{[\lambda + 2 + \Psi(1-\lambda)]} \qquad \textit{Eq. 7}$$

Maxwell's equation is valid for $\Psi \rightarrow 0$, since it was derived on the assumption that the solid spheres are sufficiently apart that they do not mutually interact. Nevertheless, it provides a lower bound for the stagnant thermal conductivity of a packed-sphere bed.

Lord Rayleigh (1892) extended Maxwell's model to higher order in the particle concentration Ψ, by taking into account the concentration of induced octupole moments. The case of a cubic array of uniform size spheres (simple cubic packing) was considered, and the effect on the potential in the neighborhood of a sphere by 248 of its closest neighbors (lying within the first 15 shells around a central sphere) was investigated. Rayleigh solved the Laplace equation for the potential inside and a sphere invoking the principle of superposition to take into account the effect of surrounding spheres

on the field in the neighborhood of the central sphere. The following expression is obtained for the effective thermal conductivity of the packed bed [40]:

$$\frac{k_m}{k_f} = \frac{\left\{\left[\frac{(\lambda+2)}{(1-\lambda)}\right] - 2\Psi - 0.525\left[\frac{(3-3\lambda)}{(4+3\lambda)}\right]\Psi^{\frac{10}{3}}\right\}}{\left\{\left[\frac{(\lambda+2)}{(1-\lambda)}\right] + \Psi - 0.525\left[\frac{(3-3\lambda)}{(4+3\lambda)}\right]\Psi^{\frac{10}{3}}\right\}} \qquad \textit{Eq. 8}$$

This expression approaches Maxwell's result by neglecting higher order terms in Ψ. At Ψ = 0.5236, the spherical particles in the cubic lattice are in point contact, and for $\lambda \rightarrow + \infty$ the effective conductivity should approach ∞ at Ψ = 0.5236. These qualitative conditions are not satisfied by Rayleigh's expression.

Meredith and Tobias (1960) modified Rayleigh's result, providing an analytical expression that agrees more satisfactorily with the data in the critical range near Ψ = 0.5236. This expression is as follows [40]:

$$\frac{k_m}{k_f} = \frac{\left\{\left[\frac{(\lambda+2)}{(1-\lambda)}\right] - 2\Psi - 0.409\left[\frac{(6+3\lambda)}{(4+3\lambda)}\right]\Psi^{\frac{7}{3}} - 2.133\left[\frac{(3-3\Psi)}{(4+3\Psi)}\right]\Psi^{\frac{10}{3}}\right\}}{\left\{\left[\frac{(\lambda+2)}{(1-\lambda)}\right] + \Psi - 0.409\left[\frac{(6+3\lambda)}{(4+3\lambda)}\right]\Psi^{\frac{7}{3}} - 2.133\left[\frac{(3-3\Psi)}{(4+3\Psi)}\right]\Psi^{\frac{10}{3}}\right\}} \qquad \textit{Eq. 9}$$

As $\lambda \rightarrow + \infty$, the data are in satisfactory agreement with the modified expression, except for Ψ = 0.5161 where the data considerably exceed the theory

Woodside (1961) considered a unit cube containing one-eighth of a sphere of radius R. The general case is considered in that the uniform spherical particles are not in contact. The final expression for the effective medium conductivity is shown to be [40]:

$$\frac{k_m}{k_f} = 1 - \left(\frac{6\Psi}{\pi}\right)^{\frac{1}{3}}\left\{1 - \left[\frac{(a^2-1)}{a}\right]\cdot \ln\left[\frac{(a+1)}{(a-1)}\right]\right\} \qquad \textit{Eq. 10}$$

$$a = \left\{1 + \frac{4}{\left[\pi(\lambda-1)\cdot\left(\frac{6\Psi}{\pi}\right)^{\frac{2}{3}}\right]}\right\}^{\frac{1}{2}} \qquad \textit{Eq. 11}$$

In deriving the above equation, it was assumed that

- the gas spaces are small enough that heat transfer by convection may be neglected,
- the isotherms are planes perpendicular to the direction of heat flow.

The second assumption is valid only when $k_s / k_f = 1$. The errors will be greater the larger the value of k_s / k_f . As with Rayleigh's model, it is limited to Ψ = 0.5236. It appears that the accuracy of the model has not been sufficiently tested against measurements.

Zehner and Schlunder (1970) arrived at an analytical expression for the effective stagnant thermal conductivity of a packed bed. They considered for the unit cell one-eighth of a cylinder (inner cylinder of unit radius and outer cylinder of radius R). Fluid is filled between the inner and outer cylinders while the inner cylinder consists of both the solid and the fluid phases with its interface A_{fs} described by [41]:

$$r^2 + \frac{z^2}{[B-(B-1)z]^2} = 1 \qquad \textit{Eq. 12}$$

Where the quantity labeled as B is the shape factor characterizing the geometrical effect of the solid particle. For B →*0*, the boundary becomes the z-axis with no solid volume; for B = 1 the solid becomes a sphere, and for B →+ ∞ the solid occupies the entire inner cylinder.
The effective thermal conductivity of a packed bed is expressed by:

$$\frac{k_m}{k_f} = 1 - \sqrt{1-\varphi} + \frac{2\sqrt{1-\varphi}}{(1-\xi B)} \cdot \left[\frac{(1-\xi)B}{(1-\xi B)^2}\ln\left(\frac{1}{\xi B}\right) - \left(\frac{B+1}{2}\right) - \frac{B-1}{1-\xi B}\right] \qquad \textit{Eq. 13}$$

$$B = C\left[\frac{(1-\varphi)}{\varphi}\right]^m \qquad \textit{Eq. 14}$$

$$\xi = \frac{1}{\lambda} = \frac{1}{\left(\frac{k_s}{k_f}\right)} = \frac{k_f}{k_s} \qquad \textit{Eq. 15}$$

With m =10/9. The constant C depends on the shape of the particle. Zehner and Schlunder suggest that C =1.25, 1.40 and 2.5 for spheres, broken (irregular particles) and cylinders respectively.

Krupiczka approximated a packed bed as a bundle of long cylinders and numerically solved a set of two heat conduction equations in two dimensions with perfect contact at the solid–fluid interface. He then extended the results to a spherical lattice and proposed a correlation for the dimensionless effective thermal conductivity [41]:

$$\frac{k_m}{k_f} = [\lambda]^{(0.208-0.757\ln\varphi-0.057\ln\lambda)} \qquad \textit{Eq. 16}$$

Hsu *et al* developed a lumped-parameter model for the effective stagnant thermal conductivity of some two-dimensional and three-dimensional spatially periodic media. The geometries under investigation include arrays of touching and non-touching in-line squares and cylinders (two-dimensional), as well as touching and non-touching in-line cubes (three-dimensional). The dimensionless effective stagnant thermal conductivity, $k_e{}^{+} = k_m/k_f$, for three-dimensional cubes with thermal resistance is expressed as [41]:

$$\frac{k_m}{k_f} = 1 - \gamma_a^2 - 2\gamma_a\gamma_c + 2\gamma_a^2\gamma_c + \frac{\gamma_a^2\gamma_c^2}{\left(\frac{1}{\lambda}\right)} + \frac{\left(\gamma_a^2 - \gamma_a^2\gamma_c^2\right)}{\left(1-\gamma_a+\frac{\gamma_a}{\lambda}\right)} + \frac{2\left(\gamma_a\gamma_c - \gamma_a^2\gamma_c^2\right)}{\left(1-\gamma_a\gamma_c+\frac{\gamma_a\gamma_c}{\lambda}\right)} \qquad \textit{Eq. 17}$$

The porosity, φ, is related to the geometrical parameters (γ_a and γ_c) by:

$$\Psi = 1 - \varphi = (1-3\gamma_c^2)\gamma_a^3 + 3\gamma_a^2\gamma_c^2 \qquad \textit{Eq. 18}$$

A comparison of the results based on *Eq. 17* with existing experimental data shows that they are in excellent agreement with the experimental data if the contact resistance parameter γ_c = 0.13 is chosen at a porosity of 0.36. However, no comparison with experimental data at different porosities was given. More refined models available for conductivity determination are reported in Ref. [41].

5.1.2 Model comparison

Comparisons of the Zehner-Schlunder model for the effective thermal conductivity of porous media containing spherical particles with the experimental data suggest that the model is satisfactory over a broad range of solid-to-fluid thermal conductivity ratio as high as 1200. The validity of the model is also confirmed over a broad range of solids fraction as high as 0.8 in certain case where data are available. It is remarkable that the one-dimensional representation of this model is able to describe the effective conductivity of porous media over such an extended range of parameters. A comparison of Zehner-Schlunder model with the data of Nozad et al. (1985), suggests that the model with φ = 0.4 agrees well with the experimental data for $\lambda < 10^3$ (*Fig. 35*). For $\lambda > 10^3$, the Zehner-Schlunder model under-predicts the effective stagnant thermal conductivity substantially. For sake of completeness, further comparisons dealing with the described theories and experimental data are reported from *Fig. 36* to *Fig. 39* (see Ref. [40] for a more exhaustive explanation).

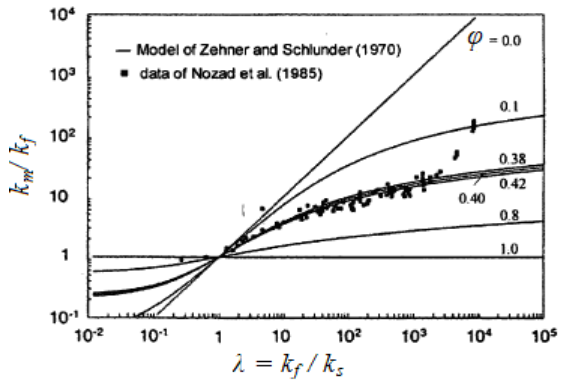

Fig. 35 – Comparison of predictions from Zehner and Schlunder model (1970) with the data of Nozad et al. (1985).

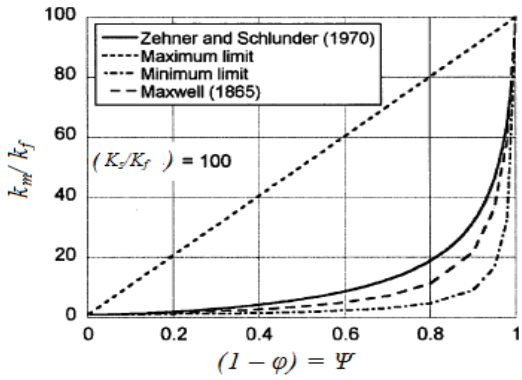

Fig. 36 – Comparison of various models for the full spectrum of porosity.

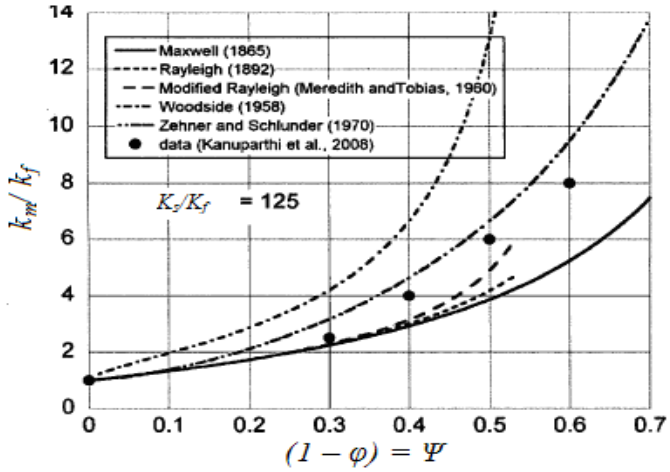

Fig. 37 – Comparison of Zehner and Schlunder model (1970) and other models with the data of Kanuparthi et al. (2008).

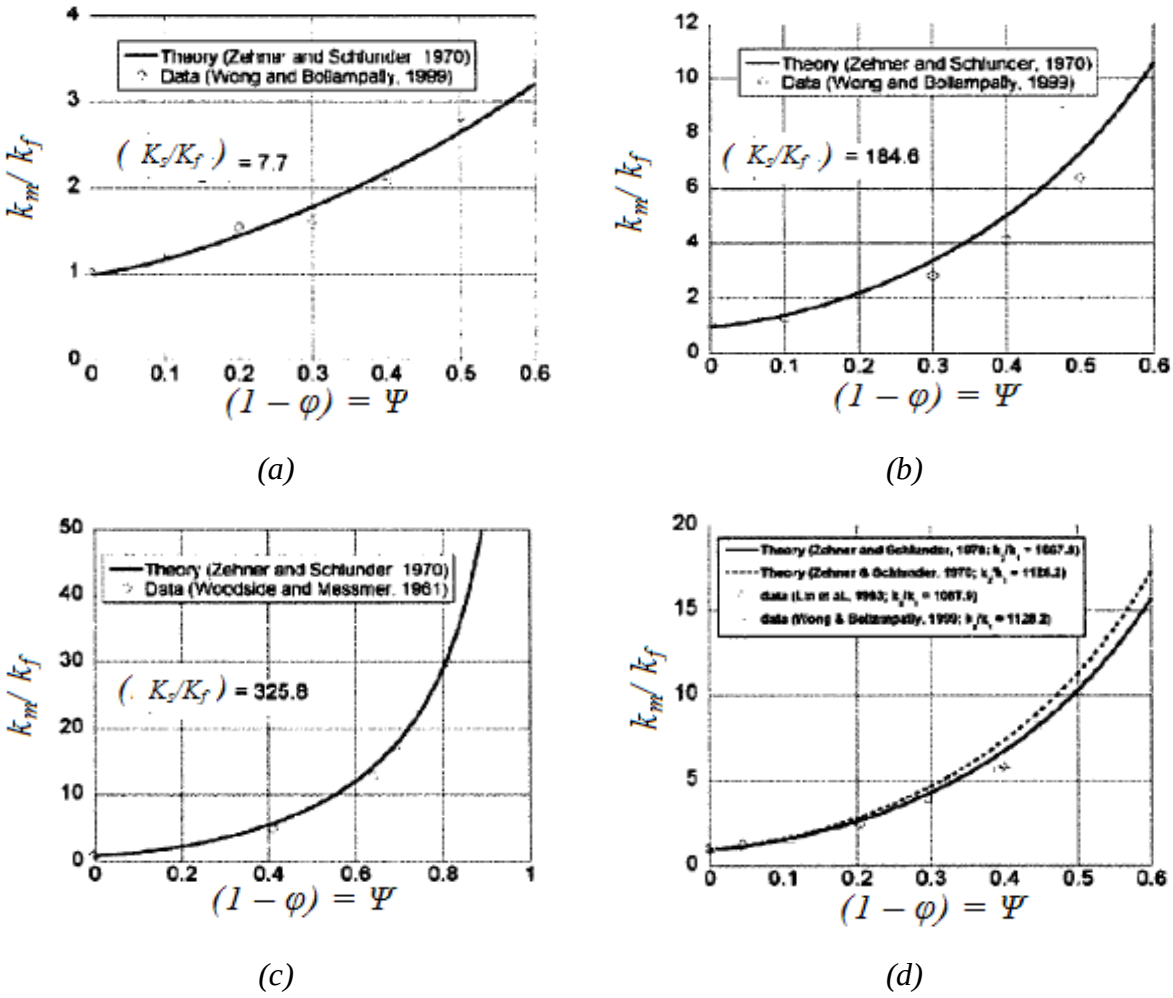

Fig. 38 – Comparison of Zehner and Schlunder model (1970) with the data for a range of thermal conductivity ratio from 8 to 1100.

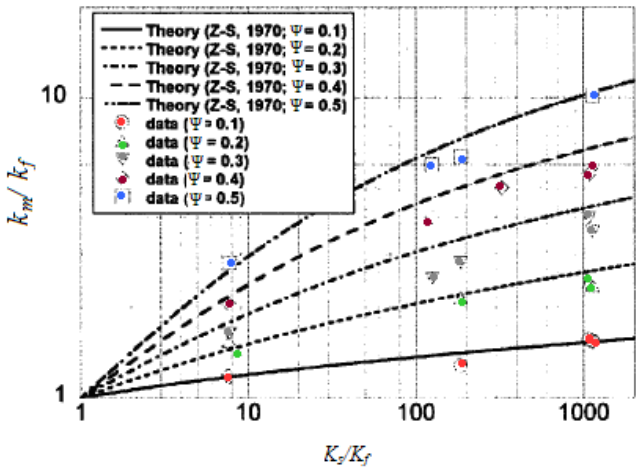

Fig. 39 – Comparison of Zehner and Schlunder model (1970) with the data with the solids fraction as a parameter.

5.1.3 Selection of models for the application to SGBT pretest-calculations

The correlations presented in the previous sections are summarized in Tab. 18. Among these models, *Eq. 5* (named Case 1) and *Eq. 16* (named Case 2) have been selected with the primary aim to support the assessment of the SGBT performance by means of RELAP-5 and to support the design of the TxP facility and the HERO test section. As example, they have been applied to synthetic diamond powder (under helium atmosphere), *Fig. 40* (the detailed calculations are reported in Ref. [42] including a large variety of materials).

Since it is clear that each material requires its own model that accounts for its status, these simple correlations that depend only upon porosity have been selected to develop pre-test calculations mainly because they provide a consistent band among the remaining correlations which is not the theoretical one (parallel and series).

However, the following limitations could in principle be a source of discrepancy between the effective conductivity of a given material and the predictions obtained with these models:

- They do not account for grain shape (it influences the contact area: it increases when deviating from spherical shape),
- They do not account for grain dimension (it influences the contact area: it increases when increasing the total surface area of the grains and their dimension heterogeneity),
- They do not account for open porosity (it reduces the contact area providing a sort of film of fluid between grains),
- They do not account for thermal effects on grain (i.e. thermal activated compaction phenomena),
- They do not account for geometrical boundaries (if the same powder is contained into a cylinder or into an annulus or into a sphere its porosity at the boundaries will be different; being the influence on the average porosity relevant for geometries that have large surface boundaries / bulk ratio, as for the annular geometry of the SGBT).

Id.	Descript.	Correlation	Notes
Case 1	--	$k_G = k_s^{1-\varphi} k_f^{\varphi}$	Ref. [39]
Case 2	Kupriczka model	$k_e^{+} = \frac{k_e}{k_f} = (\beta)^{0.280-0.757\log\varphi-0.057\log\beta}$	Ref. [41]
Case 3	Maxwell model	$\frac{k_e}{k_f} = \frac{2\varphi + (k_s/k_f)(3-2\varphi)}{3-\varphi+(k_s/k_f)\varphi}$	Ref. [40]
Case 4	Rayleigh model	$\frac{k_e}{k_f} = \frac{[(2+\lambda)/(1-\lambda)] - 2\phi - 0.525[(3-3\lambda)/(4+3\lambda)]\phi^{10/3}}{[(2+\lambda)/(1-\lambda)] + \phi - 0.525[(3-3\lambda)/(4+3\lambda)]\phi^{10/3}}$	Ref. [40]
Case 5	Rayleigh Extended model	$\frac{k_e}{k_f} = \frac{\frac{2+\lambda}{1-\lambda} - 2\phi + 0.409\frac{6+3\lambda}{4+3\lambda}\phi^{7/3} - 2.133\frac{3-3\phi}{4+3\phi}\phi^{10/3}}{\frac{2+\lambda}{1-\lambda} + \phi + 0.409\frac{6+3\lambda}{4+3\lambda}\phi^{7/3} - 0.906\frac{3-3\lambda}{4+3\lambda}\phi^{10/3}}$	Ref. [40]
Case 6	Zehner model	$\frac{k_e}{k_f} = 1-(1-\varphi)^{1/2} + \frac{2(1-\varphi)^{1/2}}{1-B/\beta}\left[\frac{(1-1/\beta)B}{(1-B/\beta)^2}\ln\frac{\beta}{B} - \frac{B+1}{2} - \frac{B-1}{1-B/\beta}\right]$ $B = 1.25\left(\frac{1-\varphi}{\varphi}\right)^{10/9} \qquad \beta = k_s/k_f$	Ref. [41]
Parallel	--	$k_m = (1-\varphi)k_s + \varphi k_f$	Ref. [39]
Series	--	$\frac{1}{k_H} = \frac{(1-\varphi)}{k_s}k_s + \frac{\varphi}{k_f}$	Ref. [39]

Tab. 18 – Summary of the correlations investigated to assess the conductivity of the powders.

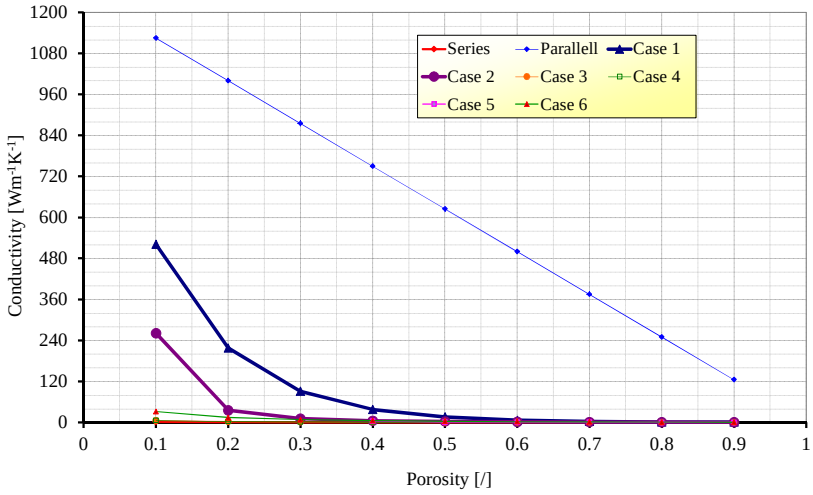

Fig. 40 – Numerical evaluation of thermal conductivity of Diamond powder: comparison of different models as function of porosity.

5.1.4 Screening of candidate powders

Six criteria have been developed in order to make a screening among candidate powders that are applicable to the SGBT and to individuate the powders to be tested. The materials that fit criterion 1 and 2 are listed in Tab. 19.

Criterion 0 Toxicity
The material should be managed with no particular cautions excepts the use of masks for powders.

Criterion 1 Thermal conductivity:
One of the most important features required by the filling material is the high value of the thermal conductivity. In order to enhance the global heat transfer coefficient, a conductivity in greater than 15 W/(mK) of the pure 99.5% dense material is required.

Criterion 2 Melting point:
The operative conditions expected in ALFRED SG are 400°C - 480°C for the primary coolant. In order to maintain the integrity of the SG in any operating condition, normal operational transient or accidental, it is required that the powder's melting temperature is sufficiently above these values. An inferior limit for this parameter can be fixed to 600 °C.

Criterion 3 Solid phase transitions temperatures:
In the expected operating conditions, allotropic phase transformations of the candidate materials have to be checked. In particular, it should be verified that phase transformations do not induce specific volume variations, or thermal conductivity deterioration, or the formation of anisotropies directions within the material.

Criterion 4 Chemical reactions:
No exothermic chemical reactions with molten lead, air, water and steam are allowed. Oxidation should also be avoided.

Criterion 5 Radiation damage
The effect of the radiation damage on thermal conductivity and on mechanical behavior of powder is more or less unknown. Nevertheless, materials that experience massive nuclear reactions with neutrons have to be avoided. It is assumed that materials with consistent neutron capture microscopic cross section (σa) that give rise to activation are excluded.

5.1.5 Selection and assessment of candidate powders

At the end of this process [42], based on the materials available at some partners of ENEA, these samples of powders where acquired for pre-test purpose:

- Copper (elettrolitic) type LT-12
- Copper type W-60-M
- Brass type OT-63
- Stainless steel type AISI-316
- Sintetic diamond
- Si-C
- Aluminum Nitride

With the exception of AISI-316, these materials allow to reach super-heated steam temperatures close to 450 °C, *Fig. 41*. The figure is obtained by RELAP-5 calculation as sensitivity analysis of the model described in section 4.1 in which the conductivity is modeled according to *Eq. 5* (case 1) and the powder is assumed 70 % TD. Even if the super-heated steam temperature decreases to 410°C if ASI-316 is adopted, this material will be checked since it has been successfully operated in the Hx of the NACIE facility and could be a back-up solution for a prototypic mockup of SG if the other materials will reveal some un-expected technological/practical limitations.

Criterion 1 Melting point **Criterion 2 Thermal conductivity**		
Material	**Melting point (°C)**	**Thermal conductivity (at 100°C) [W/mK]**
Al	660	240
Ag	961	422
Cr	1860	88
Cu	1084	391
Fe	1536	72
Mg	650	154
Mo	2620	135
Ni	1453	83
Si	1410	112
W	>2000	166
AISI1010	1510	61
Brass (30%Zn)	930	133
Boron-Nitride	>2000	160
Diamond	>2000	1250
AISI-316	1500	18
Aluminium-Nitride	>2000	90
Silicon Carbide	>2000	100

Tab. 19 – Criteria 1 and 2 conductivity and melting point.

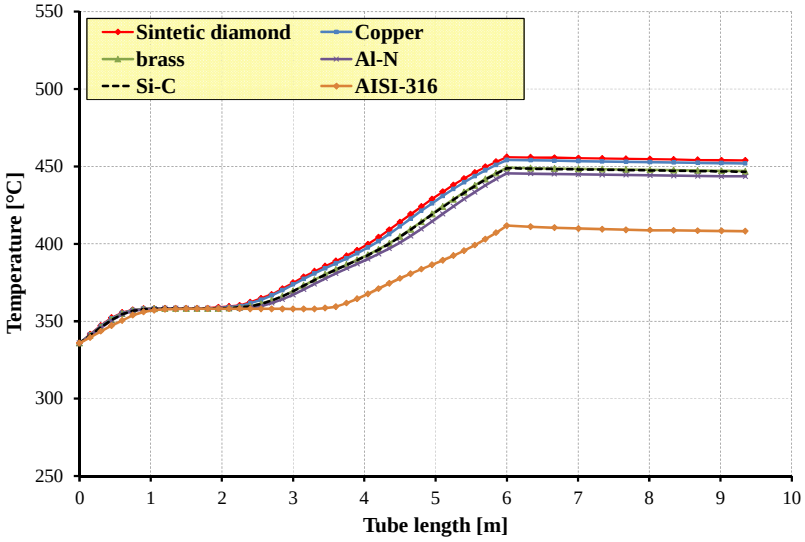

Fig. 41 – SGBT vs. RELAP5 v 3.3, sensitivity analysis, influence of the powder material, annular riser temperature as function of tube length.

5.2 Insulating materials

The present section investigates practical solutions for the minimization of the heat exchange between the feed-water that crosses in down-flow the first tube and the superheated steam that rises up in the annular space. In the SG configuration proposed by Ansaldo [11], an insulator layer has been introduced between the super-heated steam and the descending feed-water in order to prevent the loss of efficiency in the SG zone located above the active height. The preliminary solution proposed consists of a paint with a thermal conductivity in the order of 0.05 W/m K which is named RHY-12. The paint is located between the feed-water tube and the left boundaries of the annular cavity.

Two different solutions are here considered [34][35]:

- The first option is the conceptual design as depicted in *Fig. 18*. Paints, traditional fillers or other alternative composite materials at low conductivity are investigated.
- The second option is a major modification of the initial conceptual design. It consists of a single central inner tube joined with an outer insulating coating material. Ceramic coating materials are investigated.

Air or vacuum environment are also suitable back-up solutions that are in principle applicable to the first option.

5.2.1 Screening of candidate insulating materials

Six criteria have been developed in order to make a screening among the candidate materials and to individuate the most promising solutions. The criteria were assumed in a general way so that they can refer (in most situations) to all categories of materials [43].

Criterion 1 Thermal conductivity:
In order to minimize the heat transfer between feed-water and superheated steam, the conductivity has been fixed by ANSALDO Nucleare equal or lower than 0.05 W/m K. We decided to increase the limit up to 0.5 W/m K in order to investigate the alternative solution since ceramic materials coating have higher conductivities.

Criterion 2 Melting point:
The operative conditions expected in ALFRED SG are 335 °C in the feed-water line and 450 °C in the steam line. The integrity of the insulating material does not affect the heat removal safety function. Therefore, the maximum temperature can be conservatively fixed at 500 °C.

Criterion 3 Solid phase transitions temperatures:
In the expected operating conditions, allotropic phase transformations of the candidate materials have to be checked. In particular, it should be verified that phase transformations do not induce specific volume variations, or thermal insulation deterioration, or the formation of anisotropies directions within the material.

Criterion 4 Chemical reactions:
No exothermic chemical reactions with molten lead, air, water and steam are allowed. Oxidation should also be avoided.

Criterion 5 Radiation damage

The effect of the radiation damage on thermal conductivity and on mechanical behavior of insulating materials is more or less unknown. Nevertheless, materials that experience massive nuclear reactions with neutrons have to be avoided. It is assumed that materials with consistent neutron capture microscopic cross section (σa) that give rise to activation are excluded.

5.2.2 Selection and assessment of insulating materials

A series of thermal insulating materials are assessed based on the criteria provided in the previous section. The objective of this screening is the selection of the most promising solutions that can guarantee adequate thermal insulation in the conditions achieved during the operation of ALFRED SG. The investigated materials are reported in *Tab. 20* [43]. They are grouped in four categories:

- Traditional fillers: industrial solutions used in a large variety of applications.
- Alternative composite materials: new generation materials whose usage in industrial field is currently limited and which are characterized by composite nature and high cost. For example, Aerogel is a synthetic porous material derived from a gel, where the liquid component has been replaced with a gas by extracting the liquid through supercritical drying. The result is a solid with extremely low density and thermal conductivity.
- Thermal insulating paints: based on plastic materials joined with ceramic microspheres which worsen the heat transfer. When they are mixed into paint, the microscopic round hollow microspheres compress on the painted surface as the paint dries. They form a tightly packed layer close to the surface, that reflects and dissipates heat by minimizing the path for its transfer. An advantage of this solution is the space saving: paint is applied at approximately 100 µm and it dries to approximately 50% in film thickness. This allows to achieve good thermal resistance with many paint layers in small thickness.
- Ceramic coatings: ceramic materials capable to form Thermal Barrier Coatings (TBCs) on tube surfaces. These class of solutions is connected to the possibility to change the inner tube configuration realizing an external coating on the feed-water inlet tube. In general, ceramic materials for TBC applications must satisfy several items: good sintering resistance at high temperature, phase stability in operating temperature range, low thermal conductivity as to achieve desirable thermal barrier effect, capability to form a coating with stoichiometric composition and well-controlled structure. There are two manufacturing techniques which are considered as viable ways to fabricate TBCs under industrial conditions: the Plasma-Spraying (PS) technique and the evaporation technology by means of Electron Beam Physical Vapor Deposition (EBPVD). Also another recent and promising deposition technique can be considered, the detonation thermal spraying process. TBCs usually consists of a duplex system. The actual thermal barrier is a ceramic top coating with the prime function to reduce the heat transfer to the metallic substrate. Between the TBC and the substrate a metallic corrosion resistant coating is applied, which protects the substrate from oxidation and high temperature corrosion and provides the necessary adhesion of the ceramic to the metallic material. These bond coatings are either overlay or diffusion coatings. During processing and in service a Thermally Grown Oxide (TGO) layer forms as a result of bond coat oxidation: it plays the most important role for the adherence of the TBC

In the preliminary analysis, only the first two criteria are verified. In this way it is possible to exclude most of the materials and only those that survived this screening are assessed against the remaining criteria. The analysis and selection of the candidate insulating materials are summarized

in Ref. [43]. At the end of the analysis, only seven candidate materials survived the process and they may be selected for potential use in the ALFRED SG, their conductivities are attached in Tab. 21. Five materials refer to the reference design option. Stone wool [44] and Gemcowool® [45] (a high temperature insulation wool produced by Refractory Specialties Incorporated) are traditional fillers. Pyrogel® [46] (a silica aerogel insulation blanket produced by Aspen Aerogels®) is an alternative composite material. Supertherm [47] (developed by Enercheck Systems Inc. society) and RLHY-12[48] (produced by Beijing Ronglihengye Technology Company) are thermal insulating paints. ZIRCO-FOAM-250 is foam produced by the Italian society Zircofoam [51]. The last material refers to tube outer coating. It is a TBC based on a recent ceramic compound ($BaLa_2Ti_3O_{10}$ [49][50]), characterized by a thermal conductivity that is close to the acceptability limit.

The effect of the insulating material on the TH performance of the SGBT has been analyzed by means of RELAP-5 and is reported in *Fig. 42*. *Fig. 42* – (a) depicts the temperature drop along the feed-water descending tube under the hypothesis adopted to develop case 1 (see section 4.1) assuming the conductivities reported in *Tab. 21* instead of 0.05 W/mK: all the materials behave similar to the reference assumption. The assessment of TBC required to modify the input deck geometry (since it is an external coating), it is shown in *Fig. 42* – (b). Assuming a standard thickness of the coating of 400μm the temperature drop along the feed-water descending tube is un-acceptable. The analysis highlights that a theoretical coating thickness of 4.7 mm is required to achieve a temperature drop comparable to the reference case which is clearly not achievable (external coating as insulator is therefore abandoned).

In conclusion, these materials are retained suitable for SGBT application:

- Stone wool (traditional filler);
- Gemcowool® (traditional filler);
- Pyrogel® (alternative composite material);
- Supertherm (insulating paint);
- RLHY-12 (insulating paint);
- Zirco-foam 250 (traditional filler)

CATEGORY	SUB-CATEGORY	MATERIALS
Traditional fillers	Mineral or rock wool	Glass wool
		Stone wool
	High temperature insulation wools	Alkaline-earth silicate glass wool
		Aluminum-silicate glass wool
		Polycrystalline wool
	--	Fiberglass
	--	Cellular glass
	--	Vermiculite
		Perlite
	--	Calcium silicate
	Flexible elastomeric foams	Nitrile butadiene rubber
		Ethylene propylene diene monomer
	--	Polyethylene
	Rigid foam	Polyurethane
		Polyisocyanurate
		Phenolic
		Polystyrene
		ZIRCO-FOAM 250
Alternative composite materials	Silica aerogel	Spaceloft®
		Pyrogel®
Insulating paints	--	NanoAyegh
	--	Atriathermika
	--	Thermo-Shield®
	--	Supertherm
	--	RLHY-12
Ceramic coatings	--	$BaLa_2Ti_3O_{10}$

Tab. 20 - Insulating materials.

Material	Category	Conductivity [W/mK]
Stone wool	wool	0.04 (35°C) 0.22 (650°C)
Gemcowool®	wool	0.05 (200°C) 0.23 (980°C)
Pyrogel®	alternative composite	0.02 (0°C) 0.09 (600°C)
Supertherm	paint	0.019 (25°C)
RLHY-12	paint	0.03 (25°C)
$BaLa_2Ti_3O_{10}$	ceramic coating	0.6 (300°C) 0.5 (900°C)
ZIRCO-FOAM 250	foam	0.06 (150°C) 0.11 (600°C)

Tab. 21 – Conductivity of insulating materials.

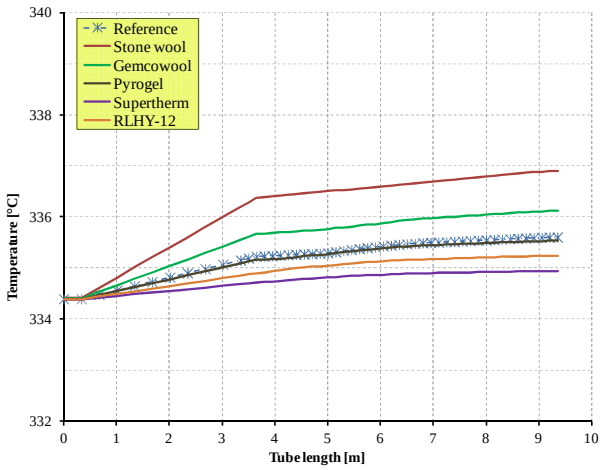

a) Case 1 – reference geometry

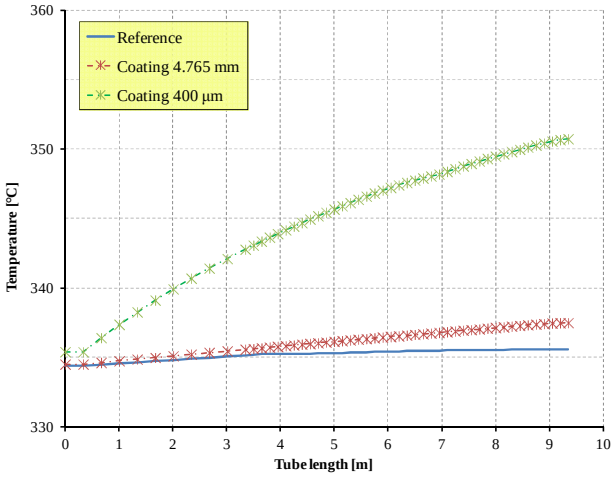

b) Case 1 – outer coating

Fig. 42 – SGBT vs. RELAP5 v 3.3, sensitivity analysis, influence of the insulating material, feed-water temperature as function of tube length.

6 Design and operation of the TxP facility

The construction and operation of the Tubes for Powder (TxP) facility is one of the main results of this doctorate. In fact, this facility has been completely designed by ENEA during the first year of this activity (2011). Its construction (by LIMAINOX), assembling (by ENEA), instrumentation (by ENEA) and subsequent operation required approximately one and half years (2012-2013). The detailed design of TxP is documented in Ref. [14].

The main objectives of TxP are:

- To determine the thermal conductivity of candidate powders.
- To determine the influence of the powder compaction grade on its thermal conductivity (i.e. the influence of the loading procedure, the influence of thermal cycling).
- To investigate the influence of the filling gas (i.e He) at different levels of pressurization.

The facility has been operated both to support the design of the SGBT and to qualify the HXs operated, under operation or under commissioning at ENEA CR Brasimone that make use of double wall design with intermediate powder (see section 3).

During one year TxP experienced several experimental campaigns that include approximately 50 subtests (each of them lasting one or two days). Five of them are retained representative and are summarized in *Tab. 22* distinguishing among the materials under testing, the experimental conditions and the procedures adopted to load the powders. The post-processing of the data points to obtain suitable values of conductivities has been standardized by means of excel routines since it involves thousands of measurements (it will not be presented in this section).

TxP underwent final disposal at the beginning of 2014 due to the cumulated structural damage that arises from its utilization.

Test Id.	Sub-Test	Powder sample	Environment	Loading procedure	Cycle N°	Grain diameter
RUN#0	RUN#0.0	AISI-316	Air	By gravity	fresh	[1-200] μm
	RUN#0.1	AISI-316	Flowing He	--	1	
	RUN#0.2	AISI-316	Air	--	2	
RUN#1	RUN#1.0	AISI-316	Air	1-S[1]	fresh	[1-200] μm
	RUN#1.1	AISI-316	Flowing He	--	1	
	RUN#1.2	AISI-316	Air	--	2	
RUN#2	RUN#2.0	Si-C	Air	2-S[2]	fresh	[149-247] μm
	RUN#2.1	Si-C	Stagnant He 1 bar	--	1	
	RUN#2.2	Si-C	Stagnant He 2 bar	--	2	
	RUN#2.3	Si-C	Stagnant He 3 bar	--	3	
	RUN#2.4	Si-C	Stagnant He 4.5 bar	--	4	
RUN#3	RUN#3.0	Si-C	Air	2-S	fresh	[1-80] μm
	RUN#3.1	Si-C	Stagnant He 1 bar	--	1	
	RUN#3.2	Si-C	Stagnant He 2 bar	--	2	
	RUN#3.3	Si-C	Stagnant He 3 bar	--	3	
	RUN#3.4	Si-C	Stagnant He 4.5 bar	--	4	
RUN#4	RUN#4.0	Si-C	Air	2-S	fresh	[80-105] μm
	RUN#4.1	Si-C	Stagnant He 1 bar	--	1	
	RUN#4.2	Si-C	Stagnant He 2 bar	--	2	
	RUN#4.3	Si-C	Stagnant He 3 bar	--	3	
	RUN#4.4	Si-C	Stagnant He 4.5 bar	--	4	
RUN#5	RUN#5.0	AISI-316	Air	2-S	fresh	[1-200] μm
	RUN#5.1	AISI-316	Air	--	1	
	RUN#5.2	AISI-316	Air	--	2	
	RUN#5.3	AISI-316	Air	--	3	
	RUN#5.4	AISI-316	Air	--	4	
	RUN#5.5	AISI-316	Stagnant He 1 bar	--	5	
	RUN#5.6	AISI-316	Stagnant He 2 bar	--	6	
	RUN#5.7	AISI-316	Stagnant He 3 bar	--	7	
	RUN#5.8	AISI-316	Stagnant He 4.5 bar	--	8	

[1] 1-S: single step vibrated loading procedure (described in section 6.3.1)
[2] 2-S: double step vibrated loading procedure (described in section 6.3.1)

Tab. 22 –TxP experimental programme.

6.1 Description of the TxP facility

6.1.1 Main layout and operating principles

The TxP facility [14][52][53][54] consists of three concentric tubes whose conceptual scheme is reported in *Fig. 43*. The tube labeled as PIPE-5 contains an Heating Rod (HR-14) that generates 25 kW (maximum). PIPE-5 is inserted in PIPE-7 which is contained in PIPE-8. This last tube allows to cool the facility by means of water. Two free volumes are realized in the facility to locate the testing powders. The first is bounded in the annular region HR-14 - PIPE-5 and the second is placed

between PIPE-5 and PIPE-7. The intent of the first zone is to obtain fruitful data on conductivity into a gap of about 15 mm in width while, the gap between PIPE-5 and PIPE-7, is designed to test powders specimens into a smaller gap (about 5 mm in width).

The design includes forty-eight N-type thermocouples located in three azimuthal and four axial directions, *Fig. 44*. Twelve are placed at HR-14 outer surface, twenty-four are located in PIPE-5 (twelve in the inner, twelve in the outer surfaces). The remaining twelve thermocouples are positioned in the inner surface of PIPE-7. The thermocouples located at the gap borders (r_{ext}, r_{int}) allow to measure the temperature difference between the tubes – walls that embed the powders under testing (T_{int}-T_{ext}). The thermal conductivity of the powder is finally calculated by *Eq. 19*.

$$k_e = \frac{q' \ln \frac{r_{ext}}{r_{int}}}{2\pi(T_{int} - T_{ext})} \qquad \textit{Eq. 19}$$

Where:

r_{ext}	powdered gap outer radius (inner radius of PIPE 5 or PIPE7) [m]
r_{int}	powdered gap inner radius (outer radius of HR-14 or PIPE5) [m]
T_{ext}	powdered gap outer surface temperature (at PIPE 5 or PIPE7) [K]
T_{int}	powdered gap inner surface temperature (at HR-14 or PIPE5) [K]
k_e	powder conductivity [W/m-K]
q'	average linear power [W/m]

The quantity q' is obtained measuring the integral power (q) with high accuracy by means of a watt-meter WT230 Digital Power Meter. Two additional thermocouples are placed in HR-14. The first is operated to control the facility ($T_{C\text{-}HR}$), the second allows to shut-down the facility if a safety set point is met ($T_{S\text{-}HR}$). The geometrical and operational data of the facility are given in *Tab. 23*. For sake of completeness, the table compares the sizing of TxP with those of the Brasimone HXs mentioned in section 3. The auxiliary systems include:

- The water line,
- The helium line,
- The control cabinet and,
- The data acquisition system.

6.1.1.1 Feed-water line

The feed-water main line removes the generated heat by flowing into the annular region between PIPE-7 and PIPE-8. It is connected to the service water by pipes and includes three valves V0, V1 and V2. V1 allows the manual regulation of the mass flow rate [0-12.5 l/min]. The service water is demineralized by means of a ionic resin filter that serves the PEC's facilities. The line is instrumented with a flow-meter and four thermo-resistances (T_{IN}, $T_{H2O\text{-}IN}$, T_{OUT}, $T_{H2O\text{-}OUT}$). Two sub-pipelines depart from the main line to cool the bottom ($V1_B$) and the top ($V1_T$) flanges. They are instrumented with two thermocouples (T_{FT}, T_{FB}).

6.1.1.2 Helium line

The helium line includes the helium storage tank (pressurized at 200vbar) with its pressure reducer and safety valves, pipes and two valves ($V1_{He}$, $V2_{He}$).

In the initial design, it was supposed to operate TxP under helium environment as follows (*Fig. 43*):

- $V1_{He}$ and $V2_{He}$ opened: the gas is pumped in the top flange of PIPE-5 (by a hole realized into an intermediate aluminum annular disk that separates the top and bottom parts of the flange), it flows in this tube, it enters PIPE-7 from the bottom by two holes realized in PIPE-5 and it leaves the tube from its top flange (again by a hole realized into an intermediate aluminum annular disk that separates the top and bottom parts of the flange). This procedure is continued for ten minutes in order to eliminate the air form the annular zones.
- After this initialization $V2_{He}$ is closed and the pressure inside TxP is measured by means of a manometer installed at the outlet of the line.
- When the fixed pressure is reached $V1_{He}$ is closed too and the test is prone to be executed.

The pre-tests highlight that this procedure was not achievable because of large Helium leakage from the PIPE-7 top flange. This required a major modification of the helium line (that guaranteed to operate TxP up to 5 bar with minor leakages):

- The holes at the end of PIPE-5 where closed (by welding). As consequence of this, the annular zone PIPE-5 – PIPE-7 can be operated under atmospheric pressure air only.
- $V2_{He}$ was mounted at the line inlet as shown in *Fig. 45*. The manometer was installed after the two valves.
- The initialization of the facility is realized by ten "washing actions" each of them consists in:
  - Pressurization at 4 bar: $V1_{He}$ opened and $V2_{He}$ closed (30 seconds).
  - De-pressurization: $V1_{He}$ closed and $V2_{He}$ opened (5 seconds).
  - The facility is operated at 200°C in order to promote the air ejection.
- At the end of the "washing actions" TxP is adjusted to the fixed pressure and the test is started.

6.1.1.3 Control cabinet and data acquisition

The control cabinet regulates the facility by means of power pulses. It is driven by the comparison between the $T_{C\text{-}HR}$ signal and $T_{C\text{-}HR\text{-}SET\text{-}POINT}$, *Fig. 45*. It automatically shuts-down the facility if $T_{S\text{-}HR}$ signal meets the $T_{S\text{-}HR\text{-}SET\text{-}POINT}$. Both the set points are selected manually. The acquisition system consists of a computer in which MX-100 (standard) software is installed, it is able to record data from the signals reported in *Fig. 45*. The main signals available at the acquisition system are given in *Tab. 24*.

TxP geometry			**TxP operating conditions**		
Description	**Unit**	**Quantity**	**Description**	**Unit**	**Quantity**
HR-14 outer radius	mm	16.0	Water inlet temp.	°C	<20
PIPE-5 inner radius	mm	31.3	Water outlet temp.	°C	<99
PIPE-5 outer radius	mm	36.5	Water mass flow	l/m	<12.0
PIPE-7 inner radius	mm	42.3	HR power	kW	≤25
PIPE-7 outer radius	mm	44.5	Helium pressure	bar	<5
PIPE-8 inner radius	mm	51.1	Maximum HR temp	°C	560
PIPE-8 outer radius	mm	57.1	Active length	mm	1200
Geometry of the gaps in TxP			**HXs at Brasimone**		
			Facility	**Gap width**	**Free vol.**
HR-14 – PIPE-5 width		15.3 mm	NACIE	5.8 mm	2.34 l
HR-14 – PIPE-5 free vol.		3.89 l	NACIE-UP	5.8 mm	1.38 l
PIPE-5 – PIPE 7 width		5.8 mm	HELENA	2.5 mm	1.17 l
PIPE-5 – PIPE 7 free vol.		2.44 l	HERO	0.6 mm	0.43 l

Tab. 23 – Main features of TxP.

Id	Module	Series	Channel	Software number	Thermocouple Type	Component	Axial position	Azimuthal position
5A0E	0	1	1	1	N	PIPE 5	A	0-esterna
5A1E			2	2	N	PIPE 5	A	1-esterna
5A2E			3	3	N	PIPE 5	A	2-esterna
5B0E			4	4	N	PIPE 5	B	0-esterna
5B1E			5	5	N	PIPE 5	B	1-esterna
5B2E		2	6	6	N	PIPE 5	B	2-esterna
5C0E			7	7	N	PIPE 5	C	0-esterna
5C1E			8	8	N	PIPE 5	C	1-esterna
5C2E			9	9	N	PIPE 5	C	2-esterna
5D0E			10	10	N	PIPE 5	D	0-esterna
5D1E	1	1	1	11	N	PIPE 5	D	1-esterna
5D2E			2	12	N	PIPE 5	D	2-esterna
5A0I			3	13	N	PIPE 5	A	0-interna
5A1I			4	14	N	PIPE 5	A	1-interna
5A2I			5	15	N	PIPE 5	A	2-interna
5B0I		2	6	16	N	PIPE 5	B	0-interna
5B1I			7	17	N	PIPE 5	B	1-interna
5B2I			8	18	N	T External	--	--
5C0I			9	19	N	PIPE 5	C	0-interna
5C1I			10	20	N	PIPE 5	C	1-interna
5C2I	2	1	1	21	N	PIPE 5	C	2-interna
5D0I			2	22	N	PIPE 5	D	0-interna
5D1I			3	23	N	PIPE 5	D	1-interna
5D2I			4	24	N	PIPE 5	D	2-interna
7A0			5	25	N	PIPE 7	A	0-esterna
7A1		2	6	26	N	PIPE 7	A	1-esterna
7A2			7	27	N	PIPE 7	A	2-esterna
7B0			8	28	N	PIPE 7	B	0-esterna
7B1			9	29	N	PIPE 7	B	1-esterna
7B2			10	30	N	PIPE 7	B	2-esterna
7C0	3	1	1	31	N	PIPE 7	C	0-esterna
7C1			2	32	N	PIPE 7	C	1-esterna
7C2			3	33	N	PIPE 7	C	2-esterna
7D0			4	34	N	PIPE 7	D	0-esterna
7D1			5	35	N	PIPE 7	D	1-esterna
7D2		2	6	36	N	PIPE 7	D	2-esterna
14A0			7	37	N	HR	A	0-esterna
14A1			8	38	N	HR	A	1-esterna
14A2			9	39	N	HR	A	2-esterna
14B0			10	40	N	HR	B	0-esterna
14B1	4	1	1	41	N	HR	B	1-esterna
14B2			2	42	N	HR	B	2-esterna
14C0			3	43	N	HR	C	0-esterna
14C1			4	44	N	HR	C	1-esterna
14C2			5	45	N	HR	C	2-esterna
14D0		2	6	46	N	HR	D	0-esterna
14D1			7	47	N	HR	D	1-esterna
14D2			8	48	N	HR	D	2-esterna
TH_2O_{IN}			9	49	K	Water in	Bottom	--
TH_2O_{OUT}			10	50	K	Water out	Top	--
TFB	5	1	1	51	K	Water bottom flange	Bottom	--
TFT			2	52	K	Water top flange	Top	--
T_{IN}			3	53	Th-resist. PT-100	Water in	Bottom	--
T_{OUT}			4	54	Th-resist. PT-100	Water out	Top	--
MASSFL			5	55	Flow meter	Water mass flow	Bottom	--
WM		2	1	56	Watt meter	HR power		--

Tab. 24 – TxP signals processed by the acquisition system.

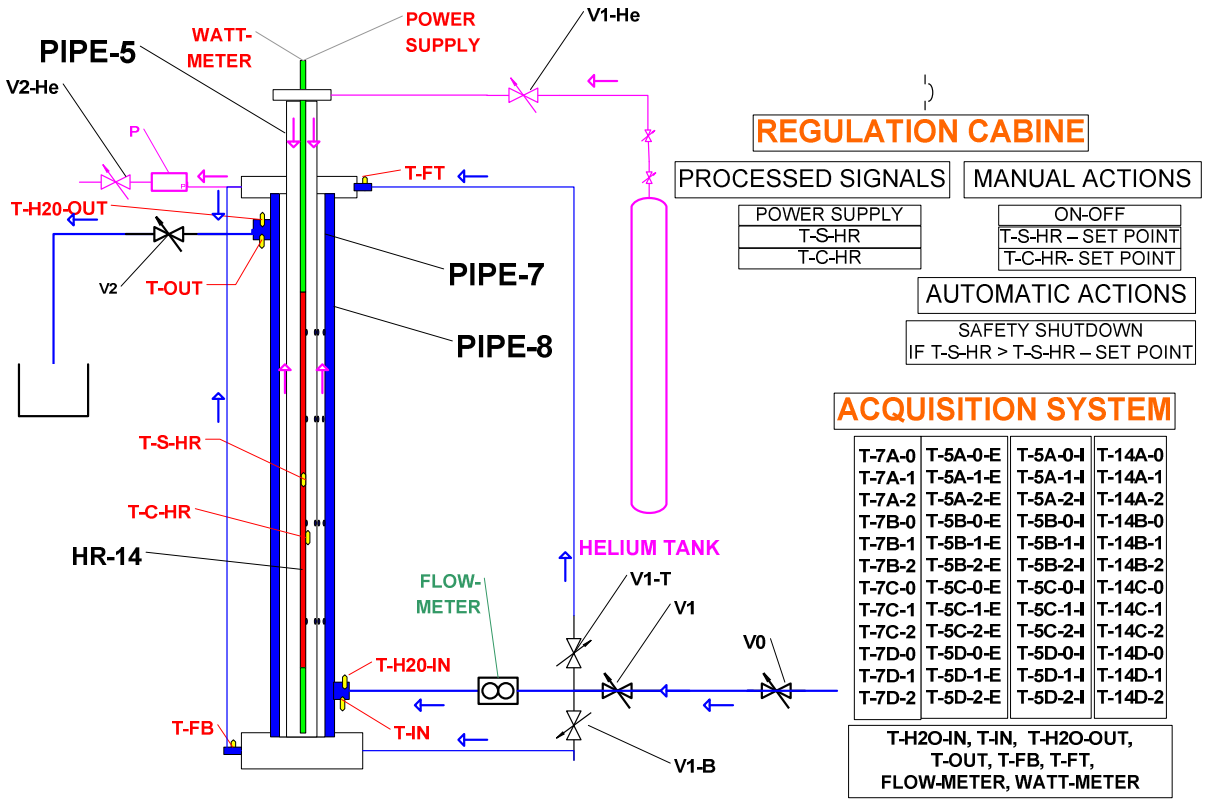

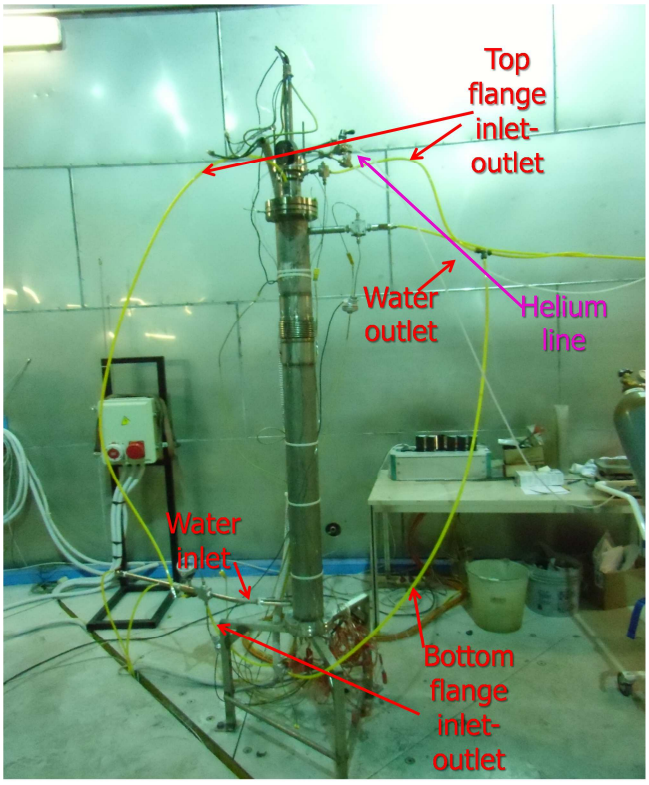

Fig. 43 – TxP initial schematic layout.

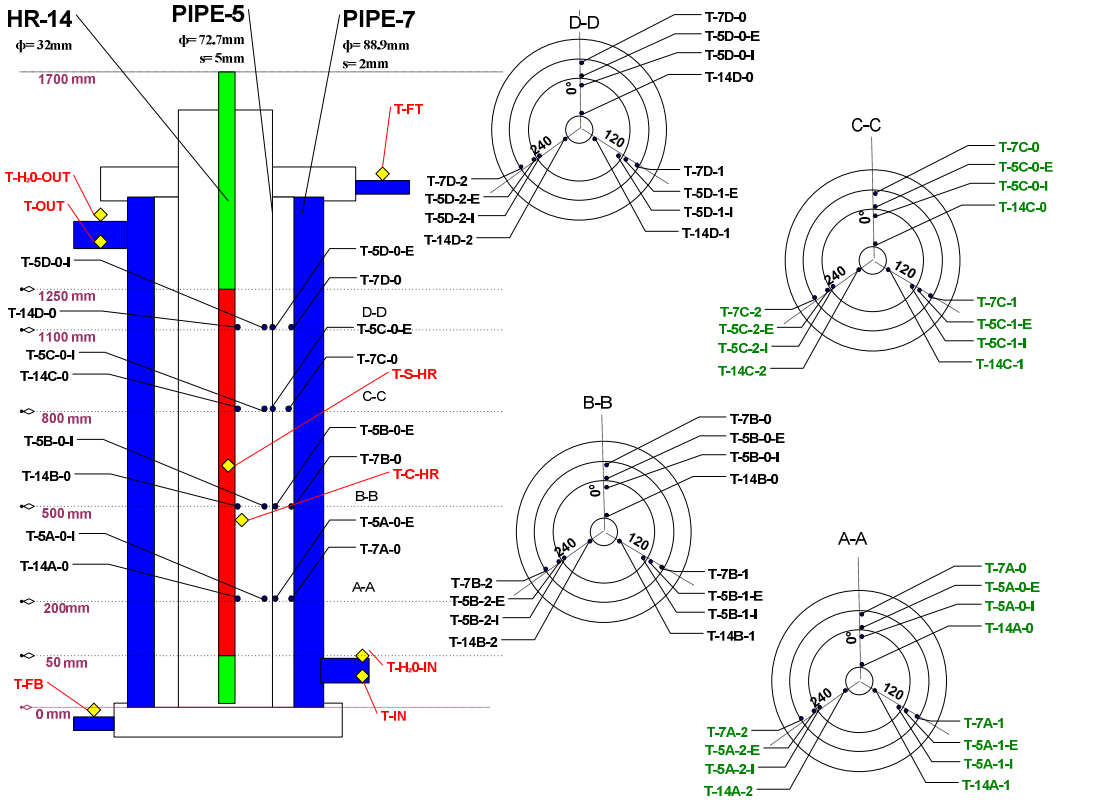

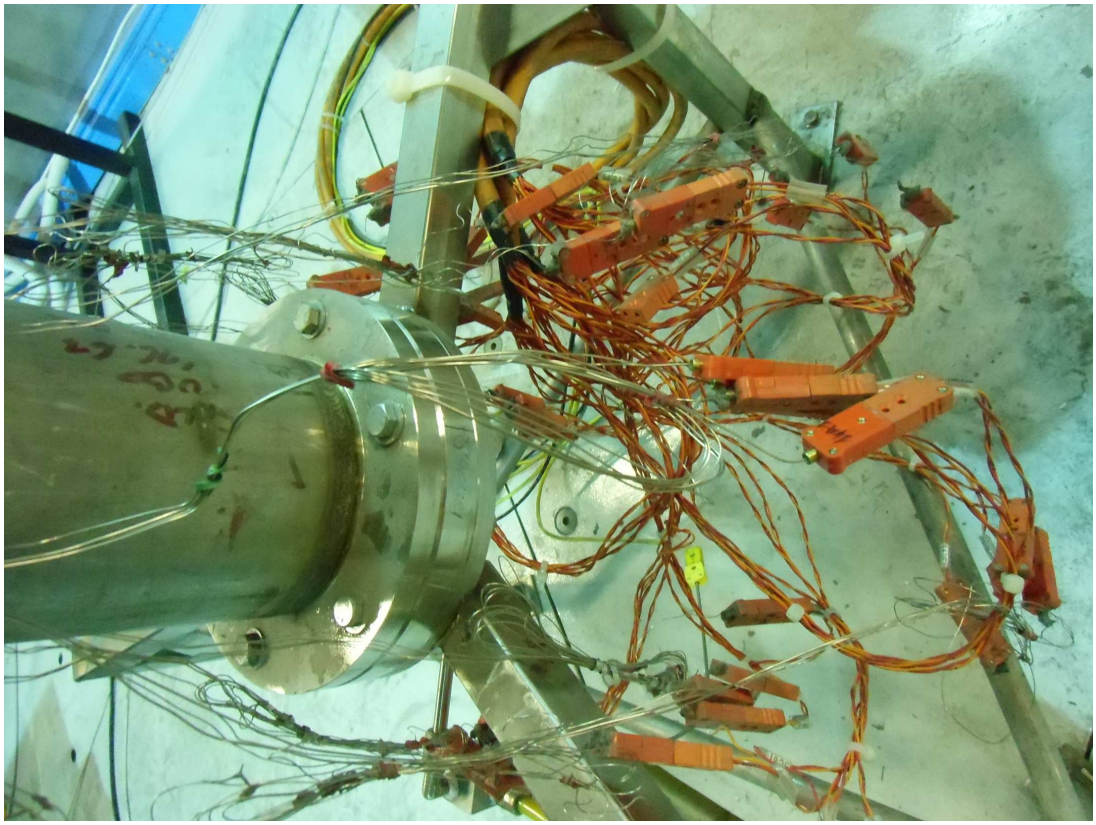

Fig. 44 – TxP instrumentation: location of the thermocouples.

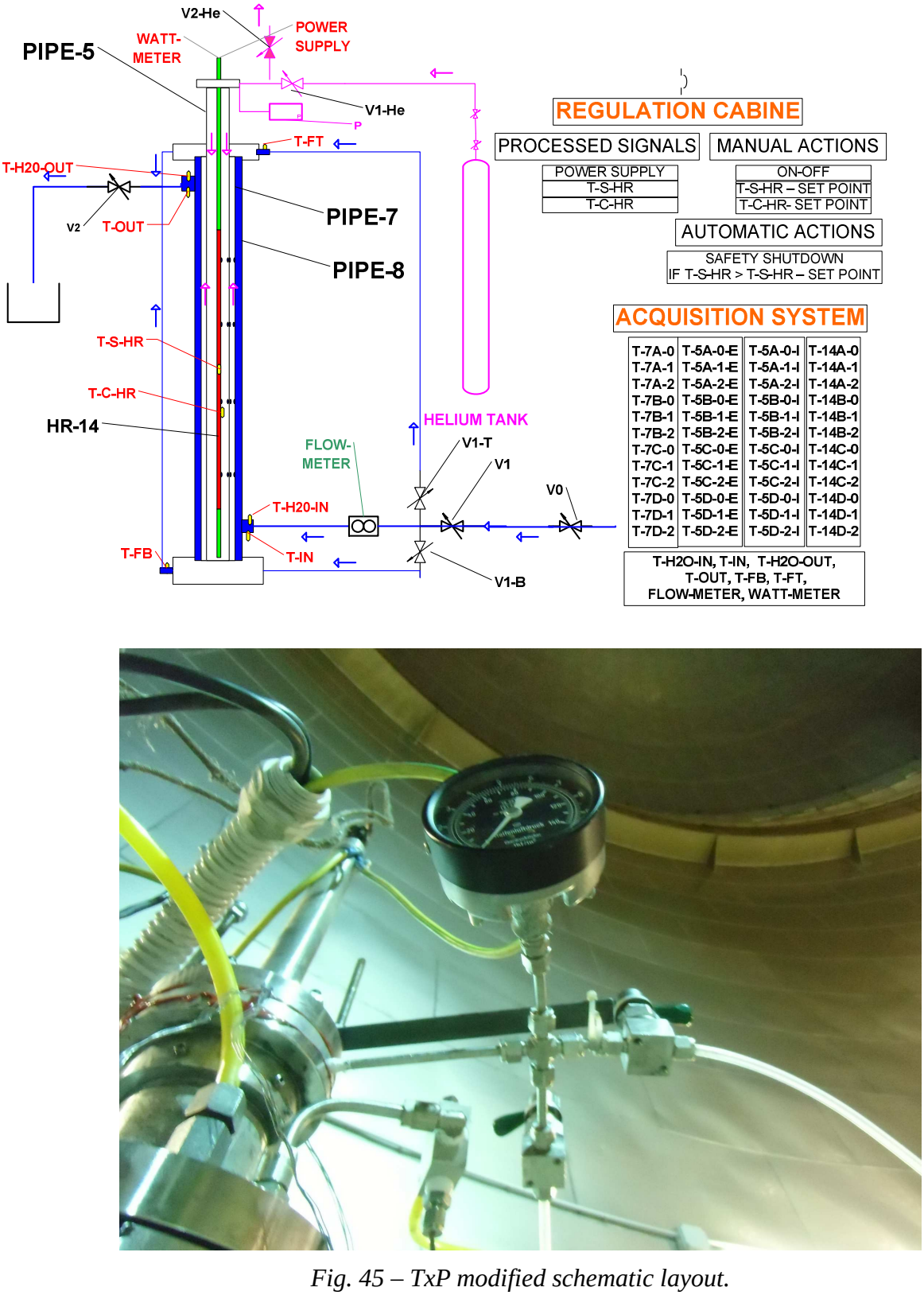

Fig. 45 – TxP modified schematic layout.

6.2 Propaedeutic tests

6.2.1 Description

On the basis of the theoretical screening presented in section 5.1.4, samples of these powders where acquired for propaedeutic test [35][55]:

- Copper (elettrolitic) type LT-12
- Copper type W-60-M
- Brass type OT-63
- Stainless steel type AISI-316
- Sintetic diamond
- Si-C
- Aluminum Nitride

The propaedeutic tests aims to study the compaction behavior of candidate powders when subjected to constant thermal loads into a furnace in which argon atmosphere is realized. The final goal of these tests is to exclude powders that will experience high compaction from further analyses in TxP since they are not suitable for SGBT application (and they may jeopardize the functionality of TxP).

The experiments consisted of, (*Fig. 46*):

- Loading the furnace with powders samples,
- Heating the furnace at 200 °C (Test 1) in Ar atmosphere,
- Keeping constant the temperature for 24 hrs,
- Repeating the procedure at 300°C (Test 2), 400°C (Test 3) and 500°C (Test 4).

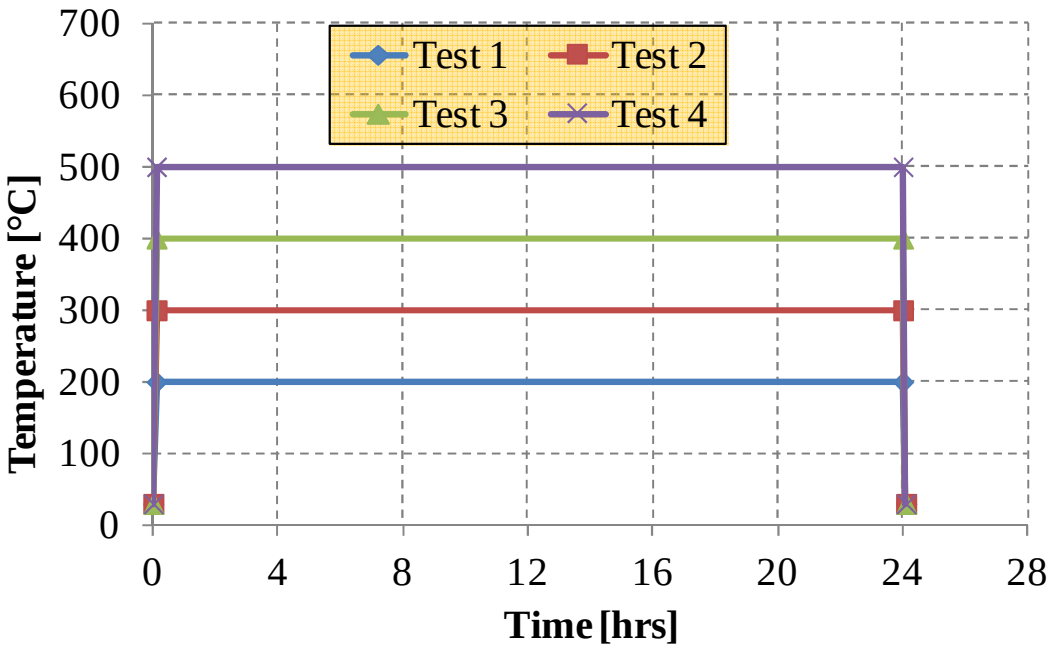

Fig. 46 – TxP- Propaedeutic tests, thermal loads applied to test the candidate powders, scheme.

The experiments require the following supporting tools:

- Furnace,
- Four stainless steel canisters to contain the powders,
- Zirconium refractory plate (as basement of the canisters),
- One pressurized vessel of Ar with relative piping and valves (to pump Ar into the fournace).

The instrumentations consist of:

- One thermocouple located inside one canister, that was ELSI type K
- One system able to record the measured temperature, Yokogawa 30 channels – with printer

The analysis consisted of measurements that are performed before the first test and after each test:

- Visual inspection,
- Stereo-scope analysis (NIKON – SMZ type),
- Scanning electron microscopy analysis (FEI - Inspect S type).

Due to the limited amount of samples, Si-C and sintetic diamond have been tested only in the fourth thermal load test. In order to simplify the examinations, powders that experience visible compaction are not tested further. Al-N has not been tested since it revealed compaction since in the pre-tests examinations at stereoscope. The main results are depicted in *Fig. 47* and summarized in *Tab. 25*. For each material the table reports an indication about the colour compared with the initial one (assumed as reference). The compaction state is given. In case of compaction, the roughest tool that capture the phenomenon is mentioned (visual inspection, stereoscopy and SEM). The grain dimensions in term of max and min measured grain lengths are included. They are obtained by atom-contrast (from SEM). Due to the limited number of measured grains, the range must be intended as a qualitative.

6.2.2 Main achievements from propaedeutic tests

Among these powders, AISI-316 (*Fig. 48*), sintetic diamond (*Fig. 49*) and Si-C (*Fig. 50*) are acceptable. Copper powders (*Fig. 51* and *Fig. 52*) and brass powder revealed un-acceptable compaction. In particular, brass powder behaves excellent up to the last test at 500°C. This last test evidenced a morphological change in the structure of the powder, *Fig. 53*. The complete set of the analysis is reported in Ref. [55].

AISI-316 powder revealed low compaction since the first test at 200 °C. It seems to be the result of large grains growing at expense of small grains. The phenomenon increases at 300 °C, 400°C and 500 °C even if, it remains limited and the compaction of the powder is considered low. However, SEM examination involves a small amount of material that may not be associated with an average value or, in the worst case, may not be representative of the general behavior (it reflects a local situation and does not allow a quantification). In order to get a more representative picture, a sample of un-heated powder and a sample of powder extracted after test 4 are delivered to FN for particle size distribution measurements by granule-meter laser MASTERSIZER 2000 Malvern Instruments. The results confirm the occurrence of compaction being the diameter of the hole to collect 50% of the powder increased of 15μm after heating at 500°C, *Fig. 54*. The detailed analyses are attached in Appendix C: *Fig C. 1* and *Fig C. 2*.

In conclusions sintetic diamond, Si-C and AISI-316 are theoretically suitable to be tested in the TxP facility. Due to the high cost, sintetic diamond has been abandoned while Si-C and AISI-316 have been acquired with the aim to assess their conductivities in TxP.

Powder	20 °C		200 °C		300 °C		400 °C		500 °C	
Copper LT-12	**Color**	ref	**Color**	Darker than ref	**Color**	Darker than ref	N/A		N/A	
	Compaction	none	**Compaction**	Total V-I	**Compaction**	**Total V-I**				
	Max grain	43 µm	**Max grain**	N/A	**Max grain**	N/A				
	Min grain	6 µm	**Min grain**	N/A	**Min grain**	N/A				
Copper W-60-M	**Color**	ref	**Color**	Darker than ref	**Color**	Darker than ref	N/A		N/A	
	Compaction	none	**Compaction**	Very Low - SEM	**Compaction**	**Total V-I**				
	Max grain	77 µm	**Max grain**	153 µm	**Max grain**	N/A				
	Min grain	16 µm	**Min grain**	44 µm	**Min grain**	N/A				
Brass OT-63	**Color**	ref	**Color**	Darker than ref	**Color**	Darker than ref	**Color**	Darker than ref	**Color**	Darker than ref
	Compaction	none	**Compaction**	Very Low - SEM	**Compaction**	Very Low - SEM	**Compaction**	Very Low - SEM	**Compaction**	**Total V-I**
	Max grain	120 µm	**Max grain**	74 µm	**Max grain**	97 µm	**Max grain**	90 µm	**Max grain**	N/A
	Min grain	17 µm	**Min grain**	58 µm	**Min grain**	58 µm	**Min grain**	49 µm	**Min grain**	N/A
SS – AISI-316	**Color**	ref	**Color**	as ref	**Color**	as ref	**Color**	Darker than ref	**Color**	Darker than ref
	Compaction	none	**Compaction**	Very Low - SEM	**Compaction**	Very Low - SEM	**Compaction**	Very Low - SEM	**Compaction**	**Beginning - SEM**
	Max grain	103 µm	**Max grain**	179 µm	**Max grain**	130 µm	**Max grain**	227 µm	**Max grain**	188 µm
	Min grain	6 µm	**Min grain**	74 µm	**Min grain**	80 µm	**Min grain**	167 µm	**Min grain**	127 µm
Sintetic diamond	**Color**	ref	N/A		N/A		N/A		**Color**	As ref
	Compaction	none							**Compaction**	**None**
	Max grain	124 µm							**Max grain**	137 µm
	Min grain	82 µm							**Min grain**	78 µm
Si-C	**Color**	ref	N/A		N/A		N/A		**Color**	As ref
	Compaction	none							**Compaction**	**None**
	Max grain	80 µm							**Max grain**	80 µm
	Min grain	5 µm							**Min grain**	5 µm

Tab. 25 – TxP-Propaedeutic tests, summary of the results.

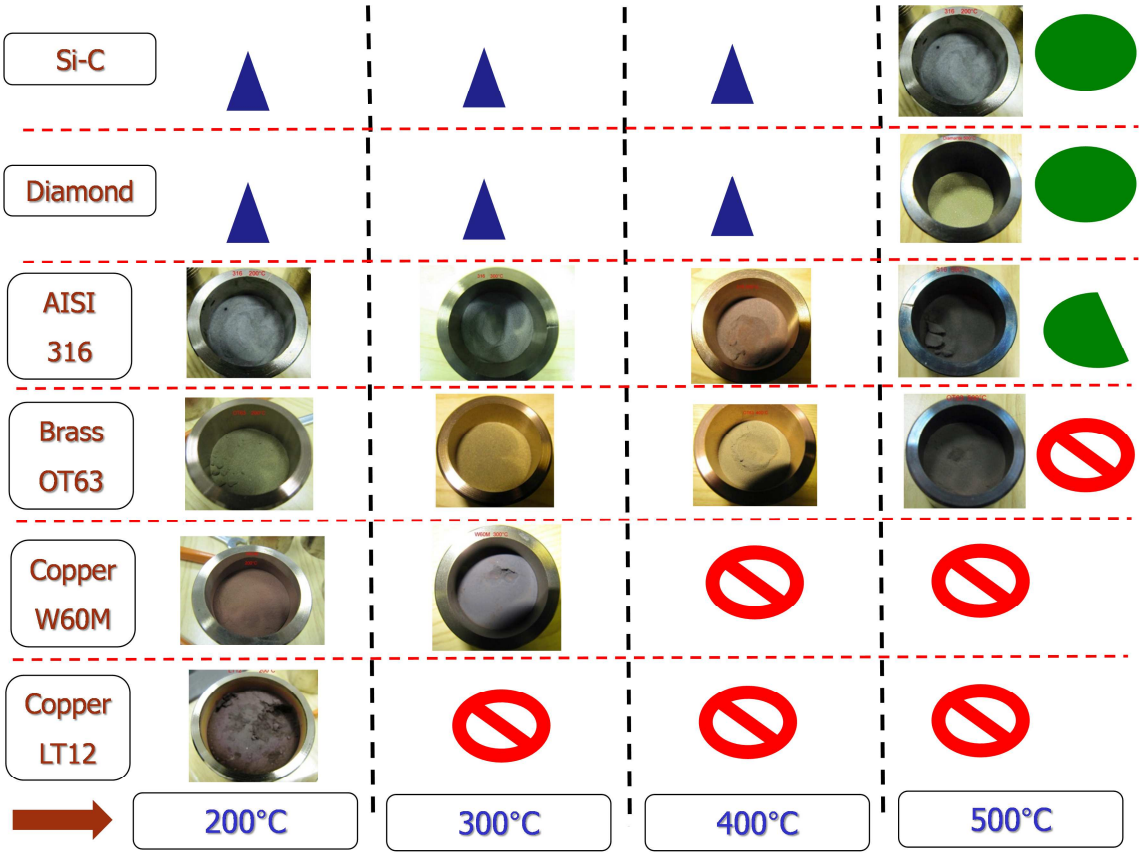

Fig. 47 – TxP-Propaedeutic test, main results.

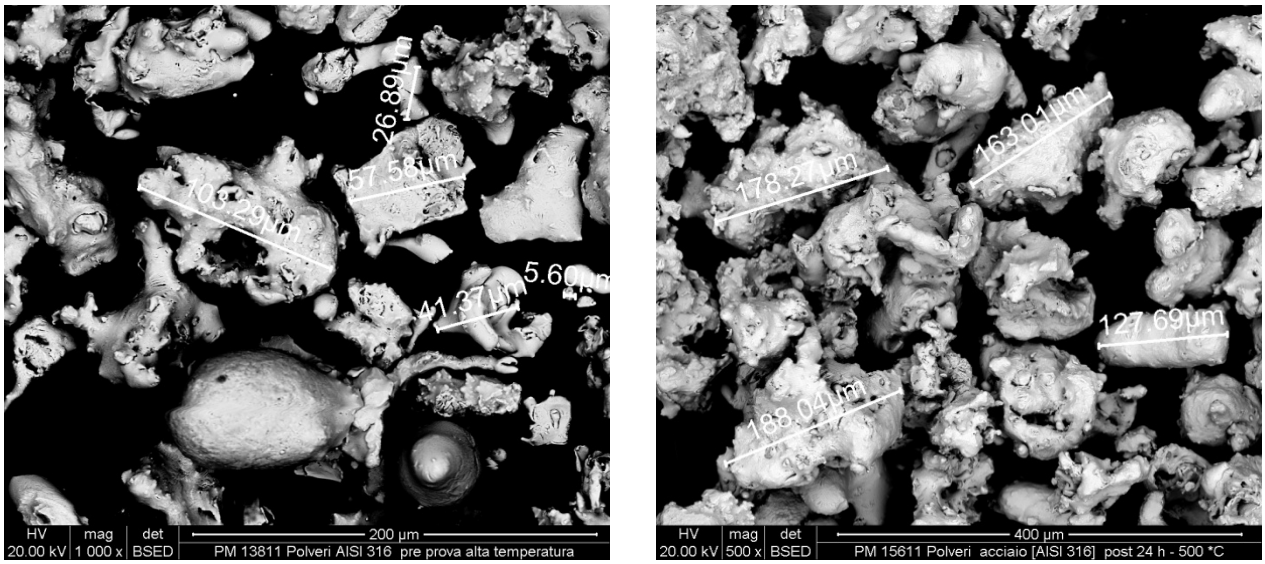

AISI-316, 20°C *AISI-316 500°C*

Fig. 48 – TxP-Propaedeutic test, AISI-316, SEM examinations.

Sintetic diamon, 20°C

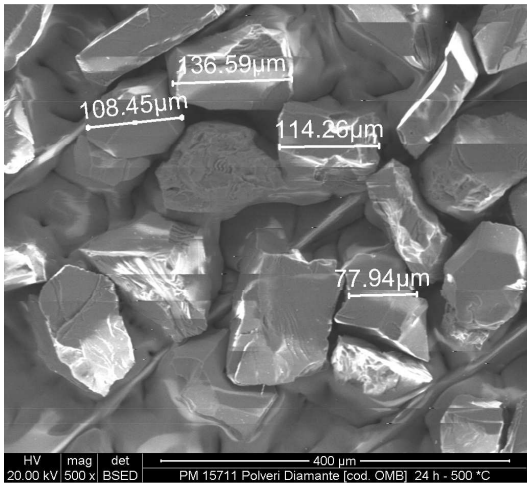

Sintetic diamond 500°C

Fig. 49 – TxP-Propaedeutic test, sintetic diamond, SEM examinations.

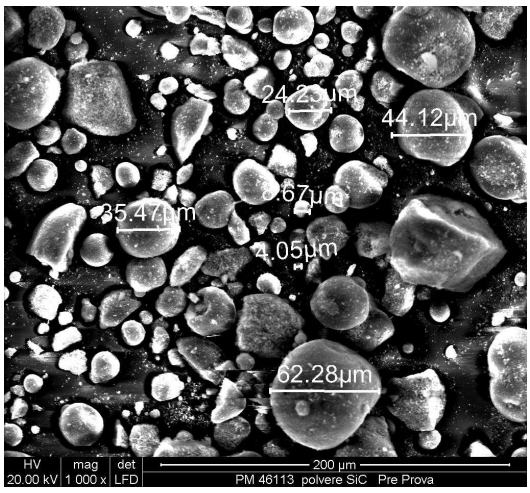

Si-C, 20°C

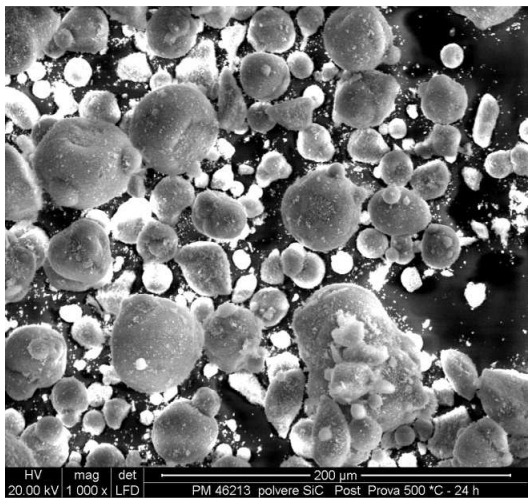

Si-C, 500°C

Fig. 50 – TxP-Propaedeutic test, Si-C, SEM examinations.

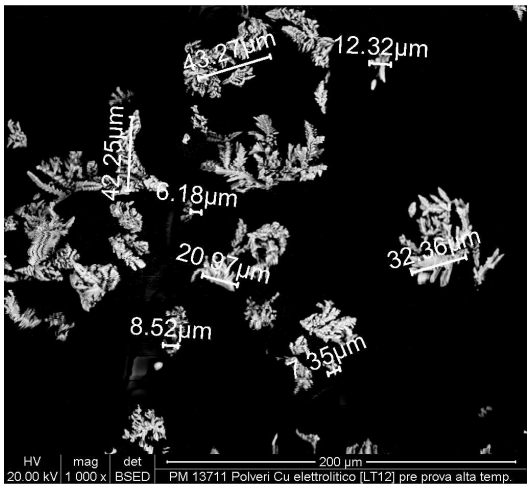

Copper LT-12, 20°C

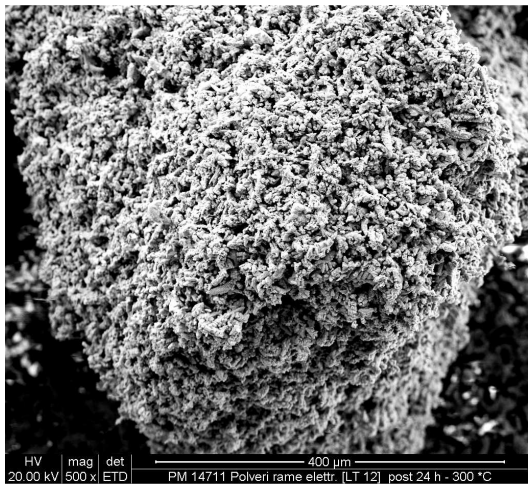

Copper LT-12, 200°C

Fig. 51 – TxP-Propaedeutic test, Copper LT-12, SEM examinations.

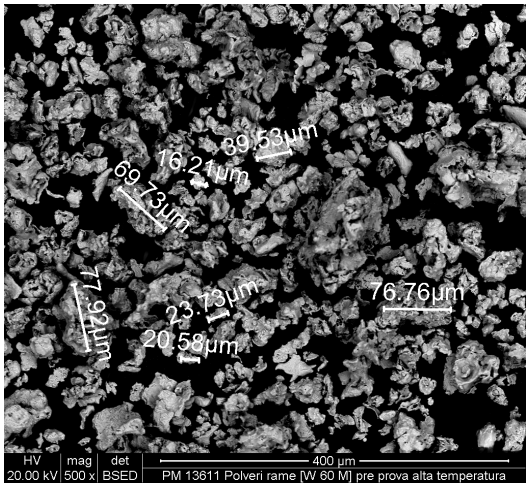

Copper W-60-M, 20°C

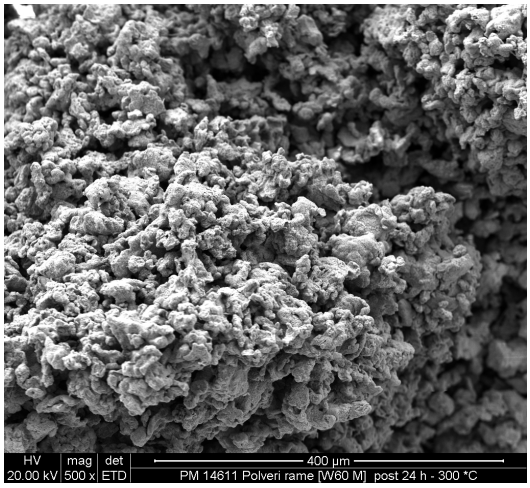

Copper W-60-M, 300°C

Fig. 52 – TxP-Propaedeutic test, Copper W-60-M, SEM examinations.

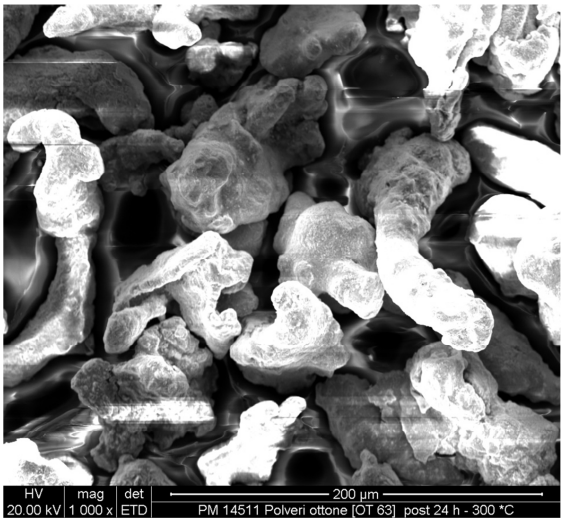

Brass OT-63, heated at 300°C

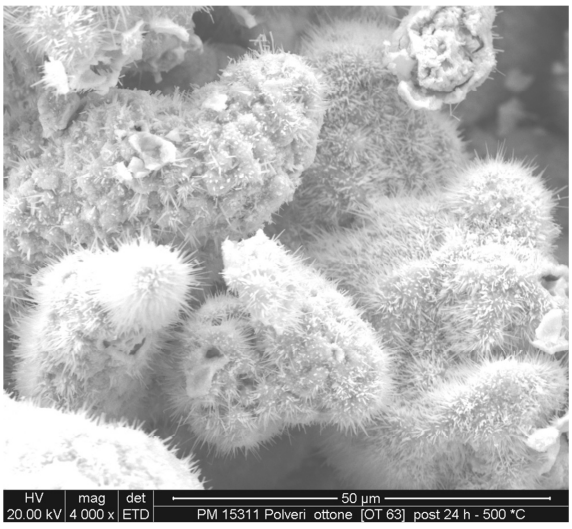

Brass OT-63, heated at 500°C

Fig. 53 – TxP-Propaedeutic test, Brass OT-63, SEM examinations.

Description	Un heated	Heated at 500°C
Minimum diameter to collect 10% of the powder	$D_{10\%}$ = 16.1 µm	$D_{10\%}$ = 20.0 µm
Minimum diameter to collect 50% of the powder	$D_{50\%}$ = 30.6 µm	$D_{50\%}$ = 45.6 µm
Minimum diameter to collect 90% of the powder	$D_{90\%}$ = 63.5 µm	$D_{90\%}$ = 100.9 µm

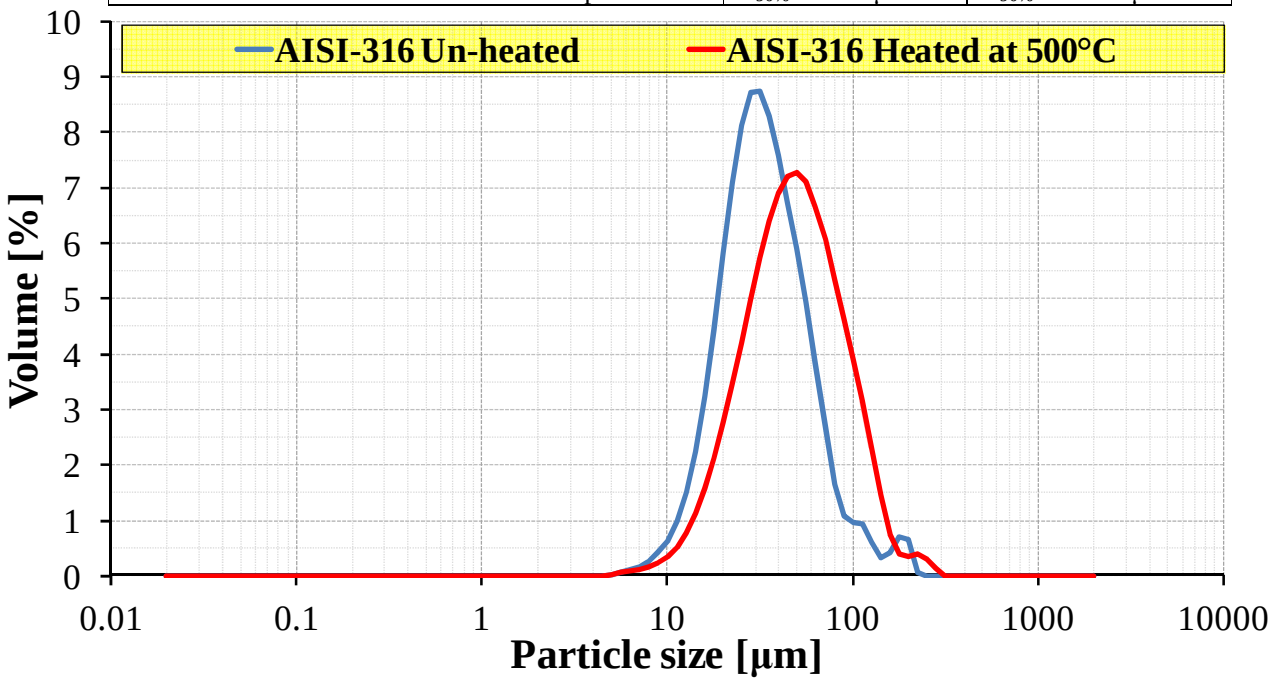

Fig. 54 – TxP-Propaedeutic test, AISI-316 particles size distribution measured by FN.

6.3 Pathfinder tests

6.3.1 Description

The experimental campaign conducted in TxP consisted of several tests each of them is subdivided in subtests. Thre series of subtests are presented in this section. They are RUN#0.0, RUN#1.0 and RUN#5.0 and are grouped as pathfinder tests.

The common objective of these sub-tests is to investigate the effect of the procedure adopted to load the powder in the facility on its conductivity. The final goal is to develop a standard procedure to load the powder inside TxP (and inside the HERO SGBT). These tests are conducted with the same powder installed in the HELENA Hx: AISI-316 (used also in the propaedeutic test) whose grain size is given in *Tab. 25*.

Test RUN#0 is experienced loading fresh powder by gravity and leaving a free volume in the upper part of the annular regions. In particular, 3.000 l of powder are loaded in HR-14 - PIPE-5 (measured capacity 3.812 l).

- The subtest RUN#0.0 took place in un-pressurized air environment in the temperature range [100-350]°C with a temperature increase of 10°C. The holding time to achieve steady state condition between two set of measurements was about 15 minutes and the acquisition time was 6 minutes.

Test RUN#1 is conducted loading fresh powder with the procedure named Single Step (1-S) vibrated. It consists in filling the region PIPE-5 - PIPE-7 with powder while the facility is vibrated on PIPE-8 by means of a pneumatic hammer operated by compressed air (at 6 bar), *Fig. 55*. Then, HR-14 is installed in TxP and the region HR-14 - PIPE-5 is filled with powder while the facility is vibrated again on PIPE-8. The disadvantage of this procedure is that it does not vibrate PIPE-5 directly. On the other hand, HR-14 is preserved from damages due to vibration.

- The subtest RUN#1.0 is experienced in un-pressurized air environment in the temperature range [100-450]°C with a temperature step increase of 10°C. The holding time to achieve steady state condition between two set of measurements was about 15 minutes and the acquisition time was 6 minutes.

RUN#5 is conducted loading fresh powder with the procedure Double Step (2-S) vibrated. It consists in filling the region HR-14 - PIPE-5 outside the facility: PIPE-5 is fixed into a mechanical equipment HR-14 is mounted and the vibration is applied directly on PIPE-5 during the loading. At the end of this first step, PIPE-5 is mounted in TxP and the region PIPE-5 - PIPE-7 is filled with powder while the facility is vibrated on PIPE-8, *Fig. 55*.

- The subtest RUN#5.0 is experienced in un-pressurized air environment in the temperature range [100-450]°C with a temperature increase of 20-30°C. The holding time to achieve steady state condition between two set of measurements was about 15 minutes and the acquisition time was 6 minutes.

The main specifications of the tests are reported in *Tab. 26*. The reference density is reported in row (b) with the aim to compare it with the density achieved into the annular region HR-14 - PIPE-5. It has been estimated weighting the powder into a graduated cylinder of 1 l. Contrarily to RUN#1.0, the estimated density of RUN#5.0 was higher than the reference density (RUN#0.0 is unknown due to the free volume), row (c). The porosity is calculated based on the theoretical density.

It should be pointed out that the porosity effectively achieved in this experiment (about 0.5) is higher than the assumption that has been done to develop TH calculations (0.3).

#	Description	Unit	RUN#0.0	RUN#1.0	RUN#5.0
	Material	--	AISI-316	AISI-316	AISI-316
(a)	Theoretical density	kg/dm^3	7.96	7.96	7.96
(b)	Reference density[1]	kg/dm^3	3.40	3.40	3.40
(c)	Estimated density[2]	kg/dm^3	unknown	3.31	3.70
(d)	Loaded powder	kg	10.20	12.64	14.12
(e)	Estimated porosity[3]	--	unknown	0.584	0.535
(f)	Filling gas	--	air	air	air
(g)	HR-14 - PIPE-5 free vol.[4]	l	3.812	3.812	3.812
(h)	Powder content	l	3.000	totally filled	totally filled
(i)	Powder vibration	--	no	procedure 1S	procedure 2S
(j)	Testing temperature range	°C	100-350	100-450	100-450
(k)	Temperature increase	°C	10	10	20-30
(l)	Holding time	min	15	15	15
(m)	Data acquisition time	min	6	6	6
(n)	Grain diameter range[5]	µm	1-200	1-200	1-200

[1] obtained weighting the powder without vibration into a graduated cylinder of 1 l
[2] obtained as [kg of powder introduced in HR-14 - PIPE-5] / [measured HR-14 - PIPE-5 free volume dm^3]
[3] obtained as [estimated density] / [theoretical density]
[4] measured by injection of water
[5] intended as max and min measured average diameter as documented in Appendix C, Fig C. 1

Tab. 26 – TxP-Pathfinder tests, summary of the test matrix.

Pneumatic hammer used in 1-S and 2-S

2-S procedure, PIPE-5 support

2-S procedure, last step loading PIPE-5 – PIPE-7 GAP

Fig. 55 – TxP-Pathfinder tests, selected pictures form loading procedures.

6.3.2 Main achievements from pathfinder tests

In order to compare the experimental results, the correlations labeled as Case1 and Case2 have been adopted (section 5.1.3). These correlations account for the average porosity, the conductivity of the solid and those of the fluid. They are expected to give a qualitative trend since they do not account for a large variety of parameters such as:

- The grain shape (they assume spherical shape) and grain size
- The open porosity
- Thermal cycling effects
- Geometrical effects at boundaries (due to the annulus)

The conductivities are given at the average temperature across the gap and they are obtained from the thermocouples located on HR-14 outer surface and on PIPE-5 inner surface since the experimental data obtained in the region PIPE-5 outer surface – PIPE-7 inner surface fall into a low temperature range and are not suitable for our purpose.

RUN#0.0 is depicted in *Fig. 56*. The figure includes two different data on conductivity labeled as C1 and C2 (*Eq. 20* and *Eq. 21*). These last indexes refer to the azimuthal position in the facility (see *Fig. 44*). Due to an ovalization of HR-14 in the azimuthal direction 0, C0 is not included in this analysis. Their linear interpolations are also evidenced (continuous lines) including the mean quadratic deviation (R2). Case1 and Case2 are calculated based on the estimated porosity of RUN#1.0. At about 90°C, the measured conductivity overpasses the case 2 curve and it slightly increases up to 0.32 W/m°C at 220°C. C1 and C2 are practically identical and the data exhibit a limited spreading (see R2) probably due to HR-14 ovalization.

RUN#1.0 and RUN#5.0 are given, respectively, in *Fig. 57* and *Fig. 58*. The figures include the same quantities defined before. In these cases, the empirical correlations are calculated according to the estimated porosity (*Tab. 26*). Both RUN#1.0 and RUN#5.0 stay always above case 2. In particular, around 200°C, the measured conductivity overpasses case 1 and it increases up to 0.72 W/m°C (RUN#1.0) or 1.05 W/m°C (RUN#5.0). C1 and C2 (*Eq. 22*, *Eq. 23*, *Eq. 24* and *Eq. 25*) highlight minor differences and the data exhibit a limited spreading (see R2). The increased slope of the curves (compared to RUN#0.0) is probably due the effect of thermal expansion of the powder in the radial direction (which tends to reduce the porosity). These tests revealed that the loading procedure 1-S with vibration (RUN#1.0) enhances the conductivity up to 40% compared to the un-vibrated loading and the loading procedure 2-S with vibration (RUN#5.0) further enhances the conductivity.

Fig. 59 compares the main results obtained in RUN#0.0, RUN#1.0 and RUN#5.0. In order to include the uncertainties related to ovalization, each curve does not distinguish the azimuthal directions and each correlation fits a single set of measurements by parabolic interpolation (*Eq. 26*, *Eq. 27* and *Eq. 28*). This choice is reflected into an increasing of data spreading. The empirical correlations are not reported since they depend on porosity and it is clear that the porosity of the powder depends on the loading procedure, therefore, it is important to standardize this process and to apply it during the assembling of the heat exchangers.

In conclusion, the 2-S vibrated procedure has been assumed as standard procedure for subsequent TxP tests since it guarantees the maximum powder density and this last parameter largely affects the powder conductivity.

$$C1_{RUN\#0.0} = 5 * 10^{-4}T + 0.2089 \quad \textit{Eq. 20}$$
$$C2_{RUN\#0.0} = 5 * 10^{-4}T + +0.2108 \quad \textit{Eq. 21}$$

$$C1_{RUN\#1.0} = 15 * 10^{-4}T + 0.2287 \quad \textit{Eq. 22}$$
$$C2_{RUN\#1.0} = 15 * 10^{-4}T + +0.2178 \quad \textit{Eq. 23}$$

$$C1_{RUN\#5.0} = 23 * 10^{-4}T + 0.2771 \quad \textit{Eq. 24}$$
$$C2_{RUN\#5.0} = 20 * 10^{-4}T + +0.2782 \quad \textit{Eq. 25}$$

$$K_{no-vibration} = -1 * 10^{-6}T^2 + 9 * 10^{-4}T + 0.1881 \quad \textit{Eq. 26}$$
$$K_{1-S-vibrated} = 7 * 10^{-7}T^2 + 13 * 10^{-4}T + +0.2426 \quad \textit{Eq. 27}$$
$$K_{2-S-vibrated} = 2 * 10^{-6}T^2 14 * 10^{-4}T + +0.3368 \quad \textit{Eq. 28}$$

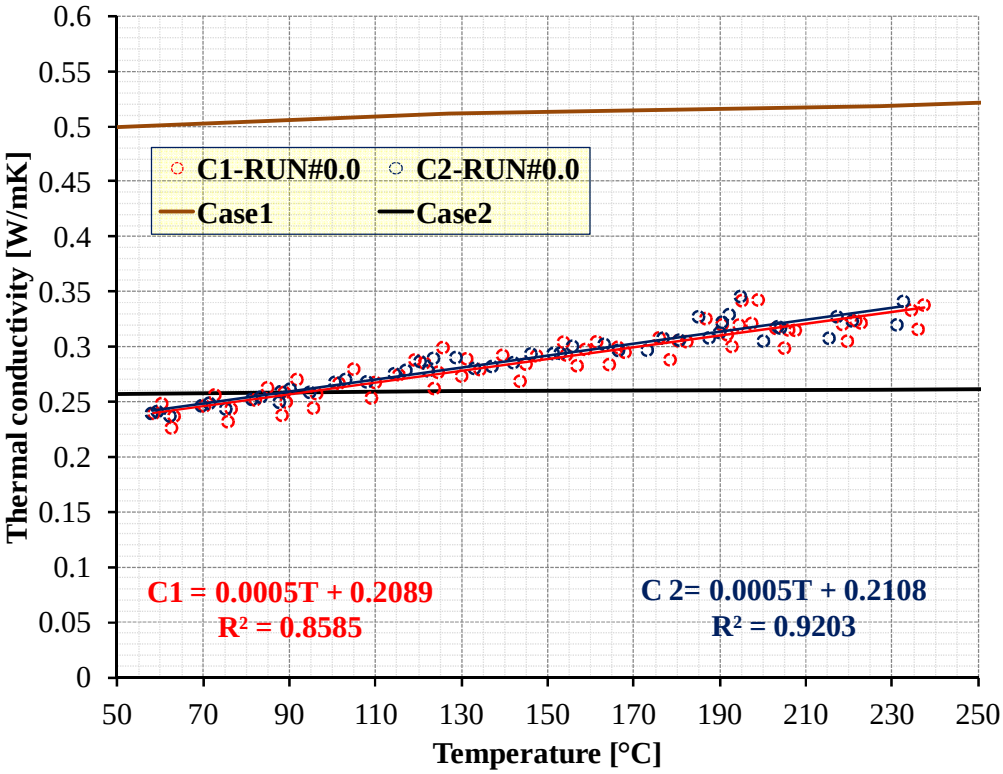

Fig. 56 – TxP-Pathfinder tests, AISI-316 powder, RUN#0.0 results.

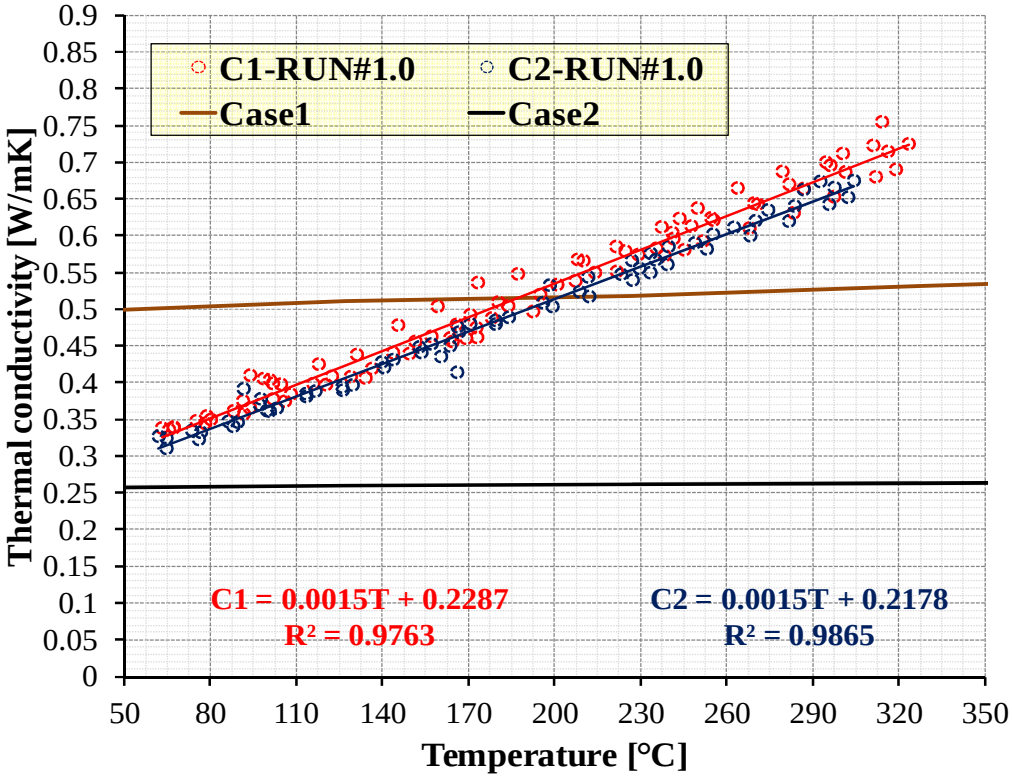

Fig. 57 – TxP-Pathfinder tests, AISI-316 powder, RUN#1.0 results.

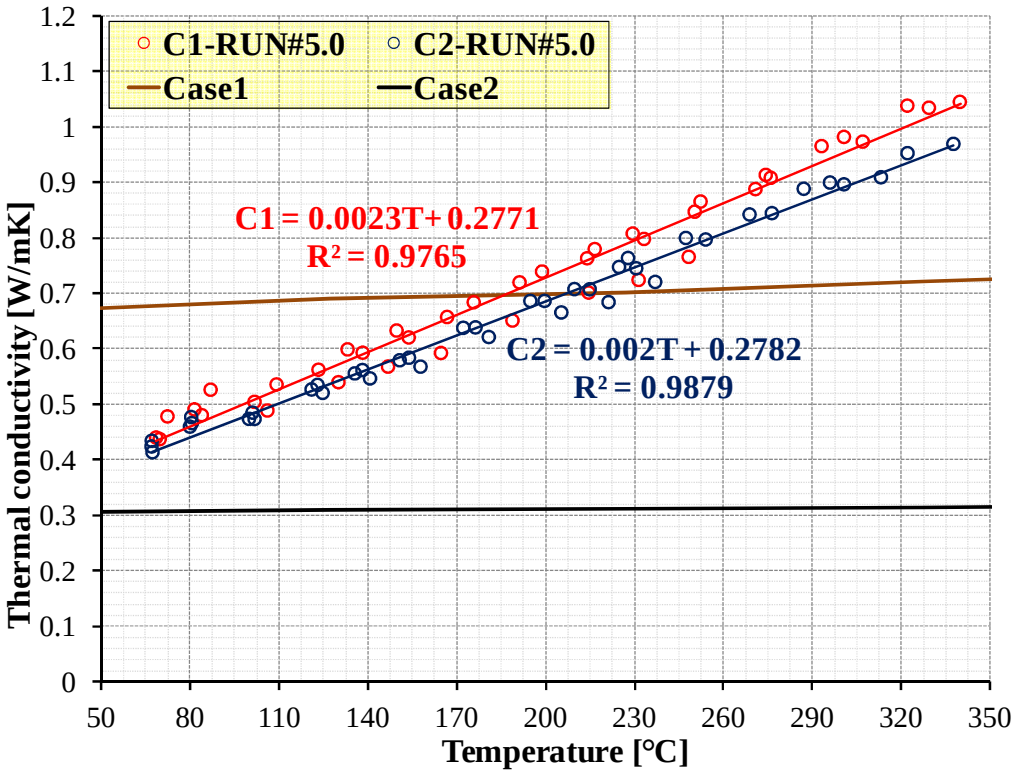

Fig. 58 – TxP-Pathfinder tests, AISI-316 powder, RUN#5.0 results.

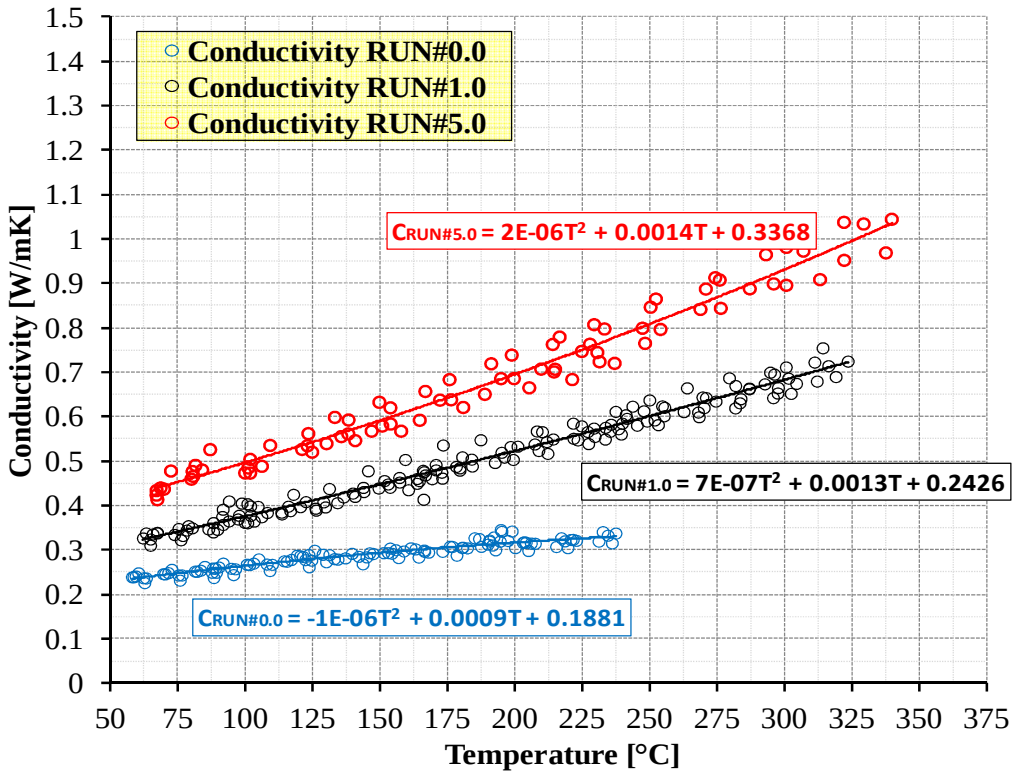

Fig. 59 – TxP-Pathfinder tests, AISI-316 powder, effect of the loading procedure on the conductivity.

6.4 Experimental campaigns in support to the HELENA and NACIE-UP Hx

6.4.1 Description

The present package of tests addresses AISI-316 powder and is based on the results obtained in pre-test heating (6.2.2, *Fig. 54*). The main aim is to investigate the effect of grain growth induced by thermal cycling on the conductivity and to develop empirical correlations suitable for the analysis of the NACIE-UP and HELENA HXs. They include the test named RUN#5 which is composed by the sub-tests RUN#5.0, RUN#5.1, RUN#5.2, RUN#5.3 and RUN#5.4 [56][57].

RUN#5 is conducted loading the fresh powder with the procedure Double Step (2-S) vibrated.

- The subtest RUN#5.0 is experienced loading fresh powder in un-pressurized air environment in the temperature range [100-450]°C with a temperature increase of 20-30°C. The holding time to achieve steady state condition between two set of measurements was about 15 minutes and the acquisition time was 6 minutes.
- The subtests RUN#5.1 to RUN#5.4 are identical to RUN#5.0. They have been conducted using the same sample of powder loaded in RUN#5.0 in order to achieve its compaction by realizing four equal cycles. Due to high temperature signals at the HR-14 outer surface, RUN#5.2-3-4 have been stopped at 400°C instead of 450°C.

The main specifications of the tests are reported in *Tab. 27*. The reference density is reported in row (b) with the aim to compare it with the density achieved into the annular region. It has been estimated weighting the powder into a graduated cylinder of 1 l. The estimated density of RUN#5.0

was higher than the reference density, row (c). Since the powder experiences compaction during the thermal cycles these quantities are applicable only to RUN#5.0.

#	Description	Unit	RUN#5.0	RUN#5.1	RUN#5.2	RUN#5.3	RUN#5.4
	Material	--	AISI-316	AISI-316	AISI-316	AISI-316	AISI-316
(a)	Theoretical density	kg/dm^3	7.96	7.96	7.96	7.96	7.96
(b)	Reference density[1]	kg/dm^3	3.40	3.40	3.40	3.40	3.40
(c)	Estimated density[2]	kg/dm^3	3.70	unknown	unknown	unknown	unknown
(d)	Loaded powder	kg	14.12	14.12	14.12	14.12	14.12
(e)	Estimated porosity[3]	--	0.535	unknown	unknown	unknown	unknown
(f)	Filling gas	--	air	air	air	air	air
(g)	HR-14 - PIPE-5 free vol.[4]	l	3.812	3.812	3.812	3.812	3.812
(h)	Powder content	l	totally filled	unknown	unknown	unknown	unknown
(i)	Powder vibration	--	procedure 2S	--	--	--	--
(j)	Testing temperature range	°C	100-450	100-450	100-400	100-400	100-400
(k)	Temperature increase	°C	20-30	20-30	20-30	20-30	20-30
(l)	Holding time	min	15	15	15	15	15
(m)	Data acquisition time	min	6	6	6	6	6
(n)	Grain diameter range[5]	µm	1-200	--	--	--	--
(o)	Cycle N°	--	fresh	1	2	3	4

[1] obtained weighting the powder without vibration into a graduated cylinder of 1 l
[2] obtained as [kg of powder introduced in HR-14 - PIPE-5] / [measured HR-14 - PIPE-5 free volume dm^3]
[3] obtained as [estimated density] / [theoretical density]
[4] measured by injection of water
[5] intended as max and min measured average diameter as documented in Appendix C, Fig C. 1

Tab. 27 – TxP experimental campaign on AISI-316 powder, RUN#5, summary of the test matrix under un-pressurized helium environment.

6.4.2 Main achievements

The main results are depicted in *Fig. 60*. It includes RUN#5.0, RUN#5.1, RUN#5.2, RUN#5.3 and RUN#5.4. Each set of points does not distinguish the azimuthal directions in order to include the uncertainty due to HR-14 ovalization. Two correlations obtained by parabolic interpolation have been identified. The first (*Eq. 29*), is representative of the fresh powder and groups RUN#5.0 and RUN#5.1. The second (*Eq. 30*), highlights the effect of powder compaction and groups the subsequent tests RUN#5.2, RUN#5.3, RUN#5.4. The increase of grain induced by high temperature achieved in previous tests tends to enhance the thermal conductivity. This last curve ends at 300°C since it was not possible to achieve the target temperature (450°C). Therefore, the phenomenon of grain growth observed in 6.2.2 increases the powder density being beneficial to its conductivity.

In conclusion, *Eq. 30* is retained representative for the pre-test simulations of the HELENA and NACIE-UP HXs.

$$C_{RUN\#5.0-1} = 2 * 10^{-6}T^2 + 13 * 10^{-4}T + 0.3601 \qquad \textit{Eq. 29}$$

$$C_{RUN\#5.2-3-4} = 9 * 10^{-6}T^2 - 8 * 10^{-4}T + 0.5231 \qquad \textit{Eq. 30}$$

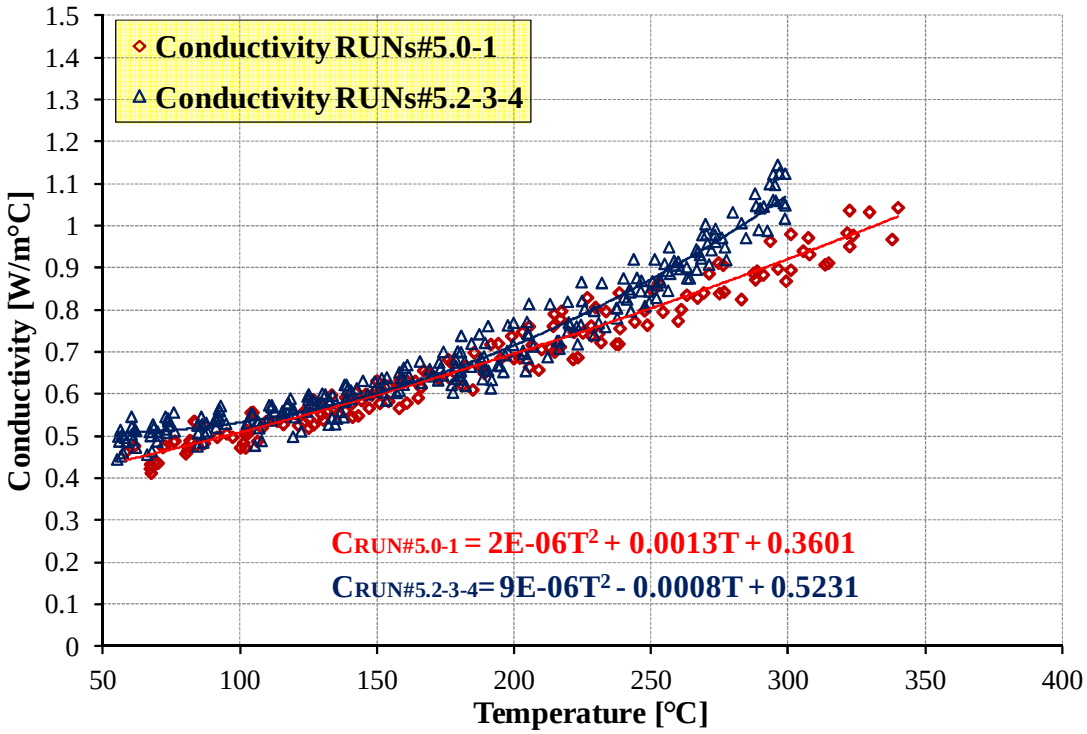

Fig. 60 – TxP experimental campaign on AISI-316 powder, effect of thermal cycling on conductivity.

6.4.3 Verification against Test-301

The present section aims to verify the correlation reported in *Eq. 30* based on an experimental campaign carried out in NACIE: test #301. The goal of this analysis is to assess the conductivity of the SS powder (AISI-304) based on the Logarithmic Mean Temperature Drop (LMTD) method [58]. The selected experiment lasted about 27000s and reached stationary conditions after 22000s, when the measured power (at the heater) is balanced by the removed power (at the HX), *Fig. 61*. The calculation is therefore conducted after 22000s based on the measured quantities reported in *Fig. 62*.

Four different values of conductivity have been calculated with this method, they are depicted in *Fig. 63*, it includes:

- The conductivity of AISI-304 powder according to the geometrical design (k-design).
- The effect of geometrical tolerances: k-Max gap and k-Min gap (the gap size in which the powder was located in to the NACIE HX is $5.83^{\pm 0.80}$ mm).
- The effect of thermal expansion (applied to the lead side tube equal to 0.4 mm): k-design-Th.exp.
- The combined effect of both geometrical tolerances and thermal expansion: k-Max gap-Th.exp and k-Min gap-Th.exp.

The estimated conductivity is in the range 1.11 – 1.49 W/mK being the effective geometry the main source of uncertainty. The powder is predicted to operate in the temperature range 100 – 290 °C (gap borders). According to the correlation that considers five thermal cycles (*Eq. 30*), this corresponds to a conductivity between 0.55 – 1.02 W/mK being therefore under estimated.

The reasons for this are substantially five:

- The first is the thermal cycling effect. TxP experienced only five cycles while test #301 is conducted after years of operation of NACIE. Furthermore, the effective fraction of powder that experiences compaction in TxP is smaller than that of NACIE. This is because, compared to TxP, NACIE has a smaller gap (5.8 mm vs 15.3 mm) and therefore a smaller cold zone in the powder (grain increase depends on the temperature level).
- The second is related to the material: the correlation is derived for AISI-316 (density ≥ 3.70 kg/dm^3, grain diameter range 10-150μm) NACIE is loaded with AISI-304 (unknown density, unknown average grain size).
- The third is connected to the different geometry of the gap. In the annular geometry, the local porosity of the powder at the gap boundaries is generally lower than the average porosity inside the gap [39] being this deviation affected by the geometry itself, the tube wall roughness, and the grain average diameter and shape.
- The fourth one is connected to the uncertainties of the measurements in test #301 (temperatures, mass flows and power). In particular, the calculation based on test #301 relies on four thermocouples whereas the correlation obtained in RUN#5.2-3-4 is an average among 72 points obtained with 24 thermocouples.
- The last one is connected to the limits of the LMTD that is substantially based on a logarithmic averaged temperature drop between the hot fluid and the cold fluid.

In conclusion, *Eq. 30* is confirmed to be applicable to HELENA ad NACIE-UP HXs with a margin of conservatism.

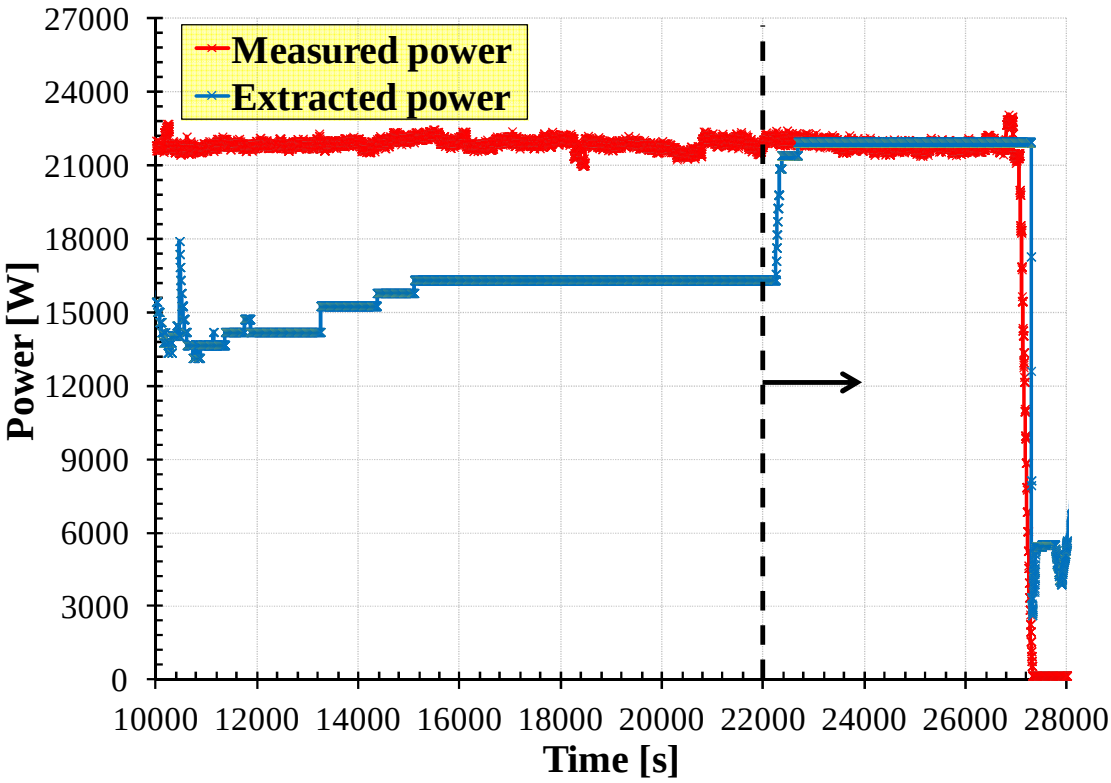

Fig. 61 – NACIE, test #301, power trend.

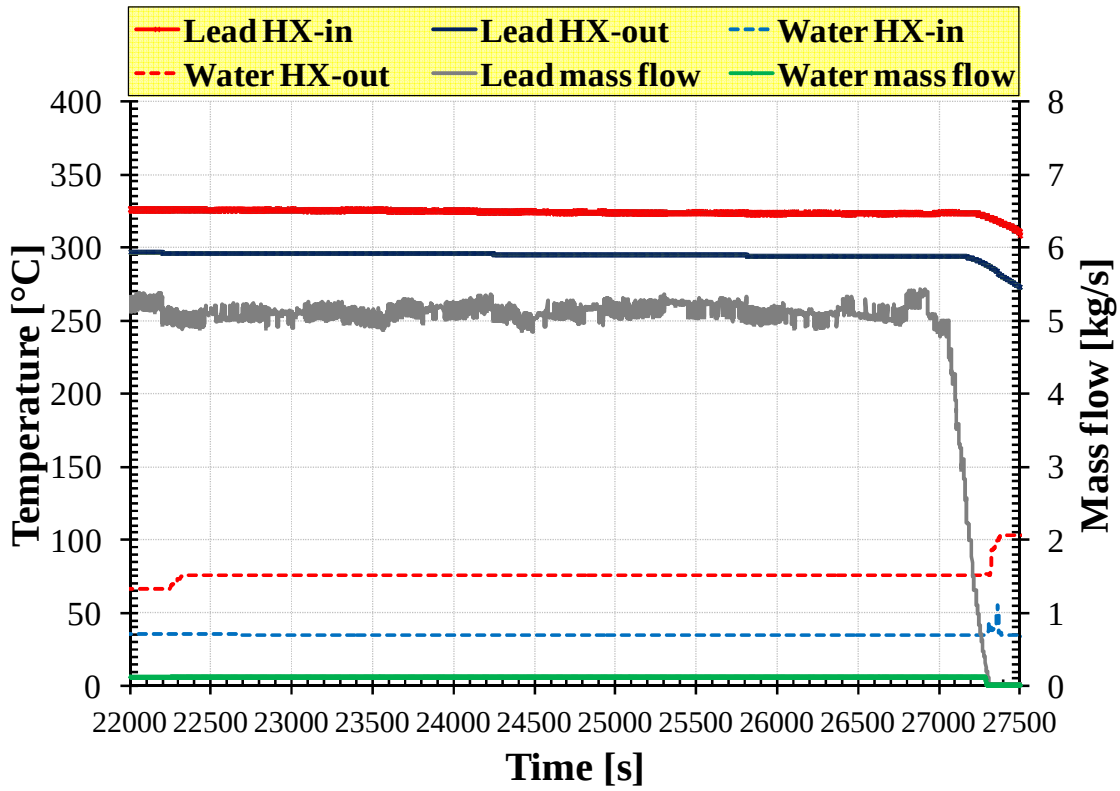

Fig. 62 – NACIE, test #301, , temperatures and mass flow rates at stationary conditions.

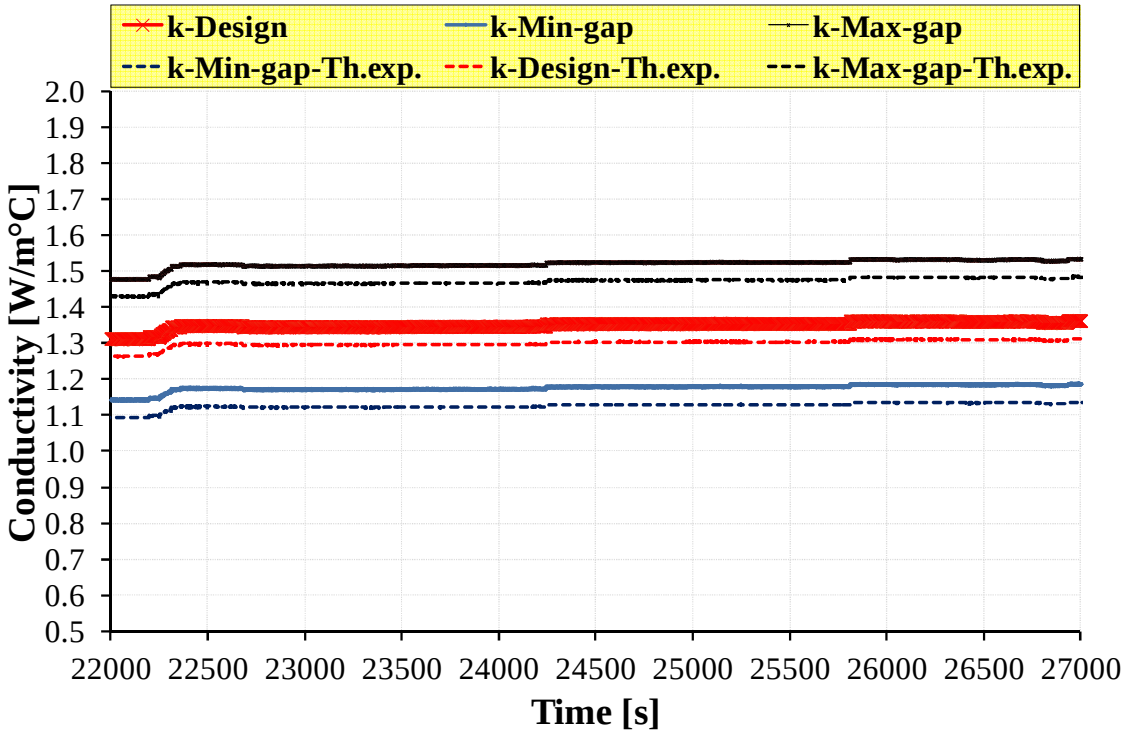

Fig. 63 – NACIE, test #301, AISI-304 powder: estimated conductivity.

6.5 Experimental campaigns in support to the HERO test section

6.5.1 Assessment of Si-C powder

6.5.1.1 Description

The present package of tests addresses Si-C powder with the aim to assess the suitability of this powder for the development of the HERO SG unit and the design of the ALFRED SGBT. Five different lots of Si-C of selected grain diameter have been supplied by FN to this purpose. They are obtained by multiple filtering of pre-heated Si-C powder at 700°C.

- RUN#2: Si-C powder having grain diameter in the range [149-247] μm
- RUN#3: Si-C powder having grain diameter in the range [1-80] μm
- RUN#4: Si-C powder having grain diameter in the range [80-105] μm
- RUN#6: Si-C powder having grain diameter in the range [105-125] μm (not executed)
- RUN#7: Si-C powder having grain diameter in the range [125-149] μm (not executed)

RUN#*i* (i = 2,3,4) is conducted with the loading procedure Double Step (2-S) vibrated.

- The subtest RUN#i.0 is experienced loading fresh powder in un-pressurized air environment in the temperature range [100-450]°C with a temperature increase of 20-30°C. The holding time to achieve steady state condition between two set of measurements was about 15 minutes and the acquisition time was 6 minutes.
- The subtests RUN#i.1 to RUN#i.4 use the same powder loaded in RUN#i.0. They have been conducted under helium atmosphere at four different pressures: 1, 2, 3, 4.5 bar in order to investigate the influence of the pressure level. In this case, it is believed that Si-C compaction will not occur and therefore it is neglected the influence of cycling.

The main specifications of the tests are reported in *Tab. 28*. RUN#6-7 where not executed (see 6.5.1.2). The reference density is reported in row (b) with the aim to compare it with the density achieved into the annular region. It has been estimated weighting the powder into a graduated cylinder of 1 l. The estimated density of RUN#3-4 were higher than the reference density, row (c). Contrarily, the estimated density of RUN#2 was lower than the reference density. This seems to be connected to the grain diameter: the lower is the grain diameter the higher is the capability to compact the powder by vibration.

#	Description	RUN#2.0 to RUN#2.4	RUN#3.0 to RUN#3.4	RUN#4.0 to RUN#4.4
	Material	Si-C	Si-C	Si-C
(a)	Theoretical density [kg/dm^3]	3.21	3.21	3.21
(b)	Reference density[1] [kg/dm^3]	0.93	1.13	1.00
(c)	Estimated density[2] [kg/dm^3]	0.80	1.17	1.03
(d)	Loaded powder [kg]	3.04	4.47	3.91
(e)	Estimated porosity[3] [/]	0.751	0.635	0.684
(f)	Filling gas	RUN#2.0 Air-He [1-4.5bar]	RUN#3.0 Air-He [1-4.5bar]	RUN#4.0 Air-He [1-4.5bar]
(g)	HR-14 - PIPE-5 free vol.[4] [l]	3.812	3.812	3.812
(h)	Testing temperature [°C]	100-450	100-450	100-450
(i)	Temperature increase [°C]	20-30	20-30	20-30
(j)	Holding time [min]	15	15	15
(k)	Data acquisition time [min]	6	6	6
(l)	Initial loading procedure	2-S	2-S	2-S
(m)	Grain diameter[5] [µm]	[149-247]	[1-80]	[80-105]

[1] obtained weighting the powder without vibration into a graduated cylinder of 1 l
[2] obtained as [kg of powder introduced in HR-14 - PIPE-5] / [measured HR-14 - PIPE-5 free volume dm^3]
[3] obtained as [estimated density] / [theoretical density]
[4] measured by injection of water
[5] realized by FN by means of multiple filtering of pre-heated Si-C powder at 700°C.

Tab. 28 – TxP experimental campaign on Si-C powder, RUN#2-3-4, summary of the test matrix.

6.5.1.2 Main achievements

The post-processing of RUN#2 is reported *Fig. 64*. The figure includes the experimental data from the five cycles and the average trend of conductivity (with an uncertainty band of ±10%). Si-C powder in the diameter range [149-247]µm highlights an un-expected low conductivity with respect to the 99% dense material (see Tab. 19). The maximum value is about 0.3 W/m°C which is obtained in He atmosphere at 4.5 bar and it should be noted that it is lower than those obtained for AISI-316 under un-pressurized air (*Fig. 59*).

Due to this occurrence, the comparison with the empirical correlations *Eq. 5* (Case 1) and *Eq. 16* (case 2) is not reported since they largely overestimate the measured trends. In general, the experimental trends are approximately constant with a slight increase with temperature and a large spreading which is due to the fact that these low values of conductivity are close to the accuracy of the measurements (therefore we decided to do not develop correlations). The introduction of He at 1 bar instead of un-pressurized air increases the conductivity of about 40%. The conductivity increases also with pressure being, compared to 1 bar, more or less doubled at 4.5 bar.

RUN#3 is analysed in *Fig. 65*. Si-C powder in the diameter range [1-80]µm confimed the low conductivity obtained in RUN#2. The maximum value is about 0.5 W/m°C, it is obtained in He atmosphere at 4.5 bar again lower than those obtained for AISI-316 under un-pressurized air (*Fig. 59*). In general, the experimental trends slightly increase with temperature. The introduction of He at 1 bar instead of un-pressurized air increases the conductivity of about 40%. The conductivity increases also increasing the helium pressure being, compared to 1 bar, more or less doubled at 4.5 bar.

RUN#4 (diameter range [80-125]µm, *Fig. 66*) definitively confirms the un-acceptability of Si-C powder as heat transfer enhancer for the SGBT being the maximum measured value around 0.4 W/m°C.

For sake of completeness, the effect of grain diameter on Si-C conductivity is given in *Fig. 67*: the lower is the grain diameter the higher is the conductivity.

In conclusion, since RUN#3 and RUN#2 bound the investigated grain diameter ranges, and, considering their results, it has been decided to do avoid the execution of RUN#6 and RUN#7 and to investigate AISI-316 as back-up solution for the design of the HERO SG unit.

In order to explain the unexpected behavior of Si-C, a sample of powder from RUN#2 has been compared with a sample of powder of AISI-316 from the propaedeutic test n° 3 (heated at 400°C for 24 hr) by SEM examination. The pictures are given in *Fig. 68*. Compared to AISI-316, it is qualitatively evident that Si-C grains have larger surface porosity (open porosity) that causes reduction of contact points among the particles. This is reflected in strong degradation of conductivity.

Therefore, if further materials will be acquired for conductivity measurements, a preliminary analysis by SEM (with resolution 1000x) should be performed to check the powder structure in order to avoid materials that are similar to Si-C.

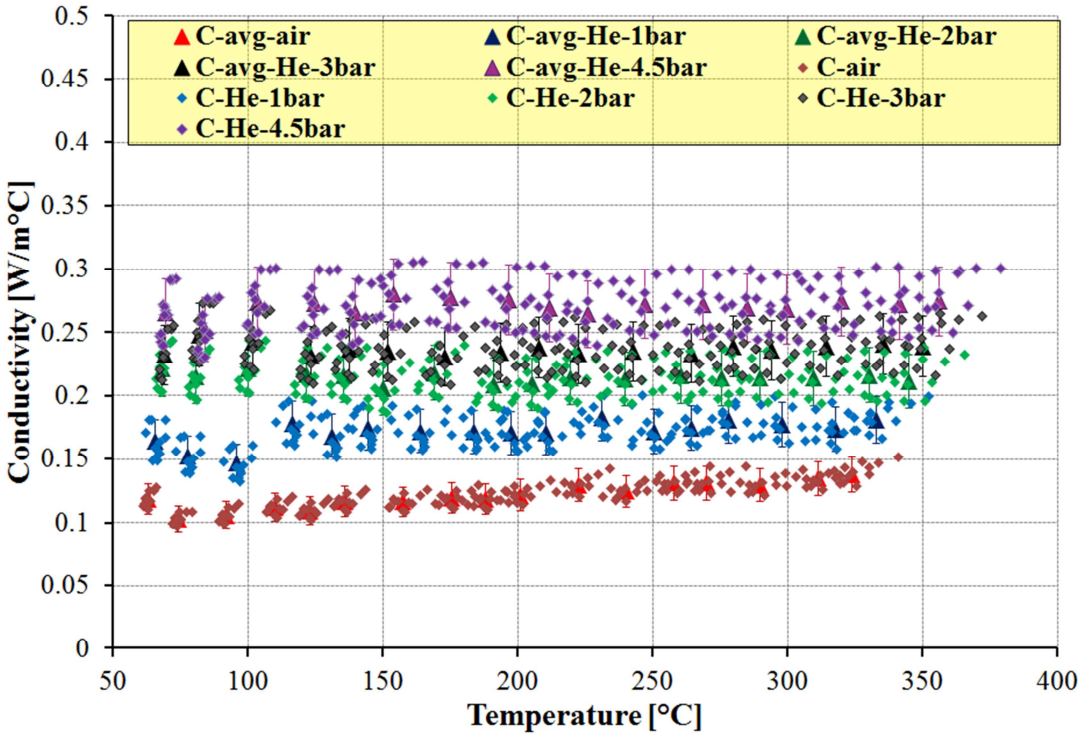

Fig. 64 – TxP experimental campaign on Si-C powder, RUN#2.

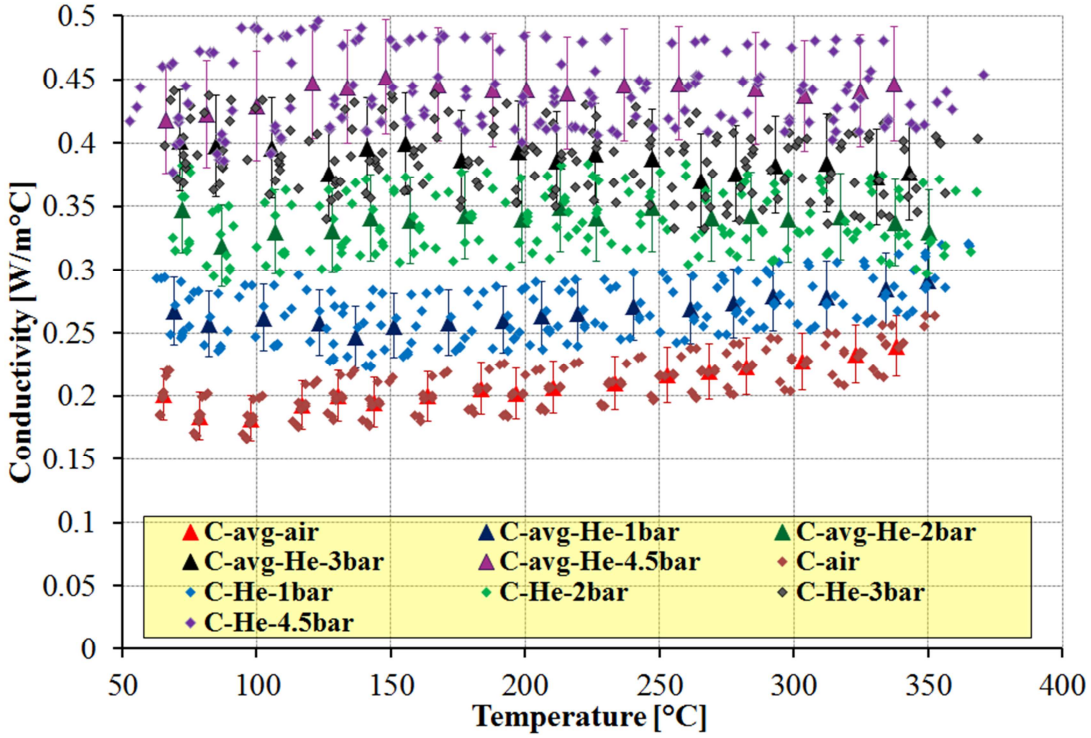

Fig. 65 – TxP experimental campaign on Si-C powder, RUN#3.

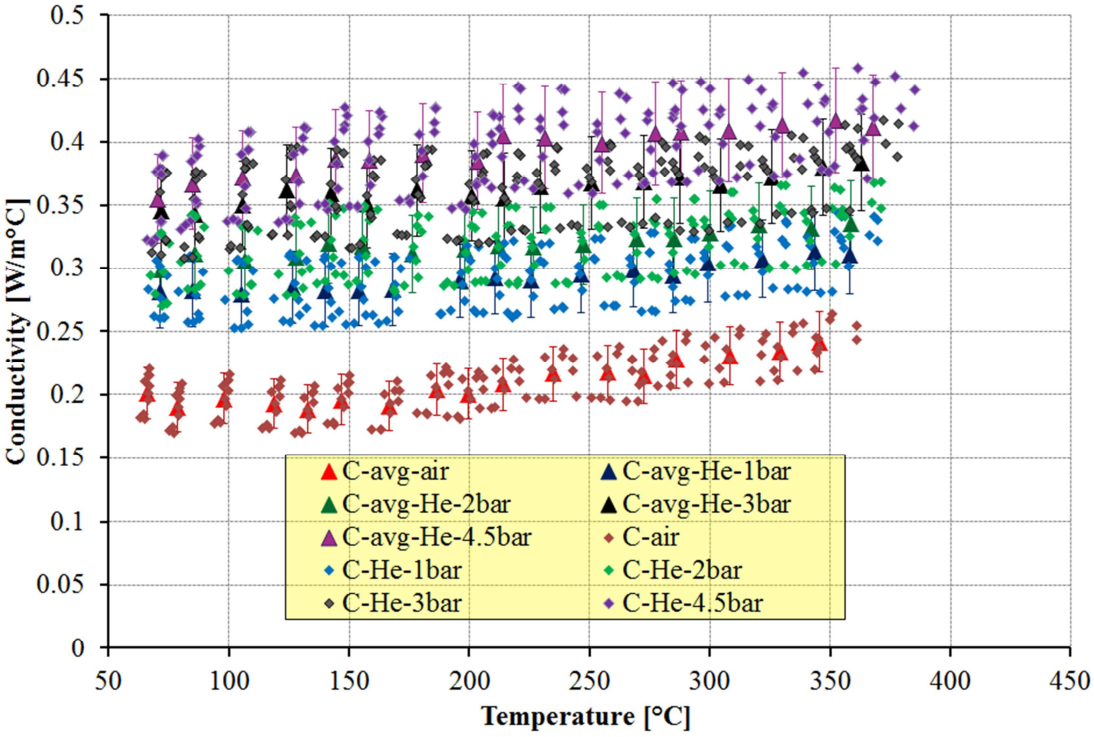

Fig. 66 – TxP experimental campaign on Si-C powder, RUN#4.

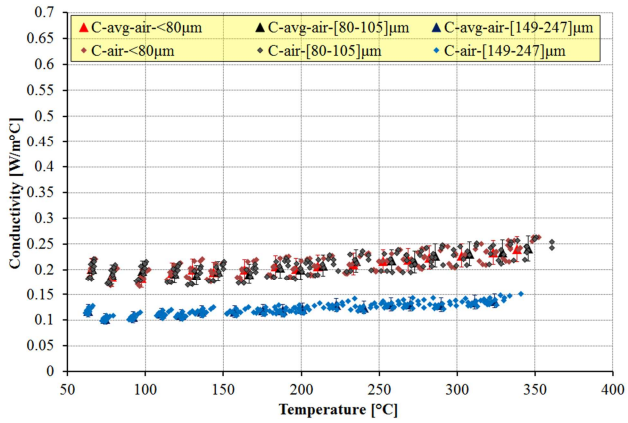

Effect of grain diameter under air unpressurized

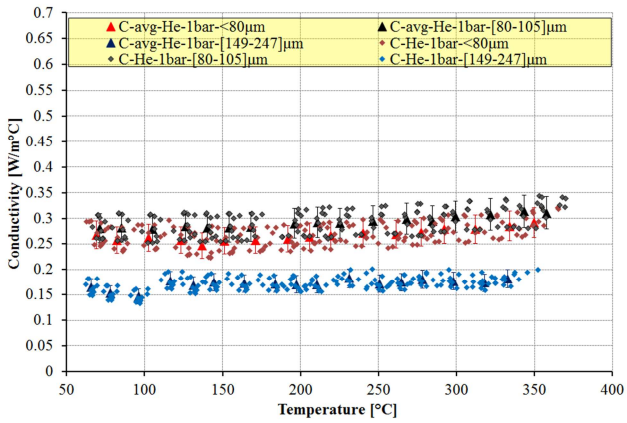

Effect of grain diameter under He 1bar

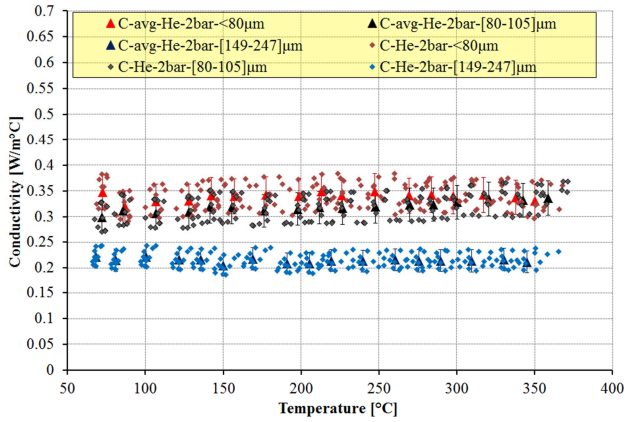

Effect of grain diameter under He 2bar

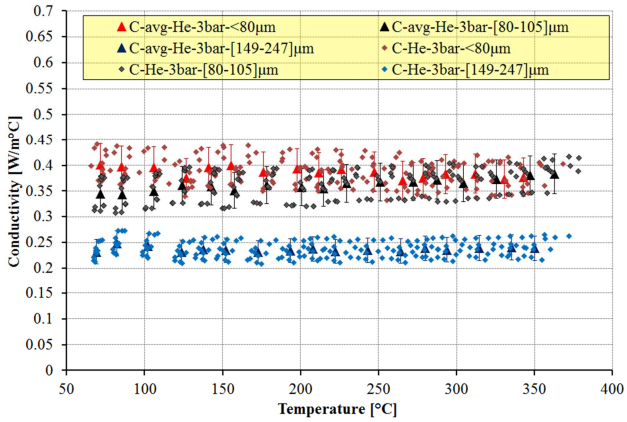

Effect of grain diameter under He 3bar

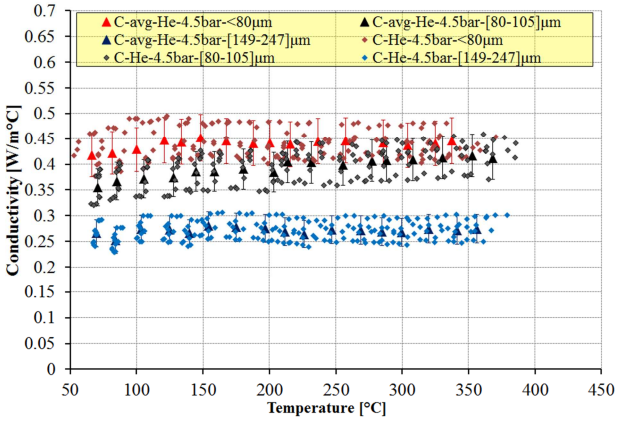

Effect of grain diameter under He 4.5bar

Fig. 67 – TxP experimental campaign on Si-C powder, comparison of tests RUN#2-3-4.

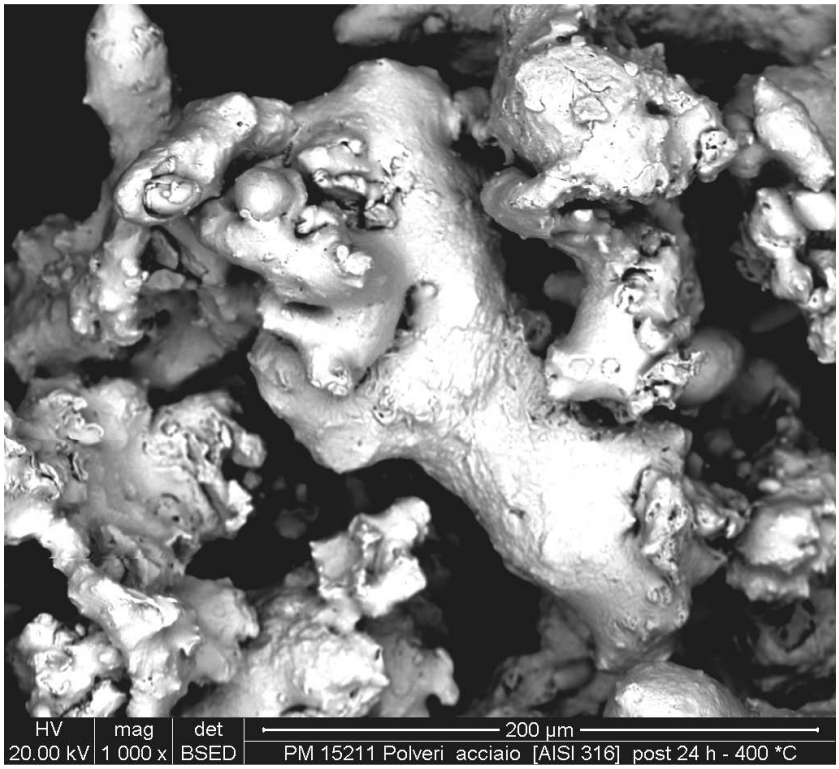

AISI-316 heated at 400°C

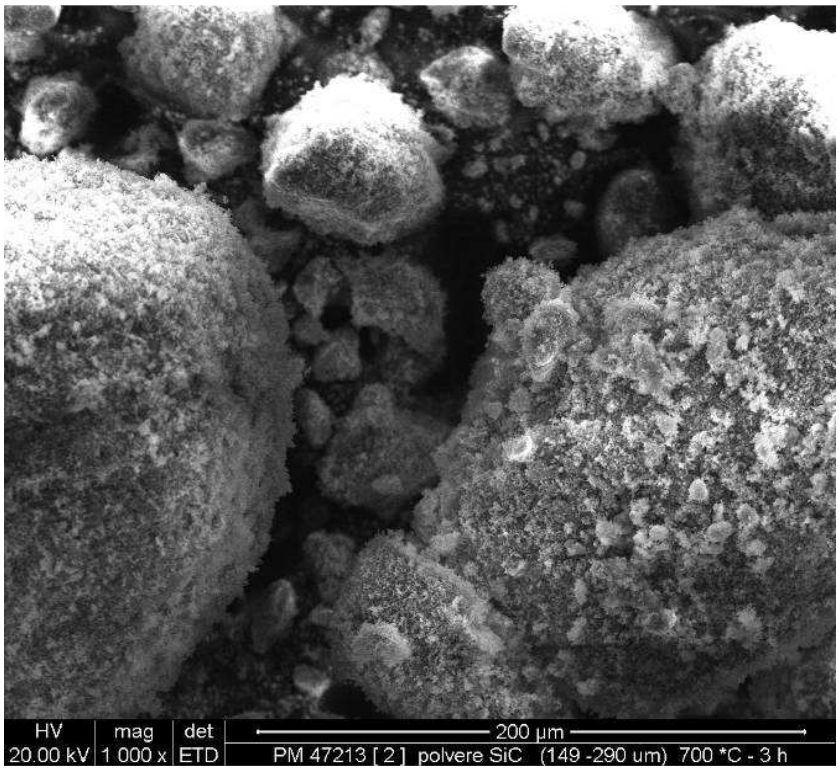

Si-C powder lot 149-290 µm (RUN#2)

Fig. 68 – SEM analysis, comparison between heated AISI-316 and Si-C.

6.5.2 Assessment of AISI-316 powder

6.5.2.1 Description

The present package of tests addresses AISI-316 powder with the aim to assess the suitability of this powder for the development of the HERO SG unit. In order to avoid the effect of thermal cycling on conductivity, these tests have been conducted as continuation of RUN#5.

- The subtests from RUN#5.5 to RUN#5.8 have been conducted using the same sample of powder loaded in RUN#5.0 (see also *Tab. 27*) in order to investigate the effect of helium introduction at different pressure levels once grain growth has saturated. They have been conducted under helium atmosphere at four different pressures: 1, 2, 3 and 4 bar. The temperature range was [100-450]°C with a temperature increase of 20-30°C. The holding time to achieve steady state condition between two set of measurements was about 15 minutes and the acquisition time was 6 minutes

The specifications of the tests are reported in *Tab. 29*. Since the powder experiences compaction during the first thermal cycles estimated porosity and density are unknown.

#	Description	Unit	RUN#5.5	RUN#5.6	RUN#5.7	RUN#5.8
	Material	--	AISI-316	AISI-316	AISI-316	AISI-316
(a)	Theoretical density	kg/dm^3	7.96	7.96	7.96	7.96
(b)	Reference density[1]	kg/dm^3	3.40	3.40	3.40	3.40
(c)	Estimated density[2]	kg/dm^3	unknown	unknown	unknown	unknown
(d)	Loaded powder	kg	14.12	14.12	14.12	14.12
(e)	Estimated porosity[3]	--	unknown	unknown	unknown	unknown
(f)	Filling gas	--	He 1bar	He 2bar	He 3bar	He 4bar
(g)	HR-14 - PIPE-5 free vol.[4]	l	3.812	3.812	3.812	3.812
(h)	Powder content	l	unknown	unknown	unknown	unknown
(i)	Powder vibration	--	--	--	--	--
(j)	Testing temperature range	°C	100-450	100-450	100-450	100-450
(k)	Temperature increase	°C	20-30	20-30	20-30	20-30
(l)	Holding time	min	15	15	15	15
(m)	Data acquisition time	min	6	6	6	6
(n)	Grain diameter range[5]	µm	--	--	--	--
(o)	Cycle N°	--	5	1	1	1

[1] obtained weighting the powder without vibration into a graduated cylinder of 1 l
[2] obtained as [kg of powder introduced in HR-14 - PIPE-5] / [measured HR-14 - PIPE-5 free volume dm^3]
[3] obtained as [estimated density] / [theoretical density]
[4] measured by injection of water
[5] intended as max and min measured average diameter as documented in Appendix C, Fig C. 1

Tab. 29 – TxP experimental campaign on Si-C powder, RUN#5, summary of the test matrix under helium environment.

6.5.2.2 Main achievements

The experimental findings are reported *Fig. 69*. The figure includes a correlation obtained by parabolic interpolation for each test (reported from *Eq. 31* to *Eq. 34*). The data points do not distinguish the azimuthal and axial location of the thermocouples. As in the case of Si-C,

pressurizing the facility it is possible to increase the conductivity up to a value that is about 400% greater than the maximum value measured for Si-C.

Therefore, since at the end of these tests the HERO SG unit was still under construction, it was confirmed to load it with AISI-316 powder instead of Si-C and to design the helium chamber to operate without leakages at 4 bar. The effect of this modification is discussed in section 7.2.1.3.

$$C_{RUN\#5.5} = C_{He-1bar} = 9 * 10^{-6}T^2 - 9 * 10^{-4}T + 1.0963 \quad \textit{Eq. 31}$$

$$C_{RUN\#5.6} = C_{He-2bar} = 7 * 10^{-6}T^2 + 2 * 10^{-4}T + 1.112 \quad \textit{Eq. 32}$$

$$C_{RUN\#5.7} = C_{He-3bar} = 7 * 10^{-6}T^2 + 2 * 10^{-4}T + 1.2412 \quad \textit{Eq. 33}$$

$$C_{RUN\#5.8} = C_{He-4bar} = 5 * 10^{-6}T^2 + 8 * 10^{-4}T + 1.3198 \quad \textit{Eq. 34}$$

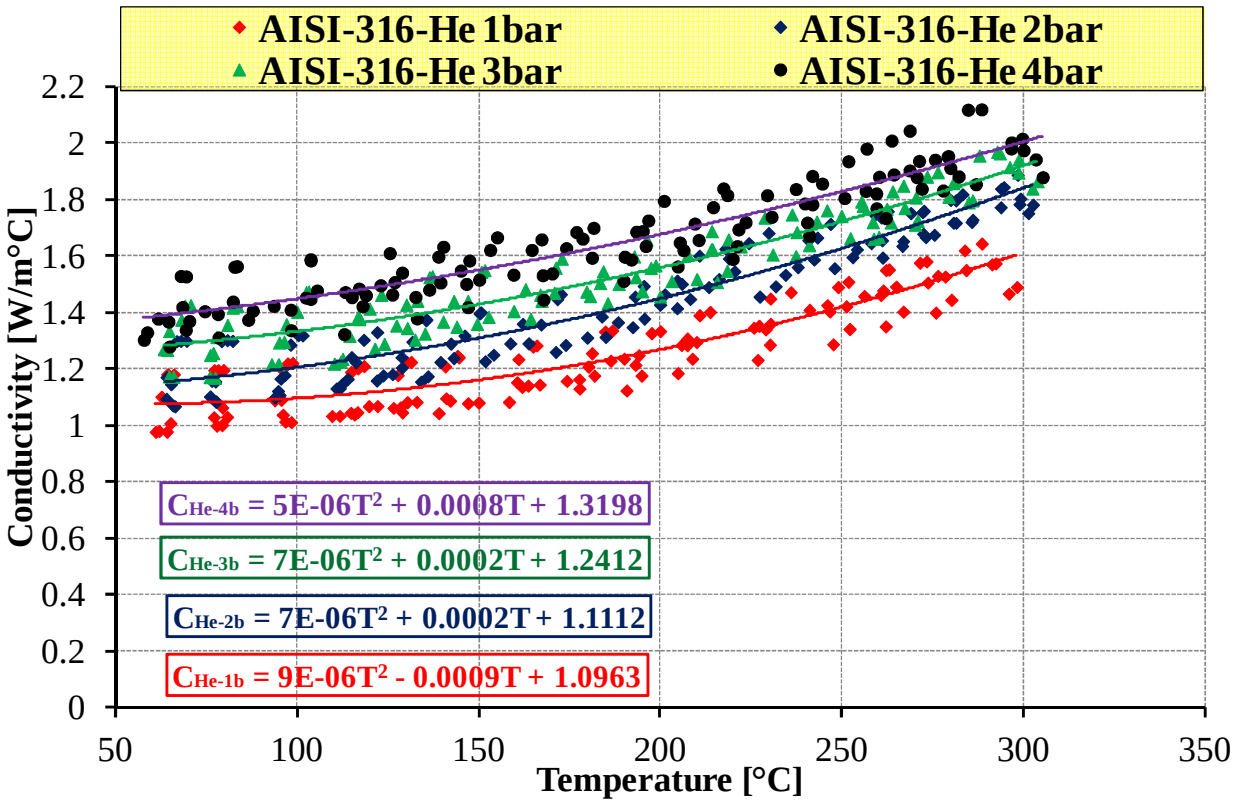

Fig. 69 – TxP experimental campaign on Si-C powder, RUN#5.5-6-7-8 effect of helium pressure on conductivity.

7 Design and construction of the Heavy liquid mEtal – pRessurized water cOoled tube (HERO)

The Heavy liquid mEtal – pRessurized water cOoled tube (HERO) aims to study a 1:1 bayonet tube/s under conditions that represent, as much as possible, the operation of the ALFRED SG. The facility is expected to be a suitable tool to support the validation process of TH-Sy codes and CFD codes coupled simulations. Two different conceptual configurations have been assessed to check their feasibility and then, the most promising solution has been designed and constructed.

The first one deals with a standalone facility to test a single tube and is based on natural circulation into the lead side [35]. The second one deals with a test section to be introduced in CIRCE to investigate an hexagonal bundle of seven tubes and is based on gas enhanced circulation into the lead side [59]. This last configuration has been selected, designed, constructed (the SG bundle) and test section is under commissioning.

7.1 Feasibility analysis of HERO

7.1.1 HERO standalone facility based on natural circulation

7.1.1.1 Conceptualization of the primary side

The schematic configuration is based on natural circulation flowing lead, it basically consists of a single bayonet tube immersed into a channel of a pool that is heated at the bottom to promote natural circulation into the annular riser that feed the bayonet tube channel, as reported in *Fig. 70*.

Lead side:

- The submerged height of the bayonet tube is 6 meters, according to the SG conditions.
- Argon atmosphere is realized above the active length (1 m in height as in the SG).
- The liquid lead heats-up in the bottom part of the facility. The power is supplied by electrically heated rods located inside the facility and it corresponds to the power removed by the single bayonet unit (about 74 kW).
- The liquid lead flows by natural circulation in the outer annular region (*Fig. 70*). Then it enters in down flow the bayonet tube channel from the top (as in the SG). The lead channel and the outer annular region are separated by a sandwich wall composed of AISI-304-insulating medium-AISI-304. In the preliminary concept, the insulating medium consists of paint, the same adopted in the bayonet tube to avoid heat exchange between the descending feed-water and the superheated steam annular riser.
- The bayonet tube channel has appropriate fissures to allow the lead flow. In the preliminary configuration, 16 identical fissures are considered 8 located at the top and 8 at the bottom.
- The zone located below the bayonet tube is fixed to 3.1 m in length to promote natural circulation (verified by calculations considering the maximum elevation that could be realized). The power is supplied in the lead side by means of 8 heating rods located between the sandwich wall and the outermost tube (*Fig. 71 a)*). In the preliminary concept, their active length is fixed to 1 m.

The main requirement of the lead loop is to provide a mass flow rate of 6.367 kg/s and 74 kW in the lead channel (as in the SG) in order to be representative of the SG. Therefore, the main parameters to be calculated are X and Y, *Fig. 70*. Should be pointed out that Y affects the simulation of the P/D of the ALFRED SG. It is expected that P/D will not be reproduced (the facility must provide 6.367 kg/s without pumps). Therefore, any deviation from P/D = 1.45 (as in the SG) must be assessed in term of discrepancies from the in reactor behavior. In order to be conservative, the lead mass flow rate should have a certain flexibility. This is realized by means of (lead) level regulation at the top fissures, *Fig. 71 b)*.

Bayonet tube: the bayonet tube is that designed by ANSALDO.

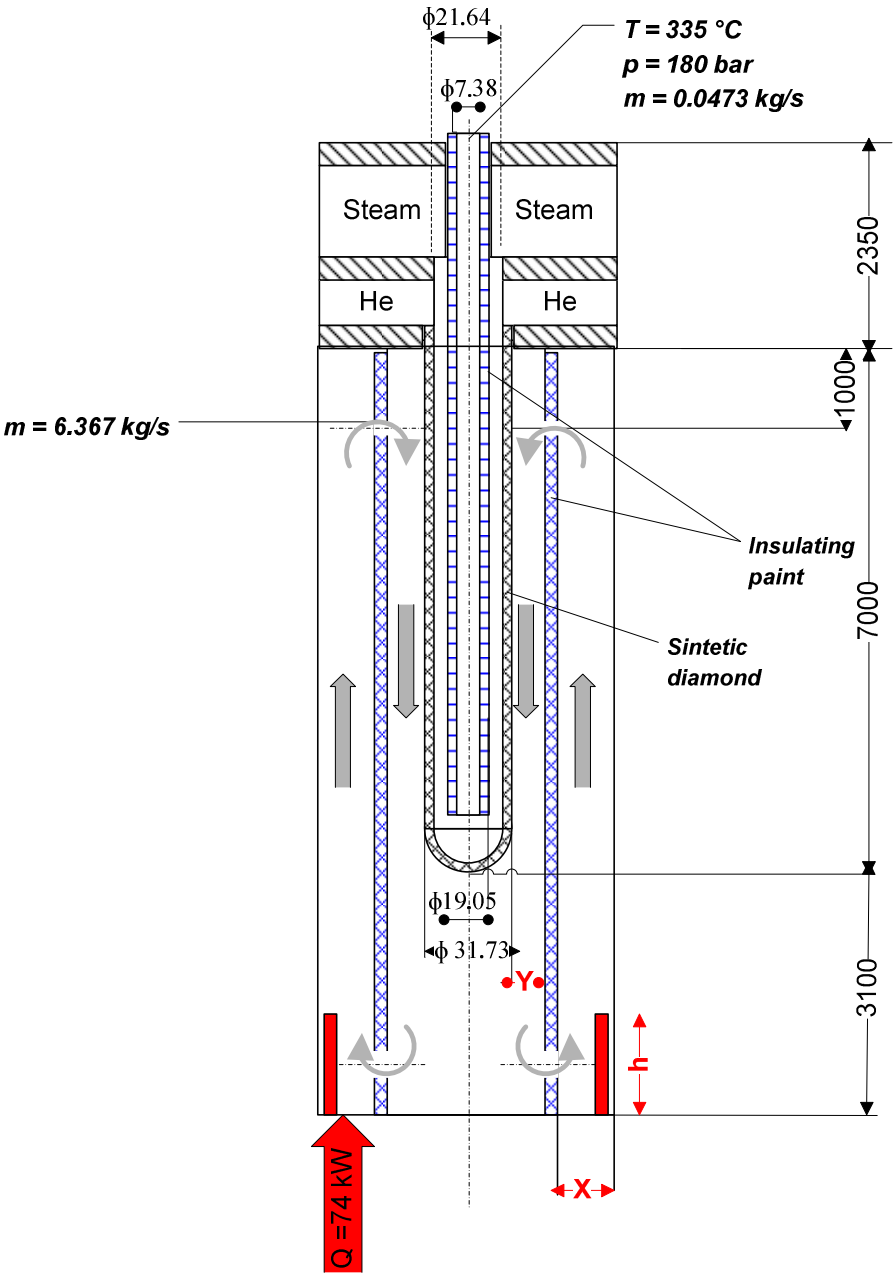

Fig. 70 – HERO standalone facility configuration, lead loop scheme with internal heating rods.

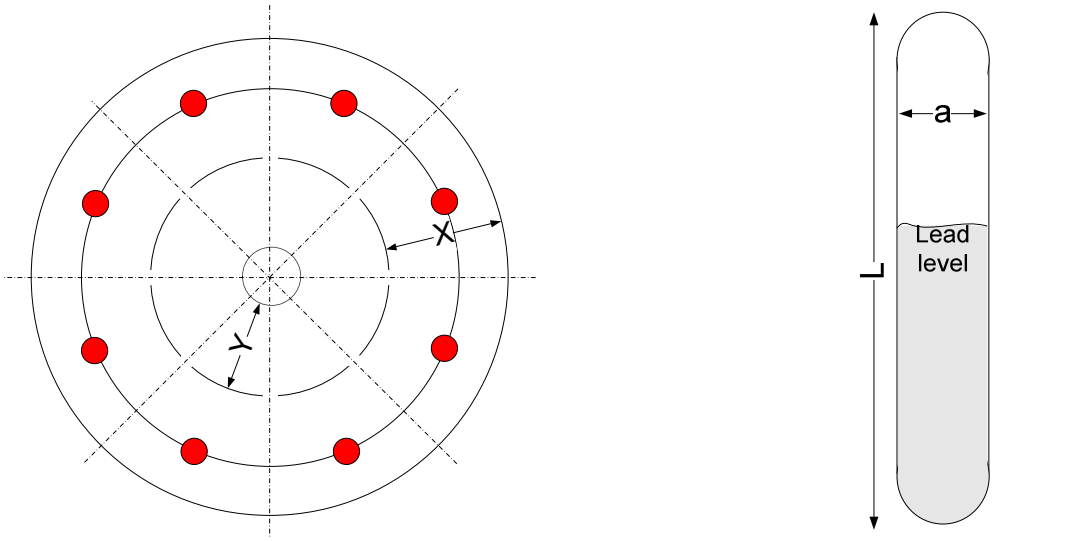

a) Heating rods position b) Top fissure schematization

Fig. 71 – HERO standalone facility configuration, heating rods and fissure.

7.1.1.2 Initialization of the primary side model

The first RELAP-5 input deck is developed according to the scheme reported in *Fig. 72*. For feasibility analysis purpose, the bayonet tube is modeled according to section 4 when not differently specified. The hydraulic model includes: the feed-water descending tube (pipe 100), the annular riser (pipe 110) the lead down flow region (pipe 140 and pipe 160) the lead up flow region (pipe 170 and pipe 180) and the fissures (branches 165-166 and branches 136-137). The bayonet tube heat structures include the T91-paint-T91 double wall (HS1100), the T91-sintetic diamond-T91 double wall (HS1110). The remaining heat structures are the AISI-304-paint-AISI-304 double wall (HS1140) and the outermost AISI-304 tube wall in which the heat source is modeled in the lower nodes of its outer surface (Power999). In steady state conditions, it represents the scheme reported in *Fig. 70* since the heating source is modeled without heat losses. The detailed input deck is reported in Ref. [35]. The main geometrical data of initial configuration are summarized in *Tab. 30*. The following assumptions have been introduced:

- The heat exchange between the annular steam riser and the Argon zone has been neglected, that means adiabatic behavior of the non-active region located outside the tube.
- The conductivity of the insulating paint in structure HS1140 has been fixed equal to those adopted for the SGBT: 0.05 W/mK.
- The lead channel, Pipe 140, is modeled as in section 4 excepts the hydraulic diameter that considers the tube outer surface. This means that the lead flow area corresponds to the SG configuration, Y = 7.8 mm (even if its hydraulic diameter is different).
- The heat transfer between the lead side and the steam annular riser is modeled according to the Seban correlation [32][33] instead of Mykitiuk since it is not a bundle.
- The annular lead riser is modeled by Pipe 170 and Pipe 180. Their flow area is assumed double time the flow area of pipe 140 that means X = 8.8 mm.
- The outermost tube outer surface is considered adiabatic.
- The 8 fissures at the top and those at the bottom are modeled assuming to keep as constant their flow area. The initial value is selected equal to the bottom holes inlet flow area (0.0017 m^2). They are modeled as branches 136, 137 and 165, 166.

- The local pressure loss coefficients are modeled as boundaries of a range that has been calculated based on Ref. [60]. Two calculations are thus performed assuming maximum and minimum local pressure losses.

Component	Description	Quantity	Component	Description	Quantity
Inner feedwater tube	OD	9.52 mm	***Lead Down flow double wall***	OD	51.23 mm
	T91 thickness	1.07 mm		SS thickness	2.00 mm
	Paint thickness	2.88 mm		Paint thickness	3.00 mm
	OD	19.05 mm		OD	61.25 mm
	T91 thickness	1.07 mm		SS thickness	2.00 mm
Annular riser	OD	25.40 mm	***Outermost tube***	OD	88.77 mm
	T91 thickness	1.88 mm		SS thickness	5 mm
	diamond thickness	1.07 mm	***Fissures***	Total flow area	1740 mm^2
	OD	31.73 mm	--	X	8.76 mm
	T91 thickness	2.11 mm	--	Y	7.76 mm

Tab. 30 – HERO standalone facility configuration, summary of the initial geometry.

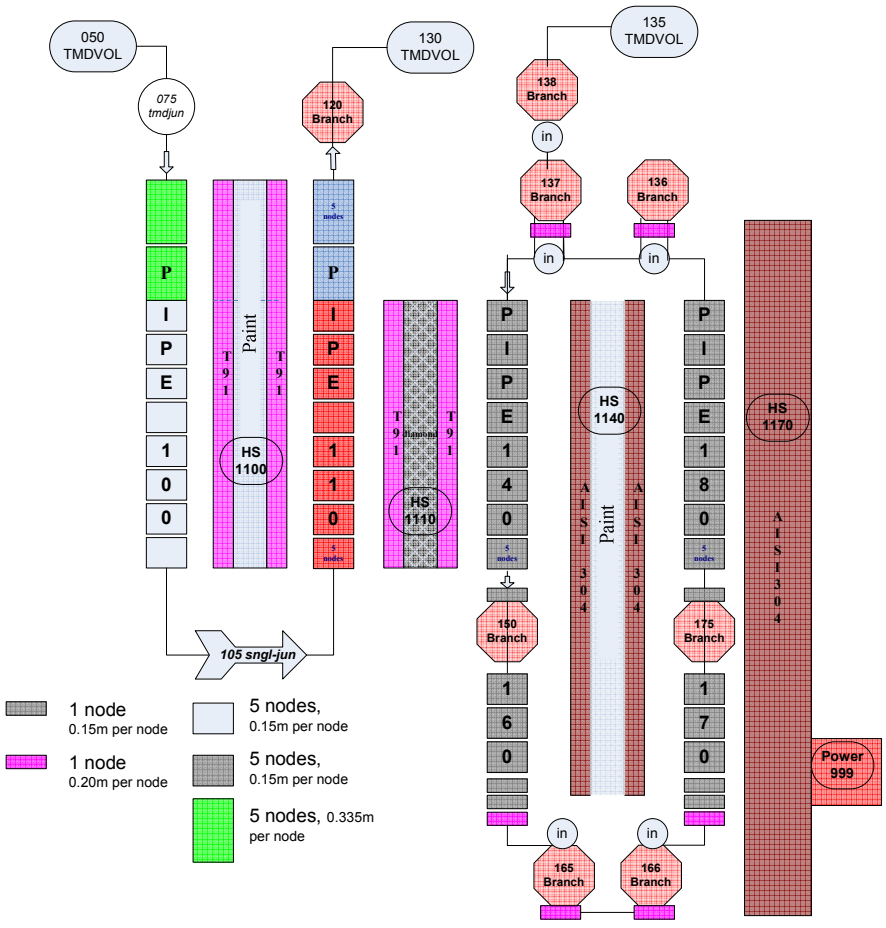

Fig. 72 – HERO standalone facility configuration, RELAP-5 input deck scheme.

7.1.1.3 Determination of the acceptable geometry

The main aim of the analysis is to point out the reference geometry. In order to get an appropriate margin of operation, the goal is to obtain a mass flow rate larger than 6.367 kg/s, possibly close to 7.0-7.5 kg/s. The lead flow area is expected to dominate the mass flow rate. Therefore, three types of simulations are performed starting from the initial configuration.

- The first investigates the influence of the outer flow area AX. The initial flow area is assumed two times those of the bayonet tube lead channel (in the SG configuration): 2AX. The analysis exploits 4AX, 6AX and 10AX that means 4, 6 and 10 times the bayonet tube lead channel flow area in the SG configuration.
- The second one investigates the influence of the bayonet tube channel flow area AY. The initial flow area is modeled equal to the SG lead channel configuration: AY (=AX). 1.5AY, 2AY, 2.5AY and 3AY are analysed (that means 1.5, 2, 2.5 and 3 times the bayonet tube lead channel flow area in the SG configuration).
- The last one deals with the combination of the previous, AX-AY.

Fig. 73 reports the flow area of the up flow outer channel (x axis) and the lead mass flow rate (y axis). Both maximum and minimum concentrated pressure losses are accounted (k-max and k-min). The green dotted curve represents the SGBT lead mass flow rate.

- At constant down-flow channel flow area AY, the lead mass flow rate does not reach 4 kg/s whatever is the up flow outer channel flow area (i.e. 10 AX), red - black labeled points.
- On the other hands, at constant outer channel flow area 2AX, the lead mass flow rate does not reach 5 kg/s whatever is the down-flow channel flow area (i. e. 3 AY), black – blue labeled points.
- It is therefore necessary to reduce the distributed pressure losses limiting the lead velocity and thus increasing both the flow areas (red – blue labeled points). In particular, 4AX-2.5AY, and 6AX-2.5AY have been selected as potential geometries. They allows to reach 6.5 – 7.4 kg/s.
- Concentrated pressure losses have in general a minor impact on the simulations, particularly at low flow areas. At high flow areas (i. e. 6AX-2.5AY), the concentrated pressure losses highlight a certain influence on the results.

The main results are summarized in *Tab. 31*. The table reports the mass flow rates achieved in the simulations. In order to confirms that steady state conditions are reached the calculation are repeated increasing the final time from 900 to 1100 seconds. In conclusion, the potential geometries have been fixed according to *Tab. 32*.

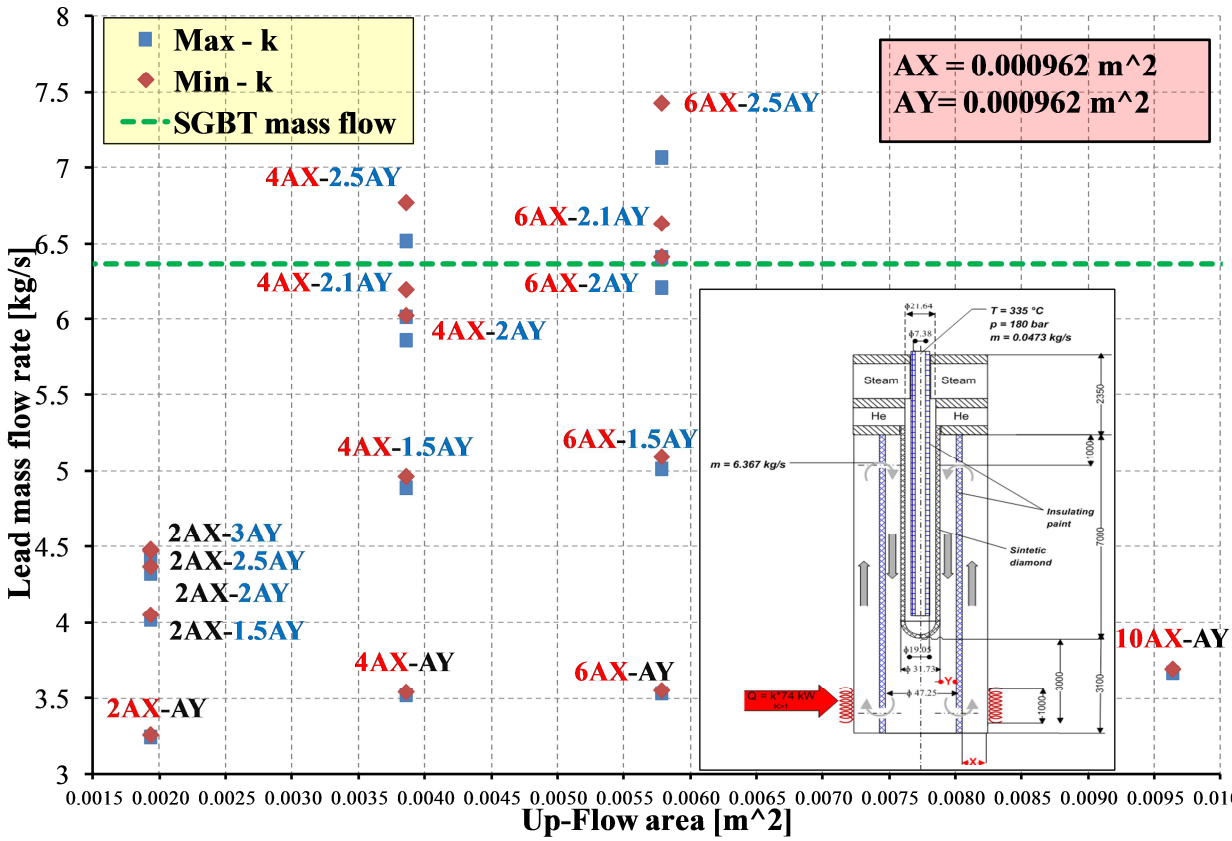

Fig. 73 – HERO standalone facility configuration, calculations in support to the determination of the radial geometry.

Description	Max k		Min k	
	Mass flow 900 s [kg/s]	Mass flow 1100 s [kg/s]	Mass flow 900 s [kg/s]	Mass flow 1100 s [kg/s]
2Ax-Ay	3.25	3.25	3.26	3.26
4Ax-Ay	3.52	3.51	3.54	3.53
6Ax-Ay	3.53	3.52	3.55	3.54
10Ax-Ay	3.67	3.56	3.70	3.57
2Ax-1.5Ay	4.02	4.01	4.05	4.04
4Ax-1.5Ay	4.89	4.87	4.96	4.94
6Ax-1.5Ay	5.01	5.01	5.09	5.10
2Ax-2Ay	4.32	4.31	4.37	4.36
4Ax-2Ay	5.86	5.85	6.03	6.01
6Ax-2Ay	6.21	6.19	6.41	6.39
4Ax-2.1Ay	6.02	6.00	6.20	6.19
6Ax-2.1Ay	6.41	6.38	6.63	6.62
2Ax-2.5Ay	4.42	4.41	4.47	4.46
4Ax-2.5Ay	**6.52**	**6.50**	**6.77**	**6.76**
6Ax-2.5Ay	**7.07**	**7.06**	**7.43**	**7.41**
2Ax-3Ay	4.43	4.42	4.48	4.47

Tab. 31 – HERO standalone facility configuration, calculations in support to the determination of the radial geometry, summary of the results.

Label	Parameter	Unit	Quantity
4AX-2.5AY	**4AX up-flow area**	m^2	0.003852
	2.5AY down-flow area	m^2	0.002407
	X	m	0.013437
	Y	m	0.016041
6AX-2.5AY	**6 AX up-flow area**	m^2	0.005778
	2.5 AY down-flow area	m^2	0.002407
	X	m	0.018997
	Y	m	0.014058

Tab. 32 – HERO standalone facility configuration, definition of the potential radial geometries.

7.1.1.4 Feasibly of regulation

This calculation aims to assess the influence of the fissure geometry on the lead mass flow rate considering the possibility to regulate it by changing the submerged area of the fissures inside the lead and therefore changing the lead level. This feature is retained the most important issue that influence the feasibility of the standalone HERO facility based on natural circulation.

Eight fissures at the bottom and eight at the top are considered in this calculation. Each fissure is assumed 0.005m x 0.100m which is considered feasible in terms of mechanical realization. The fissures are located as depicted in *Fig. 71*. Their maximum flow area is 0.004 m^2.

The regulation curves are depicted in *Fig. 74*, *Fig. 75* and summarized in *Tab. 33*.

The configuration 4AX-2.5AY allows to achieve a flow rate in the range 6.9-7.0 kg/s (*Fig. 74*) at maximum flow area. The lead level largely affects the lead mass flow rate up to 50mm. Beyond this value, the lead level has a minor influence on the mass flow rate. The lead levels 25mm (min -k) and 35mm (max-k) correspond to the desired mass flow rate. Their total flow areas are 0.0010 m^2 and 0.0014 m^2 respectively, *Tab. 33*.

The configuration 6AX-2.5AY allows to achieve a flow rate in the range 7.7-7.8 kg/s at maximum flow area, *Fig. 75*. The lead level largely affects the lead mass flow rate up to 50 mm. Beyond this value, the lead level has a minor influence on the mass flow rate. The lead levels 17.5 mm (min -k) and 25 mm (max-k) correspond to the desired mass flow rate. Their total flow areas are 0.0007 m^2 and 0.0010 m^2 respectively, *Tab. 33*.

In conclusion, nor 4AX-2.5AY and nor 6AX-2.5AY have been selected as reference standalone configuration of HERO since in their operating conditions (6.367 kg/s), the lead level seems to play high influence on the lead mass flow even if the fissures are distributed along four axial elevations, Fig. 76.

A possible alternative is to adopt gas enhanced circulation. In this last case, the initial purpose of HERO to operate as tool for V&V of CFD – TH-sy coupling has same limits. However, from the TH point of view it better represents the SG geometry since it allows to keep unchanged the SGBT channel geometry.

Level [mm]	Total flow area [m^2]	6AX-2.5AY		4AX-2.5AY	
		Max – k mass flow [kg/s]	Min – k mass flow [kg/s]	Max – k mass flow [kg/s]	Min – k mass flow [kg/s]
100.0	0.004	7.6530	7.7536	6.9140	6.9758
87.5	0.0035	7.6190	7.7343	6.8894	6.9635
75.0	0.0030	7.5633	7.7041	6.8518	6.9444
62.5	0.0025	7.4732	7.6507	6.7915	6.9127
50.0	0.0020	7.3172	7.5700	6.6850	6.8552
47.5	0.0019	7.2736	7.5428	6.6537	6.8382
45.0	0.0018	7.2240	7.5136	6.6183	6.8187
42.5	0.0017	7.1671	7.4795	6.5792	6.7960
40.0	0.0016	7.1003	7.4394	6.5326	6.7692
37.5	0.0015	7.0240	7.3919	6.4732	6.7371
35.0	**0.0014**	6.9363	7.3363	**6.4099**	6.6987
32.5	0.0013	6.8287	7.2703	6.3336	6.6515
30.0	0.0012	6.7056	7.1909	6.2426	6.5957
27.5	0.0011	6.5606	7.0923	6.1330	6.5268
25.0	**0.0010**	**6.3885**	6.9734	6.0003	**6.4367**
22.5	0.0009	6.1839	6.8175	5.8400	6.3269
20.0	0.0008	5.9345	6.6286	5.6394	6.1848
17.5	**0.0007**	5.6385	**6.3870**	5.3945	5.9996
15.0	0.0006	5.2800	6.0760	5.0885	5.7522
12.5	0.0005	4.8462	5.6735	4.7079	5.4244
10.0	0.0004	4.3207	5.1485	4.2305	4.9759
7.5	0.0003	3.6768	4.4625	3.6309	4.3625
5.0	0.0002	2.8901	3.5598	2.8700	3.5160
2.5	0.0001	1.9333	2.3339	1.8173	2.3188
0.0	0.0000	0.0000	0.0000	0.0000	0.0000

Tab. 33 – HERO standalone facility configuration, assessment of the potential configurations, mass flow rates as function of fissures flow area (and lead level).

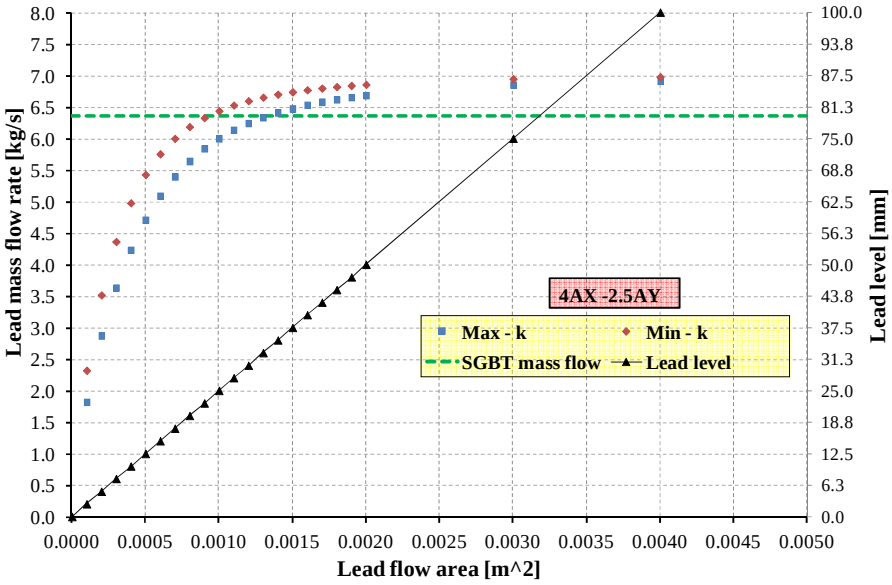

Fig. 74 – HERO standalone facility configuration, 4AX-2.5AY, mass flow rate as function of lead level at the fissures inlet.

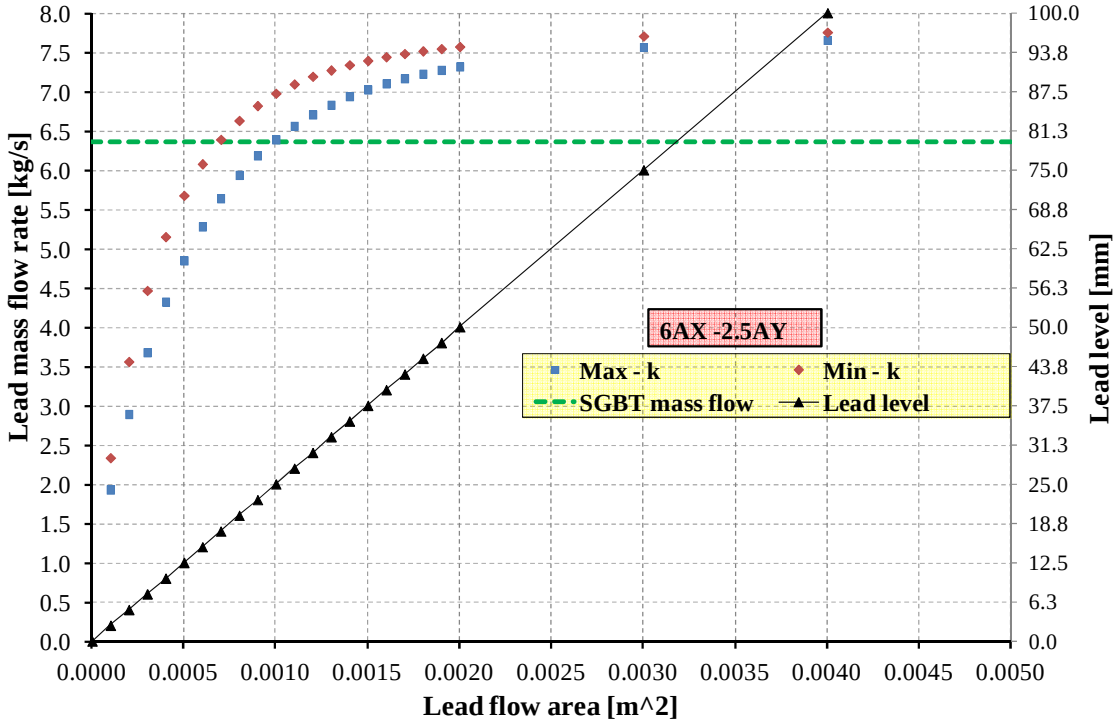

Fig. 75 – HERO standalone facility configuration, 6AX-2.5AY, mass flow rate as function of lead level at the fissures inlet.

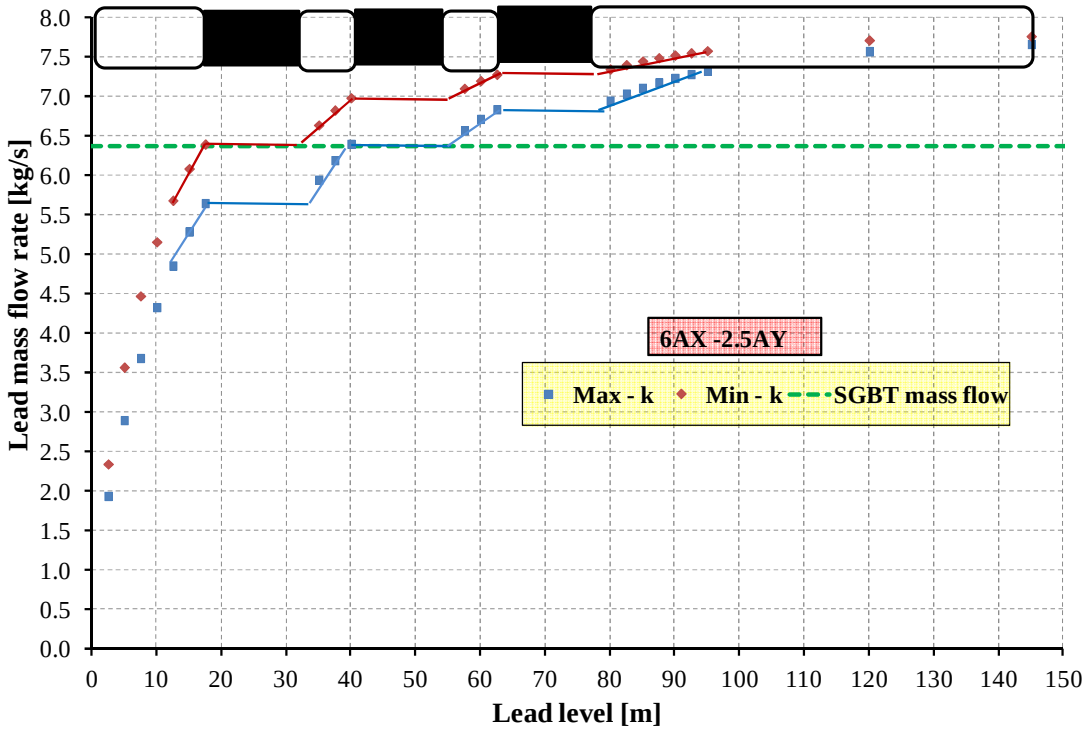

Fig. 76 – HERO standalone facility configuration, 6AX-2.5AY, mass flow rate as function of lead level at the fissures inlet with axially distributed fissures.

7.1.2 HERO as CIRCE test section

CIRCE basically consists of a cylindrical vessel (Main Vessel S100) filled with about 70 tons of molten Lead-Bismuth Eutectic (LBE) with argon cover gas and recirculation system, LBE heating and cooling system, several test sections welded to and hung from bolted vessel heads for separate-effect and integral testing, and auxiliary equipment for eutectic gas enhanced circulation [13].

In *Fig. 77*, an isometric view of the facility is shown. The facility can be considered made up of two parts, the first being dedicated to the LBE containment and management, and the other consisting of the auxiliary systems.

Concerning the first part, the main components are the above mentioned vessel S100, the storage tank S200 and the intermediate vessel S300, this later one being used during the handling of the LBE between the two other vessels. During the loading operations, the LBE is gradually transferred from the storage tank to the S300 vessel. In this way, step by step, S100 is gradually filled from the bottom. This main vessel consists of a vertical vessel which is 8500mm in height, connected by gates to the other systems, from both the LBE and gas sides. It is equipped with electrical heating cables, installed on its bottom and lateral surface. This heating system allows operating in a temperature range of 200÷400 °C. The main vessel is also equipped by a skimming line and a passive pressure safety system, in order to guarantee the LBE top level and to prevent accidental overpressure. The main parameters of CIRCE are listed in *Tab. 34*.

Parameters	**Value**
Outside diameter [mm]	1200
Wall thickness [mm]	15
Material	AISI 316L
Max LBE Inventory [kg]	90000
Electrical Heating [kW]	47
Cooling Air Flow Rate [Nm^3/s]	3
Temperature Range [°C]	200 to 500
Operating Pressure [kPa]	15 (gauge)
Design Pressure [kPa]	450 (gauge)
Argon Flow Rate [Nl/s]	15
Argon Injection Pressure [kPa]	600 (gauge)

Tab. 34 –CIRCE main data.

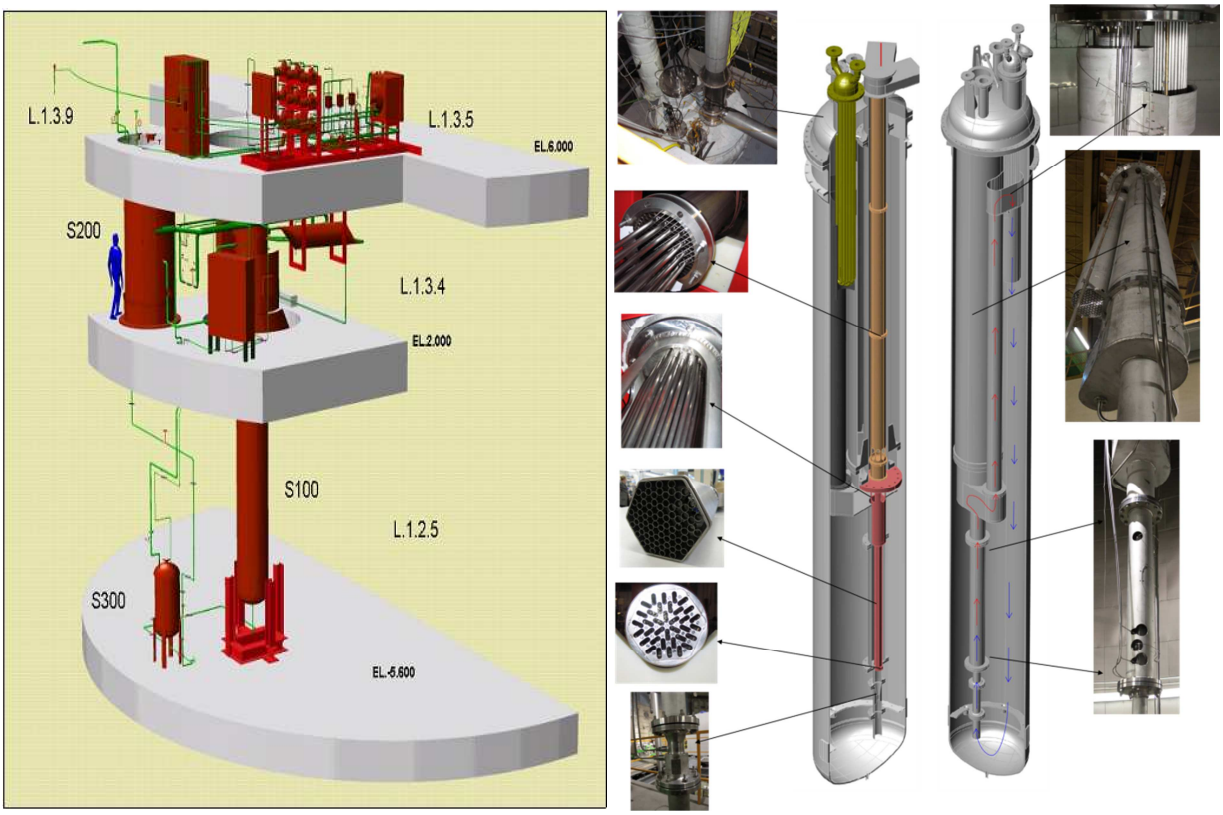

Fig. 77 – CIRCE isometric view.

7.1.2.1 Conceptualization of the primary side

This configuration is based on a hexagonal shroud that contains seven SGBT of same geometry of the ALFRED SG Fig. 78. This device is placed inside CIRCE and is fed by LBE which flows by gas enhanced circulation from the top by means of fissures that communicate with the CIRCE pool. The LBE flows inside the tube bundle for six meters (as in the SG of ALFRED) and then it leaves the device from the bottom which is opened. Thermal insulation of the shroud from CIRCE is required.

This system does not pose problems that could impair its feasibility. Furthermore, it has the following advantages compared to the standalone facility:

- The SGBT design of ALFRED could be reproduced as much as technological limits or market limits will impair its construction (i.e. F/M steel T91 could not be used as tube material due to welding problems and the difficulty to acquire it only for seven tubes).
- Seven tubes are more representative of the SG than one tube and they allow the experimental assessment of dynamic instabilities.
- The lead mass flow is regulated by enhanced circulation using a system that is already available in CIRCE.
- The required power (443 kW) is supplied by a system that is already available in CIRCE.
- The cost of the test section is lower than those of a standalone facility

Therefore, it has been decided to design and construct HERO as a CIRCE test section.

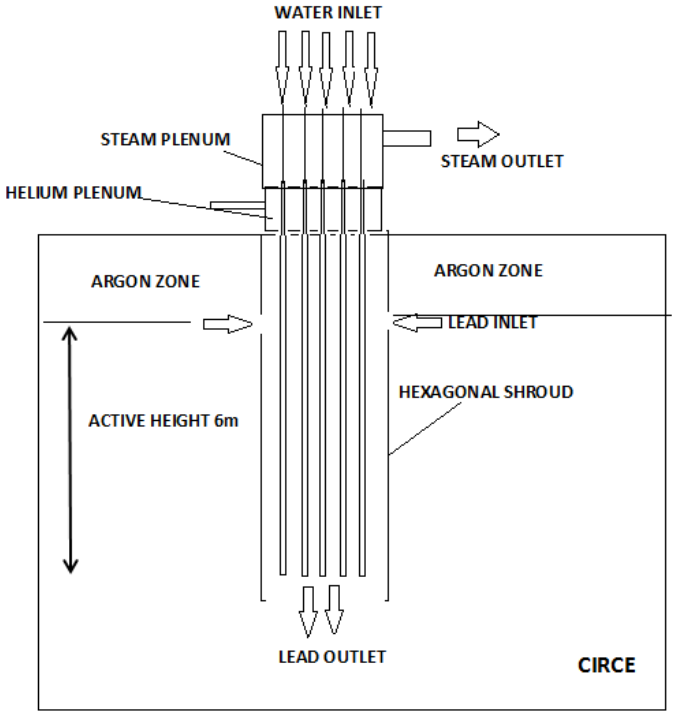

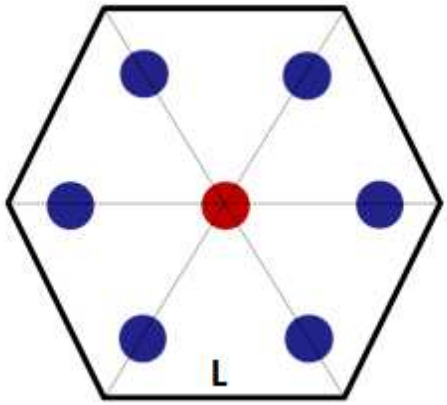

Shroud geometry		
L	m	0.0726
Transversal area	m^2	0.0137
Power	kW	504

Schematic layout *Transversal section of the SG*

Fig. 78 – HERO test section, conceptual scheme of the SG unit.

7.2 Design and construction of the HERO test section SG bundle

7.2.1 Bayonet tube design

7.2.1.1 Material selection

In order to construct the bayonet tubes it is necessary to modify some of the materials adopted for the ALFRED SG and to define the materials still not identified. These design choices are given in *Tab. 35*. In order to assess the relative influence of the materials on the reference calculation presented in section 4, four distinct calculations have been executed by means of RELAP-5:

- SiC: the high conductivity material used to fill the annular region between the lead and the water-steam sides was not yet defined by ANSALDO. The reference analysis was conducted assuming sintetic diamond (see section 4). Due to the cost of this material Silicon Carbide is assumed as alternative powder. The conductivity of this material has been modeled in the powder gap thermal structure instead of sintetic diamond. As in the reference calculation, it is assumed as 0.3 porosity Si-C and its conductivity has been selected on the basis of correlations Case 1 and Case 2. Since Si-C has lower conductivity than sintetic diamond, it is expected a degradation of the TH performance.
- AISI: The conductivity of AISI-304 has been modeled in the thermal structures of the tubes instead of T91. This choice is justified by the un-availability of small lots of T91 and by the complexity to realize and qualify T91 welded joints. Since T91 has higher conductivity and higher mechanical resistance than AISI-304, it is expected a degradation of the TH performance due to both lower conductivity and higher thicknesses.
- FOAM: ZIRCOFOAM 250 has been modeled in the feed-water tube thermal structure instead of insulating paint RHY-12. Its conductivity is given in *Tab. 36*. ZIRCOFOAM 250

has similar properties compared to RHY-12. The choice of this material is justified by its availability (RHY-12 is fabricated by a Chinese society while ZIRCOFOAM is fabricated by an Italian society). It is expected to has minor influence on the tube performance.

- SiC + AISI + FOAM: this analysis assumes all the hypothesis reported above.

The steam outlet temperature has been selected as figure of merit to assess the tube performance. *Fig. 79* and *Fig. 80* report the steam temperature along the annular riser ascending region for case1 and case2, respectively. The following conclusions can be drawn:

- ZIRCOFOAM-250 has negligible influence on the SGBT performance.
- The use of AISI-304 decreases the outlet temperature of about 15 °C.
- The use of SiC decreases the outlet temperature from 7 to 15 °C depending on the correlation adopted.
- SiC + AISI + FOAM highlight a global decrease of the outlet temperature from 20 to 30 °C depending on the correlation adopted to model the powder. Case1 predicts an outlet temperature of 435°C while the case2 predicts 409°C. Both these values are acceptable.

Component	***ANSALDO***	***Reference case***	***HERO-SGBT***
Annular gap powder	55 time the conductivity of He	Sintetic diamond	**Silicon Carbide**
Insulating material	RHY-12 paint	RHY-12 paint	**ZIRCOFOAM-250**
Tube	T91	T91	**AISI-304**

Tab. 35 – HERO-CIRCE SGBT unit: materials.

Temperature [K]	***Thermal conductivity [W/mK]***
423.15	0.060
523.15	0.071
673.15	0.088
873.15	0.113
1073.15	0.179

Tab. 36 – HERO-CIRCE SGBT unit vs. RELAP5, thermal conductivity of ZIRCOFOAM 250.

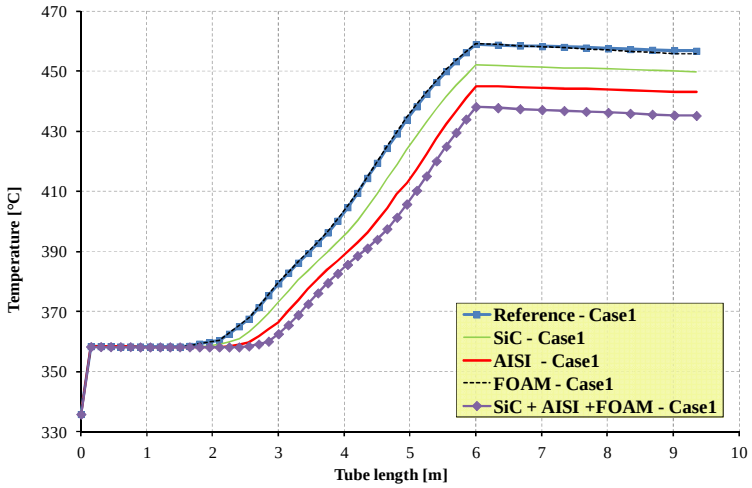

Fig. 79 – HERO-CIRCE SGBT unit vs. RELAP5 investigations on materials, steam temperature, case 1.

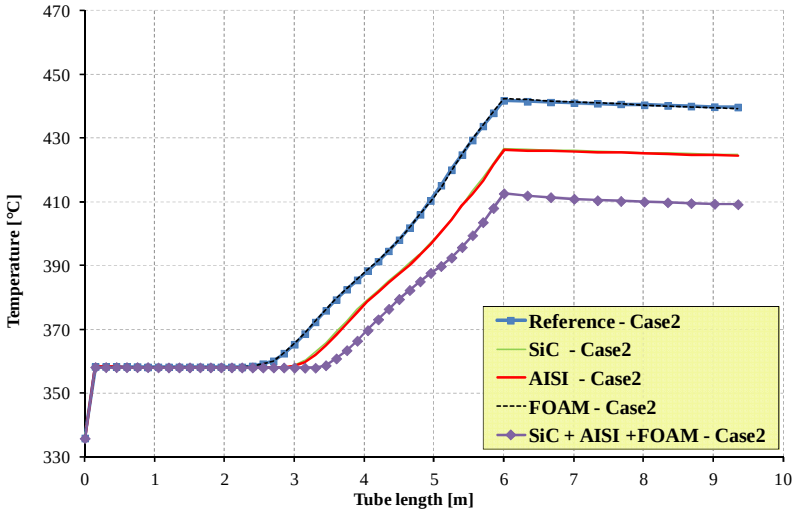

Fig. 80 – HERO-CIRCE SGBT unit vs. RELAP5 investigations on materials, steam temperature, case 2.

7.2.1.2 Determination of the tube geometry

In order to construct few prototypic tubes it is necessary to modify the geometry of the tubes because of two main reasons:

- The tube geometry adopted in the reference calculations does not agree to the standard ANSI/ASME B.36.19.
- The use of AISI-304 instead of T91 requires to increase the tube thickness because of the reduced mechanical properties.

Five configurations have been analysed, they are described in *Tab. 37* and *Tab. 39*. The operating conditions have not been modified (see *Tab. 38*). The steam temperature along the annular riser is depicted in *Fig. 81*, *Fig. 82*. RUN1 has been selected as up-dated configuration to be implemented in HERO. It allows to reach a steam temperature between 410°C and 427°C depending on the correlation adopted to model the powder.

Compared to the design of ANSALDO, this configuration has:

- Larger tube outermost diameter that means larger pitch (since P/D has been preserved),
- Larger thickness of the tubes (excepts the inner tube),
- Larger insulating gap width that enhances the insulation of the feed-water tube,
- Smaller annular riser gap that tends to increase the fluid velocity and therefore the distributed pressure drops,
- Smaller powder gap width that reduce the impact of the correlation adopted to model the powder on the TH tube performance.

The mechanical verifications substantially confirm the geometrical quantities selected by TH analysis even if, due to the reduced thickness of the inner tube, the SG bayonet tube unit could be licenced to operate at a maximum pressure of 174 bar instead of 180 bar.

#	Description	REF.	RUN1	RUN2	RUN3	RUN4	RUN5
1	Slave tube outer diameter [mm]	**9.52**	***9.53***	***9.53***	***9.53***	***9.53***	***9.53***
2	Inner tube outer diameter [mm]	**19.05**	***19.05***	***19.05***	***19.05***	***17.15***	***25.40***
3	Second tube outer diameter [mm]	**25.40**	***25.40***	***26.67***	***26.67***	***25.40***	***33.40***
4	Third tube outer diameter [mm]	**31.73**	***33.40***	***33.40***	***33.40***	***33.40***	***42.16***
5	Powder annular gap width [mm]	1.07	***0.62***	***1.72***	***0.59***	***0.62***	***0.82***
6	Water steam gap [mm]	1.30	***1.07***	***0.94***	***0.94***	***2.06***	***0.71***
7	Paint gap	2.89	***3.11***	***3.11***	***3.11***	***2.16***	***6.29***
8	Slave tube thickness [mm]	1.07	***1.22***	***1.22***	***1.22***	***1.22***	***1.22***
9	Inner tube thickness [mm]	1.88	***1.65***	***1.65***	***1.65***	***1.65***	***1.65***
10	Second tube thickness[mm]	1.88	***2.11***	***2.87***	***2.87***	***2.87***	***3.38***
11	Third tube thickness [mm]	2.11	***3.38***	***1.65***	***2.77***	***2.77***	***3.56***
12	P/D	**1.42**	***1.42***	***1.42***	***1.42***	***1.42***	***1.42***
13	P [mm]	**45.1**	***47.4***	***47.4***	***47.4***	***47.4***	***59.9***

Tab. 37 – HERO-CIRCE SGBT unit vs. RELAP5 v 3.3, modified geometries.

#	Operating conditions	REF.	RUN1	RUN2	RUN3	RUN4	RUN5
1	Feed-water inlet temperature [°C]	**335**	*335*	*335*	*335*	*335*	*335*
2	Feed-water mass flow [kg/s]	**0.047**	*0.047*	*0.047*	*0.047*	*0.047*	*0.047*
3	Steam outlet pressure [MPa]	**18.0**	*18.0*	*18.0*	*18.0*	*18.0*	*18.0*
4	Lead inlet temperature [°C]	**480**	*480*	*480*	*480*	*480*	*480*
5	Lead mass flow [kg/s]	**6.367**	*6.367*	*6.367*	*6.367*	*6.367*	*6.367*

Tab. 38 – HERO-CIRCE SGBT unit vs. RELAP5 v 3.3, operating conditions of one tube.

Component	Description	REF	RUN1	RUN2	RUN3	RUN4	RUN5
Feedwater tube	**Water flow area [m^2]**	**4.278E-05**	***3.948E-05***	***3.948E-05***	***3.948E-05***	***3.948E-05***	***3.948E-05***
	Hydraulic diameter [m]	**0.00738**	***0.00709***	***0.00709***	***0.00709***	***0.00709***	***0.00709***
	Left Dth [m]	**0.00738**	***0.00709***	***0.00709***	***0.00709***	***0.00709***	***0.00709***
	Right Dth [m]	**0.00553**	***0.004498***	***0.00395***	***0.00395***	***0.00901***	***0.00254***
Annular riser	**Water-steam flow area [m^2]**	**8.277E-05**	***6.730E-05***	***5.903E-05***	***5.903E-05***	***0.00012***	***5.068E-05***
	Hydraulic diameter [m]	**0.00259**	***0.00213***	***0.00188***	***0.00188***	***0.00403***	***0.00124***
	Left Dth [m]	**0.00487**	***0.00405***	***0.003591***	***0.003591***	***0.00729***	***0.00242***
	Right Dth [m]	**0.03864**	***0.04093***	***0.04093***	***0.04093***	***0.04093***	***0.05110***
Lead channel	**Lead flow area [m^2]**	**0.00096**	***0.00107***	***0.00107***	***0.00107***	***0.00107***	***0.00172***
	Hydraulic diameter [m]	**0.03864**	***0.04093***	***0.04093***	***0.04093***	***0.04093***	***0.05110***

Tab. 39 – HERO-CIRCE SGBT unit vs. RELAP5, main input deck modifications.

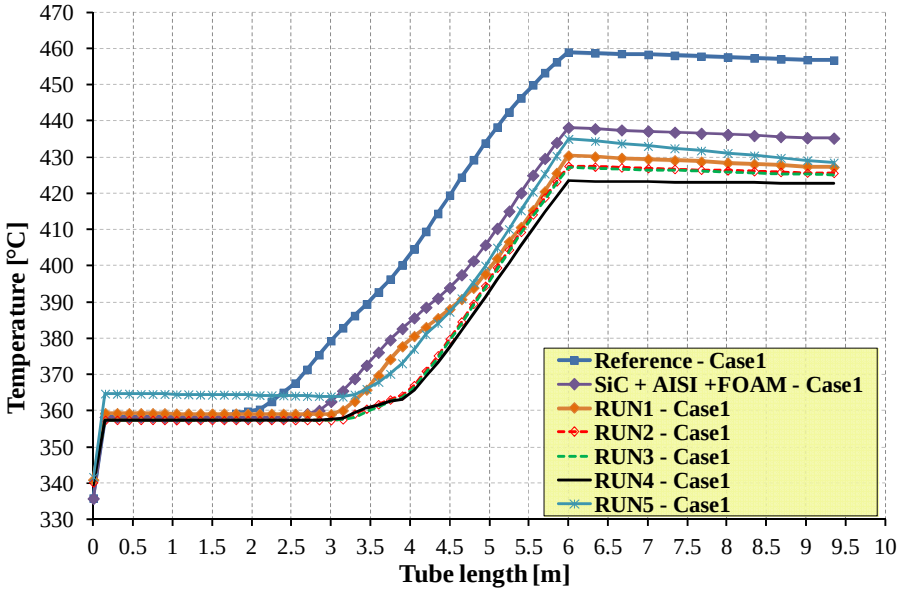

Fig. 81 – HERO-CIRCE SGBT unit vs. RELAP5, investigations on tube geometry, steam temperature, case 1.

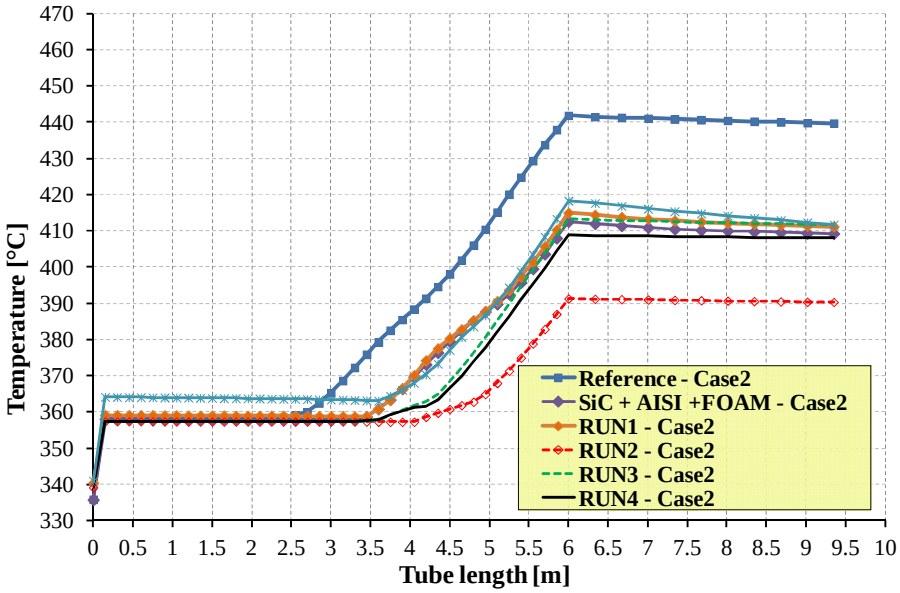

Fig. 82 – HERO-CIRCE SGBT unit vs. RELAP5 investigations on tube geometry, steam temperature, case 2.

7.2.1.3 Feedback from the SGBT construction and from the TxP campaigns

During the construction phase of the SG bayonet tube unit two main feedback arise and required the modification of its design and the development of an up-dated design:

- The experimental campaigns experienced in TxP on the Si-C powder acquired for the SG bayonet tube unit revealed an un-expected low conductivity of this material (section 6.5.1). Therefore, as a back-up solution, AISI-316 powder has been selected as heat enhancer medium instead of Si-C.

- The society that takes in charge the construction of the SG bayonet tube unit (CRIOTEC) performed some preliminary tests on ZIRCO-FOAM-250 insulating foam. This material revealed low adhesive properties when coated to the slave tube outer surface, *Fig. 83*. Therefore, in order to avoid the detachment of ZIRCO-FOAM-250 during the operation of the SG bayonet tube unit, and considering the experience of CRIOTEC in the realization of under vacuum components, dry air was introduced instead of ZIRCO-FOAM-250 and slight vacuum was then realized between the slave tube and the first tube.

Due to these modifications (and particularly the use of AISI-316 powder), the HERO test section is expected to produce superheated steam at a maximum temperature of about 400°C, *Fig. 84*. The calculation reported in this figure has been obtained based on the input deck described in section 7.2.1.2 assuming AISI-316 powder whose conductivity is according to *Eq. 34*.

Fig. 83 – HERO-CIRCE SGBT unit, coating of ZIRCO-FOAM-250 on the slave tube outer surface.

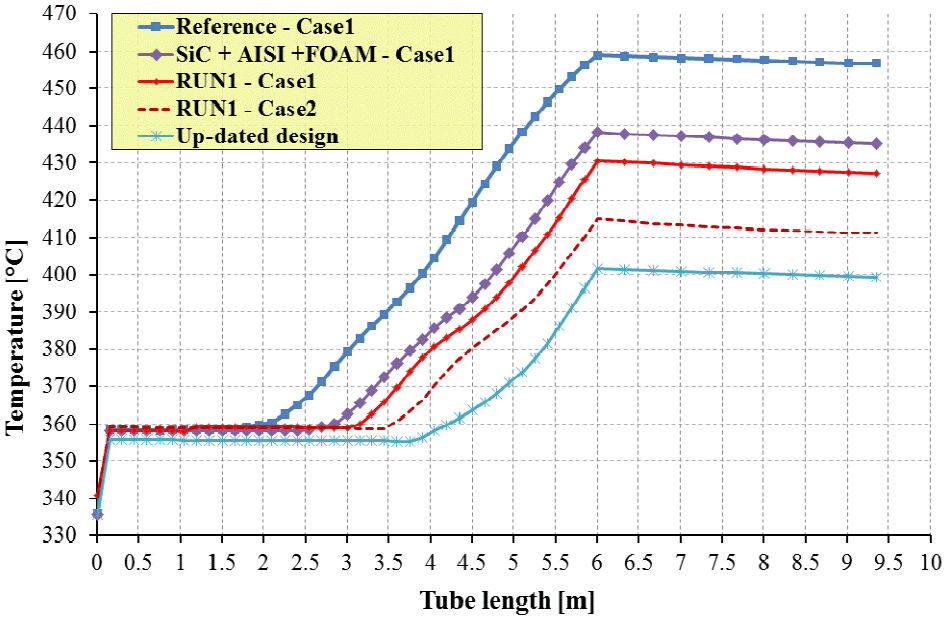

Fig. 84 – HERO-CIRCE SGBT unit vs RELAP-5 calculations: steam temperature along the annular riser.

7.2.2 Bayonet Tube SG construction

The construction of the device was assigned to CRIOTEC. The detailed constructive design is reported in Appendix D. The main operating parameters of the unit are summarized in *Tab. 40* and *Tab. 41*.
The bayonet tube bundle is given in *Fig. 85* and *Fig. 86*, it is composed of:

- A top flange with seven holes to accommodate the bayonet tubes (labeled as item 1 in *Fig. 85*) and one hole for the instrumentation. It connects the SG bayonet tube unit to the CIRCE S-100 component and sustains the helium chamber, the steam chamber, the bayonet tubes and the hexagonal shroud. This flange is Φ356 mm with a thickness of 30 mm and is made of AISI-304.
- Welded above the top flange (and therefore located outside CIRCE), there is the Helium chamber (item 2 in *Fig. 85*). It is constituted by a AISI-304 tube 6" sch.40 with an integral roof. The helium chamber have appropriate holes to accommodate the bayonet tubes. These have been fixed to the holes by sealing joints to guarantee no helium leakages up to 5 bars.
- On the top of the helium chamber there is the steam chamber that accommodates the superheated steam and contains the feed-water tubes (sealed by joints that are capable to sustain superheated steam at 180 bar). It is basically constituted by a tube with an integral roof (item 3 in *Fig. 85*).
- The bayonet tube dimensions are reported in *Tab. 41*, its main length is about 7360mm being the active length equal to 6000mm.
    - In order to measure differential pressure drops in the feed-water tube and in the annular riser, the bottom ends of the tubes have been modified as reported in *Fig. 87*. Instead of hemispherical separated ends, they have been welded to a plate with a hole. This required the use of seven thermal compensators (item 18) to accommodate the differential elongation between the third and the second tube.
    - In order to experimentally investigate the 2 phase flow stability of the unit, a special device has been introduced at the feed-water tube inlet. It allows to install a removable orifice whose diameter can be changed simply substituting the Swagelok. It is designed with the possibility to measure the pressure drop of the feed-water across the orifice, *Fig. 88*.
- The bayonet tubes are kept in position by means of five hexagonal spacer grids whose design is reported in *Fig. 89*.

The SGBT unit (*Fig. 90*) is contained into a double wall wrap depicted in *Fig. 91*. It consists of:

- An hexagonal wrap with spacers (to keep a given meatus between the wrap and the external shroud), which is 6795mm in length and whose inner and outer transversal heights are, respectively, 126mm and 132mm. Six fissures 180mm x 40mm are realized in the wrap at the top of the active length. The fissures are designed to be placed inside the cylindrical distributor of CIRCE being totally submerged by the LBE that feed the SGBT unit.
- A cylindrical external shroud that is located below the fissures and which is concentric to the hexagonal wrap. It is sealed at the bottom and at the top in order to provide a meatus which is filled by air to avoid heat exchange between the pool of CIRCE and the SGBT unit. The external shroud includes a thermal compensator to accommodate the differential elongation between the shroud and the hexagonal wrap.

- A cylinder hexagon adaptor tube which is welded at the top of the hexagon by means of a disc. The cylinder upper end has four buttonholes each of them consisting in a drilled plate welded to the cylinder to fix the wrap at the CIRCE top flange (S-100) inner surface. In order to keep in communication the argon inside the wrap with those inside the external pool, the adaptor has a transversal fissure at its top. This fissure also acts as exit for the cables of the thermocouples located in the lead side, inside the wrap.

Description	Unit	Steam line	Helium line	LBE side
Fluid	--	Water - steam	Helium	LBE
Circulation mechanism	--	Axial pump + accumulator	Storage tank for leakage refilling	Gas enhanced
Main components	--	7 bayonet tubes, steam chamber	Helium chamber	SGBT unit shell
Bundle type and P/D	-	Triangular	--	Shell
Operating inlet temperature	°C	335	--	480
Operating mass flow	kg/s	0.330785	stagnant	44.573529
Design pressure	bar	172	5.0	As CIRCE
Operating pressure	bar	170	4.5	Hydraulic head
Hydraulic head in design condition	bar	0.7	--	--
Hydraulic head in test condition	bar	0.7	--	--
Test pressure	bar	180	--	--
Design temperature	°C	432	432	As CIRCE
Volume	m^3	0.0083	0.0054	--
Empty weight	kg	135	--	--
Code	--	EN13445	--	--
Welding joint efficiency	--	1	--	--
Notified body	--	TUV0948	--	--
Welding specification	--	WKF/3479/1	--	--
Serial number	--	13173	--	--
CE - PED	--	III Category	B1+F Module	--

Tab. 40 – HERO-CIRCE SGBT unit, main data.

Label	Inner diameter [mm]	Outer diameter [mm]	Thickness [mm]	Material
Feed-water slave tube	7.09	9.53	1.22	AISI-304
Feed-water tube gap	9.53	15.75	3.11	Slight vacuum
Feed-water outer tube	15.75	19.05	1.65	AISI-304
Annular riser gap	19.05	21.18	1.07	Water-steam
Second tube	21.18	25.40	2.11	AISI-304
Annular gap	25.40	26.64	0.62	AISI 316 powder
Third tube	26.64	33.40	3.38	AISI-304

Tab. 41 – HERO-CIRCE SGBT unit, tube design

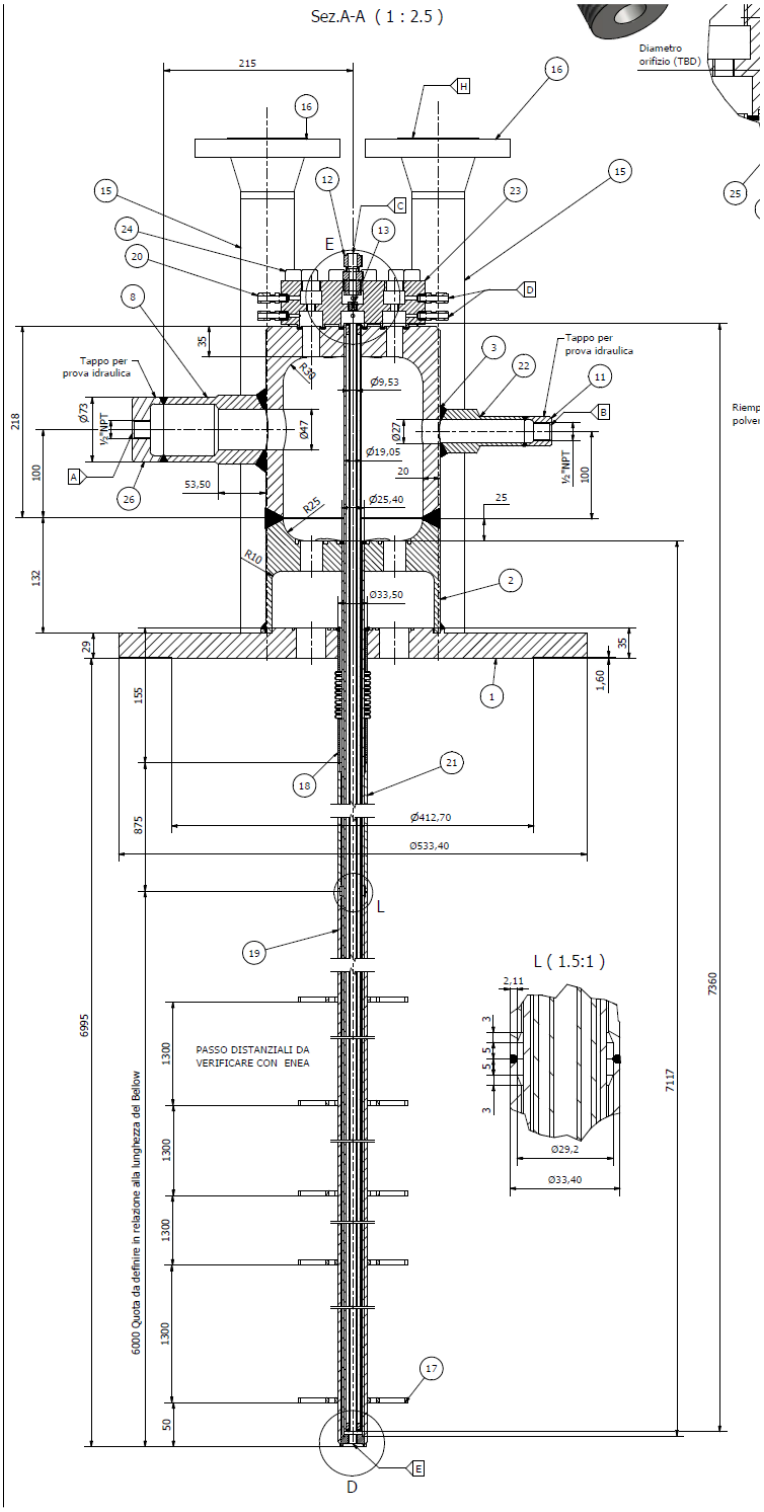

Position	N°	Description
1	1	Flange to S-100
2	1	Helium chamber
3	1	Steam chamber
4	7	Second tube Φ25.4mm s 2.11mm
5	7	Inner tube Φ19.05mm s 1.65mm
6	7	Slave tube Φ9.53mm s 1.22mm
7	14	Ring spacer
8	1	Steam outlet
9	2	Swagelok SS-6MO-1-2W
10	1	Thermocouple outlet
11	2	Threaded plug case
12	7	Swagelok SS-10MO-1-8
13	7	Orifice 1/8 "
14	7	End cap 25.4mm
15	3	Oxygen sensor tube
16	3	Flange
17	5	Grid spacer
18	7	Thermal stress accommodator
19	7	Third tube Φ33.4mm s 3.38mm
20	14	Swagelok SS-6MO-1-2
21	1	Third tube Φ33.4mm 1000mm
22	1	Steam thermocouples casing
23	1	Water flange
24	12	UNI 5931 M12 x 70
25	7	Seal
26	1	Plug

Fig. 85 – HERO-CIRCE SGBT unit: main overview.

Fig. 86 – HERO-CIRCE SGBT unit: bundle arrangement.

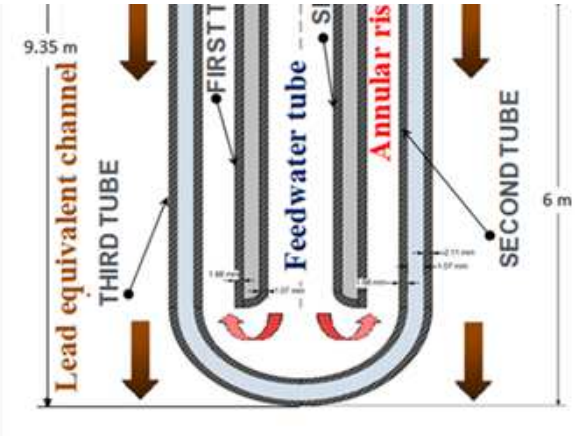

a) ALFRED

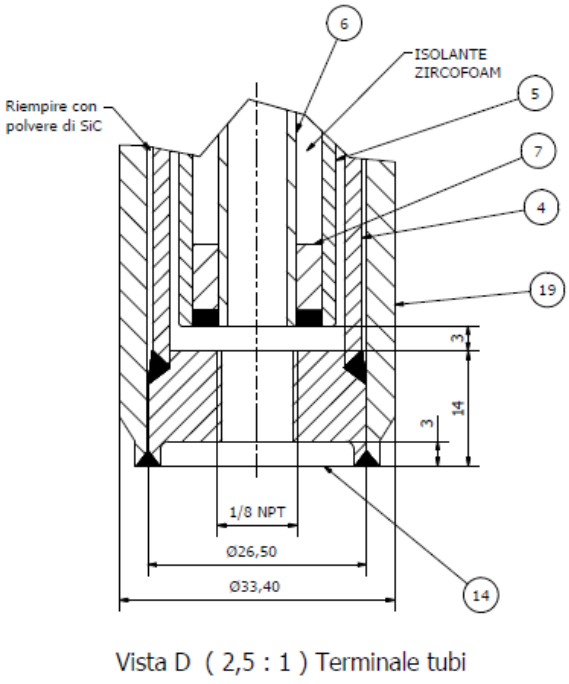

b) HERO test section

d) HERO test section, bayonet tubes ends

d) HERO test section, thermal compensators

Fig. 87 – HERO-CIRCE SGBT unit: bayonet tube bottom ends.

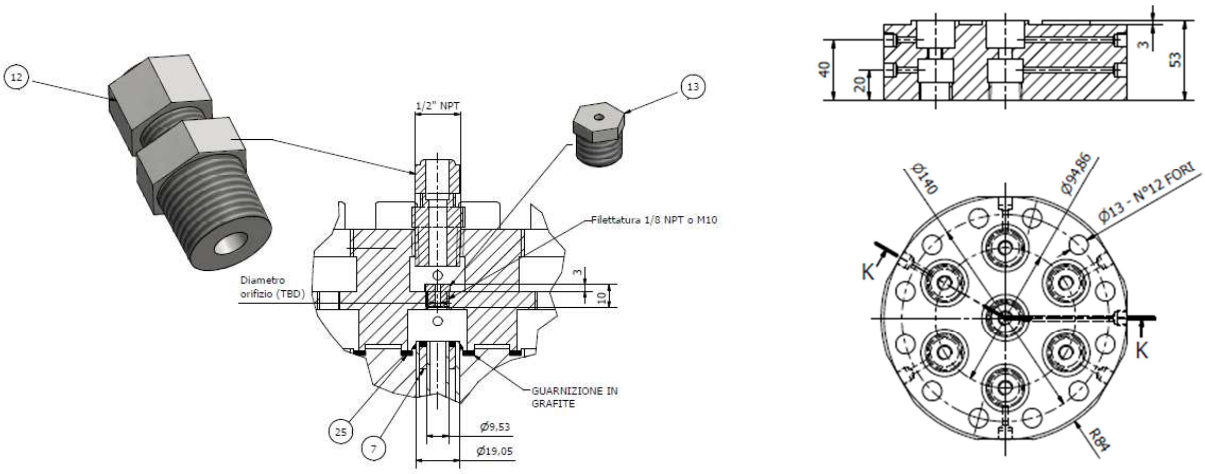

Fig. 88 – HERO-CIRCE SGBT unit: feed-water tube inlet.

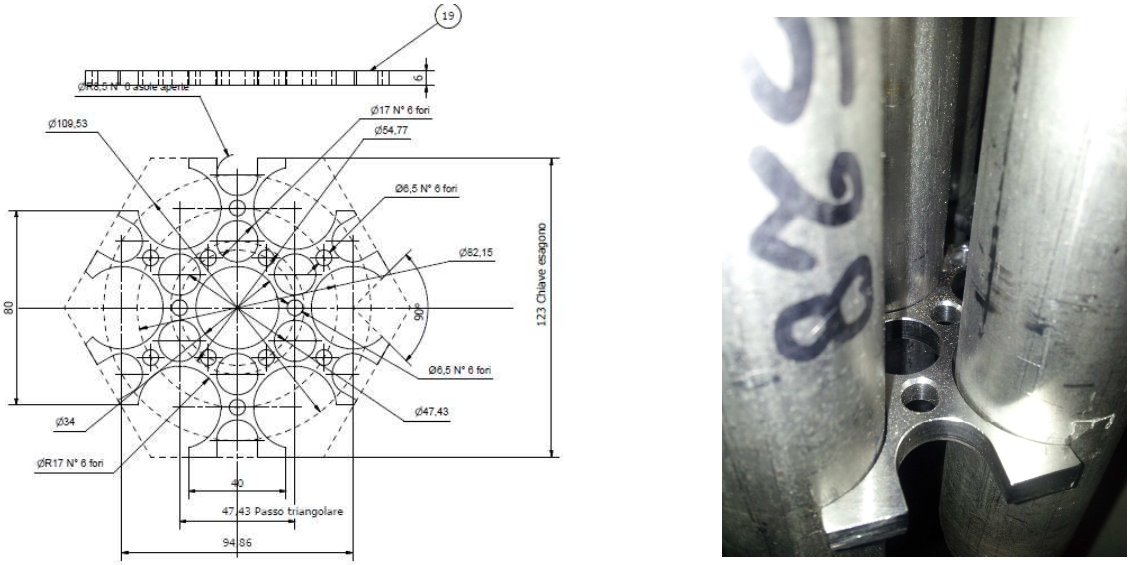

Fig. 89 – HERO-CIRCE SGBT unit: spacer grid.

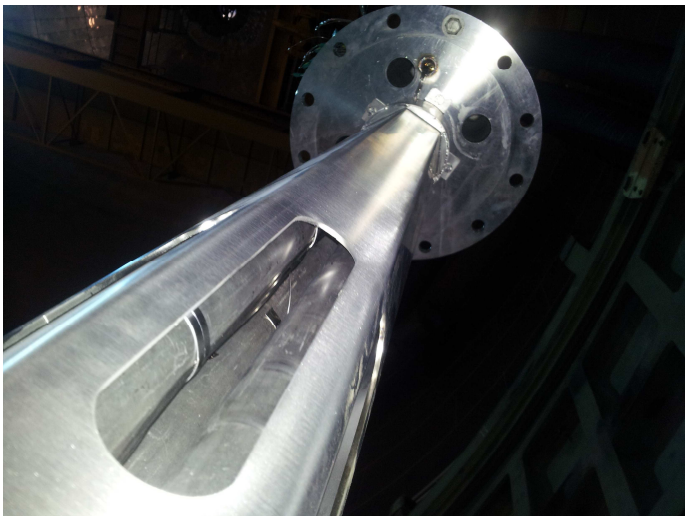

Fig. 90 – HERO-CIRCE SGBT unit: bayonet tubes inserted inside the wrap.

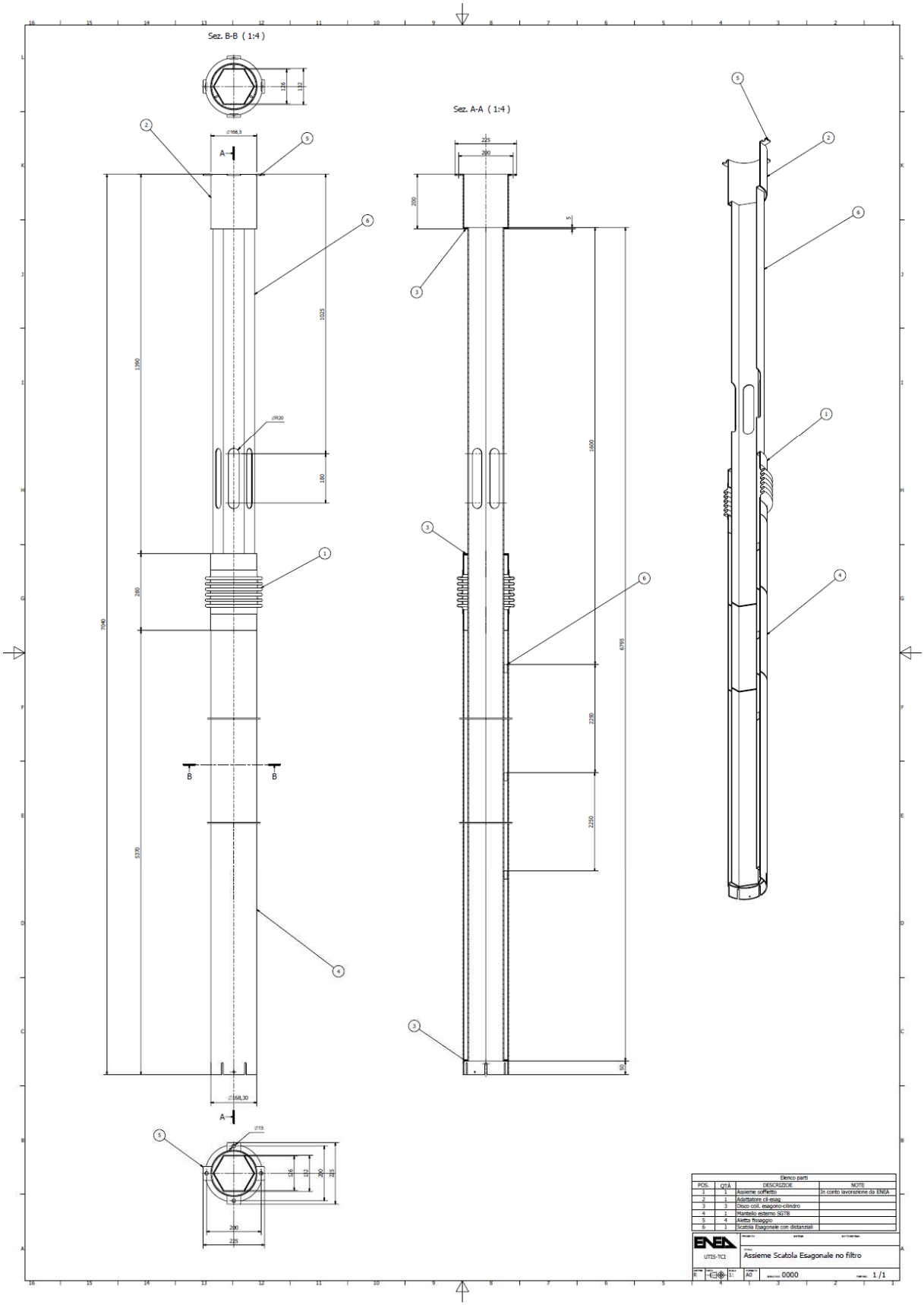

Fig. 91 – HERO-CIRCE SGBT unit: hexagonal wrap.

7.2.3 Bayonet Tube SG instrumentation

The SGBT unit is instrumented with 65 thermocouples (TCs), 13 differential pressure transducers, 2 absolute pressure transducers and 8 flow meters, *Tab. 42*.

The central tube (labeled as tube 0) is instrumented with 31 thermocouples, *Fig. 92*:

- The water-steam path is monitored by four TCs whose diameter is 0.5mm. They are placed in the center of the bulk. The first is at feed-water tube inlet, the second is at the feed-water tube end, the third is at annular riser active length end and the last one is closed to the steam plenum.
- Ten TCs (Φ 0.5mm) are placed in the annular riser active length (starting from 1500mm to the bottom with a distance of 300mm), at the center of the bulk in order to monitor the boiling length.
- One TC (Φ 0.5mm) is placed at the feed-water tube inlet on its outer surface in order to capture condensation phenomena that may in principle take place above the active length because of the heat exchange between the superheated steam that is leaving the unit and the feed-water that is entering it.
- Four TCs (Φ 0.5mm) are located inside the powder gap at four representative axial elevations (1500mm, 3000mm, 4200mm and 6000mm). These TCs where not installed because they break during their assembling.
- Twelve TCs (Φ 1mm) are located at the third tube outer wall surface (LBE side) at four axial elevations (1500mm, 3000mm, 4200mm and 6000mm) and three azimuthal positions (0, 120°, 240°). The first three elevations are combined with other TCs located inside the wrap to monitor the equivalent sub-channels while the last elevation (6000mm) will provide a characterization of the LBE temperature profile at its inlet level (fissures level).

The remaining tubes (labeled as tube 1 to 6) are instrumented with 18 TCs, *Fig. 93*:

- Two TCs (Φ 0.5mm) are placed in each tube one at its inlet (feed-water tube bulk) and the other at its outlet (annular riser bulk).
- The remaining six TCs (Φ 1mm) are placed at three axial elevations (1500mm, 3000mm, 4200mm) in the outer side (LBE side) of two tubes: tube 1 and tube 2.

The equivalent LBE sub-channel bounded by tube 0, tube 1 and tube 2 is monitored at its periphery at three axial elevations by the TCs located at the outer surface of these tubes and at its center by means of three TCs, *Fig. 94* (one at each elevation, Φ 1mm). Three boundary sub-channels bounded by tubes 1-2, tubes 3-4, and tubes 5-6 are monitored by 3 center-bulk TCs at three axial elevations (totally 9 TCs Φ 1mm). Finally, four TCs (Φ 1mm) are located in the steam plenum. *Fig. 95* reports some details of the instrumentation.

The differential pressure transducers allow to measure, per each tube, the pressure drop across the orifice, the total pressure drop along the tube (feed-water tube and annular riser), the descended pressure drop (feed-water tube only) and the ascendant pressure drop (annular riser only). Absolute pressure is measured in the steam chamber and in the feed-water collector. The mass flow rate is measured at each bayonet tube inlet and at the feed-water collector inlet, *Fig. 96*.

#	ID	Instrument location			Measurement		Type
		Zone	Elev (1). / Position	Medium	Quantity	Dim	
1	TC-C0-I00	Tube 0 – Inner tube	Inlet	Water	Temperature	°C	D=0.5mm
2	TC-C0-I01	Tube 0 – Inner tube	Outlet	Water	Temperature	°C	D=0.5mm
3	TC-C0-O15	Tube 0 – Second tube	1500mm	Water	Temperature	°C	D=0.5mm
4	TC-C0-O18	Tube 0 – Second tube	1800mm	Water	Temperature	°C	D=0.5mm
5	TC-C0-O21	Tube 0 – Second tube	2100mm	Water	Temperature	°C	D=0.5mm
6	TC-C0-O24	Tube 0 – Second tube	2400mm	Water	Temperature	°C	D=0.5mm
7	TC-C0-O27	Tube 0 – Second tube	2700mm	Water	Temperature	°C	D=0.5mm
8	TC-C0-O30	Tube 0 – Second tube	3000mm	Water	Temperature	°C	D=0.5mm
9	TC-C0-O33	Tube 0 – Second tube	3300mm	Water	Temperature	°C	D=0.5mm
10	TC-C0-O36	Tube 0 – Second tube	3600mm	Water	Temperature	°C	D=0.5mm
11	TC-C0-O39	Tube 0 – Second tube	3900mm	Water	Temperature	°C	D=0.5mm
12	TC-C0-O42	Tube 0 – Second tube	4200mm	Water	Temperature	°C	D=0.5mm
13	TC-C0-O60	Tube 0 – Second tube	6000mm	Water	Temperature	°C	D=0.5mm
14	TC-C0-O70	Tube 0 – Second tube	7016mm	Water	Temperature	°C	D=0.5mm
15	TC-W0-W68	Tube 0 – Inner tube	6800mm	Wall – Water	Temperature	°C	D=0.5mm
16	TC-W0-P15	Tube 0 – Second tube	1500mm / 0°	Wall – SiC	Temperature	°C	D=0.5mm- **BREAKED**
17	TC-W0-P30	Tube 0 – Second tube	3000mm / 0°	Wall – SiC	Temperature	°C	D=0.5mm **BREAKED**
18	TC-W0-P40	Tube 0 – Second tube	4200mm / 0°	Wall – SiC	Temperature	°C	D=0.5mm **BREAKED**
19	TC-W0-P60	Tube 0 – Second tube	6000mm / 0°	Wall – SiC	Temperature	°C	D=0.5mm **BREAKED**
20	TC-W0-L10	Tube 0 – Third tube	1500mm / 0°	Wall – LBE	Temperature	°C	D=1mm
21	TC-W0-L11	Tube 0 – Third tube	1500mm / 120°	Wall – LBE	Temperature	°C	D=1mm
22	TC-W0-L12	Tube 0 – Third tube	1500mm / 240°	Wall – LBE	Temperature	°C	D=1mm
23	TC-W0-L30	Tube 0 – Third tube	3000mm / 0°	Wall – LBE	Temperature	°C	D=1mm
24	TC-W0-L31	Tube 0 – Third tube	3000mm / 120°	Wall – LBE	Temperature	°C	D=1mm
25	TC-W0-L32	Tube 0 – Third tube	3000mm / 240°	Wall – LBE	Temperature	°C	D=1mm
26	TC-W0-L40	Tube 0 – Third tube	4200mm / 0°	Wall – LBE	Temperature	°C	D=1mm
27	TC-W0-L41	Tube 0 – Third tube	4200mm / 120°	Wall – LBE	Temperature	°C	D=1mm
28	TC-W0-L42	Tube 0 – Third tube	4200mm / 240°	Wall – LBE	Temperature	°C	D=1mm
29	TC-W0-L60	Tube 0 – Third tube	6000mm / 0°	Wall – LBE	Temperature	°C	D=1mm
30	TC-W0-L61	Tube 0 – Third tube	6000mm / 120°	Wall – LBE	Temperature	°C	D=1mm
31	TC-W0-L62	Tube 0 – Third tube	6000mm / 240°	Wall – LBE	Temperature	°C	D=1mm
32	TC-C1-I00	Tube 1 – Inner tube	Inlet	Water	Temperature	°C	D=0.5mm
33	TC-C1-O70	Tube 1 – Second tube	7016mm	Water	Temperature	°C	D=0.5mm
34	TC-C2-I00	Tube 2 – Inner tube	Inlet	Water	Temperature	°C	D=0.5mm
35	TC-C2-O70	Tube 2 – Second tube	7016mm	Water	Temperature	°C	D=0.5mm
36	TC-C3-I00	Tube 3 – Inner tube	Inlet	Water	Temperature	°C	D=0.5mm
37	TC-C3-O70	Tube 3 – Second tube	7016mm	Water	Temperature	°C	D=0.5mm
38	TC-C4-I00	Tube 4 – Inner tube	Inlet	Water	Temperature	°C	D=0.5mm
39	TC-C4-O70	Tube 4 – Second tube	7016mm	Water	Temperature	°C	D=0.5mm
40	TC-C5-I00	Tube 5 – Inner tube	Inlet	Water	Temperature	°C	D=0.5mm

#	ID	Instrument location			Measurement		Type
		Zone	Elev (1). / Position	Medium	Quantity	Dim	
41	TC-C5-O70	Tube 5 – Second tube	7016mm	Water	Temperature	°C	D=0.5mm
42	TC-C6-I00	Tube 6 – Inner tube	Inlet	Water	Temperature	°C	D=0.5mm
43	TC-C6-O70	Tube 6 – Second tube	7016mm	Water	Temperature	°C	D=0.5mm
44	TC-W1-L11	Tube 1 – Third tube	1500mm / 120°	Wall – LBE	Temperature	°C	D=1mm
45	TC-W2-L12	Tube 2 – Third tube	1500mm / 240°	Wall – LBE	Temperature	°C	D=1mm
46	TC-W1-L31	Tube 1 – Third tube	3000mm / 120°	Wall – LBE	Temperature	°C	D=1mm
47	TC-W2-L32	Tube 2 – Third tube	3000mm / 240°	Wall – LBE	Temperature	°C	D=1mm
48	TC-W1-L41	Tube 1 – Third tube	4200mm / 120°	Wall – LBE	Temperature	°C	D=1mm
49	TC-W2-L42	Tube 2 – Third tube	4200mm / 240°	Wall – LBE	Temperature	°C	D=1mm
50	TC-01-L15	Sub-channel 1 centre	1500mm	LBE	Temperature	°C	D=1mm
51	TC-07-L15	Sub-channel 7 centre	1500mm	LBE	Temperature	°C	D=1mm
52	TC-09-L15	Sub-channel 9 centre	1500mm	LBE	Temperature	°C	D=1mm
53	TC-11-L15	Sub-channel 11 centre	1500mm	LBE	Temperature	°C	D=1mm
54	TC-01-L30	Sub-channel 1 centre	3000mm	LBE	Temperature	°C	D=1mm
55	TC-07-L30	Sub-channel 7 centre	3000mm	LBE	Temperature	°C	D=1mm
56	TC-09-L30	Sub-channel 9 centre	3000mm	LBE	Temperature	°C	D=1mm
57	TC-11-L30	Sub-channel 11 centre	3000mm	LBE	Temperature	°C	D=1mm
58	TC-01-L42	Sub-channel 1 centre	4200mm	LBE	Temperature	°C	D=1mm
59	TC-07-L42	Sub-channel 7 centre	4200mm	LBE	Temperature	°C	D=1mm
60	TC-09-L42	Sub-channel 9 centre	4200mm	LBE	Temperature	°C	D=1mm
61	TC-11-L42	Sub-channel 11 centre	4200mm	LBE	Temperature	°C	D=1mm
62	TC-SL-W01	Steam-chamber outlet	--	Water	Temperature	°C	D=1mm
63	TC-SL-W02	Steam-chamber outlet	--	Water	Temperature	°C	D=1mm
64	TC-SL-W03	Steam-chamber outlet	--	Water	Temperature	°C	D=1mm
65	TC-SL-W04	Steam-chamber outlet	--	Water	Temperature	°C	D=1mm
1	DP-C0-W00	Tube 0	Overall	Water	Press. diff.	kPa	
2	DP-C0-W01	Tube 0	Descending	Water	Press. diff.	kPa	
3	DP-C0-W02	Tube 0	Ascending	Water	Press. diff.	kPa	
4	DP-C1-W00	Tube 1	Overall	Water	Press. diff.	kPa	
5	DP-C1-W01	Tube 1	Descending	Water	Press. diff.	kPa	
6	DP-C1-W02	Tube 1	Ascending	Water	Press. diff.	kPa	
7	DP-C2-W00	Tube 2	Overall	Water	Press. diff.	kPa	
8	DP-C2-W01	Tube 2	Descending	Water	Press. diff.	kPa	
9	DP-C2-W02	Tube 2	Ascending	Water	Press. diff.	kPa	
10	DP-C3-W00	Tube 3	Overall	Water	Press. diff.	kPa	
11	DP-C3-W01	Tube 3	Descending	Water	Press. diff.	kPa	
12	DP-C3-W02	Tube 3	Ascending	Water	Press. diff.	kPa	
13	DP-C4-W00	Tube 4	Overall	Water	Press. diff.	kPa	
14	DP-C4-W01	Tube 4	Descending	Water	Press. diff.	kPa	
15	DP-C4-W02	Tube 4	Ascending	Water	Press. diff.	kPa	
16	DP-C5-W00	Tube 5	Overall	Water	Press. diff.	kPa	
17	DP-C5-W01	Tube 5	Descending	Water	Press. diff.	kPa	
18	DP-C5-W02	Tube 5	Ascending	Water	Press. diff.	kPa	
19	DP-C6-W00	Tube 6	Overall	Water	Press. diff.	kPa	

#	ID	Instrument location			Measurement		Type
		Zone	Elev (1). / Position	Medium	Quantity	Dim	
20	DP-C6-W01	Tube 6	Descending	Water	Press. diff.	kPa	
21	DP-C6-W02	Tube 6	Ascending	Water	Press. diff.	kPa	
22	PC-00-I00	FW collector	--	Water	Pressure	MPa	
22	PC-00-O00	Steam collector	--	Water	Pressure	MPa	
1	MF-00-I00	Tube 0 – inlet	--	Water	Mass flow	g/s	
2	MF-01-I00	Tube 1 – inlet	--	Water	Mass flow	g/s	
3	MF-02-I00	Tube 2 – inlet	--	Water	Mass flow	g/s	
4	MF-03-I00	Tube 3 – inlet	--	Water	Mass flow	g/s	
5	MF-04-I00	Tube 4 – inlet	--	Water	Mass flow	g/s	
6	MF-05-I00	Tube 5 – inlet	--	Water	Mass flow	g/s	
7	MF-06-I00	Tube 6 – inlet	--	Water	Mass flow	g/s	
8	MF-FW-I00	FW collector	--	Water	Mass flow	g/s	

(1) *0.00m located at tube bottom*

Tab. 42 – HERO-CIRCE SGBT unit, instrumentation.

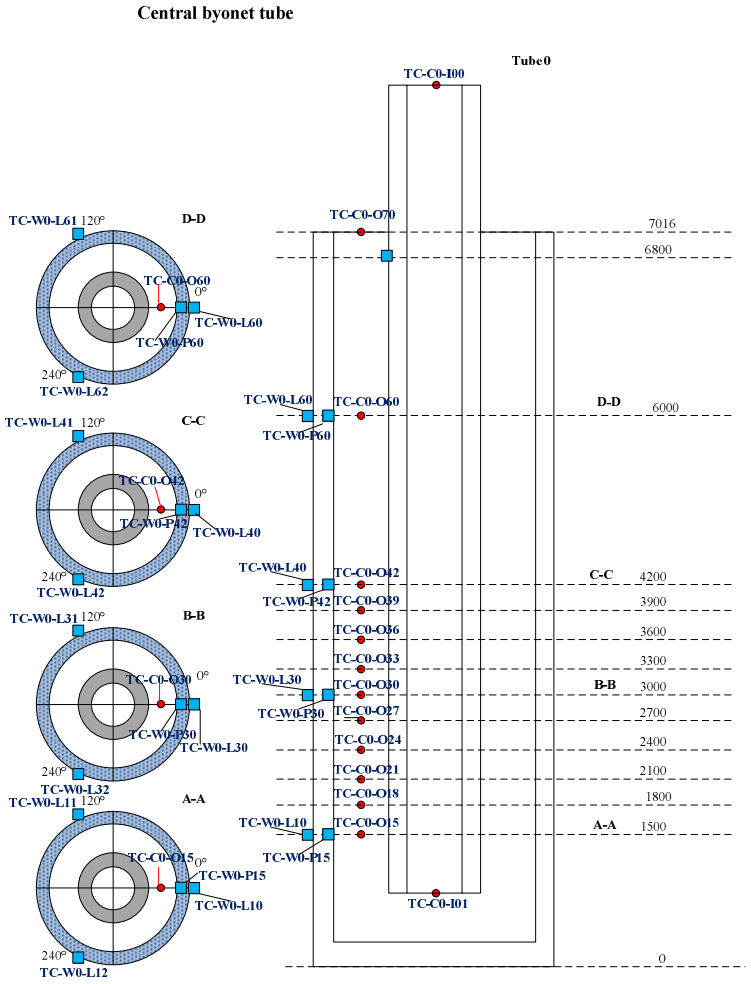

Fig. 92 – HERO-CIRCE SGBT unit instrumentation: TCs in the central tube.

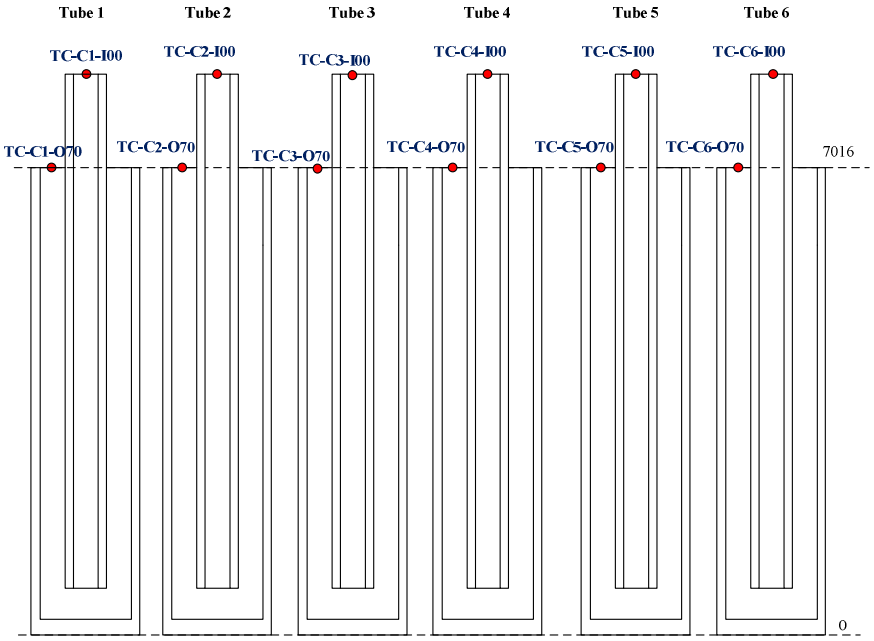

Fig. 93 – HERO-CIRCE SGBT unit instrumentation: TCs in tubes 1-2-3-4-5-6.

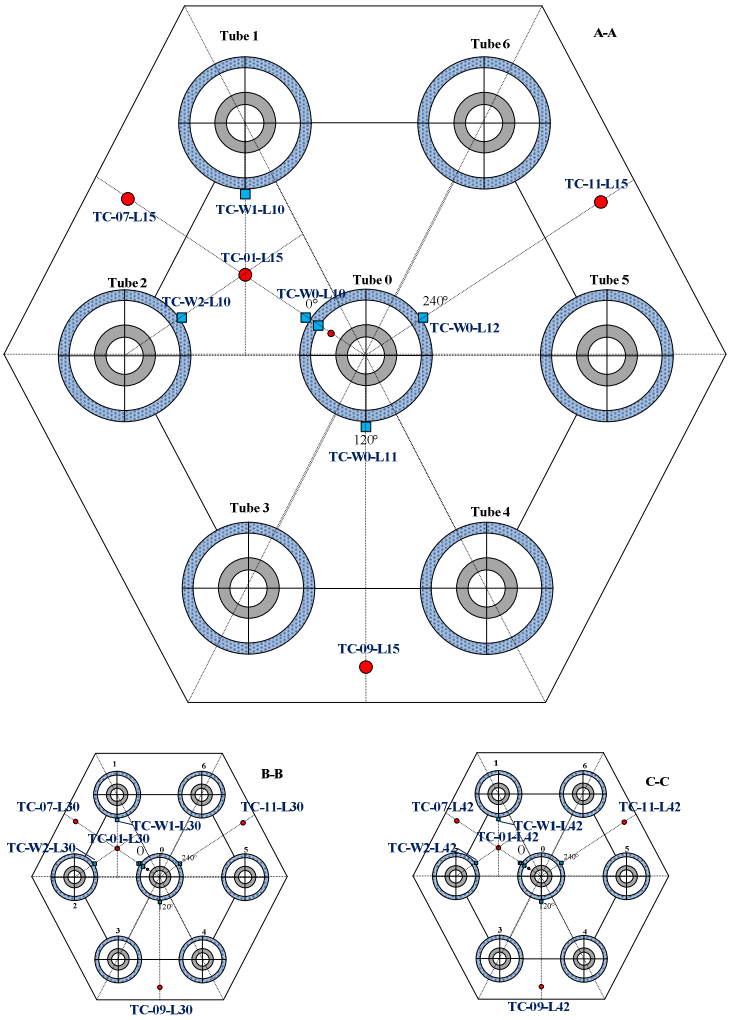

Fig. 94 – HERO-CIRCE SGBT unit instrumentation: TCs in the LBE channel.

(a) TC in the central tube wall

(a) TCs in the lead sub-channels

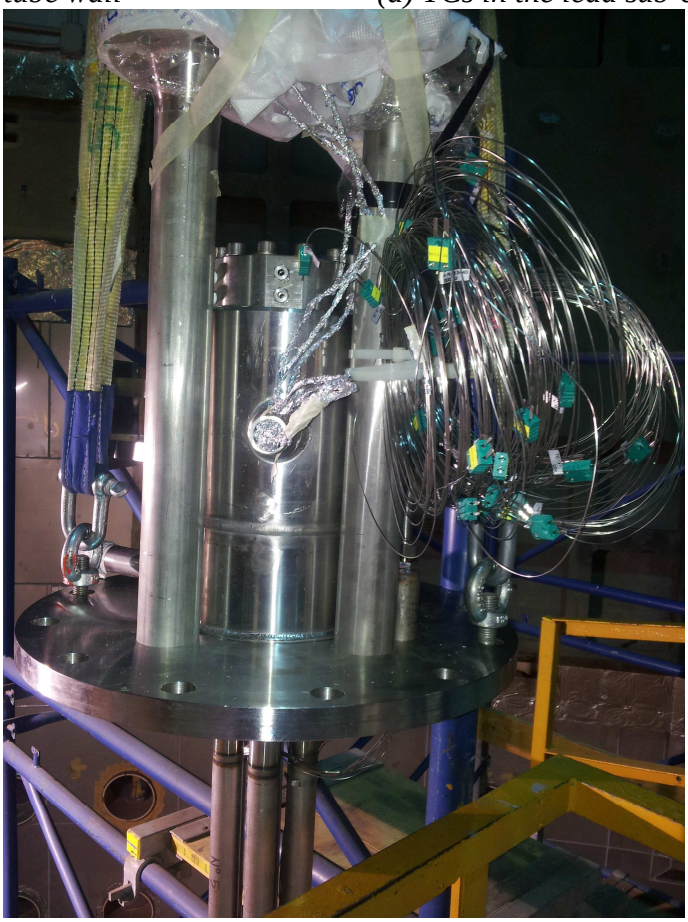

(c) TC exit (both steam-water side from the steam chamber and the LBE side from the flange)

Fig. 95 – HERO-CIRCE SGBT unit instrumentation: TCs.

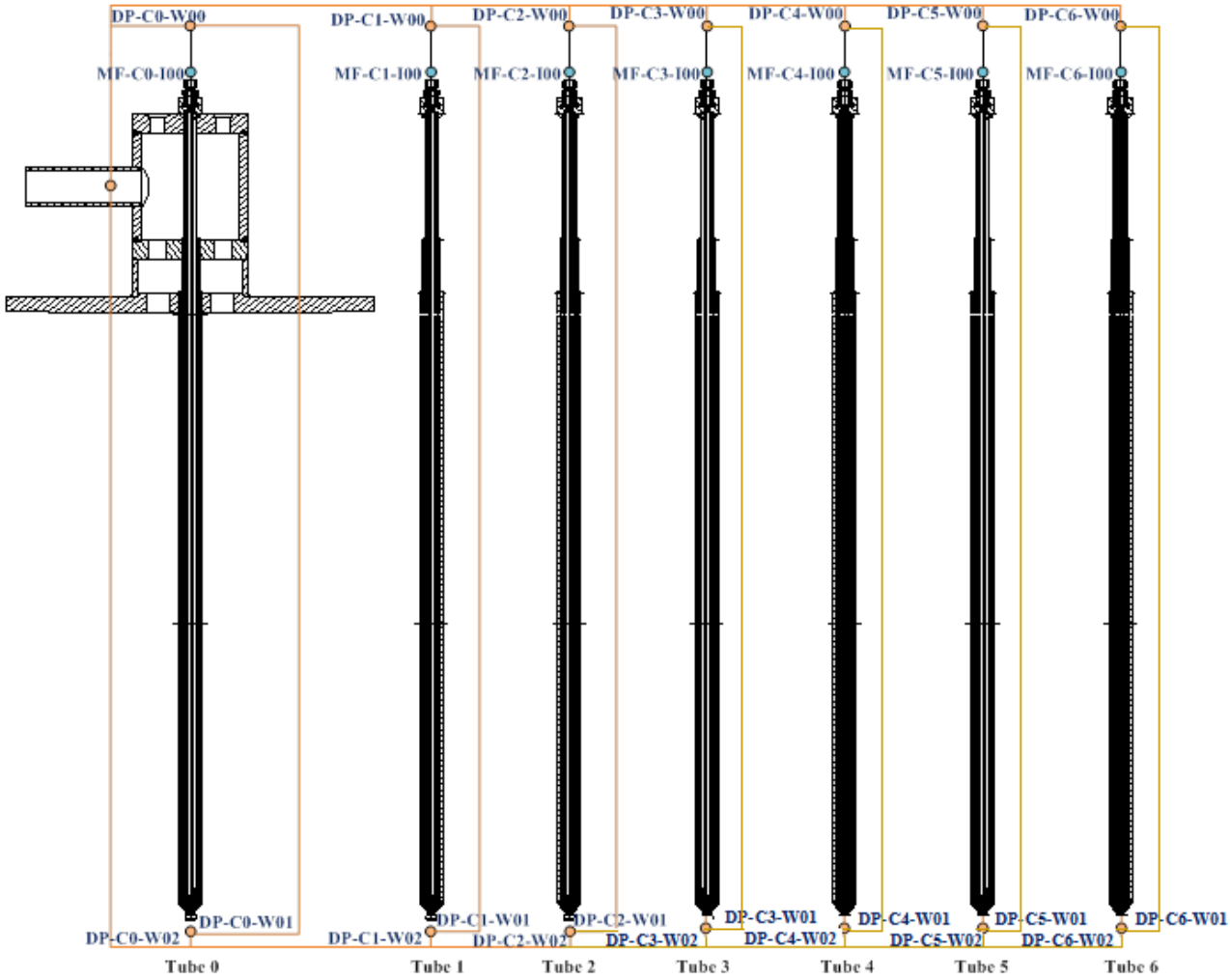

Fig. 96 – HERO-CIRCE SGBT unit instrumentation: pressure transducers and mass-flow meters in the steam-water side.

7.2.4 Modeling of the Bayonet Tube SG unit by RELAP-5

The SGBT unit has been modeled by means of RELAP version 5.3.3[28][29][30]. A schematic overview of the nodalization adopted is reported in *Fig. 97* and *Fig. 98*. The model includes: one single tube that represents seven tubes. In particular, the following main hydrodynamic components are considered: the feed-water tube (pipe 100), the annular steam riser (pipe 110), the equivalent lead channel (pipe 140), the steam plenum (branch 111) and the argon zone (branch 136). The analysis has been developed on the basis of the following assumptions:

- The heat exchange between the annular steam riser and the Argon zone has been neglected, that means adiabatic behavior of the non-active outer-side tube surface region.
- The materials and the geometry are according to the design of HERO.
- The powder (AISI-316) conductivity is according to the experimental finding achieved in the TxP campaign (*Eq. 34*).
- The heat transfer between the lead side and the annular riser is modeled according to the Mikityuk correlation that has been developed for fuel rod bundle [32][33].

- The hexagonal wrap has been considered in the model.
- The spacer grids are modeled as concentrated pressure drops calculated according to Ref. [60].

The description of the main hydrodynamic components is given in *Tab. 43*, *Tab. 44* and *Tab. 45*. The heat structures are summarized from *Tab. 46* to *Tab. 48*.

The main results are summarized in *Tab. 49*. *Fig. 99* reports the fluid temperature in the bayonet tube, the void fraction in the annular riser and the LBE temperature in the corresponding channel and. The system is capable to remove 443 kW (*Tab. 49*) and the submerged maximum steam temperature is about 400°C. The fluid becomes 95% steam after the 3.4m.

Fig. 100 highlights the profile velocities of the fluids along the bayonet tube. They contribute to a pressure drop mainly concentrated in the annular riser in the order of 1.69 bar (*Tab. 49*).

Description	**Unit**	**Quantity**	**Notes**
Label	--	--	Pipe-100 slave tube
Flow area	m^2	$2.763635\ 10^{-4}$	
N° axial volumes	--	49	--
Axial volume basic length	m	0.15000	
Axial volume lengths: min - max	m	0.13125 – 0.21000	--
Angle	°	-90	--
Wall roughness	m	$3.2\ 10^{-6}$	--
Reynolds energy loss coefficient	--	$1.00\ 10^{-3}$	--
Hydraulic diameter	m	$7.09\ 10^{-3}$	--
Reynolds reverse energy loss coefficient	--	$1.00\ 10^{-3}$	--
Pressure	Pa	$1.72\ 10^{7}$	--
Temperature	K	608	--
Mass flow	kg/s	3.3078510^{-1}	--

Tab. 43 – HERO-CIRCE SGBT unit modelling: hydrodynamic component pipe 100.

Description	Unit	Quantity	Notes
Label	--	--	Pipe-110 annular riser
Flow area	m^2	$4.711049\ 10^{-4}$	--
N° axial volumes	--	48	--
Axial volume basic length	m	0.15000	--
Axial volume lengths: min - max	m	0.13125 – 0.17800	--
Angle	°	+90	--
Wall roughness	m	$3.2\ 10^{-6}$	--
Reynolds energy loss coefficient	--	$1.00\ 10^{-3}$	--
Hydraulic diameter	m	$2.13\ 10^{-3}$	--
Reynolds reverse energy loss coefficient	--	$1.00\ 10^{-3}$	--
Pressure	Pa	$1.72\ 10^{7}$	--
Temperature	K	608	--
Mass flow	kg/s	3.3078510^{-1}	--

Tab. 44 – HERO-CIRCE SGBT unit modelling: hydrodynamic component pipe 110.

Description	Unit	Quantity	Notes
Label	--	--	Channel-140 lead channel
Flow area	m^2	$7.616311\ 10^{-3}$	
N° axial volumes	--	41	--
Axial volume basic length	m	0.15000	--
Axial volume lengths: min - max	m	0.13125 – 0.17800	--
Angle	°	+90	--
Wall roughness	m	$3.2\ 10^{-6}$	--
Reynolds energy loss coefficient	--	$1.00\ 10^{-3}$	--
Hydraulic diameters	m	$2.6017\ 10^{-2}$	--
Reynolds reverse energy loss coefficient	--	$1.00\ 10^{-3}$	--
Pressure	Pa	$1.0\text{-}7.0\ 10^{6}$	--
Temperature	K	608	--
Mass flow	kg/s	44.573529	--

Tab. 45 – HERO-CIRCE SGBT unit modelling: hydrodynamic component channel 140.

COMPONENT LABEL	**TYPE**	**DESCRIPTION**	
Heat structure	1100	Heat transfer between feed-water and riser	
Parameter	**Unit**	**Quantity**	**Notes**
Axial heat structures n°	--	49	--
Radial meshes n°	--	20	--
Slave tube inner radius	m	$3.545\ 10^{-3}$	--
Slave tube outer radius	m	$4.765\ 10^{-3}$	--
Slave tube radial nodes n°	--	5	
Gap outer radius	m	$7.875\ 10^{-3}$	--
Gap radial nodes n°	--	9	--
Inner tube outer radius	m	$9.525\ 10^{-3}$	--
Inner tube radial node n°	--	5	--
Slave tube material	--	AISI-316	--
Gap material	--	Air	--
First tube material		AISI-316	--
Temperature	K	700	--
Multiplying factor	--	7	Applied on the heated length
Heat transfer left diameter	m	$7.090\ 10^{-3}$	--
Heat transfer right diameter	m	$4.498\ 10^{-3}$	-

Tab. 46 – HERO-CIRCE SGBT unit modelling: heat structure between the feed-water tube and the annular riser.

COMPONENT LABEL	**TYPE**	**DESCRIPTION**	
Heat structure	1110	Heat transfer between Pipe 110 - 140	
Parameter	**Unit**	**Quantity**	**Notes**
Axial heat structures n°	--	41	--
Radial meshes n°	--	31	--
Second tube inner radius	m	$1.059\ 10^{-2}$	--
Second tube outer radius	m	$1.270\ 10^{-2}$	--
Second tube radial nodes n°	10	10	--
Gap outer radius	m	$1.332\ 10^{-2}$	--
Gap radial nodes n°	--	10	--
Third tube outer radius	m	$1.670\ 10^{-2}$	--
Third tube radial nodes n°	--	10	--
Second tube material	--	AISI-316	--
Gap material	--	AISI-316 powder	--
Third tube material	--	AISI-316	--
Temperature	K	608	--
Multiplying factor	--	7	Applied on the heated length
Heat transfer left diameter	m	$4.0467\ 10^{-3}$	--
Heat transfer right diameter	m	0.040930	--

Tab. 47 – HERO-CIRCE SGBT unit modelling: heat structure between the annular riser and lead channel.

COMPONENT LABEL	**TYPE**	**DESCRIPTION**	
Heat structure	1200	Heat transfer between Hexagonal wall – Outer wall	
Parameter	**Unit**	**Quantity**	**Other**
Axial heat structures n°	--	41	--
Radial meshes n°	--	22	--
Hexagonal wall inner radius	m	$6.3\ 10^{-2}$	--
Hexagonal wall radius	m	$6.45\ 10^{-2}$	--
Hexagonal wall radial nodes n°	--	7	--
Gap outer radius	m	$8.075\ 10^{-2}$	--
Gap radial nodes n°	--	7	--
Cylinder wall outer radius	m	$8.245\ 10^{-2}$	--
Cylinder wall radial nodes n°	--	7	--
Hexagonal wall material	--	AISI-316	--
Gap material	--	Air	--
Cylinder wall material	--	AISI-316	--
Temperature	K	608	--
Multiplying factor	--	7	Applied on the heated length
Heat transfer left diameter	m	4.68310^{-3}	--
Heat transfer right diameter	m	0	--

Tab. 48 – HERO-CIRCE SGBT unit modelling: heat structure between the lead channel and outer wall.

Parameter	**Unit**	**Quantity**
Lead inlet temperature	°C	*478.5*
Lead outlet temperature	°C	*410.5*
Feed-water inlet temperature	°C	*334.4*
Feed-water tube temperature drop	°C	*334.8*
Immersed tube steam temperature	°C	*400.2*
Superheated steam outlet temperature	°C	*398.3*
Void fraction	--	*1.00*
Pressure drop in the annular riser	bar	*1.69*
Lead velocity	m/s	*0.57*
Removed power	kW	*447*

Tab. 49 – HERO-CIRCE SGBT unit modelling: summary of the results.

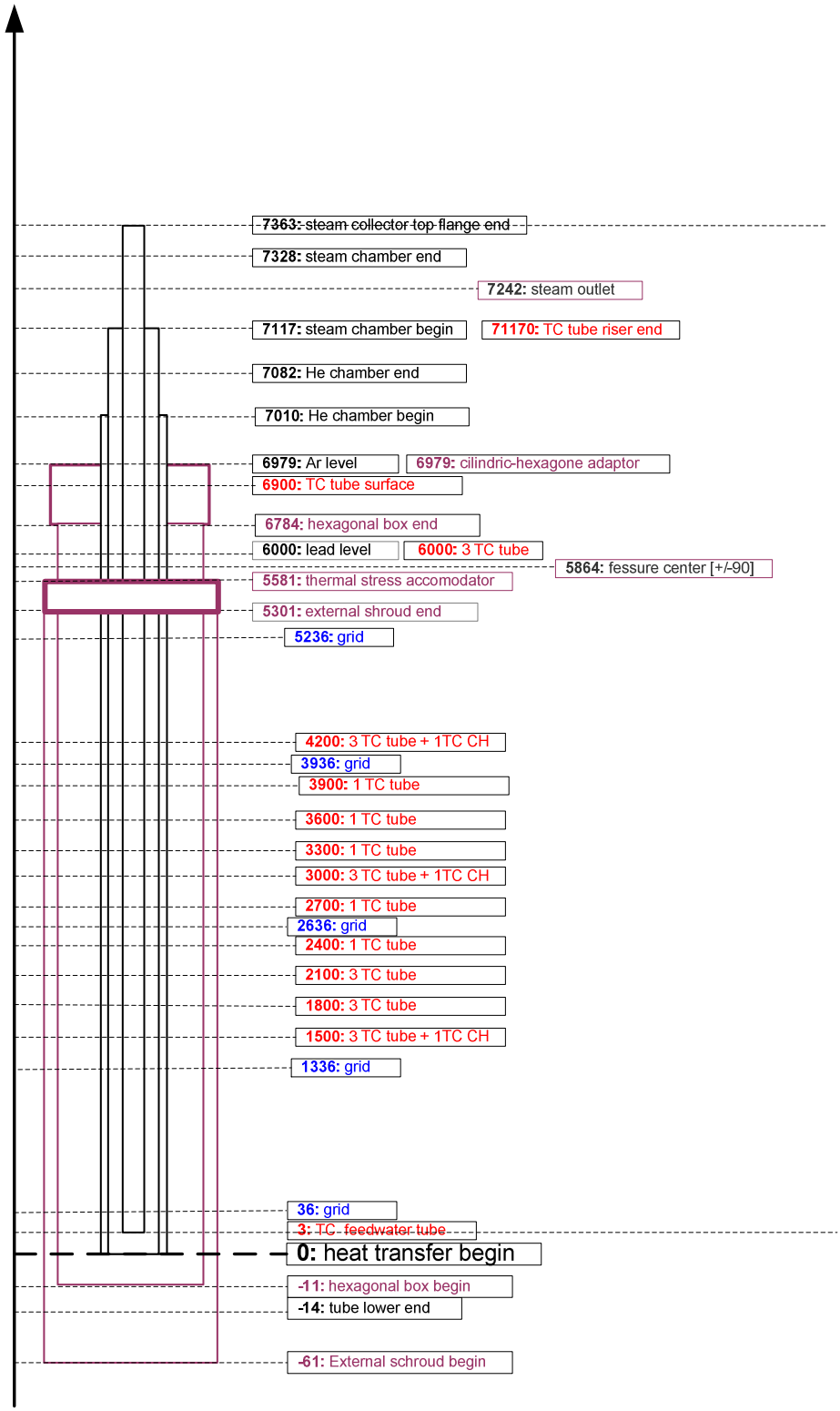

Fig. 97 – HERO-CIRCE SGBT unit modeling: axial elevations considered to develop the input deck.

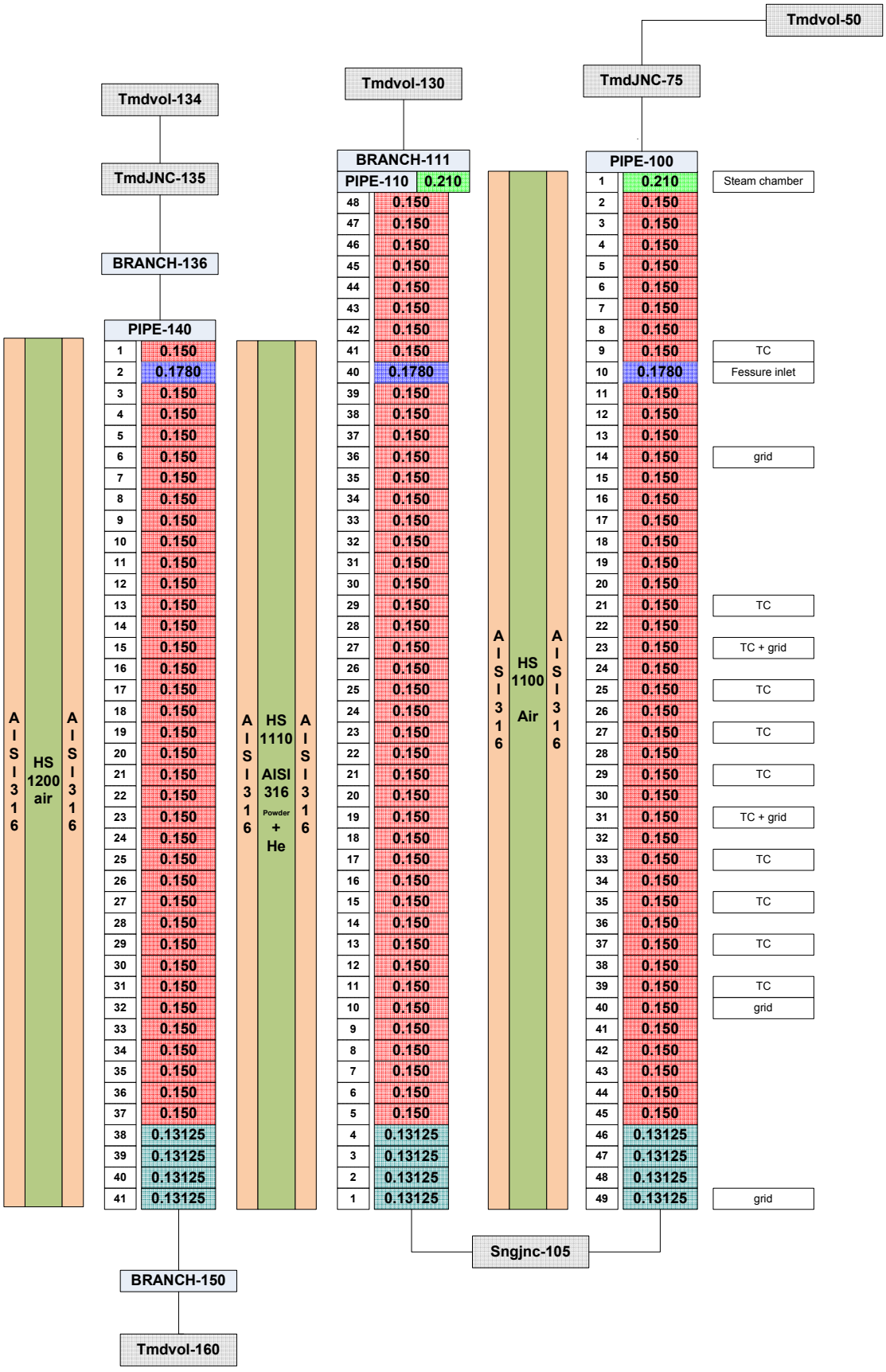

Fig. 98 – HERO-CIRCE SGBT unit modeling: nodalization scheme.

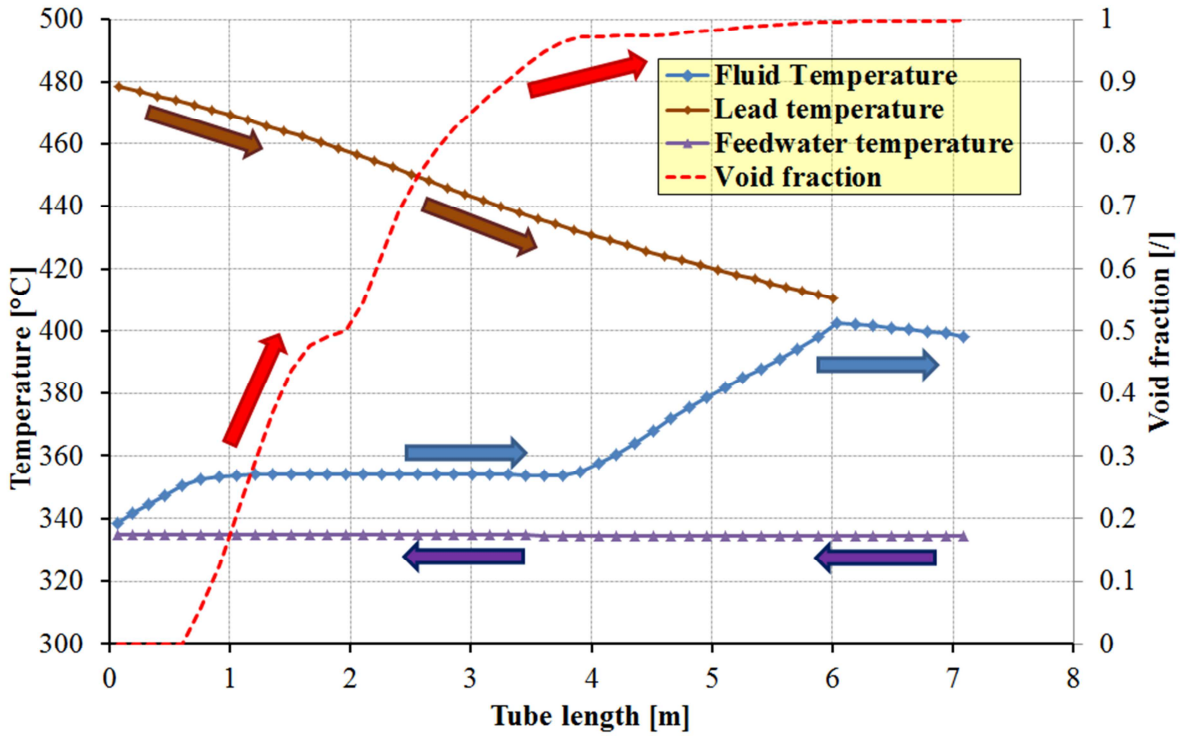

Fig. 99 – HERO-CIRCE SGBT unit vs RELAP-5 main TH parameters.

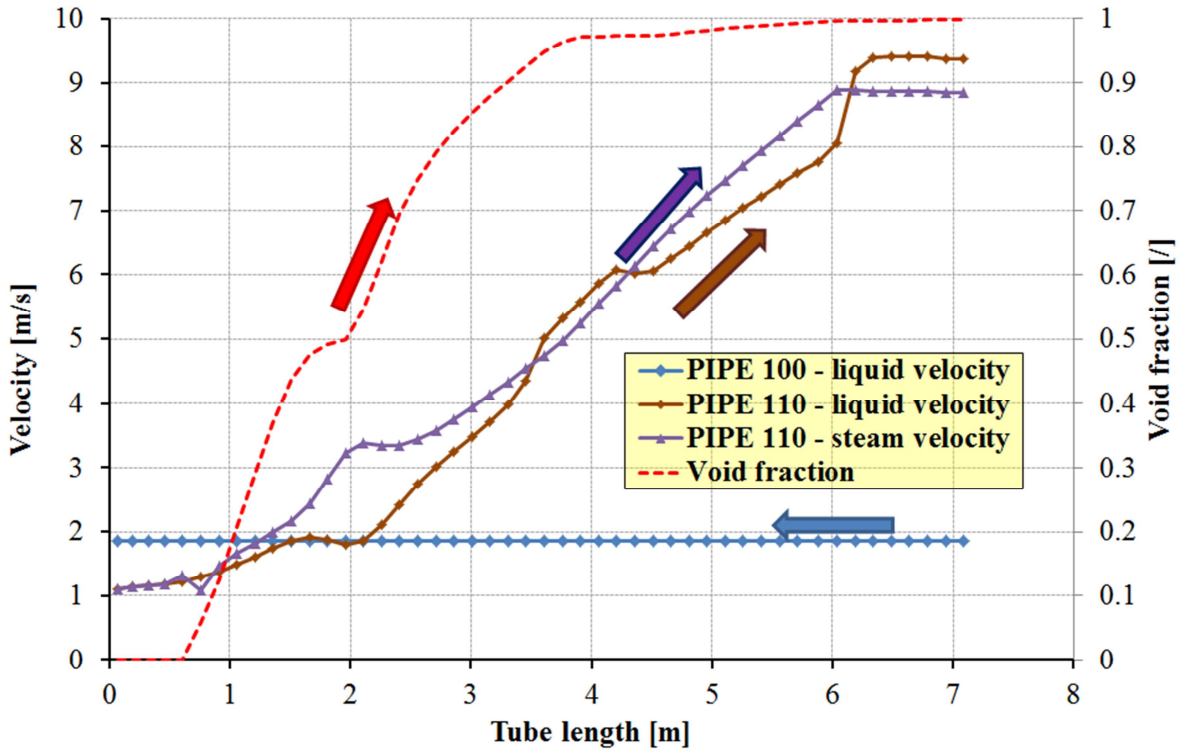

Fig. 100 – HERO-CIRCE SGBT unit vs RELAP-5 velocity profiles in the water steam side.

8 Conclusions

The present work is co-financed by ENEA-ANSALDO and aims to support the development of a SG whose tubes are double wall bayonet type with leakage monitoring. This configuration has been proposed by ANSALDO for the ALFRED reactor in the framework of the LEADER project. This project and the ADP National Project constitute the frame of this work.

The single tube vertical unit consists of three concentric tubes. Starting from the smallest one (feed-water tube), the water crosses it in down-flow and then it enters the second concentric tube (annular riser) in up-flow. In this zone the fluid starts to boil due to the heat exchange with the liquid lead that flows in counter-current at the tube outer surface up to the achievement of super-heated steam (450°C, 180bar). The liquid lead is not in direct contact with the second tube. A third concentric tube, that creates an annulus, separates it from the steam-water sides realizing the so called double wall, allowing the leakage monitoring of the system.

The study of this configuration is motivated by safety improvement. In fact, it allows the double physical separation between lead and water sides. Furthermore, by means of gap pressurization (with Helium), a leakage check system should be introduced in order to prevent incident scenarios.

On the other hands, since this unit has never been operated to produce electricity in the nuclear field, R&D is mandatory to sustain its development. In particular two main design issues are of great importance from the economic point of view. The first deals with monitor-ability of leakages: since a gas as helium is required and it has low conductivity, the gap between the double wall should be minimized and a porous heat transfer enhancer should be introduced to increase the TH performance of each unit and avoid a large SG volume (tube length or tube number), which would increase its cost and compromise the compactness of the whole primary system. The second deals with the thermal insulation of the feed-water descending tube. In fact, the water enters at its minimum temperature at the top of the SG, it is above the active length and it exchanges heat with the superheated stem that is leaving the SG unit. Therefore, in order to avoid steam condensation at the feed-water tube outer surface, this tube should be designed with sandwich wall: steel - thermal insulator – steel.

This activity is part of the R&D efforts in support to the development of a SGBT. Its main results can be subdivided in three main parts:

- Assessment of the ALFRED SG tube design and simulation of its performance by means of RELAP-5,
- Design construction and operation of a facility to test powder conductivity (Tubes for Powder facility, TxP) and
- Design and commissioning of a SG prototypic bundle based on the results achieved in TxP; the bundle hosts seven tubes which represent, as much as possible, the ALFRED SG (HERO-CIRCE SGBT unit).

Assessment of the bayonet tube performance

This part of the work is divided in two sub-parts that are strictly connected. The first is aimed to assess the performance of the tube by means of RELAP-5 v3.3 comparing the simulations with the

ANSALDO results. The second aims to investigate porous materials to be introduced as heat transfer enhancers between the double wall of the tube as well as insulating materials potentially applicable to the unit (feed-water tube).

Since the ANSALDO calculations are based on a porous material not yet identified (modeled as constant conductivity) sintetic diamond powder has been selected to develop the reference model. The insulating material is modeled according to ANSALDO (RHY-12 paint). In order to simulate the conductivity of powders, several correlations available in the open literature were investigated. Two of them are selected for the reference calculation in order to provide a band of potential results. This artifact is connected to the fact that the models that have been investigated are based on simple equations that do not consider a large variety of parameters that affects the conductivity of a porous medium such as the grain shape and size, the thermal activated mechanisms (i.e. powder grain growth and/or compaction), the open porosity effects and the boundary effects (annular geometry).

The reference simulation generally agrees with the ANSALDO results being the super-heated steam outlet temperature in the range 438-456 °C depending on the correlation adopted to model the powder. Screening, selection and computational assessment of alternative materials (to those implemented in the reference model) indicated that Si-C, Al-N, Brass, Copper and AISI-316 powders are potential solutions alternative to sintetic diamond. They have been acquired for experimental testing in the TxP facility. ZIRCOFOAM-250 insulating foam and vacuum were selected as potential solutions for the HERO-CIRCE test section instead of RHY-12 insulating paint.

Design and operation of the TxP facility

The design, construction and operation of the Tubes for Powder (TxP) facility is one of the main results of this doctorate. In fact, this facility has been completely designed during this work under the support of ENEA. The main objectives of TxP are:

- To determine the thermal conductivity of candidate powders.
- To determine the influence of the powder compaction grade on its thermal conductivity (i.e. the influence of the loading procedure, the influence of thermal cycling).
- To investigate the influence of the filling gas (i.e He) at different levels of pressurization.

The facility has been operated both to support the design of the HERO-CIRCE SGBT and to qualify the HXs operated, under operation or under commissioning at ENEA CR Brasimone that make use of double wall design with intermediate powder. The most important tests are: the propaedeutic test, the path finder test, the test in support to NACIE-UP and HELENA facilities HX, and the tests in support to the HERO-CIRCE SGBT unit.

The propaedeutic test consisted into constant temperature cycles conducted in furnace with the aim to exclude powders that experience compaction (that could not be tested in TxP). Copper, Brass, Al-N did not survive this test. Sintetic diamond, Si-C and AISI-316 survived the test and were retained suitable for testing in TxP. The first material (sintetic diamond), was excluded from the campaigns because of its high cost. Si-C was identified as first option for the application to the SGBT and acquired in five different lots (of selected grain diameter). Even if the test on AISI-316 revealed a thermal activated grain growth phenomenon, this material was identified as alternative solution for

the application to the SGBT and tested in support to the qualification of the NACIE-UP HX (the same lot of powder loaded in the NACIE-UP HX has been tested in TxP).

The pathfinder test investigated the influence of the loading procedure adopted to fill the facility with AISI-316 powder on its conductivity. Three different procedure were checked (by gravity, single step vibrated and double step vibrated) and then the procedure "double step vibrated" was selected as standard procedure (adopted also in the construction of the HX) since it tends to reduce the powder porosity increasing its conductivity.

The test in support of the NACIE-UP HX investigated AISI-316 powder loaded with the procedure double step vibrated under air un-pressurized atmosphere. The test consisted in several cycles that indicated an increase of conductivity after the second cycle which is due to grain growth. The process saturates after the third cycle and, therefore, two different correlations were released for the application to NACIE-UP HX: the first is for the first start-up, the second is for the operation.

The test in support of the SGBT investigated Si-C and AISI-316 powders loaded with the procedure double step vibrated under air un-pressurized atmosphere and under helium atmosphere at different levels of pressurization (1 - 4.5bar). Si-C revealed un-expected low conductivity (about 0.5 W/mK) which was found to be related to the structure of its grains (large open porosity at grain boundaries were identified at SEM) and was excluded for the application to the SGBT. Cycled AISI-316 under helium pressurized atmosphere revealed a maximum conductivity of 2.5 W/mK and was therefore selected as powder material for the HERO-SGBT unit.

These tests substantially confirm that each material has its own conductivity when reduced to powder that depends mainly on the grain structure and generic model could be non-representative of its behavior with large deviations.

Design and commissioning of the HERO-CIRCE test section

The Heavy liquid mEtal – pRessurized water cOoled tube (HERO) SG unit constitutes the finalization of this work. This configuration is based on a hexagonal shroud that contains 7 SGBT of similar geometry to the ALFRED SGFig. 78. It is designed to be placed inside CIRCE and is fed by LBE which flows by gas enhanced circulation from the top by means of fissures that communicate with the CIRCE pool. The LBE flows inside the tube bundle for six meters (as in the SG of ALFRED) and then it leaves the device from the bottom which is opened.

This system has been preferred to a standalone facility operated by natural circulation lead due to following advantages:

- The SGBT design of ALFRED could be reproduced as much as technological limits or market limits will impair its construction.
- Seven tubes are more representative of the SG than one tube and they allow the experimental assessment of dynamic instabilities.
- The lead mass flow is regulated by enhanced circulation using a system that is already available in CIRCE.
- The required power (447 kW) is supplied by a system that is already available in CIRCE.
- The cost of the test section is lower than those of a standalone facility.

The design and construction of the unit required several modification of the ALFRED SG tube design. The most important are:

- The tube material has been changed, stainless steel AISI-304 instead of T91 is adopted since T91 is not available in small lots and it has several problems in terms of qualification of welded joints (that should be operated at high pressure).
- Since stainless steel has lower mechanical properties than T91, the tube geometry has been slightly modified keeping as constant the original P/D.
- Based on the feed-back from the TxP experimental campaigns, AISI-316 powder has been loaded into the tubes and will operate under helium atmosphere at 4.5bar.
- ZIRCO-FOAM 250 had been selected as insulating material. During the construction phase it revealed low adhesive properties and slight vacuum has finally be realized between the feed-water tube double wall.

These modifications allows the construction of a SG unit that is expected to produce super-heated steam at 400°C, 50°C lower than the ALFRED SG goal. Two main parameters are responsible for this discrepancy:

- The tube material: stainless steel tubes require higher thicknesses than T91 and have lower conductivity.
- The powder material: AISI-316 powder has relatively low conductivity and further investigation are necessary to select alternative materials with higher conductivity.

The expected performance of HERO-CIRCE is retained acceptable for the application to a prototypic unit and can be scaled to ALFRED. However, further R&D is mandatory to design it as SG for electricity production with particular reference to the heat enhancer porous material, which impact on the cost and on the compactness of the whole systems.

REFERENCES

[1] www.gen-4.org, *GEN-IV technology website.*

[2] *DOE NERAC, GIF*, **A Technology Roadmap for Generation IV Nuclear Energy Systems**, GIF-002-00, December 2002.

[3] *D. Rozzia, M. Tarantino N. Forgione*, **State of Development of LFR and ADS Technologies and R&D Needs**, HELIMNET Project WP-5 DEL 5.1, February 2012.

[4] *C. F. Smith, L. Cinotti, H. Sekimoto*, **Lead-cooled Fast Reactor (LFR) ongoing R&D and key issues**, GIF Symposium – Paris (France) – 9-10 September, 2009.

[5] *OECD/NEA*, **Handbook on Lead-bismuth Eutectic Alloy and Lead Properties, Materials Compatibility, Thermal-hydraulics and Technologies**, ISBN 978-92-64-99002-9, 2007.

[6] *IAEA*, **Comparative assessment of thermo-physical and thermo-hydraulic characteristics of lead, lead-bismuth and sodium coolants for fast reactors**, IAEA-TECDOC-1289, Vienna, 2002.

[7] *D. Mattioli, S. Monti, D. De Bruyn and A. Alemberti*. **LFR Road-map**. LEADER Project WP1 – DEL 029-2010, December 2010.

[8] www.leader-fp7.eu. *LEADER Project website.*

[9] *A. Alemberti, S M. Grattarola*. **Project Presentation**. LEADER Project WP0 – DEL 035-2010, July 2010.

[10] *J. Carlsson*, **General Synthesis Report of ELSY**, FI6W-036439, DEL/10/04, 23 March 2010.

[11] **Leader 2nd Project Coordination Committee meeting**, Genova, May 12th 2011.

[12] *D. D. De Fur*. **LMFBR Steam Generator Development: DUPLEX Bayonet Tube Steam Generator**. Combustion Engineering, incorporated Chattanooga, Tennessee (USA) CENC-1238(Vol. 2), 1975.

[13] *M. Tarantino, et al.*. **Integral Circulation Experiment: Thermal-Hydraulic Simulator of a Heavy Liquid Metal Reactor**. Journal of Nuclear Material, vol. 415, Issue 3, pp. 433-448.

[14] *D. Rozzia, A. Toti, M. Tarantino*, **Double-wall Bayonet Tube Steam Generator for LFR Application. Preliminary Characterization**, NNFISS – LP3 – 032, September 2011.

[15] *DOE NERAC, GIF*, **A Technology Goals for Generation IV Nuclear Energy Systems**, GIF-019-00, December 2002.

[16] *IAEA.* **Liquid Metal Cooled Reactors: Experience in Design and Operation.** IAEA-TECDOC-1569, Vienna, 2007.

[17] www.ist-world.org/ProjectDetails.aspx?ProjectId=511f2e5a509041c5be90a0df653e425f, *ELSY project website.*

[18] *L. Mansani*, **Updated Design Options for the ELFR Reference Plant,** LEADER Project – WP1 – DEL 01-2011.

[19] **Leader 2nd Project Coordination Committee meeting**, Genova, May 12th 2011.

[20] http://myrrha.sckcen.be, CDT project website (MYRRHA).

[21] *D. Rozzia, A. Del Nevo, M. Tarantino,* **Preliminary Discussion on LFR Fuel Pin Design: Current Status, Fuel Modeling and Open Issues**, Proceedings of the 20th International Conference on Nuclear Engineering ICONE20 July 30-August 3, 2012, Anaheim, California, USA. Paper 54697.

[22] *C. Petrovich, G. Grasso, C. Artioli, F. Rocchi,* **Definition of the ETDR core and neutronic characterization – PART-I**, UTFISSM–P9SZ–002, March 2012.

[23] http://ww.iaea.org, *Fast Reactors Database.*

[24] *G. John Yevick*. **Fast Reactor Technology Plant Design.** The M. I. T. Press, Massachusetts Institute of Technology, Cambridge, Massachusetts, 1966, pp. 208 - 217.

[25] *G R. C. Berkan, B. R. Upadhyaya, R. A. Kisner,* **LOW-ORDER DYNAMIC MODELING OF THE EXPERIMENTAL BREEDER REACTOR II.** ORNL/TM- 11161, 1990.

[26] *L. Damiani, M. Montecucco and A. Pini Prato*. **Conceptual design of a bayonet-tube steam generator for the ALFRED lead-cooled reactor.** Nuclear Engineering and Design 2013 vol. 265 pp 154– 163.

[27] *M. Tarantino, et al.*. **Heavy Liquid Metal Natural Circulation in a One - Dimensional Loop**. Nucl. Eng. and Des., vol. 241, pp. 1301-1309, 2011.

[28] *NUREG/CR-5535*, **RELAP5/MOD3.3 Code Manual, Volume IV: Models and Correlations**, Information Systems Laboratories Inc., December 2001.

[29] *NUREG/CR-5535*, **RELAP5/MOD3.3 Code Manual, Volume I: Code Structure, System Model, and Solution Methods**, Information Systems Laboratories Inc., March 2003.

[30] *NUREG/CR-5535*, **RELAP5/MOD3.3 Code Manual, Volume II Appendix A: Input Requirements**, Information Systems Laboratories Inc., June 2004.

[31] *O. E. Dwyer, H. C. Berry*, **Heat Transfer to Liquid Metals Flowing Turbulently and Longitudinally Through Closely Spaced Rod Bundle, Part I**, Nuclear Engineering and Design Vol. 23 pp. 273-294, 1972.

[32] *W. Pfrang, D. Struwe* **Assessment of Correlations for Heat Transfer to the Coolant for Heavy Liquid Metal Cooled Core Designs** Institut für Reaktorsicherheit Forschungszentrum Karlsruhe GmbH, Karlsruhe, 2007.

[33] *R. A. Seban and T. T. Shimazaki,* "**Heat transfer to a fuid flowing turbulently in a smooth pipe with walls at constant temperature**", Transactions of the ASME, Vol. 73, May 1951, pp. 803-809.

[34] *M. Moretti, D. Rozzia, A. Del Nevo, M. Tarantino,* **Modeling of SG Bayonet Tube for GEN-IV Applications by Means of RELAP-5**. 24-04-SGBT-TR-03(12), Brasimone, June 2012.

[35] *D. Rozzia, D. Martelli, N. Forgione M. Moretti, A. Naviglio, D. Vitale Di Maio A. Del Nevo, M. Tarantino* **Activities in Support to the Assessment of SG Bayonet Tubes, for GEN-IV Applications** ENEA, NNFISS - LP3 - 054, 2012

[36] *M. Moretti,* **Analysis and modelling of a double wall bayonet tube in support to the development of innovative SG for LFR – GEN-IV nuclear systems**. Master thesis in Nuclear and Energetic Engineering, UNIROMA-1, October 2012.

[37] *D. Rozzia, M. Moretti, M. Tarantino, A. Del Nevo, N. Forgione, A. Alemberti* **Modeling of SG Bayonet Tube for GEN-IV Applications by Means of RELAP5**. Proceedings of NENE-2012, 5-7 September 2012 Ljubljana, Slovenia. Paper n°-206.

[38] *M. Palmero, F. Fionelli,* **ALFRED – Steam Generator Design,** LEADER meeting, Power Point presentation, 11 May 2011,Genova.

[39] *D. A. Nield, A. Bejan*, **Convection in Porous Media, Third Edition**, Springer Science+Business Media, Inc., 233 Spring Street, New York, NY 10013, USA.

[40] *M. Kandula*, **On the Effective Thermal Conductivity of Porous Packed Beds with Uniform Spherical Particles**, ASRC Aerospace, John F. Kennedy Space Center, FL, USA.

[41] *Y. Feng, B. Yu, M. Zou, D. Zhang,* **A generalized model for the effective thermal conductivity of porous media based on self-similarity**, J. Phys. D: Appl. Phys. 37 (2004) pp 3030–3040.

[42] *D. Rozzia, A. Toti, M. Tarantino* **Experimental Investigation on Powders Thermal Performance to Support the Design of Innovative SG for LFR**, DR_/PhD/01(11)-IIR-Rev1a, Brasimone, May 2011.

[43] *M. Moretti, D. Rozzia, M. Tarantino,* **Investigation on insulating materials and design solutions for superheated steam double wall bayonet tube bundle for Gen. IV applications**, 07-03-12-Insulating-BRR-01(12), Brasimone April 2012.

[44] http://www.energyguide.com/library/EnergyLibraryTopic.asp?bid=tva&prd=10&TID=25824&SubjectID=10171,

Wall insulation.

[45] http://www.rsifibre.com/products/mineral-wool-insulation.php,

Refractory Specialties Incorporated society.

[46] http://www.aerogel.com/,

Aspen aerogels.

[47] http://www.enerchecksystems.com/suprthrm.html,

Supertherm Insulating paint.

[48] *L. Mansani* **Direct communication**.

[49] *D. R. Clarke, S. R. Phillpot,* **Thermal barrier coating material**, ISSN 1369 7021, 2005.

[50] *R. Vaßen, M. O. Jarligo, T.a Steinke, D. E. Mack, D.v Stöver*, **Overview on advanced thermal barrier coatings**, Surface & Coatings Technology Vol. 205 pp. 938–942, 2010.

[51] http://www.zircofoam.com

ZIRCOFOAM-250 Insulating foam.

[52] *D. Rozzia, G. Fasano, M. Tarantino*, **Manuale operativo della facility TxP**, ENEA CR BRASIMONE interim report, 09/2013.

[53] *D. Rozzia, A. Toti, G. Venturi, I. Di Piazza, L. Rapezzi, M. Tarantino, A. Alemberti* **Experimental Evaluation of Thermal Performance of Powders for GEN-IV Technology Applications,** Proceeding of Nat. Conf. of UIT 2011, June, 20-22, 2011, Torino, Italy.

[54] *D. Rozzia, A. Toti, G. Venturi, A. Del Nevo, M. Tarantino, A. Alemberti*, **Basis for the Experimental Evaluation of Powders conductivity in the TxP Facility for Generation IV Technology Application,** Proceeding of Int. Conf. of NENE 2011, September, 12-15, 2011, Bovec, Slovenia. Paper n°-815.

[55] *D. Rozzia, M. Agostini, A. Ventura, G Venturi, M. Tarantino*, **Experimental Assessment of Powders Compaction When Subjected to Thermal Loads,** DR_/PhD/01(12)-IIR-Rev0a, Brasimone, February 2012.

[56] *D. Rozzia, G. Fasano, M. Tarantino, P. Agostini, A. Alemberti*, **Powder's Conductivity Measurements in the TxP Facility**. Proceedings of NENE-2013, paper n° 206, Bled, Slovenia, 9-12 September 2013.

[57] *D. Rozzia, G. Fasano, I. Di Piazza, M. Tarantino,* **Experimental Investigation on Powder Conductivity for the Application to Double Wall Heat Exchanger (NACIE-UP).** Nuclear Engineering and Design manuscript number NED-D-14-00179, **under printing**.

[58] *J. H. Lienhard IV, and J. H. Lienhard V,* **A Heat Transfer Textbook**. Third edition, Phlogiston press Cambridge Massachusett, 2003.

[59] *D. Rozzia, A. Del Nevo, M. Tarantino and P.A. Gaggini.* **Fornitura scambiatore di calore a tubi a baionetta (HERO)**. ADPFISS – LP2 – 028, 2013.

[60] *I. E. Idelchik* **Handbook of Hydraulic Resistance third edition**. ISBN 1-56700-074-6, Begell House, 1996.

APPENDIX A: SGBT RELAP-5 Input Deck

```
*----------------------------------------------------------------------
*---  RELAP5/MOD3.3 Analysis                    July 2011
*----------------------------------------------------------------------
*---  SG TUBE  MODEL          2012 REVISION 1
*----------------------------------------------------------------------
*--- by Alessandro Del Nevo and Davide Rozzia
(alessandro.delnevo@enea.it, daviderozzia@libero.it)
*----------------------------------------------------------------------
* Problem Type and Option
00000100     new     transnt
* Unit System
*00000102     si     si
* Noncondensible Gas
00000110     nitrogen
* CPU Time Remaining Card
00000105     5.0
* Hydrodynamic System Control
*          RefVol       Elev     Fluid     SystemName
00000120    100500000     0.0     h2o       tube
00000121    140010000     0.0     pbbi      channel
* TIME STEP
*         tend     dtmin    dtmax   NumMeth  mEFrq   MEFrq    RstFrq
00000201   100.    1.e-12   0.005   07003    2000    200000   200000
00000202   300.    1.e-12   0.005   07003    2000     40000   200000
00000203   500.    1.e-12   0.005   07003    2000     40000   200000
00000204   900.    1.e-12   0.005   07003    2000     40000   200000
* TRIPS
* end program
20600000  expanded                                    * expanded trip set
20600010  time 0  lt  null  0  1.e6  n   0.0          * always true
20600020  time 0  gt  null  0  1.e6  n  -1.0          * always false
20600030  time 0  lt  null  0  100.  n   0.0          * true  untill 100s
20600040  time 0  gt  null  0  100.  n  -1.0          * false untill 100s
20610010  2 and 2 n -1.0
20610020  2 and 2 n -1.0
20610030  2 and 2 n -1.0
20610040  4 and 1 n -1.0
20610050  4 and 1 n -1.0
20610060  2 and 2 n -1.0
* END OF PROGRAM
20600100  time 0  gt  null  0   900.  n  -1.0          *
600  10                                          * end program
*----------------------------------------------------------------------
** HYDRODYNAMIC COMPONENTS (SG bayonet tube)
*----------------------------------------------------------------------
*time dependent volume
0500000 cntvlv1 tmdpvol
```

```
0500101 0.  10.  10.  0.  -90.0  -10.0  5.e-5  0.  0*
0500200 0003  1001*
0500201    -1.0   1.9000e+07  608.0
0500202     0.0   1.9000e+07  608.0
0500203     1.e6  1.9000e+07  608.0
* COSTRUZIONE TRASFERIMENTO ACQUA DA PISCINA A PRIMO TUBO
*time dependent junct
0750000 fwpmp  tmdpjun
0750101 050010000 100000000  0.  0
0750200  1      1002
0750201 -1.0    0.047255  0.  0.
0750202  0.0    0.047255  0.  0.
0750203  1.e+6  0.047255  0.  0.
*PRIMO TUBO
1000000 sgtube-d    pipe
1000001 50
1000101 4.27762e-05 50
1000301 0.335  10     0.15    50
1000401 0.0         50
1000601 -90.0       50
1000801 4.50e-05  0.0      50
1000901 1.e-6     1.e-6    49
1001001 000000   50
1001101 000000   49
1001201 3 1.8000e+07  608.0  0.0 0.    0.  50
1001300 1
1001301 0.047255  0.  0. 49
*ATTACCO IL PRIMO AL SECONDO
1050000  junc     sngljun
1050101  100010000  110000000   4.27762e-05   0.80  1.00   000000
1050201  1   0.047255   0.0   0.0
*SECONDO TUBO
1100000 sgtubeu    pipe
1100001 50
1100101 8.27708e-05 50
1100301 0.15        40   0.335       50
1100401 0.0         50
1100601 +90.0       50
1100801 4.50e-05  0.00259      50
1100901 1.e-6     1.e-6    49
1101001 000000   50
1101101 000000   49
1101201 3 1.8000e+07  608.0  0.0 0.    0.  50
1101300 1
1101301 0.047255  0.  0. 49
*USCITA attacco il time dependent volume al tubo stiamo modellando il downcomer del vapore
1200000 h2o03 branch
1200001 2  1
1200101 3.333e-04   0.500  0.0  0.  0.  0.  4.5e-5  0.00  0000000
1200200 003 1.8000e+07  608.0
```

```
1201101 110010000  120000000   0.  0.  0.   0000
1202101 120010000  130000000   0.  0.  0.   0000
1201201 0.047255     0.0  0.0
1202201 0.047255     0.0  0.0
*downcomer del vapore
1300000 cntvlv2 tmdpvol
1300101 0.  10.  10.  0.  0.0  0.0  5.e-5  0.  0
1300200 3  1003
1300201    -1.0   1.8000e+07  723.0  0.0
1300202     0.0   1.8000e+07  723.0  0.0
1300203     1.e6  1.8000e+07  723.0  0.0
*LATO PIOMBO
*piscina piombo
*time dependent volume
1350000 cntvlv2 tmdpvol
1350101 0.  10.  10.  0.  -90.0  -10.0  5.e-5  0.  0
1350200 3  1004
1350201    -1.0   0.01150e+07  608.0
1350202     0.0   0.01150e+07  608.0
1350203   300.0   0.01150e+07  700.0
1350204   500.0   0.01150e+07  753.0
1350205     1.e6  0.01150e+07  753.0
*COSTRUZIONE TRASFERIMENTO Pb DA PISCINA A canale
*time dependent junct
1360000 fwpmp  tmdpjun
1360101 135010000 140000000  0.  0
1360200  1      1005
1360201   -1.0    0.01  0.  0.
1360202    0.0    0.01  0.  0.
1360203  300.0    0.1   0.  0.
1360204  500.0    6.367647  0.  0.
1360205    1.e+6  6.367647  0.  0.
*CANALE PIOMBO
1400000 pbtube    pipe
1400001 40
1400101 0.000962968 40
1400301 0.15      40
1400401 0.0        40
1400601 -90.0      40
1400801 4.50e-05  0.038641321    40
1400901 1.e-6     1.e-6    39
1401001 0000000   40
1401101 0000000   39
1401201 3 1.74329e+05  608.0  0.0 0.    0.   4
1401202 3 2.34824e+05  608.0  0.0 0.    0.   8
1401203 3 2.95319e+05  608.0  0.0 0.    0.  12
1401204 3 3.55814e+05  608.0  0.0 0.    0.  16
1401205 3 4.16309e+05  608.0  0.0 0.    0.  20
1401206 3 4.76804e+05  608.0  0.0 0.    0.  24
1401207 3 5.37299e+05  608.0  0.0 0.    0.  28
```

```
1401208 3 5.97794e+05  608.0  0.0 0.    0.  32
1401209 3 6.58289e+05  608.0  0.0 0.    0.  36
1401210 3 7.18784e+05  608.0  0.0 0.    0.  40
1401300 1
1401301 0.01  0.  0. 39
*
1500000 h2o04 branch
1500001 2  1
1500101 1.333e-04   0.500  0.0  0.  0.  0.  4.5e-5  0.00  0000000
1500200 003 1.00266e+06  608.0
1501101 140010000  150000000   0.  0.  0.   0000
1502101 150010000  160000000   0.  0.  0.   0000
1501201 0.01     0.0  0.0
1502201 0.01     0.0  0.0
*downcomer del pb
1600000 cntvlv3 tmdpvol
1600101 0.  10.  10.  0.  0.0  0.0  5.e-5  0.  0
1600200 3  1006
1600201    -1.0   1.07266e+06  753.0
1600202     0.0   1.07266e+06  753.0
1600203     1.e6  1.07266e+06  753.0
*---------------------------------------------------------------------
** THERMAL STRUCTURE (SG bayonet tube)
*---------------------------------------------------------------------
*primo tubo
11001000 50  20  2  1  0.00369 0
11001100 0 1
11001101 5 0.00476  9  0.007645 5 0.009525
11001201 10 5  11 14  10 19
11001301 0. 19
11001400 0
11001401 608.  20
11001501 100010000   10000      1 1 0.335    10
11001502 100110000   10000      1 1 0.15     50
11001601 110500000  -10000      1 1 0.335    10
11001602 110400000  -10000      1 1 0.15     50
11001701 0  0.0  0.0  0.0  50
11001801 0.00738 100. 100. 0. 0. 0. 0. 1. 50
11001901 0.005532131 100. 100. 0. 0. 0. 0. 1. 50
* Secondo tubo
11101000 40  31  2  1  0.01082 0
11101100 0 1
11101101 10 0.0127  10 0.01377 10   0.015865
11101201 10 10  12 20  10 30
11101301 0. 30
11101400 0
11101401 608.  31
11101501 110010000   10000      1   1 0.15        40
11101601 140400000  -10000      110 1 0.15        40
11101701 0  0.0  0.0  0.0  40
```

11101800 1
11101801 0.004870014 100. 100. 0. 0. 0. 0. 1. 9.3500 1.1000 1. 40
11101900 1
11101901 0.038641321 100. 100. 0. 0. 0. 0. 1. 6.0000 1.4182 1. 40

APPENDIX B: TxP main components

14. HR-14		
Thermocox 25 kW – 1200mm active length it has 16 TCs		
5. PIPE-5		
It contains the heating rod HR-14, it is made of AISI-304		
Id	**Sub-component**	**Instrumentation**
3	Spacer	--
4	HR - Support	--
5a	Annular rodlet	3 T-5a –i, 3 T-5a -e
5b	Annular rodlet	3 T-5b –i, 3 T-5b -e
5c	Annular rodlet	3 T-5c –i, 3 T-5c -e
5d	Annular rodlet	3 T-5d –i, 3 T-5d -e
5e	Annular rodlet	--
5f	Annular rodlet	--
7. PIPE-7		
It contains PIPE-5, it is made of AISI-304		
Id	**Sub-component**	**Instrumentation**
7a	Annular rodlet	3 T-7a -e
7b	Annular rodlet	3 T-7b –e
7c	Annular rodlet	3 T-7c –e
7d	Annular rodlet	3 T-7d –e
7e	Annular rodlet	--
8. PIPE-8		
It contains PIPE-7, it is made of AISI-304		
Id	**Sub-component**	**Instrumentation**
8a	Annular rodlet	--
8b	Thermal compensator	--
8c	Annular rodlet	--
6. Flange		
Upper bottom flange that connects Pipe-7 to Pipe-8, it is welded and has been checked against liquid penetration		
9. Flange		
Lower top flange that connects Pipe-7 to Pipe-8, it is welded and has been checked against liquid penetration		
1. TxP support		
It keeps the facility in position by anchoring to the floor		
2. Flange		
Bottom flange connected to the support and to flange 6		
10. Aluminum disk		
Connected to item 9 and item 11. It has four square channels for TCs cables		
11. Flange		
Upper top flange Pipe-7 - Pipe-8		
12. Flange		
Lower flange of pipe 5		
13. Aluminum disk		
Connected to item 12 and item 15. It has four square channels for TCs cables		
15. Flange		
Upper flange of pipe 5		
16. Flange		
HR-14 closure		

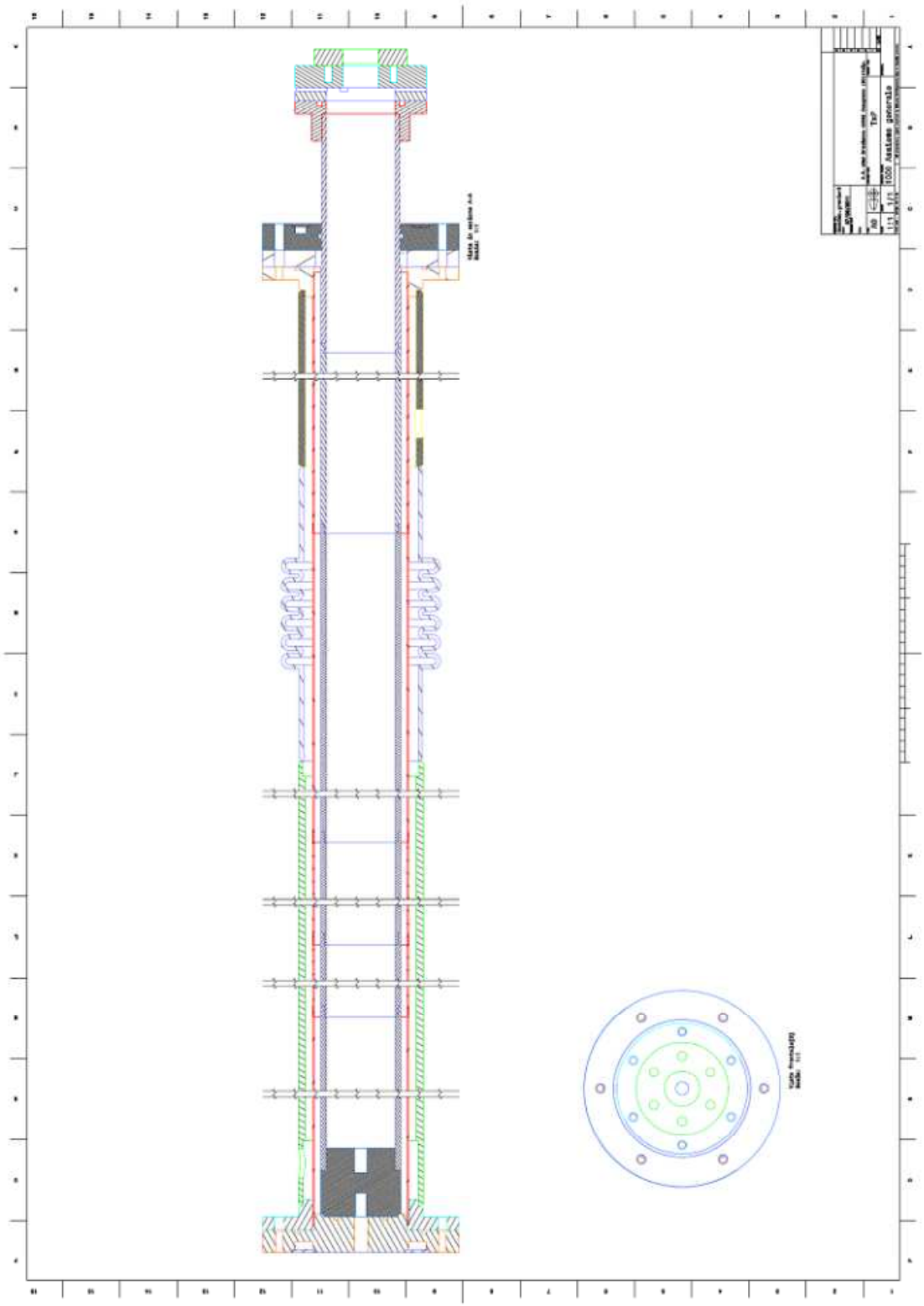

Fig. B. 1 – TxP main layout.

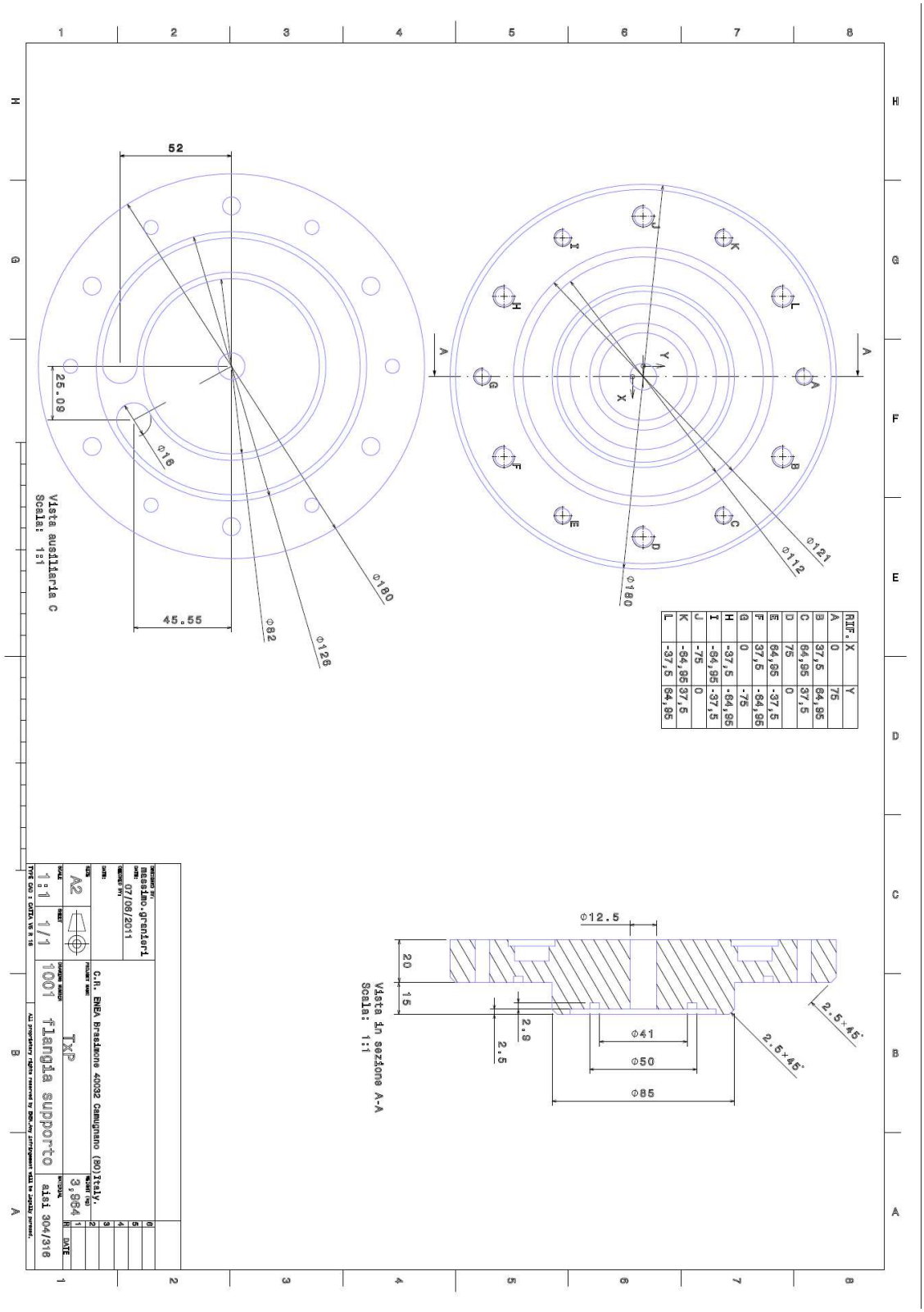

Fig. B. 2 – TxP lower bottom flange, item 2.

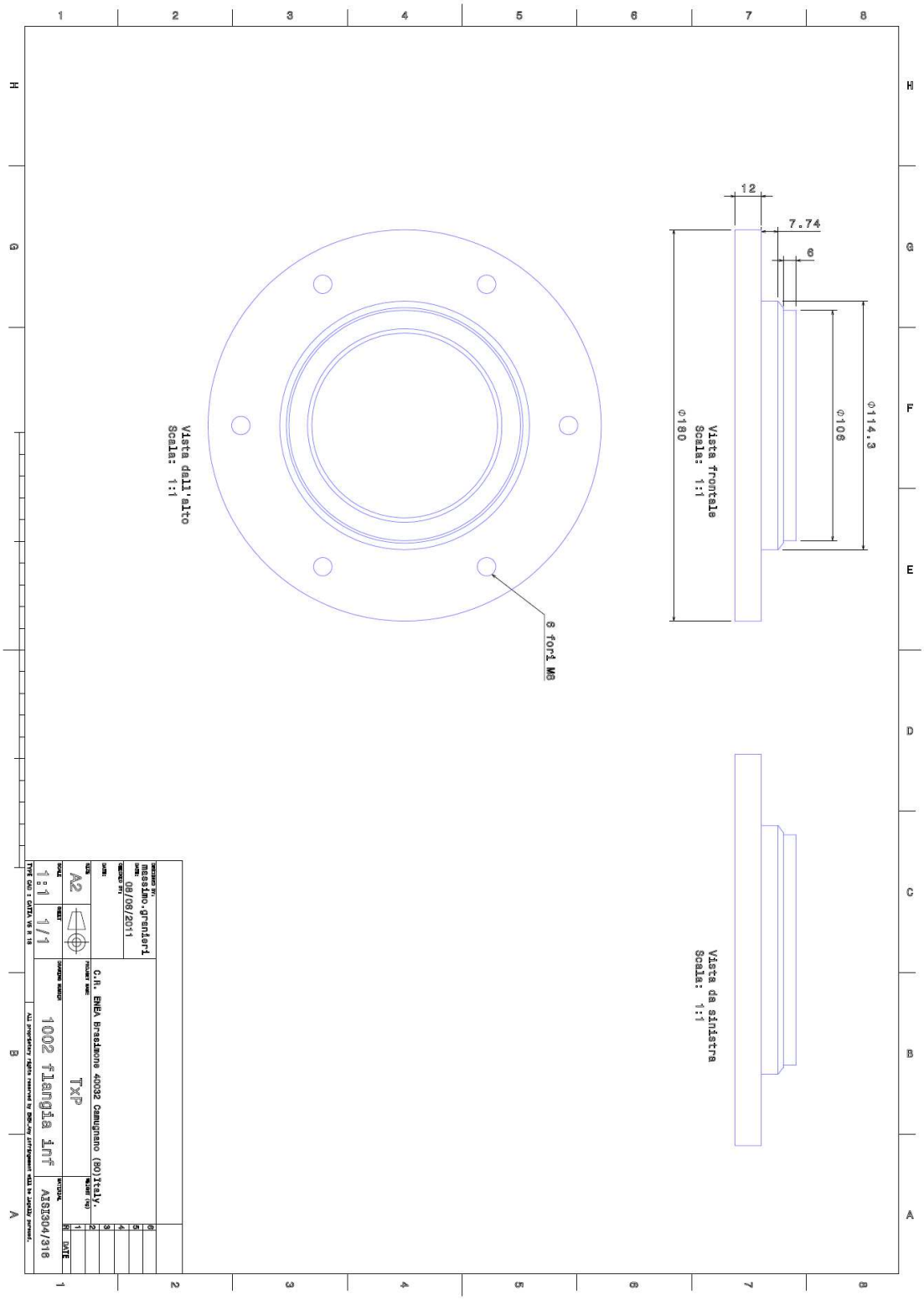

Fig. B. 3 – TxP upper bottom flange, item 6.

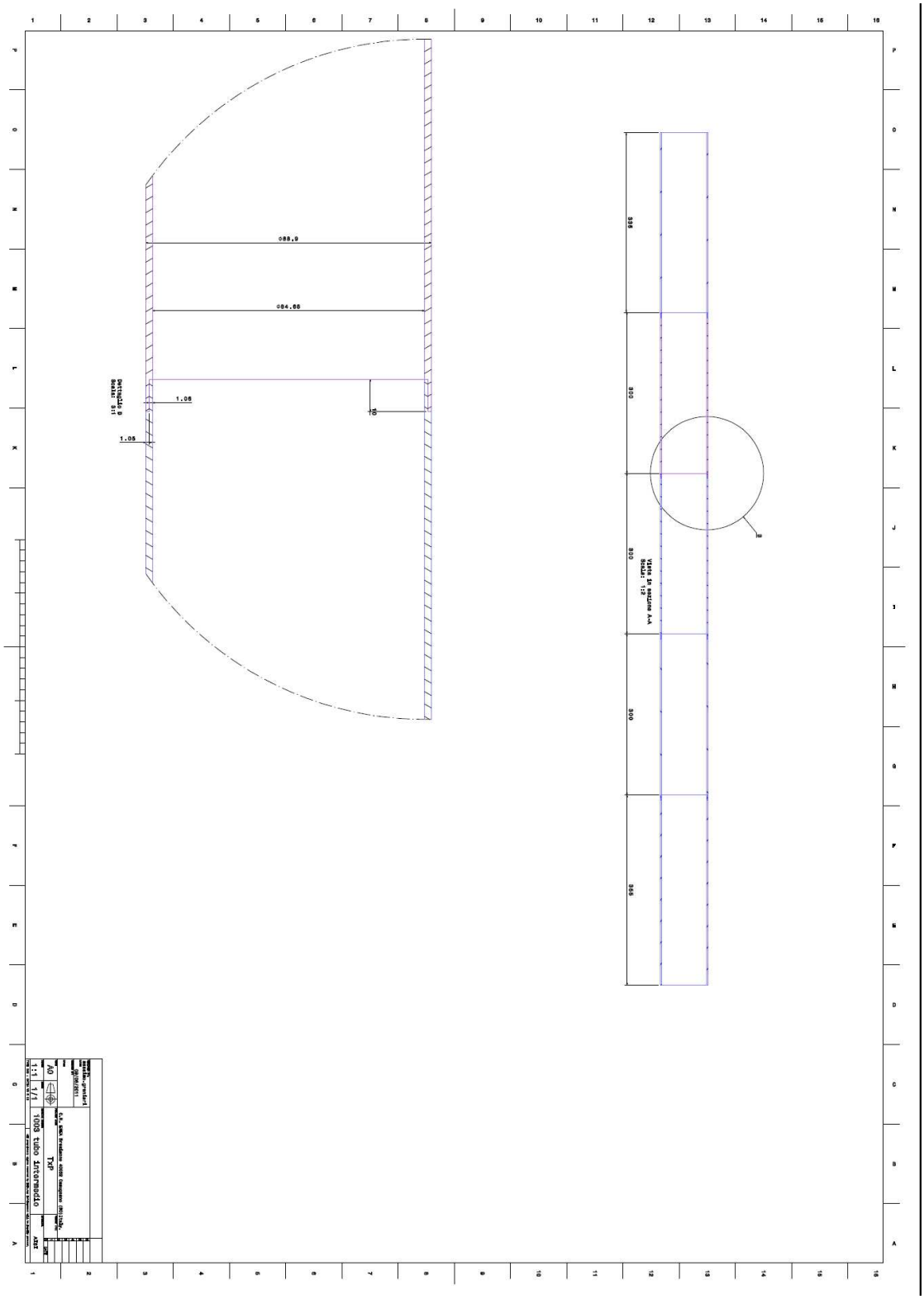

Fig. B. 4 – TxP PIPE-5, item 5.

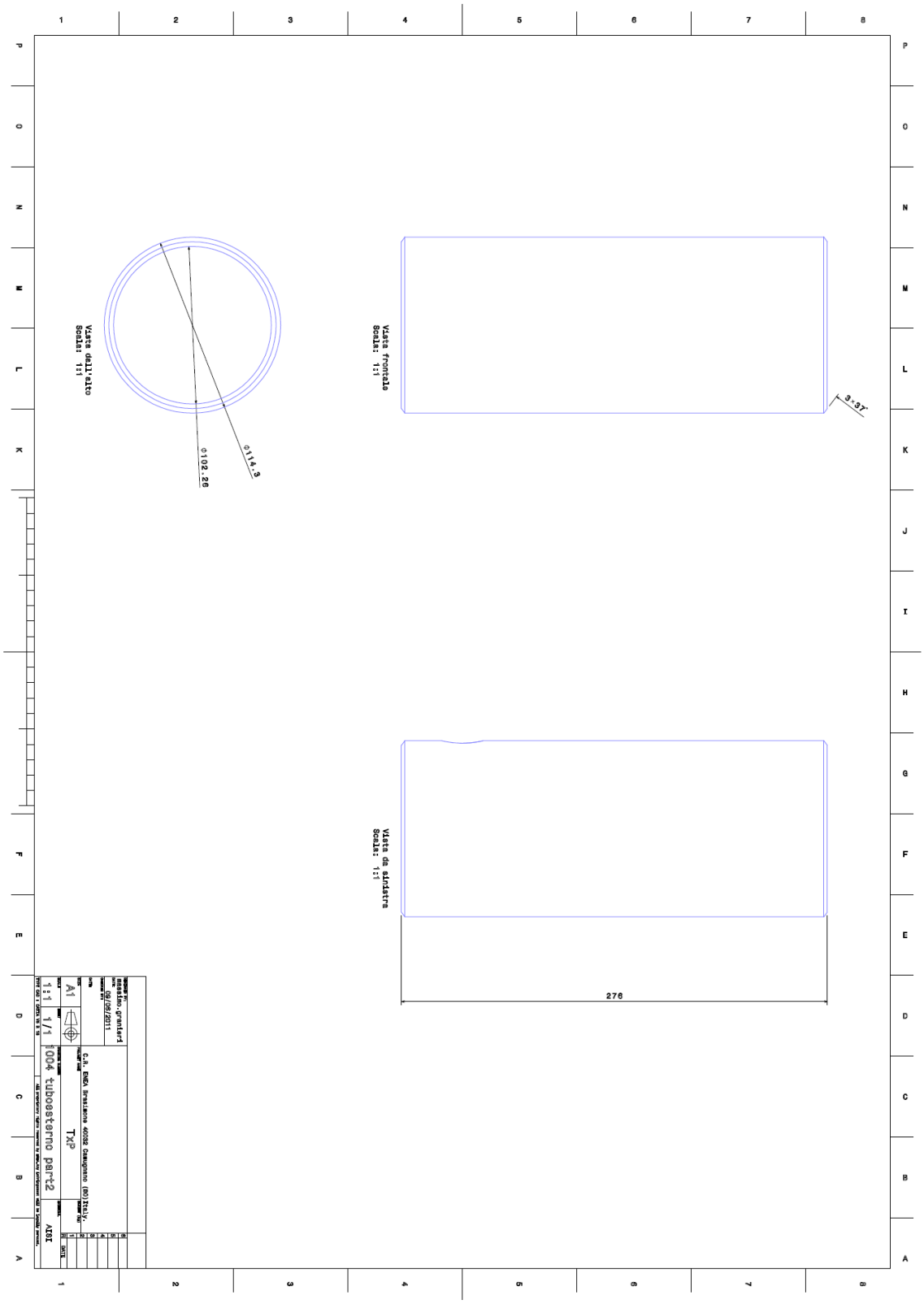

Fig. B. 5 – TxP PIPE-8, sub-component 8c.

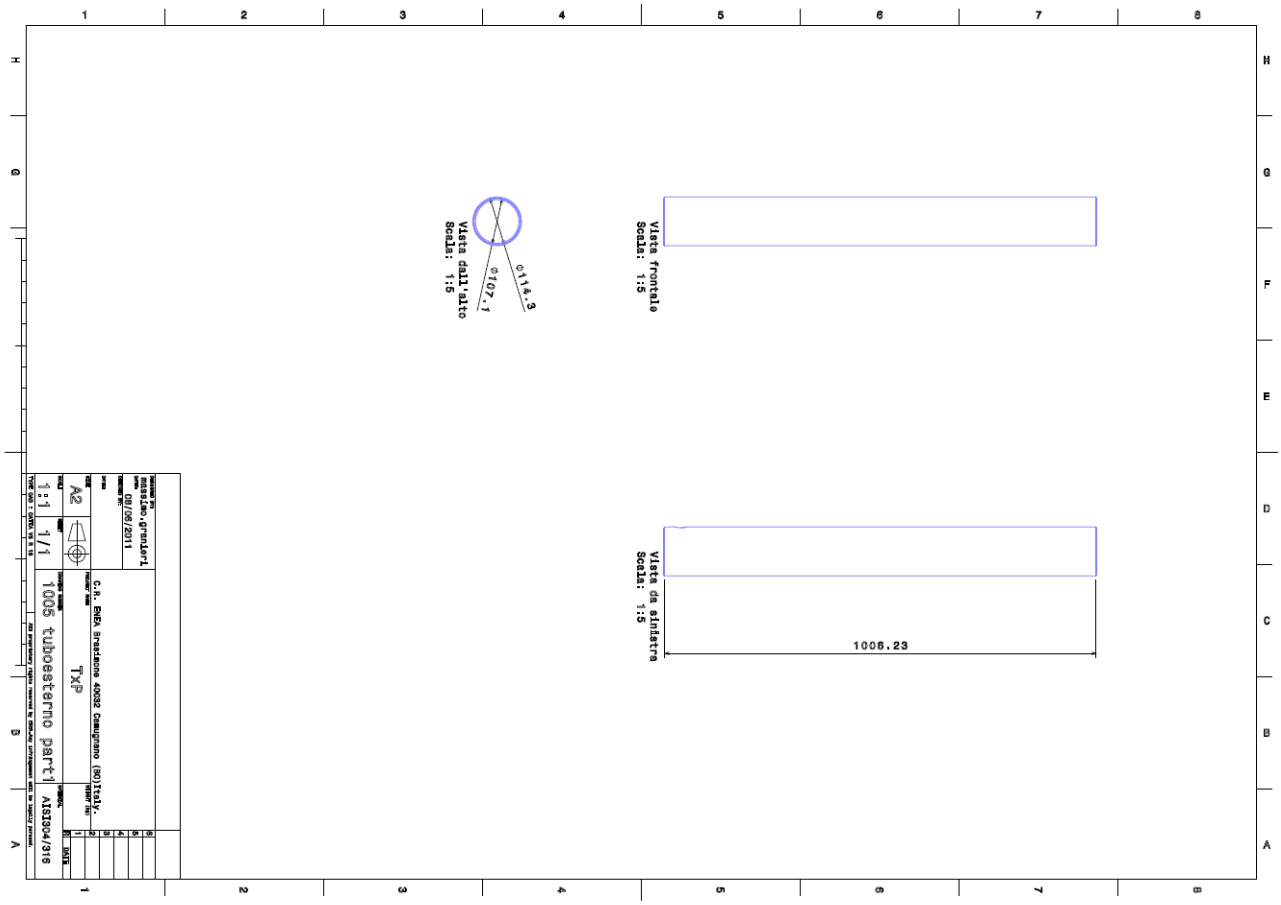

Fig. B. 6 – TxP PIPE-8, sub-component 8a.

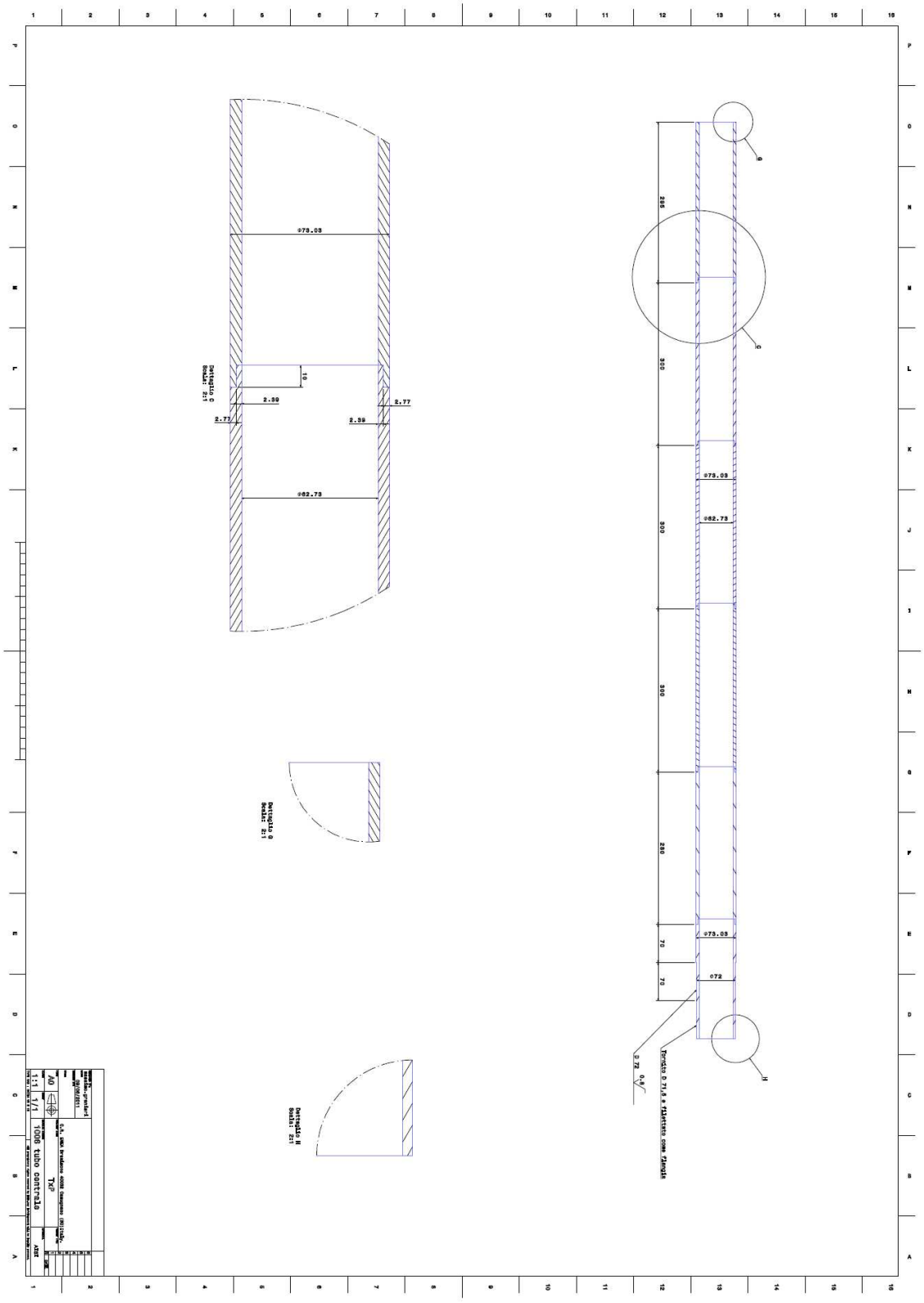

Fig. B. 7 – TxP PIPE-7, item 7.

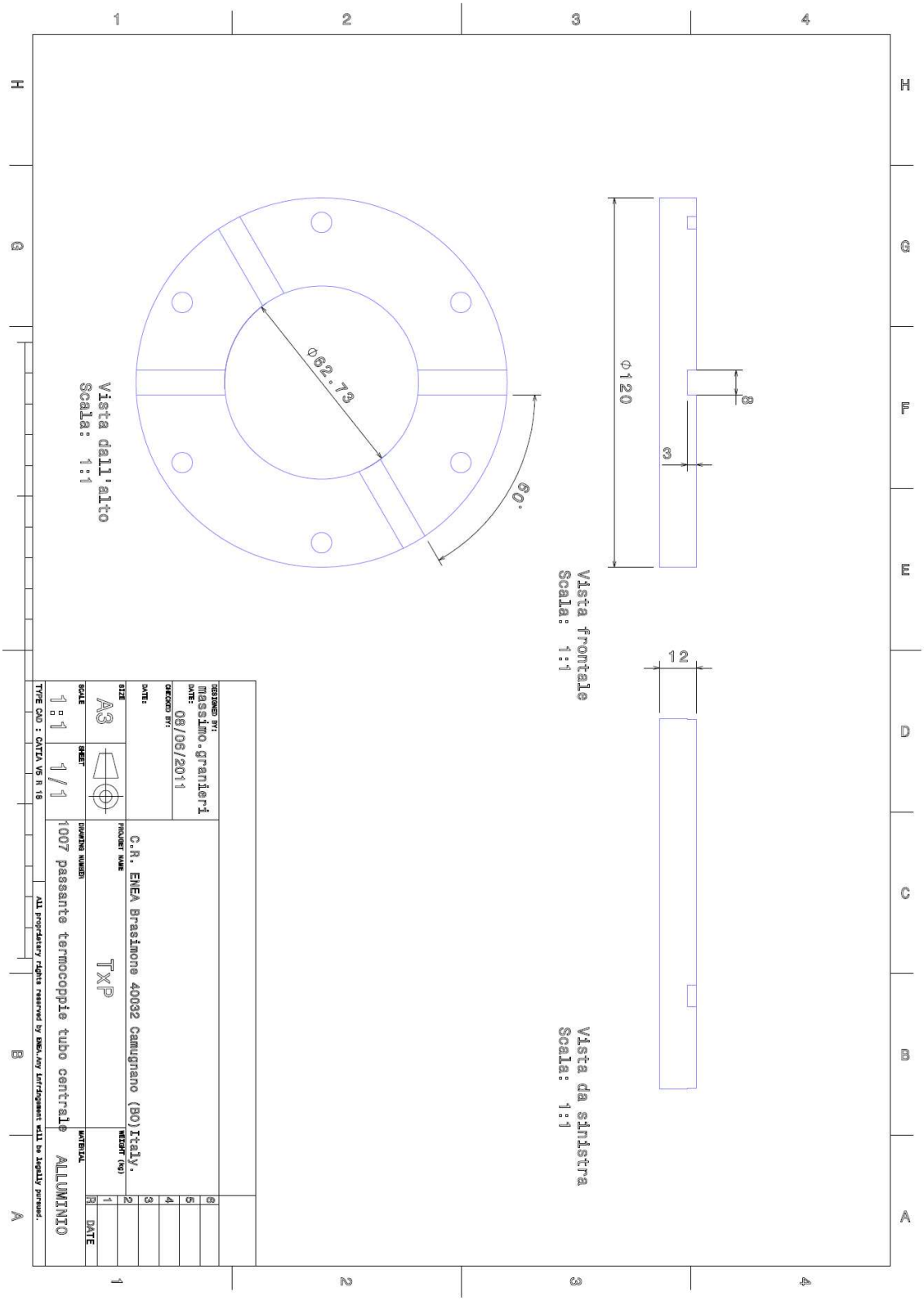

Fig. B. 8 – TxP aluminum disk, item 13.

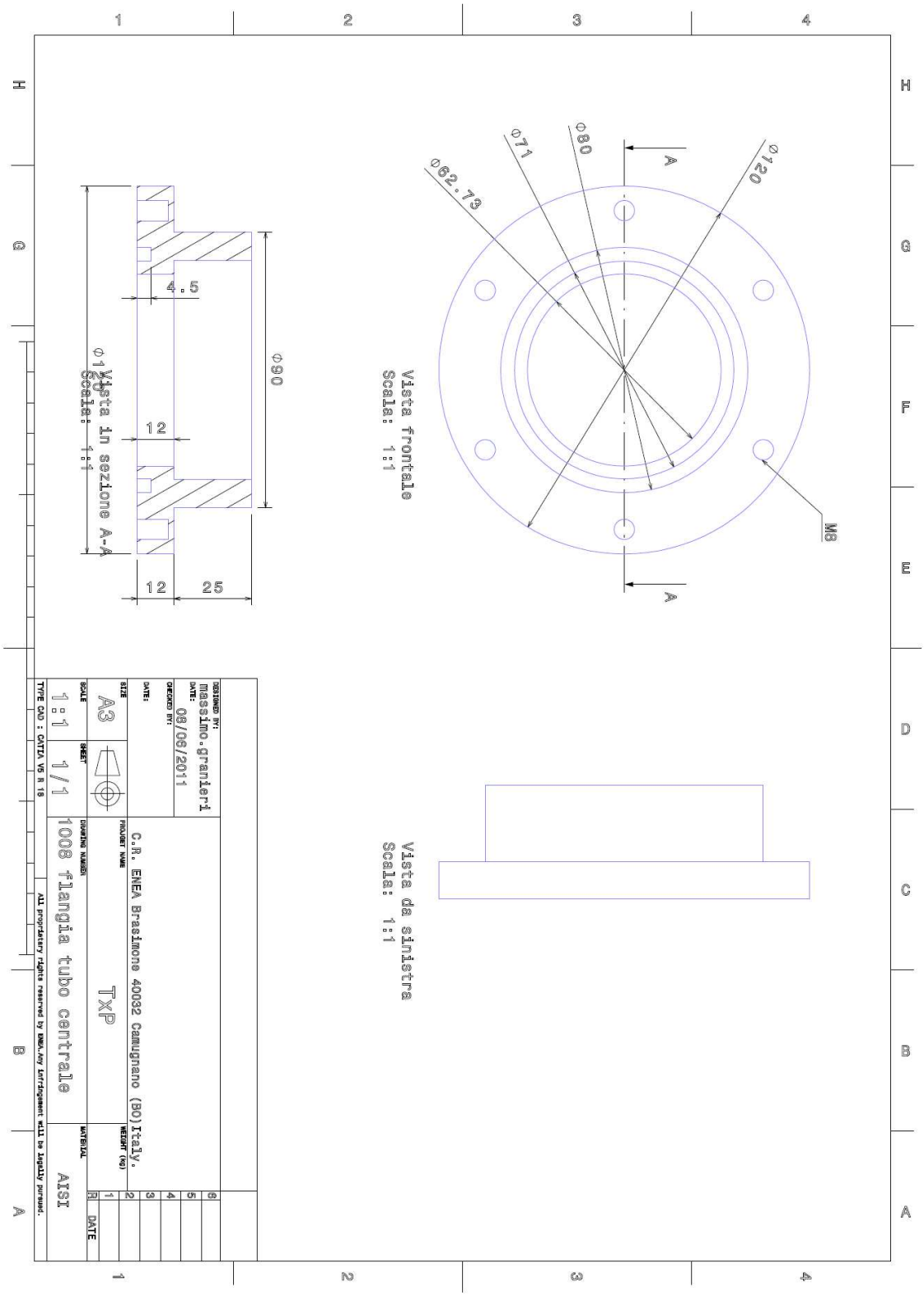

Fig. B. 9 – TxP flange, item 12.

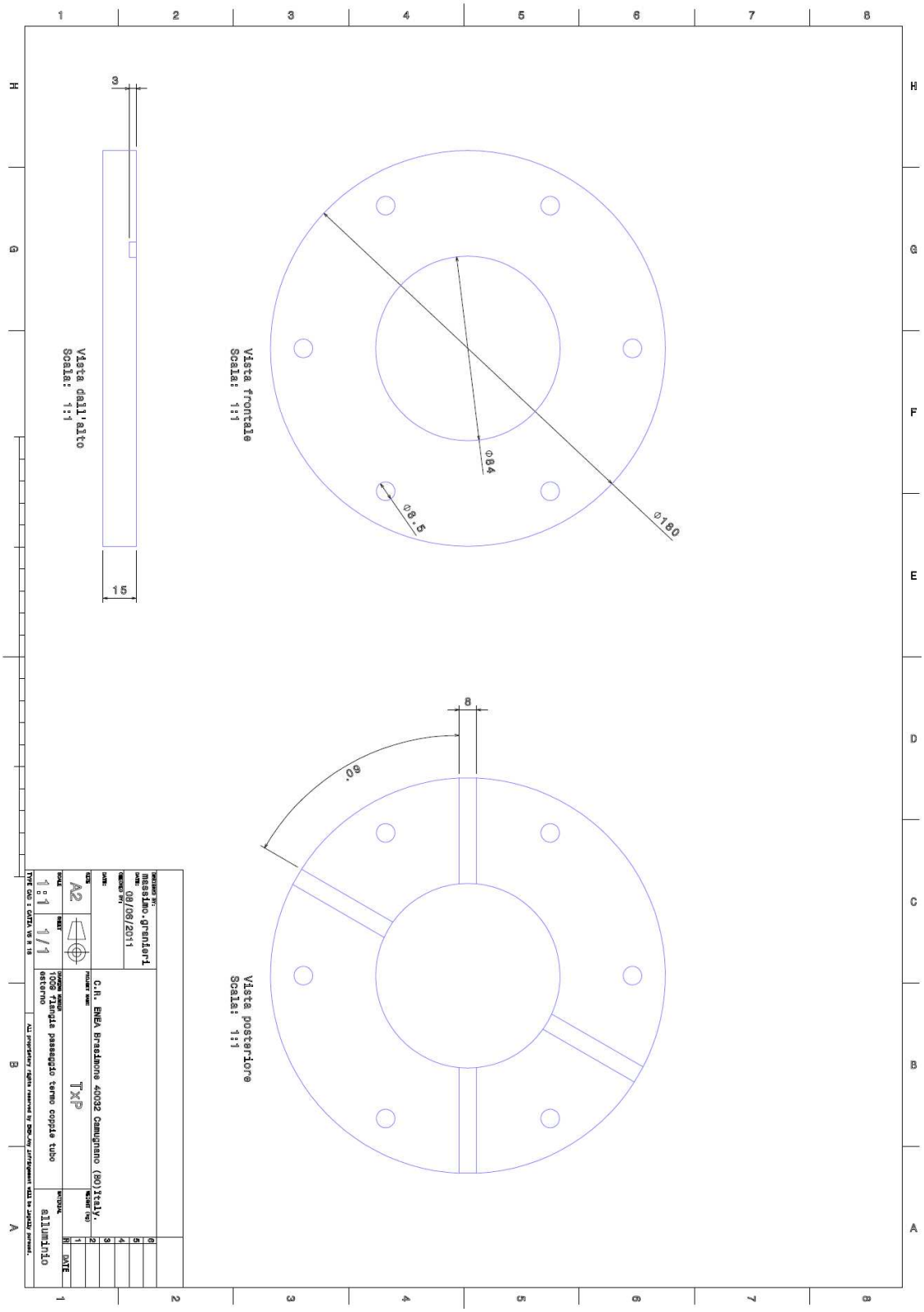

Fig. B. 10 – TxP aluminum disk, item 10.

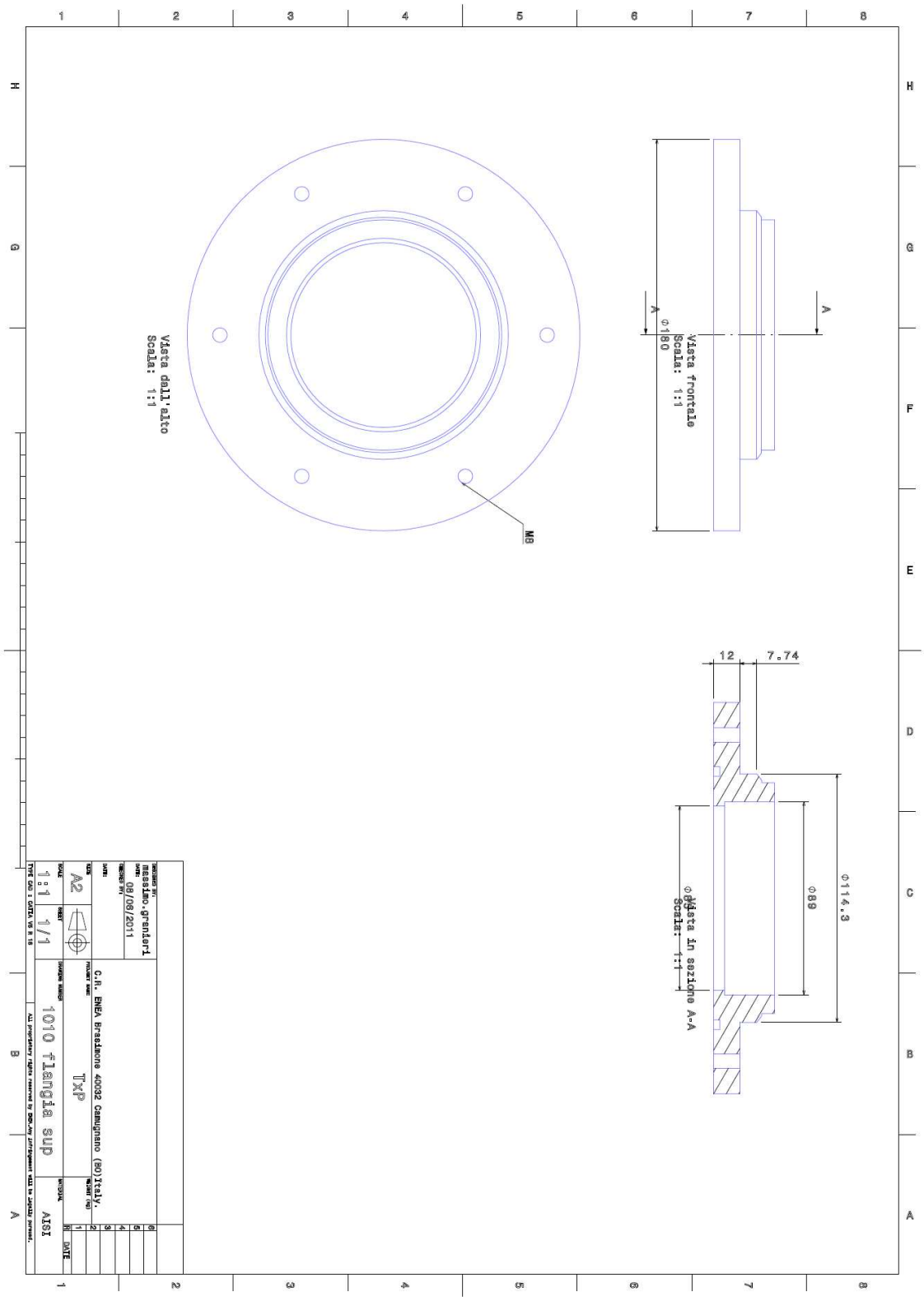

Fig. B. 11 – TxP flange, item 9.

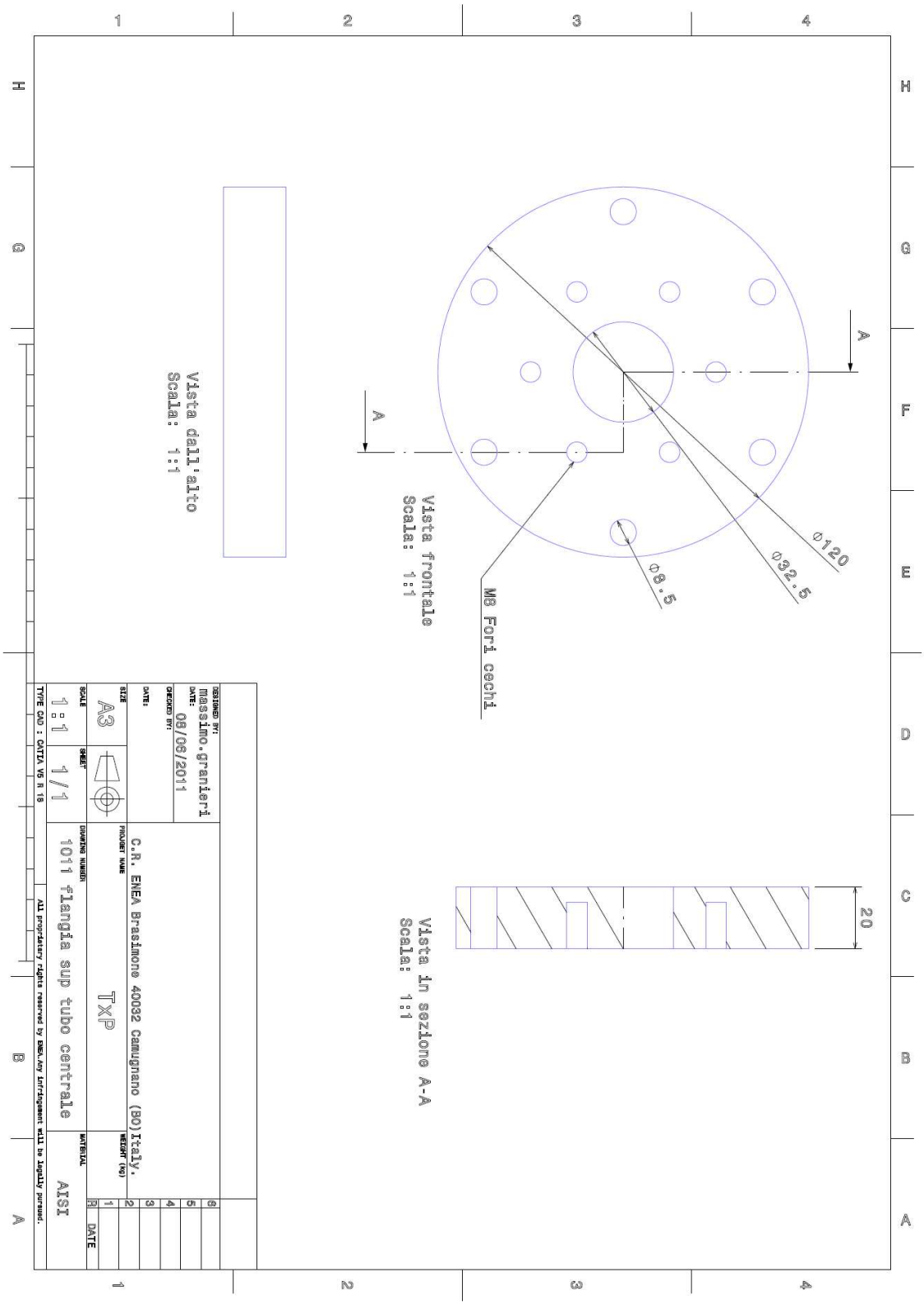

Fig. B. 12 – TxP flange, item 15.

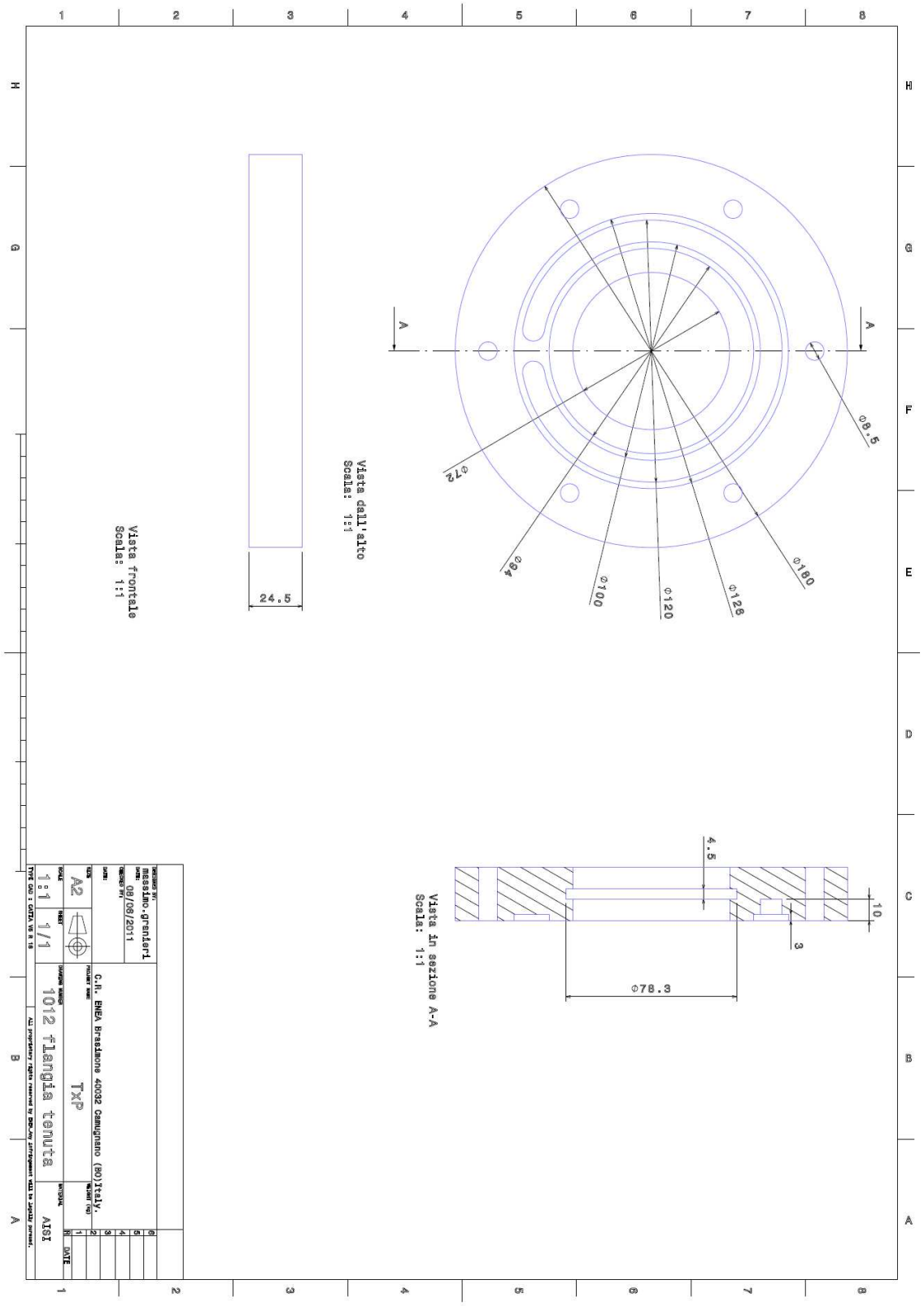

Fig. B. 13 – TxP flange, item 11.

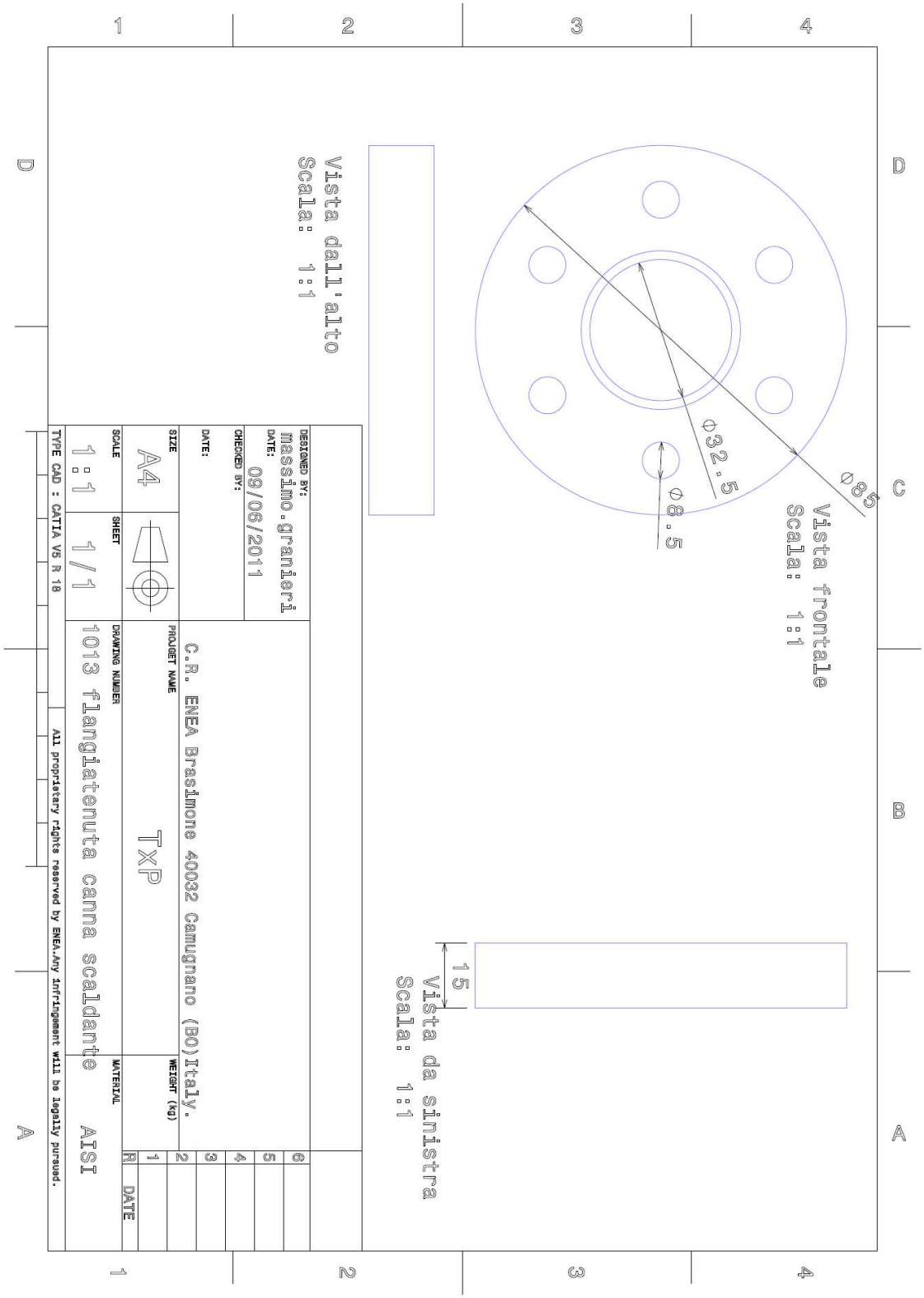

Fig. B. 14 – TxP flange, item 7.

APPENDIX C: FN measurements on AISI-316 powder

MALVERN INSTRUMENTS

MASTERSIZER 2000

Result Analysis Report

Sample Name: AISI 316 vergine - Average	**SOP Name:**	**Measured:** martedì 25 febbraio 2014 13.49.36	
Sample Source & type: Works	**Measured by:** Utente	**Analysed:** martedì 25 febbraio 2014 13.49.38	
Sample bulk lot ref: 19/04/2013	**Result Source:** Averaged		
Particle Name: Iron	**Accessory Name:** Hydro 2000SM (A)	**Analysis model:** Multiple narrow modes	**Sensitivity:** Enhanced
Particle RI: 2.860	**Absorption:** 1	**Size range:** 0.020 to 2000.000 um	**Obscuration:** 12.44 %
Dispersant Name: Water	**Dispersant RI:** 1.330	**Weighted Residual:** 0.393 %	**Result Emulation:** Off
Concentration: 0.0492 %Vol	**Span :** 1.548	**Uniformity:** 0.541	**Result units:** Volume
Specific Surface Area: 0.221 m²/g	**Surface Weighted Mean D[3,2]:** 27.128 um	**Vol. Weighted Mean D[4,3]:** 37.885 um	

d(0.1): 16.055 um **d(0.5):** 30.631 um **d(0.9):** 63.479 um

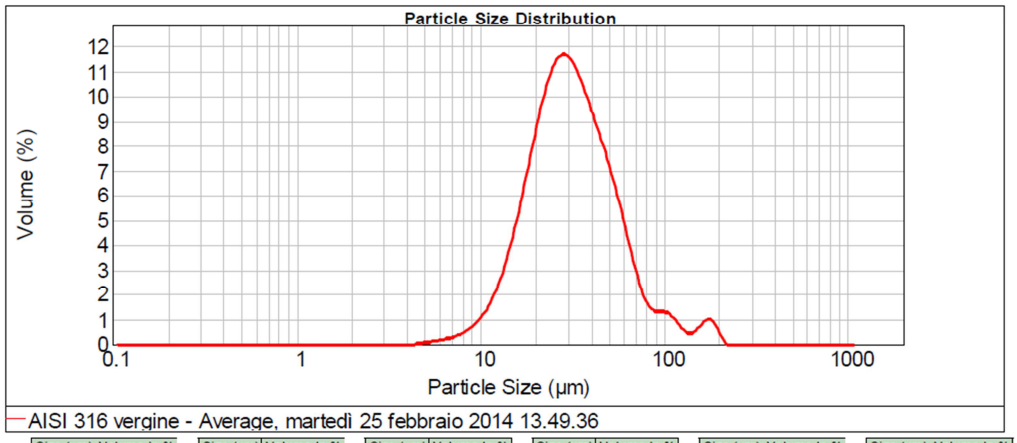

Size (µm)	Volume In %	Size (µm)	Volume In %	Size (µm)	Volume In %	Size (µm)	Volume In %	Size (µm)	Volume In %	Size (µm)	Volume In %
0.020	0.00	0.142	0.00	1.002	0.00	7.096	0.26	50.238	4.94	355.656	0.00
0.022	0.00	0.159	0.00	1.125	0.00	7.962	0.41	56.368	3.85	399.052	0.00
0.025	0.00	0.178	0.00	1.262	0.00	8.934	0.63	63.246	2.67	447.744	0.00
0.028	0.00	0.200	0.00	1.416	0.00	10.024	0.98	70.963	1.65	502.377	0.00
0.032	0.00	0.224	0.00	1.589	0.00	11.247	1.50	79.621	1.09	563.677	0.00
0.036	0.00	0.252	0.00	1.783	0.00	12.619	2.25	89.337	0.97	632.456	0.00
0.040	0.00	0.283	0.00	2.000	0.00	14.159	3.24	100.237	0.93	709.627	0.00
0.045	0.00	0.317	0.00	2.244	0.00	15.887	4.45	112.468	0.61	796.214	0.00
0.050	0.00	0.356	0.00	2.518	0.00	17.825	5.80	126.191	0.33	893.367	0.00
0.056	0.00	0.399	0.00	2.825	0.00	20.000	7.09	141.589	0.41	1002.374	0.00
0.063	0.00	0.448	0.00	3.170	0.00	22.440	8.13	158.866	0.71	1124.683	0.00
0.071	0.00	0.502	0.00	3.557	0.00	25.179	8.71	178.250	0.66	1261.915	0.00
0.080	0.00	0.564	0.00	3.991	0.00	28.251	8.75	200.000	0.06	1415.892	0.00
0.089	0.00	0.632	0.00	4.477	0.03	31.698	8.30	224.404	0.00	1588.656	0.00
0.100	0.00	0.710	0.00	5.024	0.07	35.566	7.58	251.785	0.00	1782.502	0.00
0.112	0.00	0.796	0.00	5.637	0.11	39.905	6.74	282.508	0.00	2000.000	
0.126	0.00	0.893	0.00	6.325	0.17	44.774	5.90	316.979	0.00		
0.142		1.002		7.096		50.238		355.656			

Operator notes: *in acqua*

Fig C. 1 – AISI-316, unheated sample, FN measurements.

MASTERSIZER 2000

Result Analysis Report

Sample Name: AISI 316 tFN - Average	**SOP Name:**	**Measured:** mercoledì 26 febbraio 2014 13.56.00	
Sample Source & type: Works	**Measured by:** Utente	**Analysed:** mercoledì 26 febbraio 2014 13.56.01	
Sample bulk lot ref: 19/04/2013	**Result Source:** Averaged		
Particle Name: Iron	**Accessory Name:** Hydro 2000SM (A)	**Analysis model:** Multiple narrow modes	**Sensitivity:** Enhanced
Particle RI: 2.860	**Absorption:** 1	**Size range:** 0.020 to 2000.000 um	**Obscuration:** 13.06 %
Dispersant Name: Water	**Dispersant RI:** 1.330	**Weighted Residual:** 0.120 %	**Result Emulation:** Off
Concentration: 0.0712 %Vol	**Span :** 1.773	**Uniformity:** 0.673	**Result units:** Volume
Specific Surface Area: 0.162 m²/g	**Surface Weighted Mean D[3,2]:** 36.956 um	**Vol. Weighted Mean D[4,3]:** 59.870 um	

d(0.1): 20.045 um **d(0.5):** 45.613 um **d(0.9):** 100.915 um

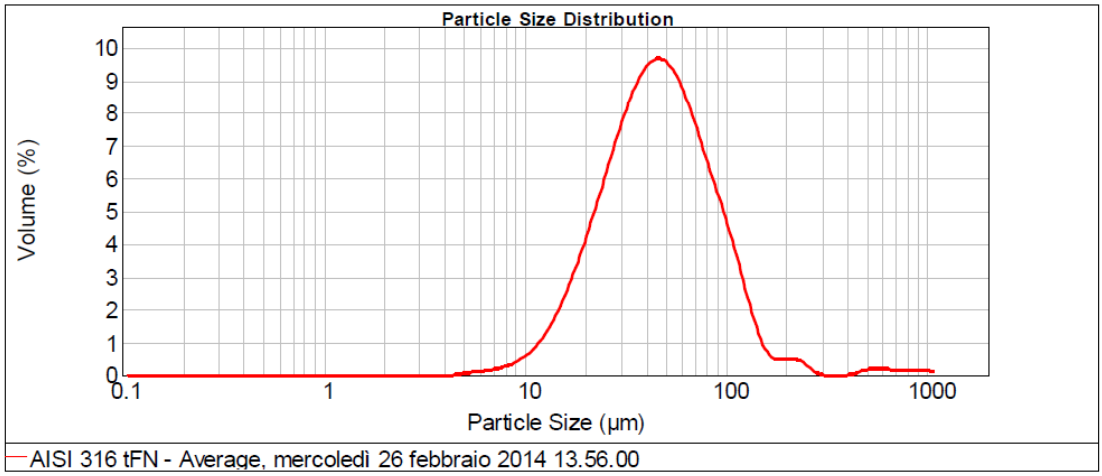

Size (µm)	Volume In %	Size (µm)	Volume In %	Size (µm)	Volume In %	Size (µm)	Volume In %	Size (µm)	Volume In %	Size (µm)	Volume In %
0.020	0.00	0.142	0.00	1.002	0.00	7.096	0.17	50.238	7.10	355.656	0.00
0.022	0.00	0.159	0.00	1.125	0.00	7.962	0.23	56.368	6.67	399.052	0.01
0.025	0.00	0.178	0.00	1.262	0.00	8.934	0.34	63.246	6.06	447.744	0.10
0.028	0.00	0.200	0.00	1.416	0.00	10.024	0.52	70.963	5.34	502.377	0.13
0.032	0.00	0.224	0.00	1.589	0.00	11.247	0.78	79.621	4.62	563.677	0.14
0.036	0.00	0.252	0.00	1.783	0.00	12.619	1.13	89.337	3.90	632.456	0.13
0.040	0.00	0.283	0.00	2.000	0.00	14.159	1.58	100.237	3.16	709.627	0.11
0.045	0.00	0.317	0.00	2.244	0.00	15.887	2.13	112.468	2.32	796.214	0.11
0.050	0.00	0.356	0.00	2.518	0.00	17.825	2.77	126.191	1.46	893.367	0.11
0.056	0.00	0.399	0.00	2.825	0.00	20.000	3.46	141.589	0.76	1002.374	0.08
0.063	0.00	0.448	0.00	3.170	0.00	22.440	4.21	158.866	0.40	1124.683	0.00
0.071	0.00	0.502	0.00	3.557	0.00	25.179	4.98	178.250	0.36	1261.915	0.00
0.080	0.00	0.564	0.00	3.991	0.00	28.251	5.73	200.000	0.39	1415.892	0.00
0.089	0.00	0.632	0.00	4.477	0.02	31.698	6.39	224.404	0.31	1588.656	0.00
0.100	0.00	0.710	0.00	5.024	0.06	35.566	6.90	251.785	0.13	1782.502	0.00
0.112	0.00	0.796	0.00	5.637	0.08	39.905	7.21	282.508	0.00	2000.000	
0.126	0.00	0.893	0.00	6.325	0.12	44.774	7.28	316.979	0.00		
0.142		1.002		7.096		50.238		355.656			

Operator notes: *campione trattato da FN messo tal quale*

Fig C. 2 – AISI-316, heated at 500°C, FN measurements.

APPENDIX D: HERO SG bayonet tube unit main components

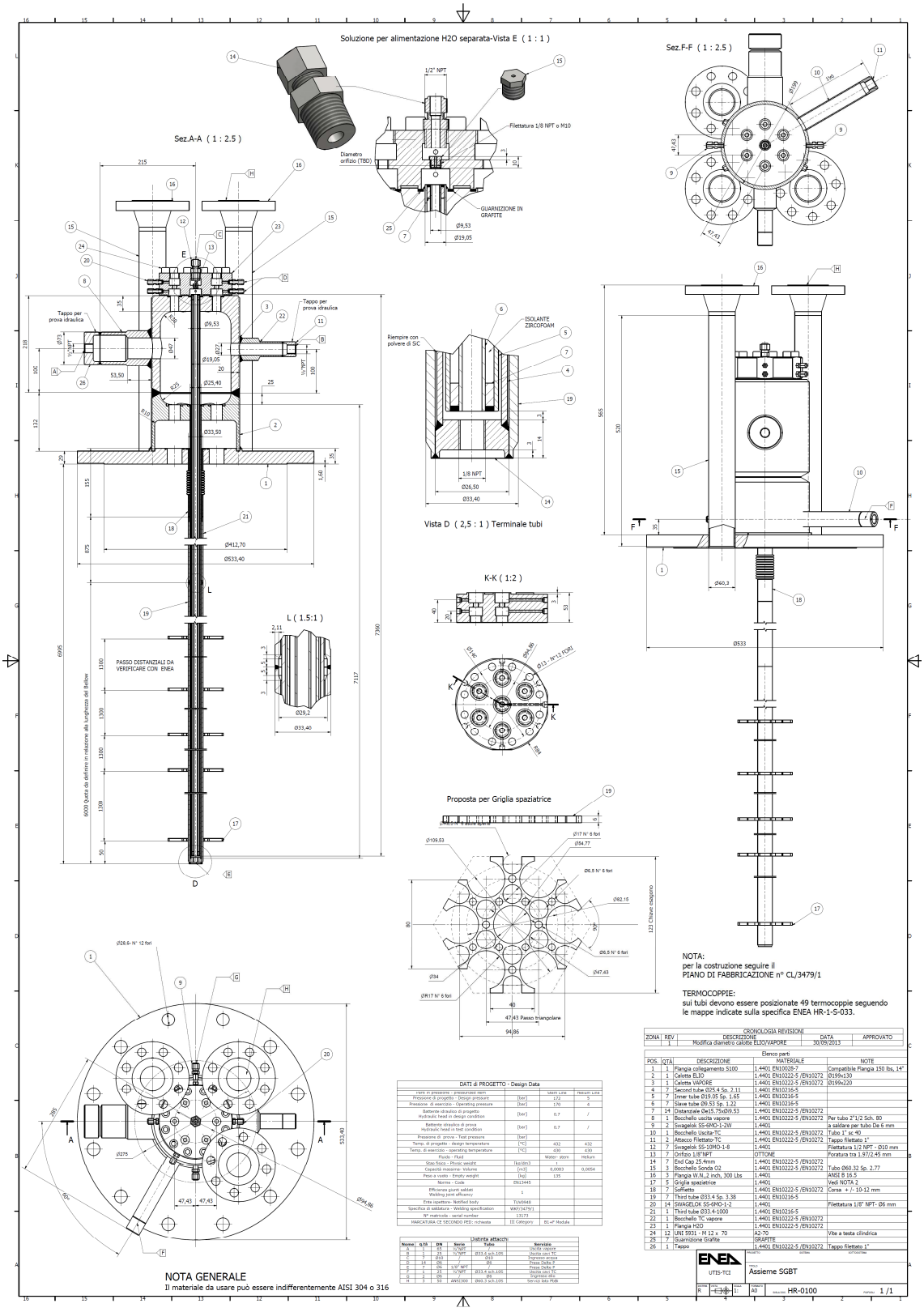

Fig. D. 1 – HERO-CIRCE SGBT unit main layout.

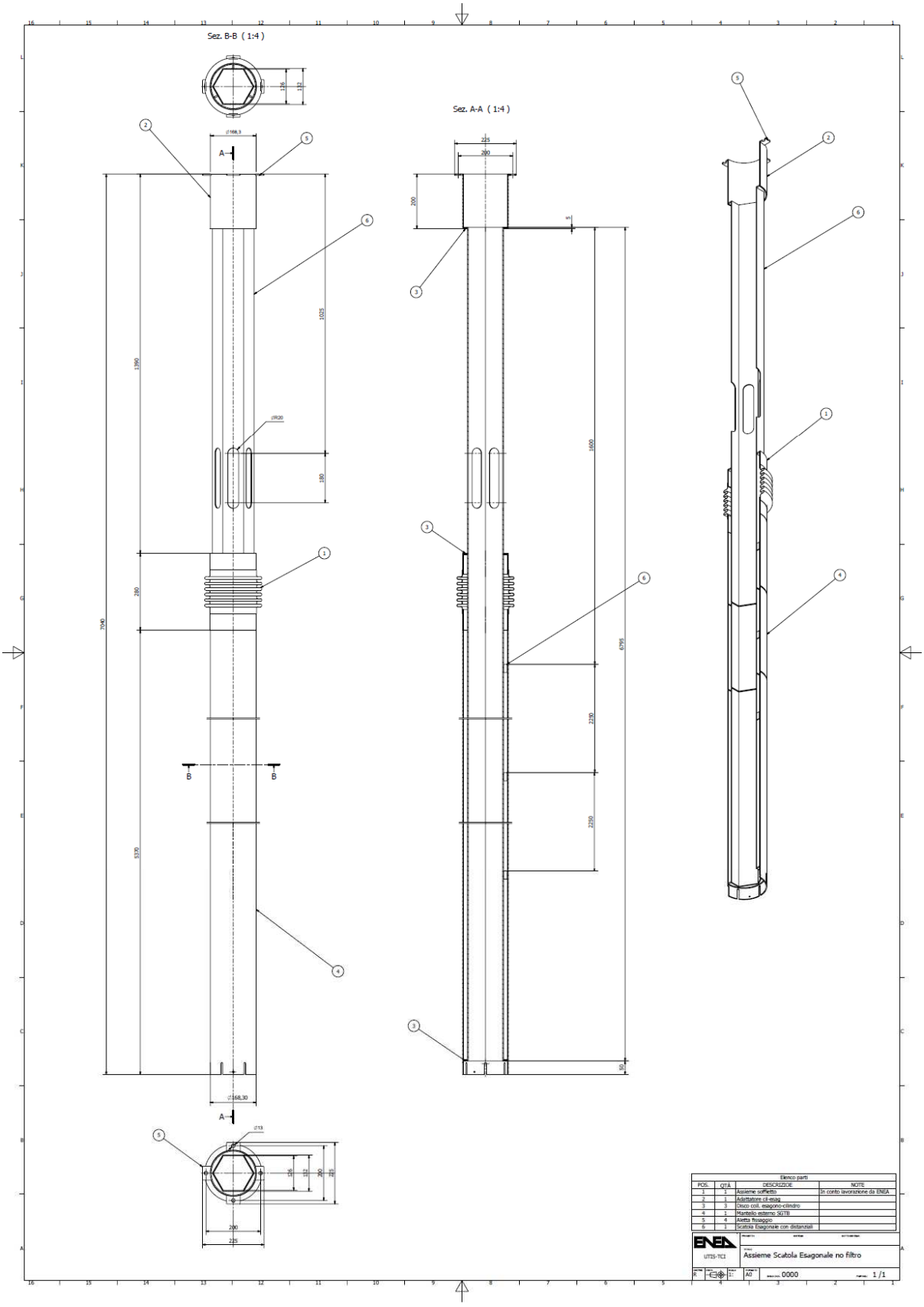

Fig. D. 2 – HERO-CIRCE SGBT external wrap layout.

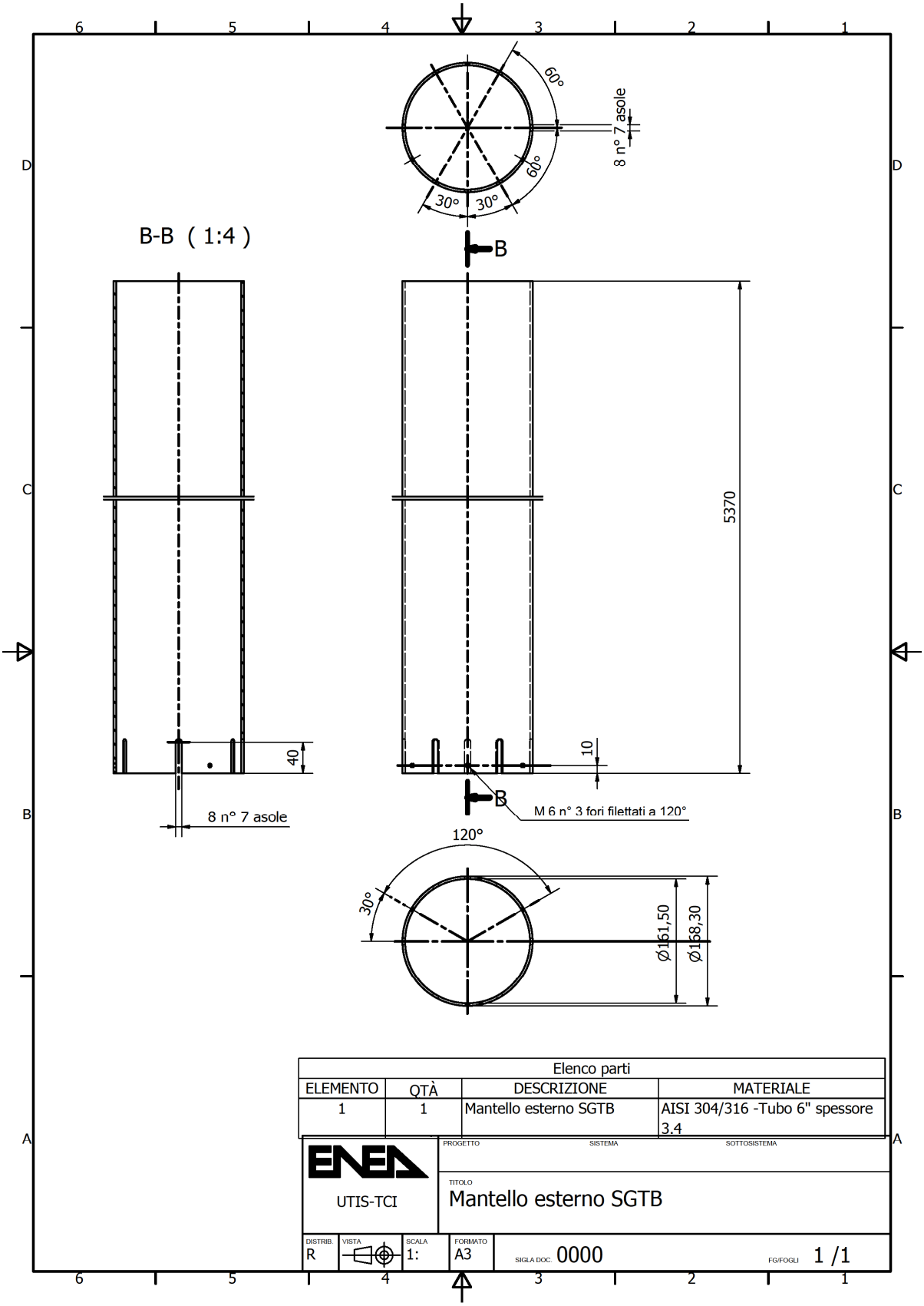

Fig. D. 3 – HERO-CIRCE SGBT wrap external shroud.

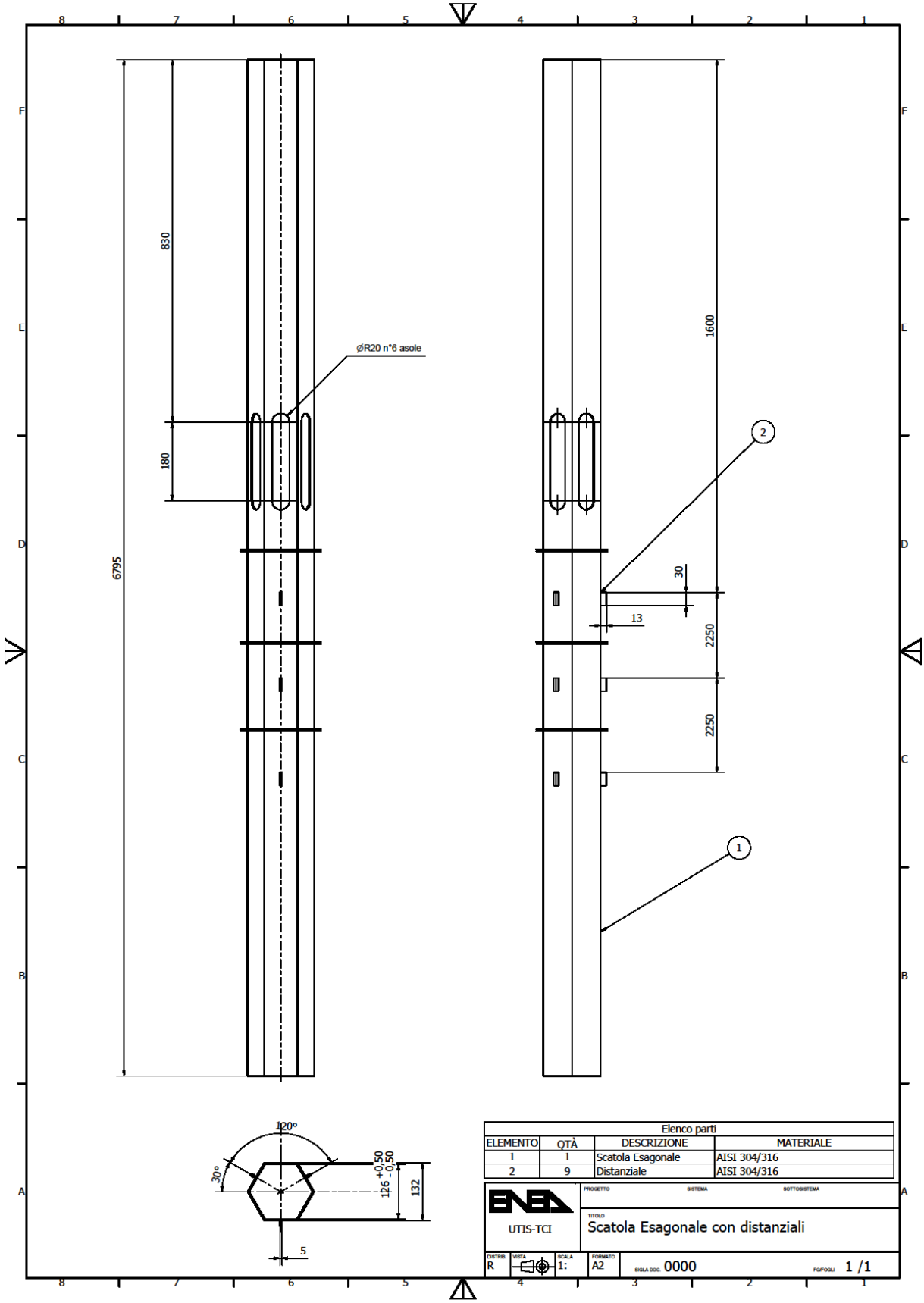

Fig. D. 4 – HERO-CIRCE SGBT hexagonal inner wrap.

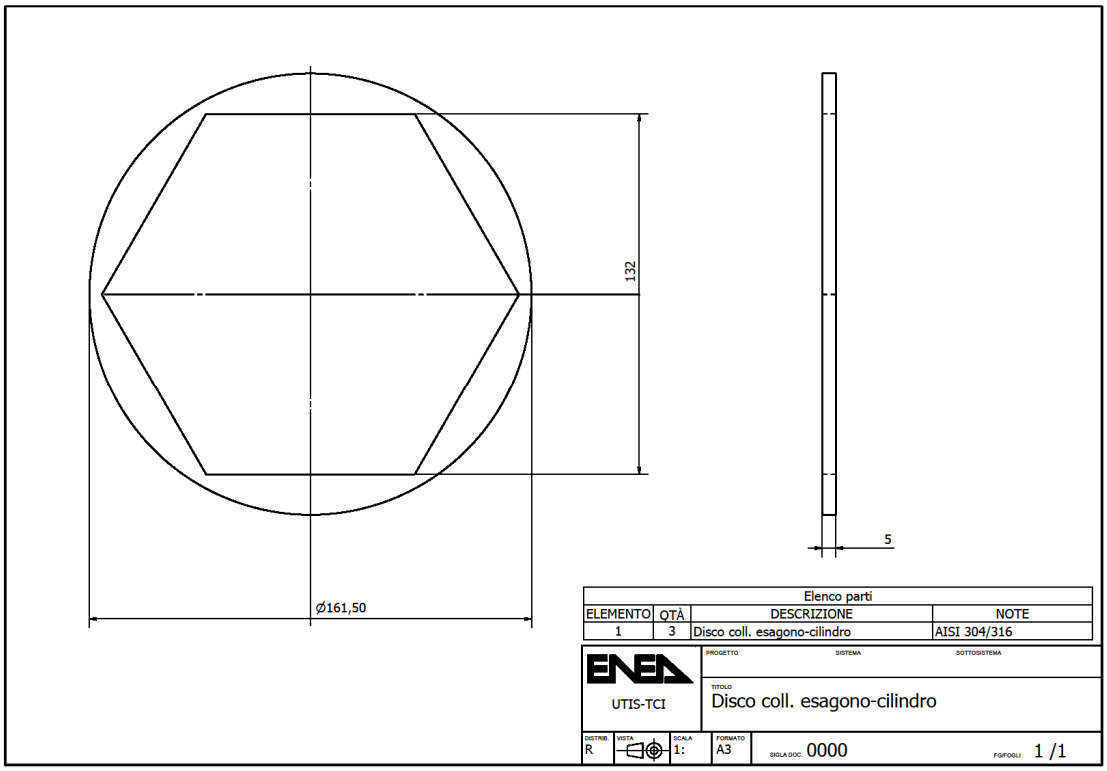

Fig. D. 5 – HERO-CIRCE SGBT hexagon cylinder adaptor.

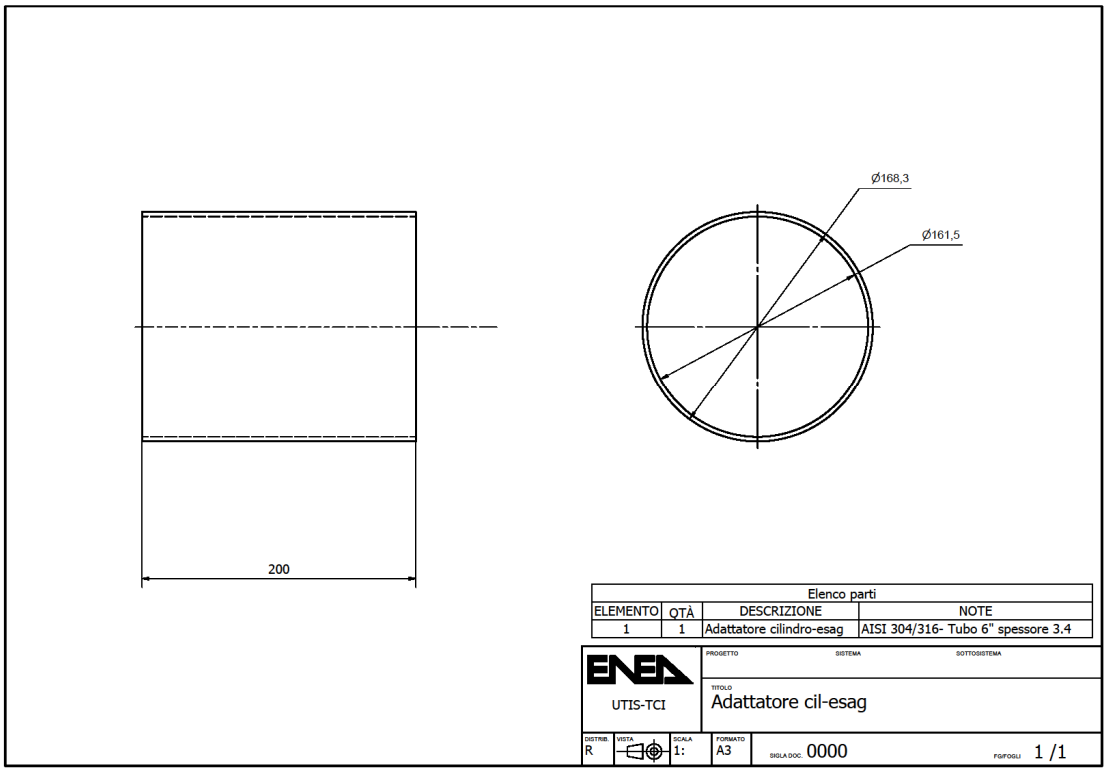

Fig. D. 6 – HERO-CIRCE SGBT hexagon cylinder adaptor.

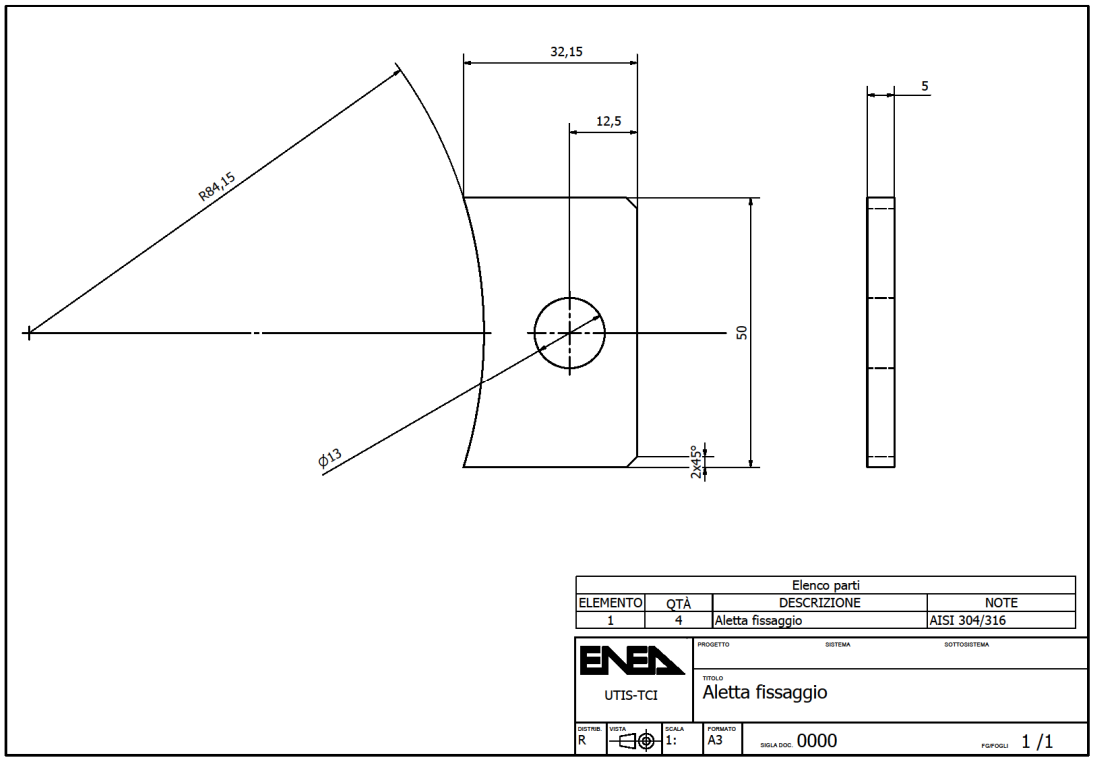

Fig. D. 7 – HERO-CIRCE SGBT fixing plate (to S-100 of CIRCE top flange).

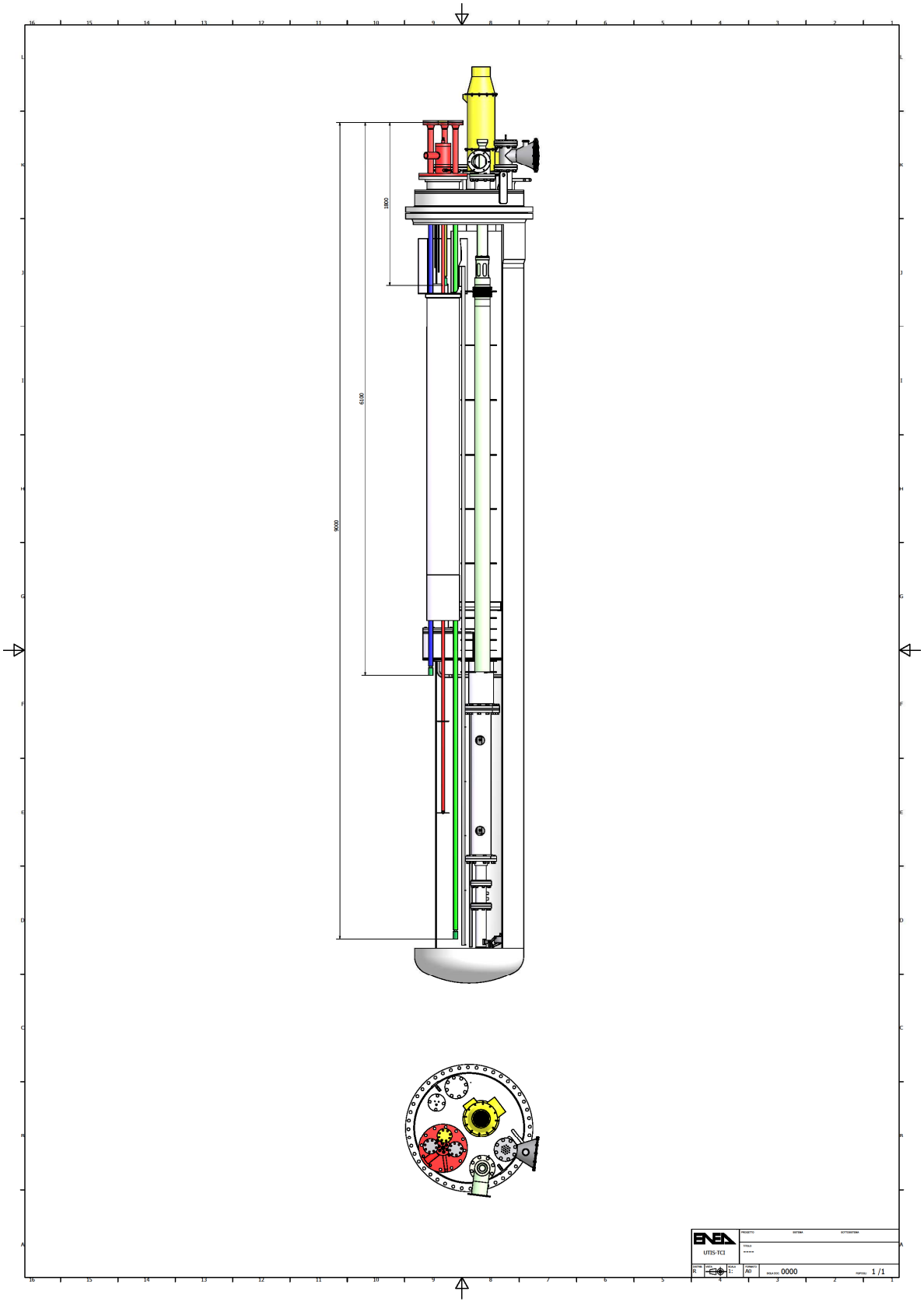

Fig. D. 8 – HERO-CIRCE SGBT inserted in the CIRCE facility.